

# Tfh Lymphoma: Analysis of a RHOA Mutation & Establishment of a Pre-Clinical Model

Thesis submitted for the degree of Doctor of Philosophy  
at the University of Leicester

Dr Rebecca L Allchin

Leicester Cancer Research Centre

Department of Genetics & Genome Biology

January 2019

# TFH LYMPHOMA: ANALYSIS OF A RHOA MUTATION & ESTABLISHMENT OF A PRE-CLINICAL MODEL

---

DR REBECCA L ALLCHIN

T cell lymphoma is a rare haematological cancer but represents an area of unmet need with little improvement in patient outcomes over the last 20 years. However, recently there has been an increase in the understanding of T cell biology and development of a subtype of T cell lymphoma known as Tfh lymphoma. This has been associated with the detection of recurrent mutations which occur in Tfh lymphoma including mutations found in RHOA.

Here I show that the expression of RHOA carrying the mutations found in Tfh lymphoma samples is lower than the WT RHOA protein, and that these mutated proteins have reduced activity. The combination of this work and other recently published work suggests that the mutated RHOA is found at lower levels which may be due to protein instability. Although it has reduced GTP binding ability the mutated protein may activate other pathways leading to its role in lymphomagenesis.

Due to the lack of preclinical models of Tfh lymphoma I have further characterised a T cell lymphoma model initially described by Ellyard et al showing that this represents a model of a genetically diverse lymphoma which occurs on an immunocompetent background.

I demonstrate the use of Magnetic Resonance Imaging (MRI) to assess the response of the lymphoma to treatment. I demonstrate the utility of MRI to monitor changes in lymph node size showing this to be a useful tool in assessment of treatment effects.

Subsequently I show the effect of ITK inhibition with ibrutinib on the T cell lymphoma in this model. Ibrutinib shows a mixed response in this model and no biomarkers of response were found.

## ACKNOWLEDGEMENTS

---

There are many people I must thank for their support and assistance in the completion of this thesis. Not least is Professor Wagner who gave me the opportunity to carry out this period of research and has been always on hand to review my work and inspire its direction.

The others in the Wagner lab have offered practical and emotional support with thanks to Dan Beck, Larissa Lezina, Matt Carr, Amy Wilson, Katie Wickenden, Sami Mamand, Nadia Nawaz, Afaf Altharhi, Sian Evans and Matt Ahearne.

I received financial support from the Scott-Waudby Charitable Trust as part of the Ernest and Helen Scott Haematological Research Institute. Part of the project received funding from Janssen. My work took place at the MRC Toxicology Unit and I was fortunate to receive assistance from that department.

I must also thank my thesis committee of Professor Jon Barrett and Professor Shaun Cowley who helped to guide my thinking and were always enthusiastic.

I had help from members in Professor Schwabe's lab with aspects of the project, particularly from Peter Watson, Louise Fairall and Chris Millward.

Aspects of the project were supported by Nucleus Genomics at the University of Leicester with assistance from Spencer Gibson & Nic Sylvius. I am also indebted to Thomas Keane (now of EMBL) and Anthony Doran for their assistance with the whole exome sequencing and subsequent data analysis. I was also helped enormously by bioinformatic training provided by BBASH at the University of Leicester

I was assisted by Lucia Pinon with much of my flow cytometry work from initial teaching to guidance in setting up and carrying out experiments.

Without the support of the Pre-Clinical Research Facility much of this project would have been impossible. Particular thanks go to Hayley Smith for her day to day care of the colony and interest in the work and Mike Kelly who leads the imaging team. I am extremely grateful to Ruth Barber for her help and advice throughout the project.

I have also been fortunate to develop a clinical interest and expertise during the period of my research and have had many opportunities supported by the clinical team at the Leicester Royal Infirmary, with special thanks to Fiona Miall.

# TABLE OF CONTENTS

---

Abstract .....	i
Acknowledgements .....	ii
Table of Contents .....	iv
Table of Figures & Tables .....	x
1 Introduction - T Cell Lymphoma .....	1
1.1 T cell lymphoma classification .....	1
1.2 T cell lymphoma treatment .....	2
1.3 T cell development and differentiation .....	5
1.3.1 Early T cell development .....	5
1.3.2 T cell maturation and differentiation .....	6
1.4 Follicular helper T cells .....	8
1.5 T cell signalling .....	10
1.6 Tfh Lymphoma .....	11
1.7 Tfh Lymphoma genetics .....	14
1.7.1 Epigenetic dysregulation .....	14
1.7.2 RHOA mutation .....	15
1.7.3 Other mutations .....	18
1.8 RHOA GTPase .....	20
1.8.1 RHOA in T cell development .....	21
1.8.2 RHOA in T cell signalling and behaviour .....	23
1.8.3 Effect of mutations on RHOA function .....	24
1.9 ITK in TFH cells and T cell lymphoma .....	26
1.9.1 Role of ITK in T cell differentiation .....	26
1.9.2 ITK inhibition .....	27

1.9.3	Role of ITK in T cell lymphoma .....	28
1.10	Mouse models of T cell Lymphoma .....	28
1.10.1	ITK:SYK translocation models .....	28
1.10.2	Models with features of Tfh lymphoma or PTCL.....	29
1.10.3	Models with expression of RHOA <sup>G17V</sup> .....	31
1.10.4	Patient derived xenografts .....	33
1.10.5	Summary of mouse models.....	34
1.11	Development of AITL.....	34
1.11.1	Speculation about clonal evolution.....	34
1.11.2	Do mutations in epigenetic modifiers cause T cell lymphoma? .....	35
1.11.3	What is the role of the RHOA pathway in lymphomagenesis? .....	36
1.12	Aims.....	37
2	Methods .....	38
2.1	Buffers.....	38
2.2	RHOA Expression constructs for Bacterial and Mammalian cells .....	40
2.2.1	Quantification of nucleic acids .....	40
2.2.2	DNA sequencing .....	40
2.2.3	Expression plasmids .....	40
2.2.4	Bacterial transformation .....	41
2.2.5	Small scale purification of plasmid DNA.....	41
2.2.6	Large scale purification of plasmid DNA for mammalian cell transfection 42	
2.2.7	Site Directed Mutagenesis.....	42
2.3	Protein expression and purification of bacterial culture.....	44
2.3.1	Cell Lysis.....	44

2.3.2	Protein purification.....	44
2.3.3	Protein concentration .....	44
2.3.4	Protein quantification.....	45
2.3.5	Protein Electrophoresis .....	45
2.3.6	Immuno-blotting .....	45
2.3.7	Coomassie staining .....	46
2.3.8	Circular Dichroism .....	46
2.4	Mammalian cell culture .....	47
2.4.1	Cell counting.....	47
2.4.2	Mammalian cell transfection.....	48
2.4.3	Mammalian cell lysis .....	48
2.4.4	RNA extraction.....	48
2.4.5	Protein extraction.....	49
2.4.6	Rhotekin pull down.....	49
2.4.7	Gel analysis with Image J.....	50
2.4.8	Ibrutinib treatment of cells .....	51
2.5	A Mouse Model of T-Cell Lymphoma .....	51
2.5.1	Husbandry and colony management .....	51
2.5.2	Adoptive transfer.....	51
2.5.3	Imaging .....	52
2.5.4	Image analysis .....	53
2.5.5	Drug treatments .....	53
2.5.6	Lymph Node Dissection .....	54
2.5.7	Serum IL-21 measurement.....	55
2.5.8	Cell suspension preparation .....	57

2.5.9	Cell counting.....	57
2.5.10	Cell separation.....	57
2.5.11	FACS staining.....	58
2.5.12	CD4 <sup>+</sup> cell culture.....	59
2.5.13	CellTiter-Glo <sup>®</sup> Luminescent Cell Viability Assay.....	60
2.5.14	Cell proliferation & differentiation.....	60
2.5.15	RNA extraction.....	61
2.5.16	Gene Expression Profiling by Microarray.....	61
2.5.17	DNA extraction.....	62
2.5.18	Whole exome sequencing.....	63
2.5.19	Clonality.....	65
3	Characterisation of RHOA Mutations.....	67
3.1	Introduction.....	67
3.2	Bacterial Expression & Purification of RHOA Mutant Proteins.....	67
3.2.1	Circular dichroism of RHOA proteins.....	70
3.3	Mammalian expression of RHOA proteins.....	72
3.4	Assessment of RHOA activity.....	75
3.5	Discussion.....	77
4	Characterisation of the San Roque Mouse Model.....	80
4.1	Introduction to the model.....	80
4.2	The San Roque Colony.....	80
4.3	Flow Cytometry Assessment.....	82
4.3.1	Comparison of SRQ and WT spleens.....	82
4.3.2	Assessment of lymph nodes.....	83
4.3.3	Paired comparison of tumour lymph nodes and spleen.....	85

4.4	T cell Clonality.....	88
4.5	In Vitro Characterisation.....	90
4.5.1	CD4 <sup>+</sup> T cell ITK expression.....	90
4.5.2	T cell stimulation and ITK inhibition.....	91
4.5.3	Interleukin stimulation and proliferation.....	94
4.5.4	Conclusions from <i>in vitro</i> experiments.....	97
4.6	Assessment of Gene Expression by Microarray.....	97
4.7	Whole Exome Sequencing.....	101
4.7.1	Analysis of reads and Mapping to the reference genome.....	101
4.7.2	Generating variants of interest.....	103
4.7.3	Description of Variants.....	106
4.7.4	Pathway analysis.....	112
4.7.5	Discussion of WES results.....	112
4.8	Characterisation of the SRQ mouse model summary.....	113
5	Results of Preclinical experiments.....	114
5.1	Introduction.....	114
5.2	Adoptive transfer to Produce Cohorts of Mice with Genetically Identical Lymphomas?.....	114
5.3	Visualising Mouse Lymphoma By Magnetic Resonance Imaging (MRI).....	115
5.4	Pilot Study to Demonstrate Sensitivity to Cyclophosphamide Treatment....	118
5.5	A Preclinical Study with the ITK/BTK inhibitor, Ibrutinib.....	124
5.5.1	Cohort 1.....	124
5.5.2	Cohort 2.....	125
5.5.3	Response assessment by MRI.....	126
5.5.4	Post mortem analysis.....	129

5.6	Discussion .....	137
6	Conclusions.....	140
6.1	RHOA mutation: could loss of protein expression contribute to lymphomagenesis?.....	140
6.2	The san roque mouse strain is a useful pre-clinical model for testing novel agents that might be beneficial in T-cell lymphoma.....	142
6.3	Future Directions .....	144
7	References.....	145

## TABLE OF FIGURES & TABLES

---

Figure 1-1: 10-year survival of the most common T cell lymphoma subtypes as described by the International T Cell Project (3) .....	1
Table 1-1: Summary of key phase 2 trials of single agents in relapsed/refractory T cell lymphoma.....	5
Figure 1-2: Representation of T cell development in the thymus. ....	6
Figure 1-3: Diagram showing the main CD4 <sup>+</sup> T cell subsets with master transcription factors and key cytokines. ....	7
Figure 1-4: Diagram representing the differentiation steps of Tfh cells.....	9
Figure 1-5: T cell signalling pathway adapted from Schwartzberg et al (72) Vallois et al (73).....	11
Table 1-2: Differentially expressed genes in the molecularly defined AITL classifier ....	13
Figure 1-6: Molecular diagnostic signatures of PTCL subgroups and survival prediction in AITL .....	14
Figure 1-7: RHOA mutations and structure .....	16
Table 1-3: RHOA mutations found in haematological malignancies as listed by COSMIC (109) in December 2018.....	17
Figure 1-8: Mutational status of TCR genes in an 85-patient cohort.....	19
Figure 1-9: The Rho GTPase cycle adapted from Etienne-Manville & Hall (118).....	21
Table 1-4: Summary of mouse models of T cell lymphoma.....	30
Figure 2-1: PROTEX expression vectors.....	40
Table 2-1: Primers used to insert RHOA cDNA into pLEICS vectors .....	41
Table 2-2: Concentration of antibiotics used for bacterial selection.....	41
Table 2-3: Primers used for site directed mutagenesis.....	42
Figure 2-2: Sanger Sequencing Chromatograms.....	43
Table 2-4: Antibodies used for immunoblotting .....	46
Figure 2-3: Lymph node anatomy of the mouse from Dunn (6) .....	55
Figure 2-4: Standard curve generated for the IL-21 ELISA. ....	56

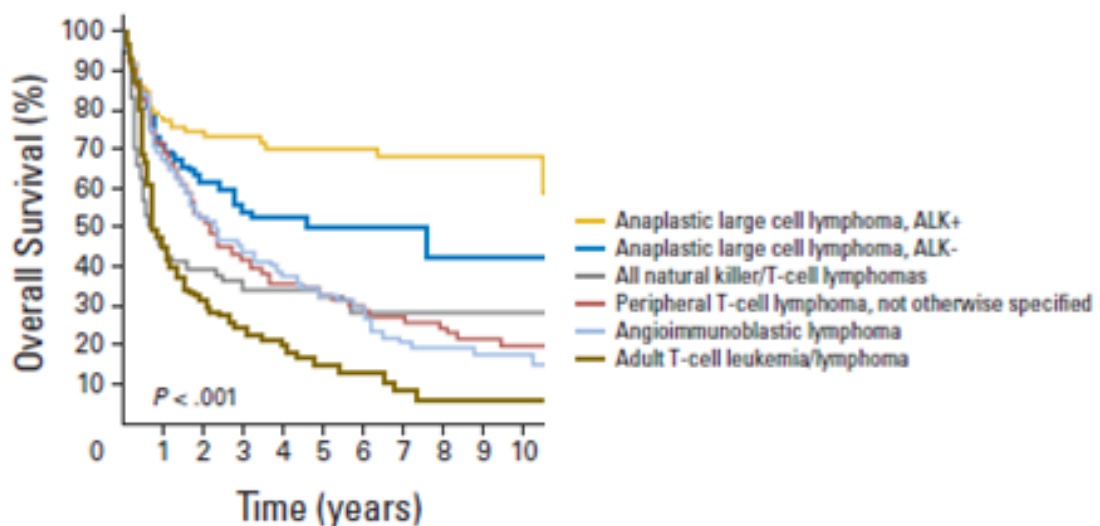
Table 2-5: Antibodies used in FACS panels .....	59
Table 2-6: Databases used in Functional Annotation Clustering analysis.....	62
Table 2-7: Filters used for determining variant quality.....	64
Table 2-8: Primers used for the assessment of T cell clonality .....	66
Figure 3-1: Coomassie stained gel showing proteins produced following bacterial expression.....	69
Figure 3-2: Circular dichroism curves for RHOA constructs. ....	70
Figure 3-3: Normalised melting curves of RHOA constructs.....	71
Table 3-1: Melting temperatures of RHOA constructs.....	71
Figure 3-4: Representative Western blots showing FLAG, RHOA and GAPDH. ....	73
Figure 3-5: Graph showing the relative expression of FLAG-RHOA protein by HEK293 cells.....	74
Figure 3-6: Coomassie stained gel showing the GST-Rhotekin-RBD.....	75
Figure 3-7: Representative Western blot showing the results of the active RHOA pulldown.....	76
Figure 3-8: Relative activation of RHOA compared to RHOA <sup>WT</sup> .....	77
Figure 3-9: Representation of RHOA generated in PYMOL.....	78
Figure 3-10: Representation of RHOA generated by Louise Fairall in PYMOL. ....	79
Figure 4-1: Lymph nodes extracted from SRQ5211. ....	81
Figure 4-2: Haematoxylin and eosin stained sections of an enlarged axillary lymph node .....	81
Figure 4-3: FACS assessment for lymphocyte subsets in WT and SRQ spleens. ....	82
Figure 4-4: FACS to determine lymphocyte subset proportions in normal and tumour lymph nodes in SRQ mice (page 84).....	83
Figure 4-5: Lymphocyte subsets in paired spleen and enlarged lymph node samples. ....	85
Figure 4-6: FACS assessment for Tfh populations in spleen and tumour pairs.....	87
Figure 4-7: TCR spectratyping results of V2-J PCR products. ....	89
Figure 4-8: Western blot showing expression of ITK in SRQ and WT mice.....	90
Figure 4-9: Response curve showing effect of ibrutinib treatment on stimulated CD4 <sup>+</sup> T cells. ....	91
Figure 4-10: Effect of stimulation and treatment on splenic CD4 <sup>+</sup> T cells. ....	92

Figure 4-11: Graph showing effect of stimulation and ibrutinib treatment on CD4 <sup>+</sup> T cells from SRQ spleens and tumours.....	93
Figure 4-12: Tfh proportions following culture with interleukins +/- ibrutinib. ....	94
Figure 4-13: Summary of CTV and proliferation of Tfh cells. ....	96
Figure 4-14: SAM graph from MeV .....	98
Figure 4-15: Hierarchical clustering generated from differentially expressed genes....	99
Figure 4-16: Heat map of hierarchical clustering of genes from AITL gene classifiers.	100
Table 4-1: BAM file statistics showing the numbers and proportions of properly mapped reads and properly paired reads for each sample. ....	102
Figure 4-17: Integrated Genomics Viewer confirming the genotype of each sample in the Roquin gene. ....	102
Figure 4-18: Summary of WES analysis to produce SNVs of interest.....	103
Table 4-2: VCF file statistics.....	104
Figure 4-19: Variants analysed by Varscan showing the number of variants found at each stage of the analysis for 5293 (A) and 5301 (B). ....	105
Figure 4-20: Variants analysed by Varscan showing the number of variants found at each stage of the analysis for 5293 and 5301 constitutional samples compared to SRQ control sample. ....	106
Table 4-3: List of genes generated by comparison of filtered VCF files.....	107
Table 4-4: Details of predicted effects of SNVs on Hsp90ab1-201. ....	108
Figure 4-21: Gene lollipop diagrams representing the six genes found to have SNVs predicted to impact protein production in tumour samples only. ....	109
Table 4-5: SNVs found in Mroh2a. ....	110
Figure 4-22: Gene lollipop diagrams showing the genes mutated in the tumour and constitutional samples of the tumour-bearing mice. ....	111
Table 4-6: SNVs found in Hjurp. ....	112
Figure 5-1: H & E stained section of bowel taken from a mouse at post mortem 5 days after receipt of adoptive transfer of tumour cells. ....	115
Figure 5-2: Montage of T2 weighted MRI scan images of axial slices (0.8mm) from a 12-month-old mouse with no enlarged lymph nodes.....	116

Figure 5-3: Montage of T2 weighted MRI scan images of axial slices (0.8mm) from an 8-month-old mouse.....	117
Table 5-1: Details of mice treated with cyclophosphamide/placebo with the age measured on the day of treatment.....	118
Figure 5-4: Graphs showing the lymph node volume by caliper measurement and the weight of mice in the cyclophosphamide study.....	119
Figure 5-5: Series of MRI scan images from SRQ5396 .....	120
Figure 5-6: Series of MRI scan images from SRQ5336 .....	121
Figure 5-7: Water fall plot demonstrating the response to cyclophosphamide.....	122
Figure 5-8: Results of FACS analysis of lymph nodes following treatment of mice with cyclophosphamide/placebo. ....	123
Figure 5-9: Graph showing the effect of ibrutinib vehicle on Jurkat cells assessed by CTG assay. ....	124
Table 5-2: Details of mice in cohort 1 with the age measured on the first day of treatment .....	125
Table 5-3: Details of mice in cohort 2 with the age measured on the first day of treatment .....	126
Figure 5-10: Water fall plot showing the change in volume of enlarged pre-treatment lymph nodes following therapy.....	127
Figure 5-11: Representative MRI scan images from the first cohort of mice treated with ibrutinib or vehicle. ....	128
Figure 5-12: FACS to assess lymphocyte subsets following ibrutinib treatment.....	130
Figure 5-13:FACS to assess Tfh populations following ibrutinib treatment. ....	131
Figure 5-14: Assessment of serum IL-21. ....	132
Figure 5-15: SAM graph from MeV .....	134
Figure 5-16: Hierarchical clustering generated from genes with significantly different upregulation by SAM analysis .....	135
Figure 5-17: Bar graph showing the effects of stimulation of CD4 <sup>+</sup> T cells in cell culture. ....	137

# 1 INTRODUCTION - T CELL LYMPHOMA

Lymphoma is a malignant proliferation of lymphocytes and can present with lymphadenopathy, bone marrow infiltration and leukaemic disease or extra-nodal tumours. The classification of lymphoma depends upon the nature of the malignant lymphocytes and the clinical features. There were 13,605 cases of non-Hodgkin lymphoma (NHL) diagnosed in the UK in 2014 of which approximately 5% were cases of T cell lymphoma (1). T cell lymphomas arise from T cells and there are a number of subtypes of T cell lymphoma described by the World Health Organisation (WHO) in the Classification of Tumours of Haematopoietic and Lymphoid Tissues, which was updated in 2017 (2).



**Figure 1-1: 10-year survival of the most common T cell lymphoma subtypes as described by the International T Cell Project (3)**

## 1.1 T CELL LYMPHOMA CLASSIFICATION

T cell lymphomas are diverse and accurate classification can be difficult due to overlapping clinical and histological features. Recent advances are reflected in the most recent update to the WHO classification with changes to classifications and the addition of new provisional entities (2). The most common types of T cell lymphoma are peripheral T cell lymphoma, not otherwise specified (PTCL-NOS) and

angioimmunoblastic T cell lymphoma (AITL) making up 29% and 18% of T cell lymphoma diagnoses respectively in UK data collected between 2004 and 2014 (1).

The median age of diagnosis with T cell lymphoma in the UK is 65.8 years with the median age for diagnosis of AITL slightly later at 70.9 years. The International T cell Project report a median age at diagnosis of AITL of 65 years with a range of 18 to 86 years (3). The vast majority of patients (89%) diagnosed with AITL present with advanced stage disease (Ann Arbor stage 3-4) (3).

The UK data shows a 5-year overall survival of 25-40% (1) which is similar to that seen in data from the International T cell Project (4), (Figure 1-1) and contrasts poorly to 10-year survival rates of 63% seen in B cell NHL diagnoses. Although T cell lymphomas are rare they represent an important area of unmet need, as demonstrated by the poor prognosis and the lack of improvement in outcomes seen over the last 20 years (5).

Studies of genetic changes and gene expression have shown similarities between AITL and cases of PTCL-NOS with a T follicular helper (Tfh) cell phenotype (6,7) leading to the new category of nodal T-cell lymphomas with Tfh phenotype which encompasses AITL, follicular T cell lymphoma and other nodal PTCL with a Tfh phenotype (8). The clinicopathological features of AITL will be discussed in section 1.6.

The ability to accurately classify cases of T cell lymphoma based on the biological understanding of these lymphomas will become more important as targeted therapies are developed and our understanding of the pathogenesis of T cell lymphoma increases.

## 1.2 T CELL LYMPHOMA TREATMENT

Nodal T cell lymphoma is an aggressive disease and patients would be considered for treatment at the time of diagnosis. In general treatment is given with curative intent although outcomes are poor with high rates of refractory and relapsed disease (9). Standard therapy for a patient diagnosed with PTCL-NOS or AITL is combination chemotherapy, usually with cyclophosphamide, doxorubicin, vincristine and prednisolone (CHOP) with the addition of etoposide (CHOEP) in some patients and centres (10). The addition of several agents to CHOP have not demonstrated better outcomes (11-13) and a recent UK trial comparing CHOP to a regimen containing

gemcitabine, cisplatin and prednisolone (GEM-P) was closed early as it was failing to show superiority of the GEM-P regimen at a planned interim analysis (14).

The addition of novel agents to CHOP for first line treatment has been assessed in phase I/II studies but no randomised studies have been reported. The addition of romidepsin, a histone deacetylase inhibitor (HDACi), to CHOP was feasible but associated with increased toxicity compared to that expected with CHOP alone (15), the study authors recommend a romidepsin dose of 12 mg/m<sup>2</sup> on D1 & D8 and this is being compared to CHOP alone in a phase 3 trial which has completed recruitment (NCT01796002). The combination of belinostat, another HDACi, and CHOP was assessed and a belinostat dose of 1000 mg/m<sup>2</sup> on D1-5 used in an expansion phase without excess toxicity (16), no phase 3 randomised trial has yet been registered. The combination of pralatrexate, an antimetabolite which is a folate analogue inhibitor of dihydrofolate reductase (DHFR), and CHOP did not show a maximum tolerated dose (MTD) and the expansion phase used a dose of 30 mg/m<sup>2</sup> on D1 & D8 (17). The authors describe the regimen as well tolerated and suggest that the response rates are good enough to warrant further evaluation in a randomised trial. Phase I/II trials with the addition of lenalidomide, an immunomodulatory drug (IMiD), to CHOP (NCT02561273) or CHOP (NCT01553786) are also underway.

Autologous stem cell transplant (ASCT) in first remission is recommended by the American Society for Blood and Marrow Transplantation (18) but this remains controversial. There has not been a randomised trial and retrospective reviews and phase 2 studies show conflicting results (19). In reality, the median age of AITL diagnosis is 70 years and due to the toxicity associated with ASCT this approach is not suitable for a high proportion of patients.

A number of patients are managed with supportive care at the time of diagnosis due to poor performance score secondary to age, co-morbidities and advanced disease. In the International T cell Project review of AITL 6% of patients were managed with supportive care. Although 82% received combination chemotherapy the 5-year progression free survival was only 18% with an overall survival of 32% at 5 years. The majority of deaths occurred due to progressive lymphoma (3).

Treatment of relapsed or refractory T cell lymphoma has dismal outcomes and few long-term responses are achieved (9,20). In suitable patients where remission can be achieved, and an appropriate donor is found, an allogeneic stem cell transplant will be considered and is associated with better outcomes. A recent review of outcomes for patients with relapsed/refractory AITL or PTCL-NOS at the MD Anderson Cancer Center (MDACC) showed a 5-year overall survival rate of 52% for patients receiving an allograft compared to 10% for those receiving no transplant therapy (20). However only 31 of 240 patients received an allograft as patients may be ineligible due to co-morbidities and poor performance scores or the failure to achieve response to therapy (13%).

Novel agents have been used in several early phase trials in the relapsed/refractory setting and key completed trials are summarised in Table 1-1 and show both low response rates and poor median progression free survival (PFS). Lenalidomide, romidepsin and belinostat have shown very durable responses in a small number of cases. However, at present there is no clear mechanism for determining which is the most suitable agent for an individual patient. Outcomes with lenalidomide, romidepsin and belinostat appear to be better in patients with AITL compared to other T cell lymphoma subtypes however numbers are too small to be statistically significant. In general, these novel agents are better tolerated than chemotherapeutic agents, but they are not without toxicity. Trials of combinations of novel agents are currently underway in patients with relapsed/refractory disease, in the UK the combination of a HDACi (romidepsin) and a proteasome inhibitor (carfilzomib) is recruiting after completion of a dose finding phase.

Preliminary results of a trial using oral 5-Azacitidine, a hypomethylating agent which is also directly cytotoxic through incorporation into DNA and RNA, and romidepsin in relapsed/refractory lymphoma have recently been reported and recruitment is ongoing (21). This follows a case report of successful treatment of AITL with 5-Azacitidine (22) and a subsequent case series (23). A study combining lenalidomide with vorinostat and dexamethasone recruited 8 patients and the combination was not further investigated due to high toxicity and poor responses (24).

Drug	Trial	Patient No	ORR	CR	DoR (median)	PFS (median)
Lenalidomide	(25)	54	22%	11%	3.6m	2.5m
	(26)	40	26%	8%	13 m	4 m
Romidepsin	(27)	130	25%	16%	28 m	4 m
Brentuximab	(28)	35	41%	24%	7.6 m	2.6 m
Bendamustine	(29)	60	50%	28%	3.5 m	3.6 m
Pralatrexate	(30)	111	29%	11%	10.1 m	3.5 m
Belinostat	(31)	129	26%	10%	13.6 m	1.6 m
	(32)	24	25%	8.3%	3.7 m	Not reported
Mogamulizumab	(33)	38	35%	14%	5.5 m	3.0 m
Alisertib	(34)	37	30%	7%	3 m	3.0 m
Everolimus	(35)	16	44%	6%	8.5 m	4.1 m

**Table 1-1: Summary of key phase 2 trials of single agents in relapsed/refractory T cell lymphoma**  
Overall response rate (ORR), Complete response (CR), Duration of response (DoR), Progression free survival (PFS)

Brentuximab vedotin (BV) is an antibody-drug conjugate which targets CD30 positive cells with monomethyl auristatin E which disrupts microtubules. A trial comparing CHOP to BV and CHP (cyclophosphamide, doxorubicin and prednisolone) for 6 – 8 cycles in patients with newly diagnosed systemic T cell lymphoma with CD30 expression has been recently published. Approximately half of AITL cases express CD30 and 12% of trial patients had AITL. Overall results showed an improvement in PFS with the use of BV + CHP although unpowered sub-group analysis suggests that the benefit is greatest in anaplastic large cell lymphoma (ALCL) and may not be present in AITL (36).

### 1.3 T CELL DEVELOPMENT AND DIFFERENTIATION

#### 1.3.1 Early T cell development

T cells develop in the thymus after migration of haemopoietic stem cell progenitors from the bone marrow. Approximately 95% of T cells carry the  $\alpha\beta$ -T cell receptor (TCR) with the remaining carrying the  $\gamma\delta$ -TCR. There are a series of maturation steps which are identified by the expression of surface markers and occur following interaction with the stromal cells of the thymus and initiation of intracellular signalling pathways. Double

negative (DN) cells undergo TCR- $\beta$  rearrangement followed by selection (Figure 1-2). Cells with successfully rearranged  $\beta$ -chains upregulate CD4 and CD8 becoming double positive (DP) cells which undergo TCR- $\alpha$  rearrangement to carry an  $\alpha\beta$ -TCR. The T cells then undergo positive selection in the cortex of the thymus followed by negative selection in the medulla to remove self-reactive T cells. Subsequently CD4 or CD8 is downregulated to produce a naïve single positive T cell which leaves the thymus and enters the peripheral circulation (37,38).

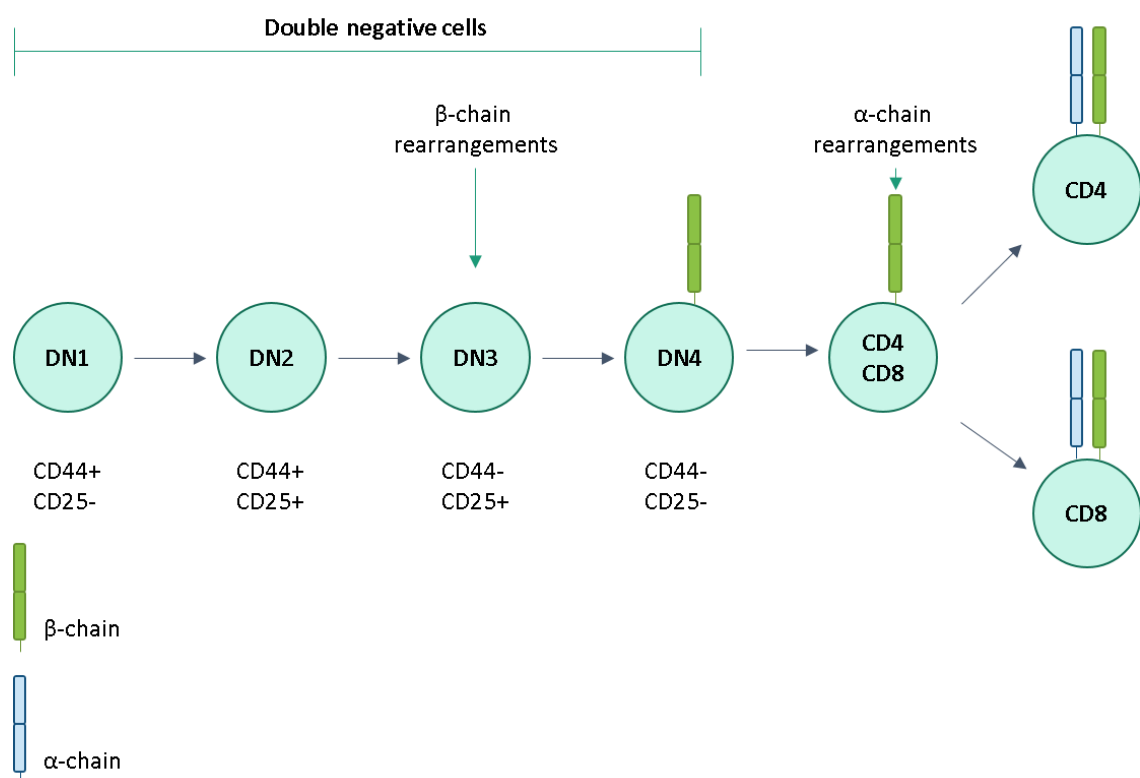


**Figure 1-2: Representation of T cell development in the thymus.**  
See text for description.

### 1.3.2 T cell maturation and differentiation

Naïve T cells undergo maturation and differentiation into mature effector T cells following interaction with antigen and exposure to specific cytokines. Naïve CD4<sup>+</sup> T cells have the potential to differentiate into several different types of effector CD4<sup>+</sup> T cells, originally described for T helper 1 (Th1) and T helper 2 (Th2) cells (39,40). Several other

types of CD4<sup>+</sup> T cell subsets, which support the immune response with different functions, have now been described; regulatory T cell (Treg), T helper 17 (Th17), follicular helper T cell (Tfh) T helper 9 (Th9) and T helper 22 (Th22) (41).

Various cytokines and transcription factors are involved in differentiation (Figure 1-3) with the aim of ensuring an appropriate immune response. Although differentiation was once thought to be an irreversible and permanent event, there is increasing evidence to support plasticity of differentiated CD4<sup>+</sup> T cells (42,43) enabling flexibility in the immune response. Correct function of the different subsets mounts an appropriate immune response whilst limiting self-recognition, autoimmune disease and allergy.

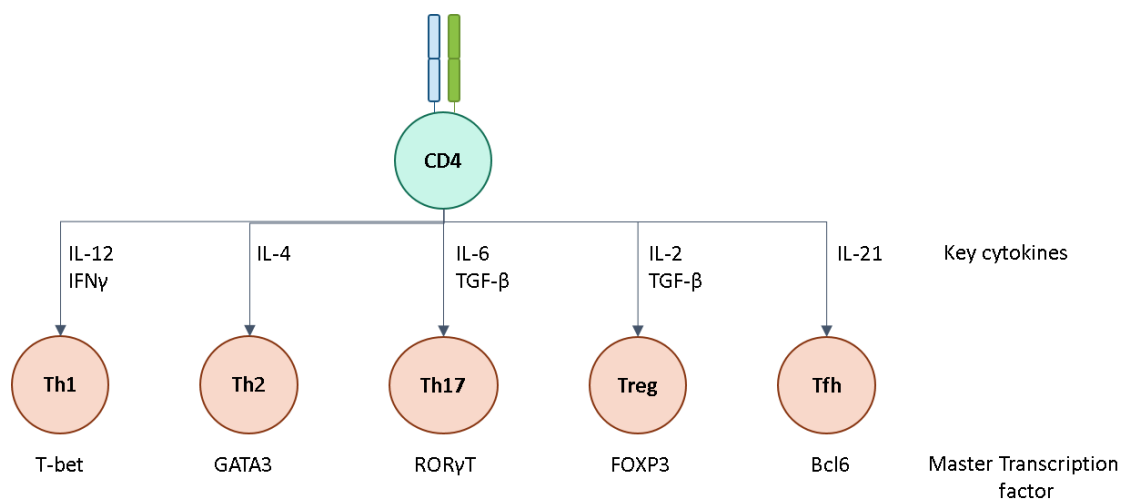


**Figure 1-3: Diagram showing the main CD4<sup>+</sup> T cell subsets with master transcription factors and key cytokines.**

*The naïve CD4<sup>+</sup> T cell is shown in green and mature CD4<sup>+</sup> T cell subsets in pink.*

The expression of transcription factors by CD4<sup>+</sup> T cells can be altered after initial maturation by cytokine and chemokine receptor signalling, leading to a change in subset specification. This occurs as a result of chromatin modifications which can be reversed by the binding of cytokines leading to changes in the expression of the master transcription factors. The plasticity of CD4<sup>+</sup> T cells reduces with increasing divisions as the chromatin modifications become less reversible (44,45). Interleukin 12 (IL-12) has

been shown to have an important role in conversion from Th17 or Th2 to Th1 cells when the original cells continue to express the IL-12 receptor (46,47).

Recent discoveries suggest that microRNAs (miRNAs) have an important role to play in the differentiation and plasticity of CD4<sup>+</sup> T cells by altering cell phenotype at the level of protein expression (48,49). They appear to have a particularly important role in the development of Tfh cells and one group have identified miRNA cluster miR-17~92 as a regulator of Tfh differentiation and subsequent T cell dependent antibody responses (50).

#### 1.4 FOLLICULAR HELPER T CELLS

Tfh cells were first proposed in 2000-2001 but were not widely accepted as a distinct CD4<sup>+</sup> T cell subset until 2009 when B-cell lymphoma 6 (BCL6) was shown to be the lineage defining master transcription factor (51-53) and their role in providing help to B cells in the germinal centre was established. Their distinct gene expression profile had already been described with differences to the established Th1 and Th2 subtypes demonstrated (54,55). Tfh cells are essential to support the development of the germinal centre and the subsequent generation of high affinity B cells and memory cells (52,53,56). Initial Tfh differentiation occurs following interaction with antigen presenting cells in an inducible co-stimulator (ICOS) dependent process (57) (Figure 1-4). Signalling through ICOS occurs through the phosphoinositide 3-kinase (PI3K) pathway (58,59) and leads to expression of the transcription factor BCL6, and suppression of B-lymphocyte-induced maturation protein 1 (BLIMP1). An early feature of Tfh differentiation is the expression of C-X-C chemokine receptor type 5 (CXCR5) leading to migration of the T cell to the T-B border of the germinal centre (GC) in response to C-X-C chemokine ligand 13 (CXCL13). BCL6 also suppresses the expression of molecules which antagonise GC localisation and represses the expression of opposing T cell differentiation programmes both directly and through co-localisation with AP1 (60).

On-going Tfh proliferation and maturation depends upon interactions with B cells, initially at the T-B border (Figure 1-4). Further stimulation through ICOS along with

CD28, IL-21 receptor and IL-6 receptor contributes to commitment to the GC Tfh subtype. This further differentiation leads to higher expression of CXCR5, ICOS and PD-1 and migration into the GC (61). There is, therefore, co-dependency between the GC-Tfh cells and GC-B cells (62).

Signalling lymphocyte activation molecule-associated protein (SAP, encoded by SH2D1 $\alpha$ ) plays an important role in T-B cell interactions and deficiency leads to reduced B cell expansion due to reduced T cell help and failure of Tfh cells to be retained in the GC (63,64). SAP binds to signalling lymphocyte activation molecule (SLAM) family receptors of which there are several. There is redundancy in this family with normal GC responses seen in mice with 3 family members knocked out (65).

High expression of PD-1 is seen in GC Tfh cells and is thought to provide inhibitory signals to prevent excessive Tfh proliferation (66,67) but there is also data to support a role for PD-1 in regulating T-cell differentiation (68,69).

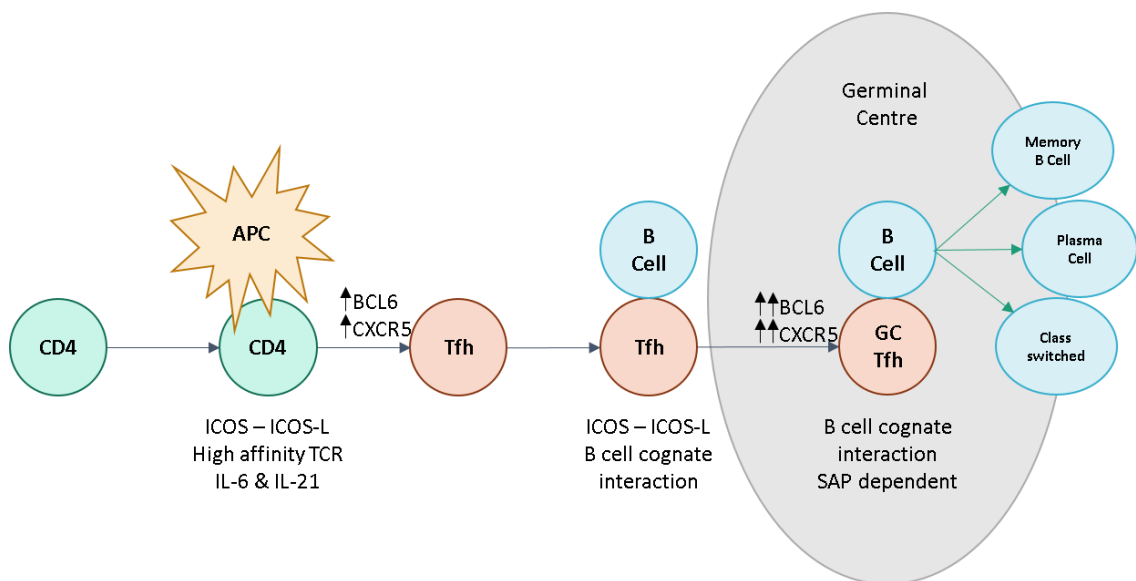


**Figure 1-4: Diagram representing the differentiation steps of Tfh cells.**

*Initiation is dependent upon interaction with an APC and the upregulation of BCL6 and CXCR5. Maintenance of the Tfh phenotype occurs following cognate interaction with B cells. Subsequent migration into the germinal centre leads to full Tfh polarisation and help for B cells. Adapted from Crotty (51).*

## 1.5 T CELL SIGNALLING

Signalling through the T cell receptor (TCR) and co-stimulatory molecules is important for T cell proliferation, differentiation and activation. Several pathways can be activated upon stimulation of the TCR. Key pathways are those leading to transcriptional changes. Firstly, activation of nuclear factor of activated T cells (NFAT), nuclear factor kappa B (NF- $\kappa$ B) and interferon regulatory factor 4 (IRF4). Secondly, activation of the activator protein 1 (AP-1) and mitogen-activated protein kinase (MAPK) pathways via c-Jun, signal transducer and activator of transcription 3 (STAT3) and general transcription factor II-I (GTF2I). Finally, activation of the phosphoinositide 3-kinase (PI3K) pathway. Another pathway of interest when thinking about Tfh lymphoma is that leading to cytoskeletal changes and effects upon adhesion and migration due to the prevalence of mutations seen in genes of this pathway as discussed further in Section 1.7.

Upon TCR activation with co-stimulation through CD28 +/- ICOS there is subsequent activation of PI3K leading to the accumulation of phosphatidylinositol (3,4,5)-triphosphate (PIP<sub>3</sub>) which recruits Interleukin-2-inducible T-cell kinase (ITK) to the membrane complex where it is phosphorylated by Lck (70). One target of ITK is PLC $\gamma$ 1 which hydrolyses phosphatidylinositol 4,5-bisphosphate (PI<sub>(4,5)</sub>P<sub>2</sub>) to produce inositol trisphosphate (IP<sub>3</sub>) and diacylglycerol (DAG) (71). IP<sub>3</sub> leads to the influx of calcium and subsequent activation of calcineurin and NFAT. DAG activates members of the protein kinase C (PKC) family and Ras guanyl-releasing protein (Ras-GRP) which is an activator of the Ras-Raf-ERK pathway leading to STAT3 activation (72). ITK can also activate the Ras-Raf-ERK pathway and GTF21 leading to activation of the AP-1/MAPK pathways.

The NF- $\kappa$ B/NFAT pathway can also be activated via PKC and subsequently Caspase recruitment domain family, member 11 (CARD11), Mucosa Associated Lymphoid Tissue Lymphoma Translocation Gene-1 (MALT1) and I $\kappa$ B kinase (IKK). This pathway can also be activated via the PI3K pathway through the interaction of RAC-alpha serine/threonine-protein kinase (AKT1) with CARD11 or IKK.

PKC is also activated by a VAV1 and RAC1 mediated pathway, both VAV1 and RAC1 are also found as part of the TCR signalling complex (72). VAV1 is a guanine exchange factor

which interacts with RhoA, Rac1 and Cdc42 which play important roles in the actin cytoskeleton and subsequent adhesion and migration.

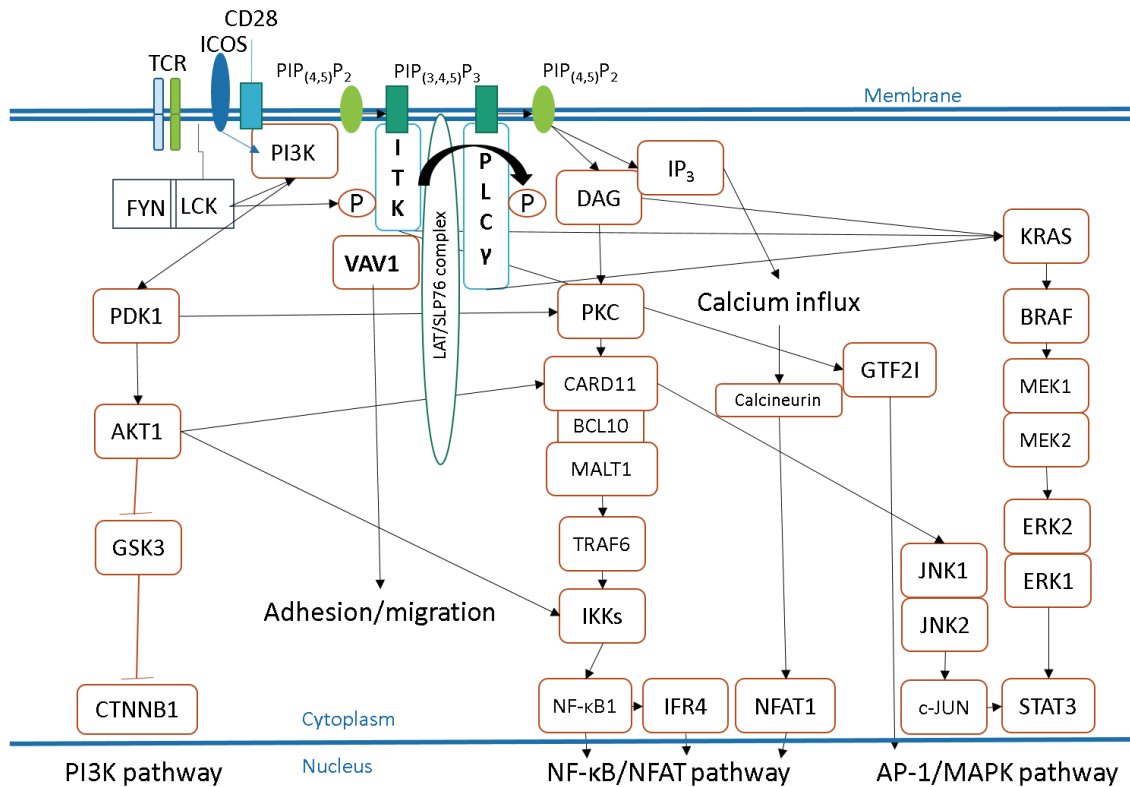


**Figure 1-5: T cell signalling pathway adapted from Schwartzberg et al (72) Vallois et al (73).**  
See section 1.5 for further description of pathway.

## 1.6 TFH LYMPHOMA

AITL is now recognised as a malignant population of Tfh cells and this helps us to understand some of its clinical features (74). AITL is associated with autoimmune phenomena and hypergammaglobulinaemia in approximately 30% of patients at presentation (3). Immunohistochemistry has shown that AITL is associated with the expression of markers found on Tfh cells including PD-1 (75,76), CXCL13 (77), ICOS (78) and SAP (79). This is confirmed by gene expression studies which show similarities between the gene expression profiles of AITL tumour cells and Tfh cells (6-8,80).

The malignant Tfh cells are rarely the prominent cell seen in the malignant lymph node as they are surrounded by numerous B cells (immunoblasts, plasma cells and centrocytes), a proliferation of follicular dendritic cells (FDCs) and high endothelial venules (81). Commonly the large B cells have active Epstein Barr Virus (EBV) infection (82) and EBV-driven B cell lymphomas develop more frequently than in association with other PTCL subtypes (83,84).

Due to the high proportion of stromal cells in AITL tumours their gene expression profile includes a significant contribution from B cells and FDCs (85), pathological review of cases in this series showed malignant T cells making up on average 28.5% of the cells. This work generated classifiers for T cell lymphoma subtypes based upon gene expression profiles. The upregulated genes in the AITL classifier include T cell specific genes and a cytokine/chemokine signature demonstrating the importance of the microenvironment (Table 1-2).

An extension of this study confirmed these findings and generated a prognostic model reflecting the importance of the microenvironment in outcomes (8). This paper lists genes unique to the AITL gene signature including genes involved in cell morphology, cell migration and the cell cycle (EFNB2, ROBO1, S1PR3, ANK2, LPAR1, SNAP91, SOX8, RAMP3, TUBB2B, ARHGEF10). Both the studies also showed that a proportion of cases diagnosed as PTCL-NOS had gene expression profiles consistent with AITL and on pathological review the cases showed some features consistent with AITL but were not sufficient to be diagnostic with histopathological criteria (85).

The data from Iqbal et al (8) demonstrates the unique gene expression signatures for the different subgroups of T cell lymphoma (Figure 1-6Figure 1-6A) with each column representing a unique patient and each row a unique gene from the classifier. There is some correlation between pathological diagnosis and molecular classification (Figure 1-6Figure 1-6B) but molecular investigation allows a proportion of cases to be reclassified including 21 cases (14%) of PTCL-NOS as AITL in this series. There were also 26 AITL cases (22%), which were not molecularly classifiable as AITL and changed to PTCL-NOS.

Genes in classifier	
<b>Cytokine/chemokine signature</b>	
Proinflammatory response	<i>LTA (TNFSF1), LTB (TNFSF3)</i>
T- and B-cell activation	<i>TNFRSF4 (OX40/CD134), TNFRSF17(BCM/CD269) TNFSF8 (CD30L/CD153), CSF2RB (CD131)</i>
Chemotactic activity for activated T cells	<i>CCL17, CCL19, CCL20, CCL21, CCL22</i>
Angiogenesis	<i>CXCL8 (IL8), CXCL5</i>
Homing of B cells and TFH cells to follicles	<i>CXCL13, its receptor (CXCR5)</i>
B-cell receptor signalling	<i>CD79a, CD19, FCRL5, CD22</i>
Immunoglobulin family	<i>IgH, IgK, IgL</i>
B-cell-associated/activation	<i>MS4A1 (CD20), CR1 (CD21), CD23, CD24, CD37, FCRLA, AICD, ID3, SpiB</i>
FDC markers	<i>CR1, CR2 (CD21), CD23, CLU, CD200, C4orf7</i>
Complement system	<i>C1S, C3, C4A, C7</i>
<b>T cell-specific genes</b>	
Costimulatory	<i>ICOS</i>
Coinhibitory	<i>CTLA4</i>
Miscellaneous genes	<i>SOX8, XKR4, GPR64, PTGDS, NTN2L, PLA2G2D, ALPK2, NT5DC4</i>

**Table 1-2: Differentially expressed genes in the molecularly defined AITL classifier**

*Adapted from Iqbal et al (85)*

The paper describes the development of a prognostic model using gene signatures from the lymphoid signature database (86) to produce 4 subgroups with a better prognosis seen in patients with a higher expression of B cell genes and a lower expression of genes associated with cytotoxic CD8<sup>+</sup> T cells, monocytes and TP53-induction. When this gene signature is applied to patients it is able to separate out prognostic groups (Figure 1-6Figure 1-6C).

The availability of gene expression profiling is generally restricted to clinical trials and is not currently routinely available. Although there is a suggestion that differences in the molecular signature within AITL are prognostic there is not yet any evidence to support different treatment strategies.

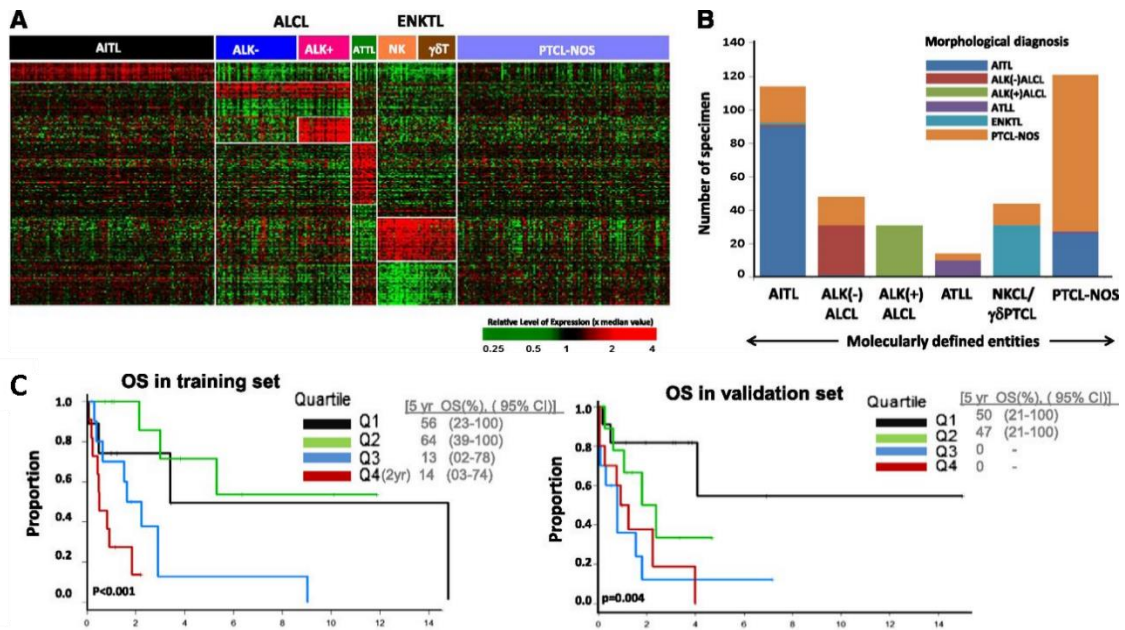


**Figure 1-6: Molecular diagnostic signatures of PTCL subgroups and survival prediction in AITL** adapted from Iqbal et al (2014) (8) A shows the gene expression signatures for cases of T cell lymphoma grouped by diagnosis based on GEP. B shows the differences in diagnosis based upon GEP and morphology. C shows the Kaplan-Meier curves generated from a prognostic gene signature in a training set (left) and a validation set (right).

## 1.7 TFH LYMPHOMA GENETICS

### 1.7.1 Epigenetic dysregulation

Advances in the availability of genome sequencing have led to discoveries of mutations associated with many cancers and AITL is no exception. There is a strong association between the AITL subtype and mutations in genes related to epigenetic changes, specifically Tet methylcytosine dioxygenase 2 (TET2) (87,88), DNA methyltransferase 3 alpha (DNMT3A) (88,89) and isocitrate dehydrogenase (NADP<sup>(+)</sup>) 2 (IDH2) with a hotspot at amino acid 172 (90,91) which are also associated with myeloid malignancies.

TET2 mutations are usually loss of function and in several cases multiple mutations are found, they have been detected in 50-85% of cases in published series (88). TET2 mutations have also been described in PTCL-NOS and Lemonnier et al found that TET2 mutations were more common in PTCL-NOS cases with Tfh-like features, suggesting an association with Tfh differentiation (87).

DNMT3A mutations are reported in 20-30% of cases (88).

IDH2 mutations are reported in 20-45% of cases and are exclusively found at an arginine residue at position 172 (IDH<sup>R172</sup>) (90). It is frequently found in individuals who also have one or more TET2 mutations, which contrasts with myeloid disease where TET2 and IDH2 mutations are predominantly exclusive (92,93). IDH2<sup>R172</sup> mutations lead to abnormal production of 2 hydroxyglutarate (2HG) which inhibits TET2 activity (94) along with other enzymes (95). 2HG was detected in the frozen extracted lymph nodes and serum of patients with IDH2 mutated AITL by Lemonnier et al (96) who showed that 2HG was restricted to ICOS<sup>+</sup> cells.

### 1.7.2 RHOA mutation

A point mutation of RHOA predicted to cause a substitution of valine for glycine at residue 17 (RHOA<sup>G17V</sup>) has been found in over 50% of AITL cases following the initial reports in 2014 (97-99), around 20% of PTCL-NOS cases also carry this mutation. Only occasional mutations at other RHOA loci have been reported in AITL, however a range of positions have been shown to be mutated in ATLL (100), Burkitt lymphoma (101,102), diffuse large B cell lymphoma (103), gastric cancer (104,105) and head and neck cancer (106) although at lower rates than seen in AITL. The recurrent mutations seen in haematological malignancies are shown in Figure 1-7A with all mutations listed in Table 1-3. The majority of the mutations seen in AITL and ATLL are found in GTP-binding regions, which consists of four parts of the RHOA sequence consisting of amino acids 12-19, 59-63, 117-120 and 157-164 (Figure 1-7)

Two groups have compared the pathological features of AITL between cases with and without RHOA<sup>G17V</sup> mutation. Both found that the RHOA mutated cases had a higher number of Tfh markers expressed on the malignant cells (107,108). One series showed an increase in vessel density correlated with RHOA mutation (108) suggesting higher vascular proliferation. This group also found that RHOA<sup>G17V</sup> mutated cases were more likely to have B symptoms and splenomegaly, the other group found a correlation with a higher performance score (PS) at diagnosis (107) but neither found an association with disease stage or survival. Both these series were small but add further to the evidence that RHOA<sup>G17V</sup> is important in the development of AITL.

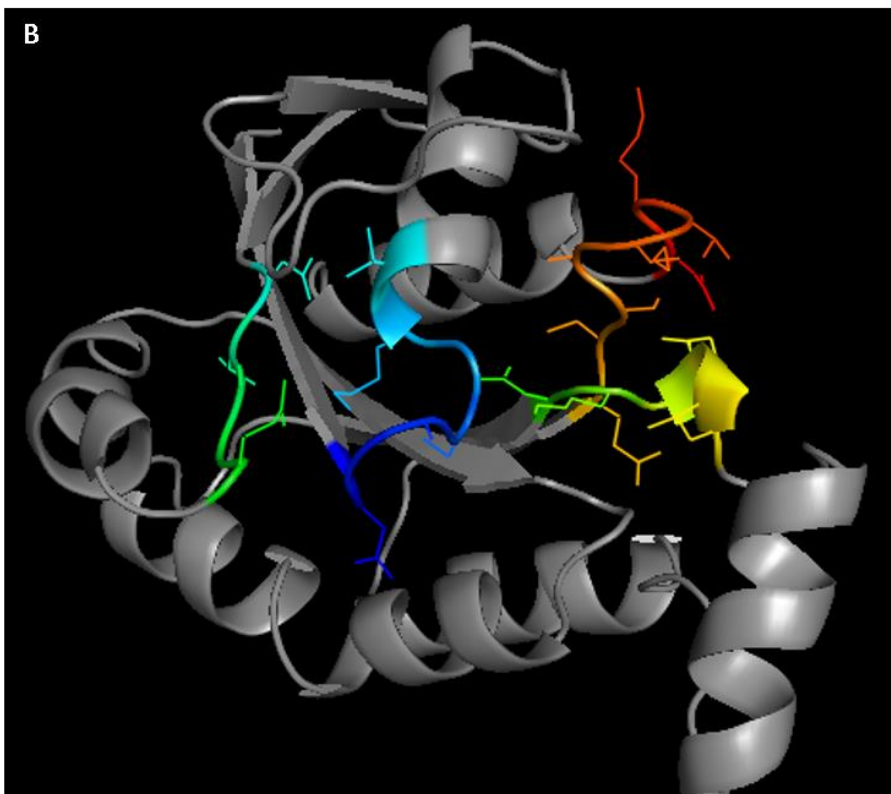
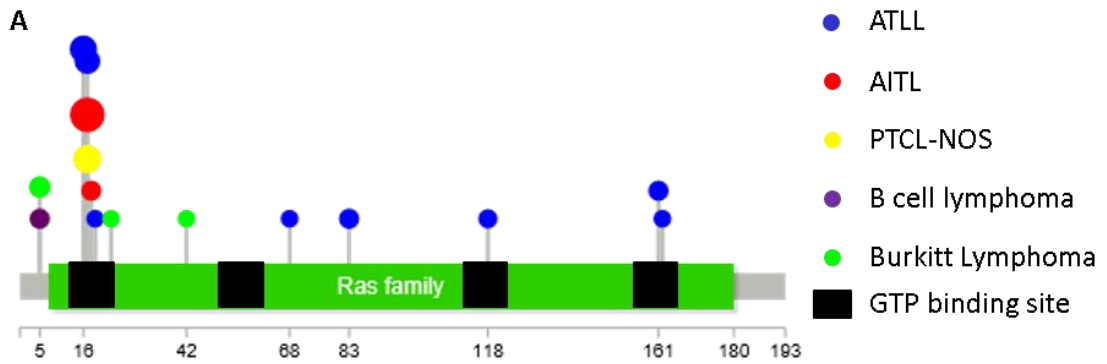


**Figure 1-7: RHOA mutations and structure**

*A: Mutations in RHOA described in haematological malignancies with regions making up the GTP binding site highlighted in black. Recurrent mutations as reported by COSMIC are shown on the diagram (109). B: representation of the wild type RHOA protein generated in PYMOL with the GTP binding site highlighted in colour.*

Site	Mutation	Diagnosis	Number of cases reported in COSMIC
5	R5Q	Burkitt lymphoma	6
	R5Q	DLBCL	3
	R5W	PTLD	1
15*	A15P	PTCL-NOS	1
16*	C16R / L / G / F	ATLL	18 / 2 / 2 / 2
	C16F	ALL	1
	C16Y	AML	1
17*	G17V / E / R	ATLL	11 / 3 / 2
	G17V / E / L	AITL	170 / 24 / 1
	G17V	PTCL-NOS	33
18*	K18N	AITL	4
19*	T19I	ATLL	2
	T19I	ALL	1
22	L22H	Burkitt lymphoma	1
23	I23R	Burkitt lymphoma	2
34	Y34N	DLBCL	1
37	T37A	Follicular lymphoma	1
39	F39L	DLBCL	1
42	Y42F / S	Burkitt lymphoma	1 / 1
56	A56V	ATLL	1
57	L57V	Marginal zone lymphoma	1
58	W58R	Follicular lymphoma	1
64	E64K	Follicular lymphoma	1
68	R68L	ATLL	2
69	L69P	B cell lymphoma	1
	L69R	Burkitt lymphoma	1
72	L72P	DLBCL	1
73	S73F	ATLL	1
76	D76V	Burkitt lymphoma	1
83	C83Y	ATLL	4
117*	N117I	ATLL	1
118*	K118E / Q	ATLL	2 / 1
120*	D120N	ATLL	1
	D120N	ALL	1
138	P138L	DLBCL	1
161*	A161E	AITL	1
	A161V / P	ATLL	3 / 1
	A161V	PTCL-NOS	1
162*	K162E	ATLL	2

**Table 1-3: RHOA mutations found in haematological malignancies as listed by COSMIC (109) in December 2018.**

*The starred sites are those located within the GTP binding site.*

### 1.7.3 Other mutations

Mutations in CD28 have been demonstrated in around 10% of AITL cases (73,110,111), 3 recurrent mutations have been reported and two of these have been shown to enhance NF- $\kappa$ B activity in vitro (111,112). Recurrent mutations in genes of the TCR signalling pathway (excluding RHOA) have been shown to present in 49% of AITL cases following targeted deep sequencing of a 69 gene panel by Vallois et al (73). They report TCR genes mutated in multiple cases: PLCG1, CTNNB1, GTF2I, PIK3R1, PDPK1, VAV1, FYN, CARD11, KRAS and STAT3 (see Section 1-5 and Figure 1-5 for the T cell signalling pathway). Further in vitro testing of the 10 missense mutations found in PLCG1 showed that most caused an increase in MALT1 protease activity and increased NFAT in a luciferase reporter assay compared to WT. Three CARD11 point mutations were found and all of these were shown to increase NF- $\kappa$ B reporter activity in response to stimulation compared to WT CARD11 and two increased MALT1 protease activity. The other mutations described (shown in Figure 1-8) have also been found in other tumour types and have either been shown to increase downstream signalling or are proposed to. The authors suggest that these findings support the role of activated TCR-signalling in AITL and Tfh-lymphoma development.

These findings suggested two major pathways to drive Tfh-lymphoma: mutated RHOA alone or mutated TCR signalling genes with or without mutated RHOA (Figure 1-8). They also showed mutations in TET2, DNMT3a and IDH2 in a high proportion of cases which had been analysed as part of previous work in which these genes were sequenced.

A fusion of Cytotoxic T-Lymphocyte Associated Protein 4 (CTLA4) and CD28 has been described and was found in 38% of T cell lymphoma in a case series, this included 26 of 45 (58%) of AITL patients (113). The fusion has been shown between exon 3 of the CTLA4 gene and exon 4 of the CD28 gene which is predicted to produce a protein with the extracellular and transmembrane portions of CTLA4 and the cytosolic signalling domain of CD28. In vitro work using the Jurkat cell line transfected with a construct expressing the fusion protein showed increased proliferation, IL-2 production and AKT and ERK phosphorylation in response to stimulation. This suggests that there would be

dysregulation of inhibitory signalling through CTLA4. In this case series there were 4 patients with a CD28 mutation and this was mutually exclusive to the CTLA4-CD28 fusion. This supports the hypothesis that dysregulation of the TCR signalling pathway plays a role in lymphomagenesis.

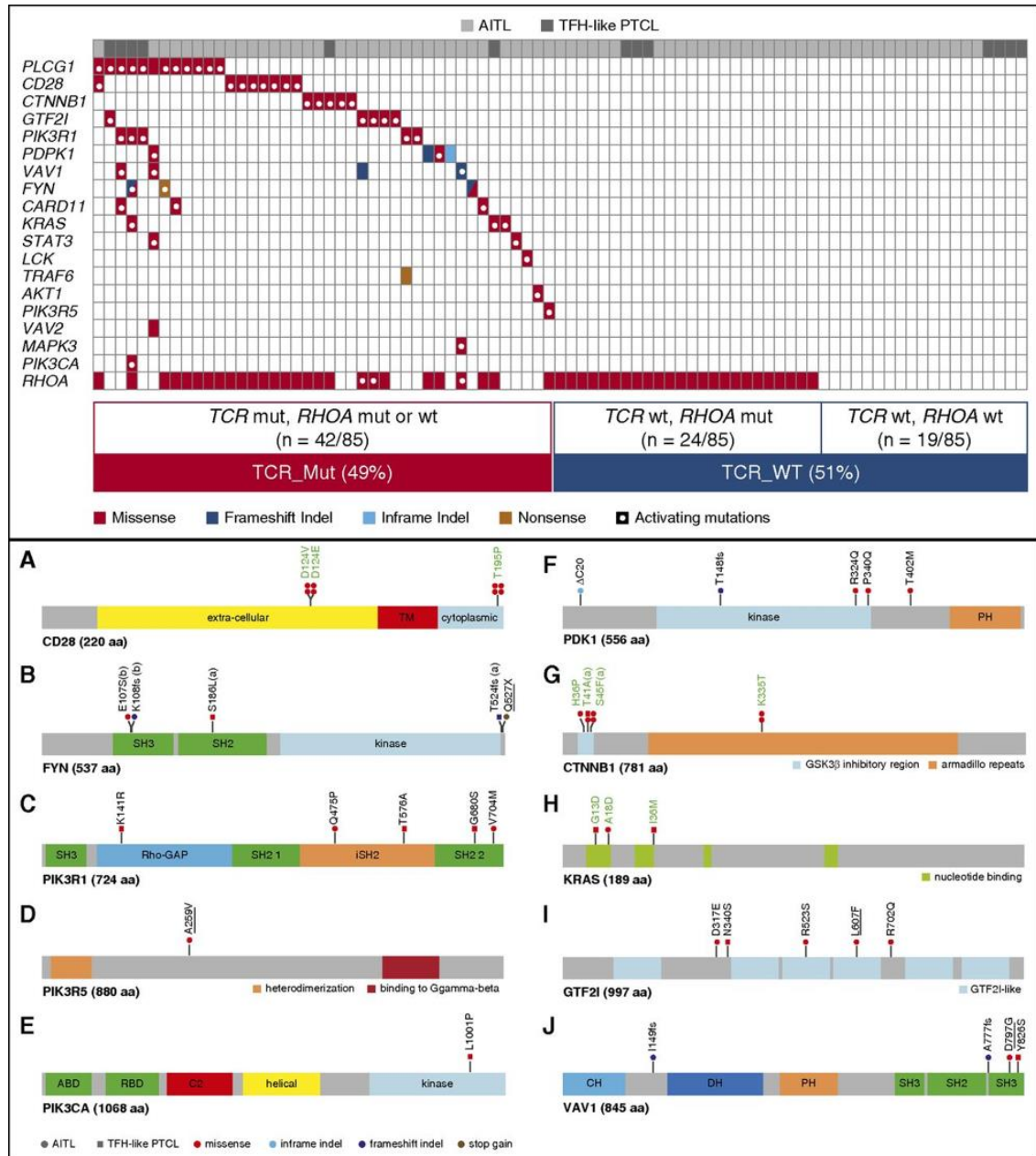


**Figure 1-8: Mutational status of TCR genes in an 85-patient cohort** (upper panel) and the mapping of variants in TCR signalling genes (lower panel A-J) which were mutated in at least 3 patients adapted from Vallois et al (73).

Analysis of 154 patients with T cell lymphoma using RNA sequencing revealed a number of VAV1 mutations as well as three VAV1 gene fusions and two cases with an inframe deletion causing the loss of 9 amino acids (114). Further DNA sequencing showed four further cases with mutations resulting in alterations in splicing leading to changes in the C-SH3 domain due to deletion of amino acids 778-786. In vitro analysis of the gene fusions and a VAV1 construct with deletion of amino acids 778-786 showed increased ERK1/2 phosphorylation in keeping with activation of this downstream pathway. Analysis of the JNK pathway using an AP1 reporter showed increased activity in the presence of the gene fusions, this activity was seen without CD3 stimulation suggesting constitutive activity. There was no increased activity seen in the VAV1 carrying the 778-786 deletion. Similar results were seen when an NFAT reporter assay was performed.

The chromosomal translocation t(5;9)(q33;q22) which fuses the IL-2-inducible T cell kinase (ITK) and the spleen tyrosine kinase (SYK) genes was initially described as a recurrent and specific genomic alteration in PTCL-NOS being found in five of 30 examined cases (115). Although initially described as being absent in AITL but found in the follicular variant of PTCL (PTCL-F) a case has subsequently been reported (116). Another group did not find the ITK:SYK translocation in AITL but did find gain of either ITK or SYK in 38% and 14% of cases respectively (117).

There appears to be co-operation between epigenetic dysregulation, RHOA mutation and activating mutations in the TCR signalling pathway which is discussed further in section 1.11.

## 1.8 RHOA GTPASE

Ras homolog family member A (RHOA) is a small GTPase which along with the other Rho GTPases have several roles within the cell. There are over 20 members of the Rho GTPase family and the best understood are RHOA, Rac1 and Cdc42. Each of these proteins cycle between an active GTP-bound state and an inactive GDP-bound state under the regulation of GTPase activating proteins (GAPs) and guanine nucleotide exchange factors (GEFs) (118). Guanine nucleotide dissociation inhibitors (GDIs) also

play a role in regulation by sequestering the GDP-bound Rho GTPases in the cytosol in their inactive form (119) (Figure 1-9Figure 1-9).

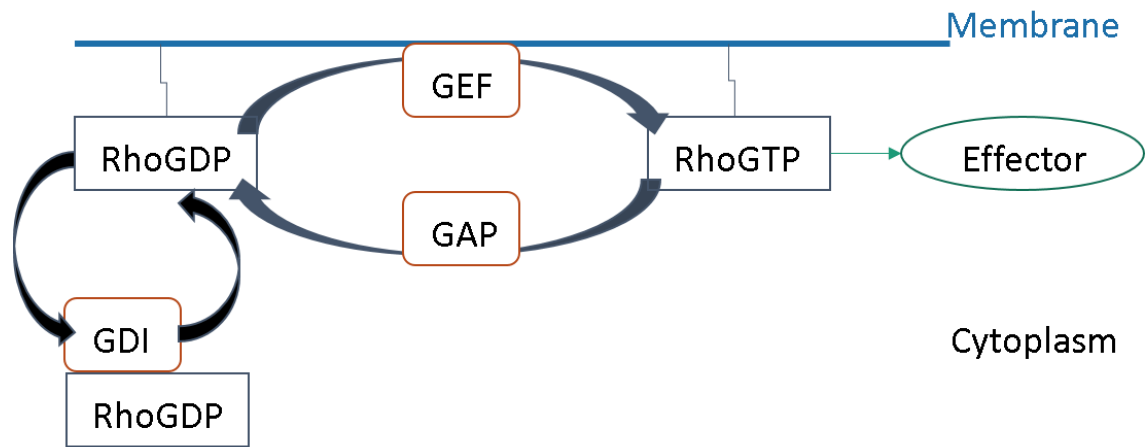


**Figure 1-9: The Rho GTPase cycle adapted from Etienne-Manville & Hall (118).**

The RhoGTPases were first identified in 1985 and in the 1990s were recognised to have an important role in cell motility and cell adhesion through the actin cytoskeleton (120). Their co-ordinated functions also play an important role in cell polarity, morphology and migration with the expression of different GEFs and GAPs in different cell types determining their precise role (118).

The RhoGTPases play a role in the cell cycle both through signal transduction and activation of transcription factors (121) and through a role in the development of the actin and myosin contractile ring which is essential for cytokinesis (122,123).

There are over 60 GAPs and over 70 GEFs which have variable specificity for RhoGTPases and approximately half are expressed in one or more lymphoid lineages (124).

### 1.8.1 RHOA in T cell development

A series of mouse experiments has examined the role of RHOA in T cell development by using the expression of bacterial enzyme C3-transferase from *Clostridium botulinum* at different stages of T cell development (37,125-127). *Clostridium botulinum* C3-transferase selectively ADP-ribosylates Rho within its effector-binding domain and thereby abolishes its biological function (128).

Firstly C3-transferase was expressed under the control of  $p56^{lck}$  which is expressed from the DN1 stage of T cell development (Figure 1-2 and section 1.3.1) until the cells exit the thymus. These mice had significantly smaller thymi with a marked reduction in cellularity (less than 20% of normal) compared to WT mice when examined at 5-6 weeks of age (125). Further analysis of the thymus showed a reduction in  $CD4^+CD8^+$  DP thymocytes which appeared to be due to a partial  $G_1$  block in the DN thymocytes. The level of  $\alpha\beta$ -TCR expression on each cell was normal suggesting that the level of proliferation is reduced but maturation does occur. Spleen cellularity was reduced by 50% with a marked reduction in  $\alpha\beta$ -TCR<sup>+</sup> T cells. Examination of the Rho<sup>-</sup> thymi during embryogenesis showed a block of  $\alpha\beta$ -TCR<sup>+</sup> T cells and impairment of  $\gamma\delta$ -TCR<sup>+</sup> T cell development (126).

Subsequently C3-transferase was expressed under the control of the human CD2 promoter leading to expression from the DN2 stage of T cell development (Figure 1-2) and throughout T cell development and on leaving the thymus (37). The thymi in these mice were also smaller than WT littermates with a 50-100-fold reduction in thymocyte numbers. These thymi contained almost exclusively  $CD4^-CD8^-$  DN cells with further stages of development almost completely absent.

The authors compare the differences between these two models showing that when C3-transferase is expressed from the DN1 stage there is increased apoptosis of  $CD25^+$  cells but normal differentiation of remaining cells whereas when C3 is expressed from the DN2 stage  $CD25^+$  cells showed normal survival but no differentiation (37).

Gene expression analysis of the DN3 T cells from the mice expressing C3-transferase under the control of the CD2 promoter was then compared to WT mice and  $Rag2^{-/-}$  mice in which there is also a differentiation block at the pre-TCR stage (129). They show that loss of Rho function in pre-T cells leads to downregulation of members of the Fos/Jun and early growth response family of transcription factors.

It was then noted that the  $lck$ -C3 mice were dying prematurely when compared to WT littermates with none surviving over 12 months and most dying between 4 and 8 months of age (127). Post mortem examination of the mice now showed dramatically

enlarged thymi causing heart and lung compression. Spleen, lymph nodes and liver were enlarged, and all organs were infiltrated with monoclonal CD25<sup>+</sup> T cells with blastic appearances. They propose that those CD25<sup>+</sup> cells which survive may undergo compensatory changes to prevent apoptosis, which ultimately leads to a predisposition to malignant transformation.

This shows that RHOA has an important role in the development of T cells and absence of RHOA in immature T cells appears to lead to compensatory changes, which predispose to the development of T cell lymphoma.

### 1.8.2 RHOA in T cell signalling and behaviour

Assessment of RHOA deficiency on T cell activation was made using a model in which exon 3 of RHOA was removed by Cre-recombinase under the control of the CD2 promoter (130). They showed a similar reduction in T cell numbers to that seen in the model from the Cantrell laboratory (37), which used a different mechanism to knockdown RHOA function. T cell activation in response to stimulation with anti-CD3 and anti-CD28 in vitro was reduced without increased apoptosis in the RHOA deficient T cells compared to normal T cells with inhibition of CD69 and CD25 upregulation. Further in vitro work suggested that RHOA was essential for Th2 differentiation but not Th1 differentiation. They also assessed the effect of RHOA deficiency on oxygen consumption and extracellular acidification rate (ECAR), an indicator of aerobic glycolysis, in response to stimulation demonstrating reduced oxygen consumption and compromised ECAR with reduced ATP production.

Another group showed defective thymocyte development in the absence of RHOA in T cells expressing CD2 (131) with an apparent block at the transition from DN3 to DN4 and defective  $\beta$ -selection. The RHOA deficient cells showed defects in mitosis and subsequently reduced proliferation. They also demonstrated reduced phosphorylation of ZAP70, ERK and JNK in response to TCR stimulation in RHOA deficient DP cells. They went on to assess mitochondrial function in the RHOA deficient cells showing that despite an upregulation in mitochondrial genes involved in oxidative phosphorylation there was a reduction in ATP production. They demonstrated a role for reactive oxygen species (ROS) with increased levels seen in RHOA deficient cells and treatment of the

RHOA deficient mice with the ROS scavenger N-acetylcysteine partially reversed the abnormalities in T cell development.

Downstream effectors of RHOA include Rho-associated kinase (ROCK) 1 and ROCK2 (132). Increased ROCK kinase activity has been shown in the peripheral blood mononuclear cells (PMBCs) of patients with systemic lupus erythematosus (SLE) and rheumatoid arthritis compared to healthy controls suggesting a role in autoimmune disease (133-135). ROCK inhibitors were shown to reduce production of IL-17 and IL-21 (133), which are key cytokines in the inflammation seen in autoimmune disease.

Inhibition of ROCK2 in vitro leads to reduced differentiation of naïve CD4<sup>+</sup> T cells, cultured in the presence of stimulation and Th17 skewing pro-inflammatory cytokines, to Tfh cells (136). This occurred through regulation of STAT3 and STAT5 activities leading to reduced BCL6 expression and increased BLIMP1 expression with ROCK2 inhibition. The same group showed that ROCK2 inhibition did not affect the differentiation of naïve CD4<sup>+</sup> T cells cultured with Th1 skewing pro-inflammatory cytokines which occurs through STAT4 dependent mechanisms (136).

Thymocytes with constitutive activation of RHOA show better adhesion to  $\beta_1$  and  $\beta_2$  integrin ligands and cells with deficient RHOA show reduced migration towards chemokines (137). The ligation of RHOA to 2 integrins appears to be mediated by amino acids 23-40 when the adhesion to ICAM-1 was assessed (138,139).

Collectively it is clear that RHOA has essential functions in T cell development but also the differentiation and function of mature T cells.

### 1.8.3 Effect of mutations on RHOA function

A variety of experiments have been carried out in attempts to explain the frequency of RHOA<sup>G17V</sup> in AITL and determine its contribution to lymphomagenesis. There are also a number of mutations which cause constitutive activation of RHOA including glycine to valine at position 14 (RHOA<sup>G14V</sup>) and glutamine to leucine at position 63 (RHOA<sup>Q63L</sup>) which is a laboratory generated mutation and has not been described in human samples (140,141). A mutation leading to the substitution of threonine to asparagine at position 19 (RHOA<sup>T19N</sup>) has been described as a dominant negative mutation (142).

The groups who initially described the RHOA<sup>G17V</sup> mutation in AITL also carried out a series of functional experiments. Over-expression of GFP-fused RHOA in fibroblasts showed similar changes including elongated morphology and increased cellular protrusions when RHOA<sup>G17V</sup> and RHOA<sup>T19N</sup> were transfected into HEK293T cells and reduced numbers of F-actin stress fibres when transfected into HeLa cells (97) and NIH3T3 cells (99).

They showed reduced interaction with rhotekin by HA-tagged RHOA<sup>G17V</sup> and RHOA<sup>T19N</sup> compared to RHOA<sup>WT</sup> in keeping with reduced levels of GTP-bound RHOA in both the mutant forms (97-99). Increased affinity for Rho-GEFs by RHOA<sup>G17V</sup> was also shown (97,99).

Overexpression of the RHOA in human T cell lymphoblastic lymphoma and leukaemia cells lines showed increased proliferation and invasiveness in cells transfected with RHOA<sup>G17V</sup> and RHOA<sup>T19N</sup> compared to RHOA<sup>WT</sup> and RHOA<sup>G14V</sup> (98). The induced expression of RHOA<sup>WT</sup> led to reduced proliferation of Jurkat cells with G1 cell cycle arrest whereas the expression of RHOA<sup>G17V</sup> did not affect proliferation or cell cycle progression (99).

The similarities with changes induced by RHOA<sup>T19N</sup> expression and the increased affinity for Rho-GEFs led to the proposal that the RHOA<sup>G17V</sup> mutation was a dominant-negative mutation and produced its effects by sequestration of Rho-GEFs and reduced RHOA activity. However, none of these groups were able to assess the effect of RHOA<sup>G17V</sup> in a model of AITL as no cell line models exist (143,144). The expression of RHOA<sup>G17V</sup> protein was found to be consistently lower in several cell lines when exogenously expressed (143).

Many of the mutations seen in AITL and ATLL are found in the GTP binding site regions which suggests that they alter the activation of RHOA.

More recent work has assessed proteins which bind specifically to RHOA<sup>G17V</sup> in both unstimulated and stimulated Jurkat cells, which are over-expressing FLAG tagged RHOA (145). It was found that RHOA<sup>G17V</sup> bound to VAV1 in both unstimulated and stimulated cells with the binding efficiency augmented by stimulation whereas there was no

binding between RHOA<sup>WT</sup> and VAV1. This interaction led to increased activity downstream of VAV1 even in unstimulated cells demonstrated by subsequent PLC $\gamma$ 1 phosphorylation. Activating mutations or translocations in VAV1 have also been described (114,145). Increased NFAT activity was shown in stimulated Jurkat cells transfected with RHOA<sup>G17V</sup> or VAV1 mutants when compared to WT (145).

Further work has assessed the effect of expression of an active mutant of RHOA with a valine substitution at amino acid 14 (RHOA<sup>G14V</sup>) under the control of the CD2 promoter (146). They showed that thymi were normal sized with normal cellular composition and thymocyte maturation. The RHOA<sup>G14V</sup> expressing thymocytes had normal morphology but showed higher levels of adhesion to fibronectin than normal thymocytes. They demonstrated lower levels of expression of  $\alpha\beta$ -TCR complexes on both CD4<sup>+</sup> and CD8<sup>+</sup> T cells however there was increased proliferation in response to stimulation with CD3 antibodies than in WT T cells.

Mutations in RHOA alter its function and lead to subsequent changes in cell behaviour. The described work all involves the induced expression of RHOA rather than assessing endogenous RHOA levels.

## 1.9 ITK IN TFH CELLS AND T CELL LYMPHOMA

ITK is a member of the TEC family of kinases and is highly expressed by T cells and plays a major role in TCR signalling (147) as discussed in section 1.5. Knockdown of ITK leads to reduced responses to TCR stimulation rather than abolition (71,148).

Through its interaction with VAV1 it is involved in the organisation of the actin cytoskeleton (149) and activation of adhesion molecules (150). ITK also plays a role in T cell migration in response to chemokine stimulation (151,152).

### 1.9.1 Role of ITK in T cell differentiation

ITK plays an important role in the differentiation of naïve CD4<sup>+</sup> T cells into mature Th2 cells due to reduced nuclear localisation of NFAT and failure of IL-4 production (153). It also has an important role in Th17 cell differentiation with CD4<sup>+</sup> T cells lacking ITK showing reduced IL-17A expression despite normal ROR- $\gamma$ T expression (154). Differentiation to Th9 cells also requires ITK. ITK deficient mice show reduced IL-9

production by T cells, which has also been demonstrated by reduced IL-9 production by human T cells after ITK inhibition (155).

### 1.9.2 ITK inhibition

There is interest in the role of ITK inhibition in prevention and management of inflammatory conditions, particularly asthma, as ITK knockout mice are resistant to the development of asthma (156,157). Analysis of an ITK inhibitor showed reduced TCR-signalling in cultured Th2 cells with reduced cytokine secretion, however in a mouse model the ITK inhibition failed to reduce airway hyper-responsiveness or inflammation (158).

In a mouse model of inflammatory skin inflammation improvement was seen in ITK knockout and with the use of an ITK inhibitor (159). Use of an ITK inhibitor in a mouse model of colitis also showed reduction in disease progression with Th1 and Th17 cells showing reduced P-selectin binding and impaired migration (160).

Ibrutinib is a Bruton's tyrosine kinase (BTK) inhibitor established in the treatment of CLL and other B cell malignancies, which also inhibits ITK (161). Using four mouse models ibrutinib was shown to reduce chronic graft-versus-host disease (cGVHD) with a reduction in the proliferation of B cells and lower levels of auto-antibodies (162). In one model ibrutinib treatment improved B cell reconstitution and reduced the percentage of Tfh cells in the spleen. In a model of acute GVHD in which T cells are the main drivers of disease ibrutinib was also able to improve clinical scores and survival (162). Ibrutinib has been approved for the treatment of cGVHD in patients after the failure of at least one systemic therapy (163) after showing clinical benefit in a phase 1b/2 study. A reduction was also shown in pro-inflammatory cytokines and chemokines.

Ibrutinib has also been shown to inhibit B cell signalling and activation in the culture of human peripheral B cell lines (164). It has also shown efficacy in the treatment of mouse models of autoimmune disease (165). BTK has been shown to alter B cell migration in response to chemokines (166) and integrin-mediated adhesion (167). There is interest in the use of ibrutinib in a number of conditions outside of B cell malignancies due to

the potential for manipulation of the tumour microenvironment in solid tumours (168-170) but it has not previously been tested in models of T cell lymphoma.

### 1.9.3 Role of ITK in T cell lymphoma

The discovery of a recurrent ITK:SYK translocation in PTCL-NOS with an association with a follicular phenotype (115) suggests that increased ITK activity may contribute to the development of T cell lymphoma. Examination of a series of 30 follicular T cell lymphoma (PTCL-F) cases showed 18% carried the ITK:SYK translocation (171). ITK has been shown to be expressed in 87% of AITL cases (172).

## 1.10 MOUSE MODELS OF T CELL LYMPHOMA

Mouse models can be a useful method for understanding the pathogenesis of human disease and potentially be used for pre-clinical testing of novel therapies to allow the most appropriate compounds being taken forward into human trials. There are also important differences between the immune systems of mice and human, which mean findings must be interpreted with caution. The spontaneous development of T cell lymphoma in mice is common due to the persistence of the thymus into adulthood, although this often resembles a lymphoblastic picture (173). Models of T cell lymphoma are discussed here and summarised in Table 1-4.

### 1.10.1 ITK:SYK translocation models

Following the demonstration of the ITK:SYK translocation in PTCL-NOS Pechloff et al (174) developed a mouse model with inducible CD4<sup>+</sup> T cell restricted expression of a patient derived ITK-SYK kinase. The mice with CD4<sup>+</sup> T cell expression of ITK-SYK developed a PTCL-like illness with clonal T cell infiltration of the bone marrow and solid organs. They propose that although the ITK:SYK translocation is relatively rare in PTCL this model is more broadly applicable as it shows the effect of aberrant activation of TCR signalling pathways which are commonly found in PTCL (7).

They refined this model by inducing ITK-SYK in CD4<sup>+</sup> T cells using tamoxifen-inducible Cre activation in CD4<sup>+</sup> T cells (175). A single dose of tamoxifen was given leading to expansion of the ITK-SYK CD4<sup>+</sup> T cells which was dose-dependent but subsequently contracted. With ongoing observation 2 of 3 mice receiving the highest tamoxifen dose

developed expansion of the ITK-SYK CD4<sup>+</sup> T cells with organ infiltration by lymphoblasts at around 200 days. In further work they developed a quadruple transgenic progeny with mutagenic ATP transposon cassettes expressed alongside ITK-SYK in CD4<sup>+</sup> T cells. Analysis of the tumours in these mice showed the site of highest transposon insertion density was located at the *Pdcd1* locus which encodes PD1, indicating that PD1 may have a tumour suppressor function in T cell lymphoma (175). This was supported by further mouse models with PD1 deficiency (*PD1<sup>-/-</sup>* & *PD1<sup>+/-</sup>*) and the treatment of mice with anti-PD1 and anti-PD-L1 where the suppression of PD1 led to increased lymphoproliferation.

#### 1.10.2 Models with features of Tfh lymphoma or PTCL

Ellyard et al (176) demonstrated tumour development in mice with a heterozygous *Roquin/Rc3h1* mutation. ROQUIN regulates ICOS mRNA stability and the mutant form has a higher affinity leading to slower mRNA decay and subsequent increased expression of ICOS (177,178). The increased ICOS expression leads to accumulation of Tfh cells and mice with a homozygous mutation develop a severe lupus-like disease (179). In their study 53% of the mice with a heterozygous mutation (*Roquin<sup>san/+</sup>*) developed one or more enlarged lymph nodes which had histopathological changes with similarities to AITL (176). They demonstrated the presence of a clonal T cell population in amongst large numbers of reactive cells.

Muto et al (180) described the development of a lymphoma-like illness in 71% of mice over 60 weeks of age with knocked down Tet2. Histology and T cell clonality showed that this was consistent with a T cell lymphoma and the gene expression profile was similar to that of Tfh cells. However, unlike the *Roquin* mutated mice there was no hypergammaglobulinaemia or B cell infiltration as seen in human AITL. They describe their model as a mimic of PTCL-NOS with Tfh-like features. Others have shown both lymphomagenesis and myeloid malignancies in mice with dysregulated TET2 (181,182).

<b>Model</b>	<b>Phenotype / Key findings</b>
<b>ITK-SYK in CD4<sup>+</sup> T cells (174)</b>	Development of increased proportions of circulating T cells and symptoms leading to sacrifice between 12 & 25 weeks in all mice. Infiltration of T cells into spleen, bone marrow and solid organs.
<b>ITK-SYK in CD4<sup>+</sup> T cells with PD1<sup>+/-</sup> (175)</b>	Development of organ infiltration with CD4 <sup>+</sup> T cells which could be transplanted.
<b>Roquin<sup>san/+</sup> (176)</b>	Development of asymmetrical lymphadenopathy in approximately 50% of mice at 4-6 months of age. Similarities to AITL and clonal T cell populations shown.
<b>Tet2 knockdown (180)</b>	Enlarged spleens with increased Tfh cells at 40-60 weeks old. Development of lymphadenopathy and organ infiltration over 60 weeks in 5 of 7 mice.
<b>Lin28b overexpression (183)</b>	Reduction in thymus size with reduced DP cells and increased CD8 <sup>+</sup> T cells. Subsequent development of lymphadenopathy, splenomegaly and symptoms at 10+ months of age. Infiltration of organs with CD3 <sup>+</sup> T cells demonstrating T cell clonality.
<b>Transplantation of Tet2<sup>-/-</sup> haematopoietic cells expressing RHOA<sup>G17V</sup> (184)</b>	Splenomegaly and lymphadenopathy developed at 200-350 days. Tumour cells showed high expression of Tfh markers and gene expression consistent with Tfh cells and AITL.
<b>Expression of RHOA<sup>G17V</sup> in Tet2<sup>-/-</sup> CD4 cells (185)</b>	Development of lymphoma in 4 of 10 mice with splenomegaly and lymphadenopathy with tumour cells expressing CD4, PD1, CXCR5 and BCL6.
<b>Transplantation of Tet2<sup>-/-</sup> haematopoietic cells expressing RHOA<sup>G17V</sup> into TCR<math>\alpha</math> deficient mice (186)</b>	Development of symptoms including weight loss, skin ulcers and lymphadenopathy in all mice. Organ infiltration with T & B cells including an increase in GC B cells.

**Table 1-4: Summary of mouse models of T cell lymphoma**

Another group developed transgenic mice overexpressing Lin28b in haematopoietic cells demonstrating aberrant T-cell development. Lin28b and Lin28a have been shown to reduce the let-7 family of miRs and subsequent alteration in expression of MYC, HMGA2 and KRAS (187). Due to these links with genes implicated with malignant transformation the group hypothesized that Lin28b may function as a proto-oncogene if over-expressed. These mice developed a peripheral T-cell lymphoma (PTCL) that occurred on the background of an inflammatory tumour microenvironment (183). They also showed the over-expression of Lin28b in PTCL samples when compared to activated CD4<sup>+</sup> T cells.

### 1.10.3 Models with expression of RHOA<sup>G17V</sup>

Three groups have recently developed mouse models with expression of RHOA<sup>G17V</sup> in CD4<sup>+</sup> T cells (184-186).

Cortes et al produced a mouse model with inducible expression of RHOA<sup>G17V</sup> in CD4<sup>+</sup> T cells and demonstrated increased Tfh differentiation both immunophenotypically and by gene expression analysis (184). They demonstrated a marked increase ICOS expression in naïve CD4<sup>+</sup> T cells with induction of RHOA<sup>G17V</sup> expression with low levels of TCR engagement. After normalising ICOS levels between RHOA<sup>G17V</sup> expressing and control cells stimulation via the TCR and ICOS led to increased PI3K-mTOR and mitogen-activated protein kinase (MAPK) signalling in the RHOA<sup>G17V</sup> expressing cells.

They went on to transplant haematopoietic cells from TET2<sup>-/-</sup> mice, which had been infected with retroviruses expressing RHOA<sup>WT</sup> or RHOA<sup>G17V</sup>. The mice receiving cells infected with RHOA<sup>G17V</sup> went onto develop lymphoid malignancies with histological appearances similar to AITL and gene expression profiles similar to AITL and Tfh cells. In this TET2<sup>-/-</sup> RHOA<sup>G17V</sup> tumour model they found high levels of expression of ICOS-ligand on CD21<sup>+</sup> follicular dendritic cells, CD11b<sup>+</sup> GR1<sup>+</sup> dendritic cells, and B220<sup>+</sup> B cells suggesting that the microenvironment has an important role to play in driving tumour development.

Ng et al developed a transgenic model in which RHOA<sup>G17V</sup> was expressed under the control of the CD4 regulatory elements, with RHOA mRNA expression at 60% of

endogenous levels (185). Expression of RHOA<sup>G17V</sup> began at the DP stage of T cell development and led to a reduction in peripheral T cell numbers. They demonstrated a lower TCR stimulation threshold in RHOA<sup>G17V</sup> CD4<sup>+</sup> T cells. Transcriptome analysis showed enrichment of the PI3K-AKT-mTOR signalling signature in naïve RHOA<sup>G17V</sup> CD4<sup>+</sup> T cells, this pathway is known to modulate T cell activation and differentiation (197,198). Enrichment of the mTORC1 signalling pathway was also seen in RHOA<sup>G17V</sup> Tfh cells from TET2<sup>-/-</sup> mice, but not in WT Tfh cells from TET2<sup>-/-</sup> mice.

These tgRHOA mice had reduced numbers of naïve T cells but a relative increase of Tfh cells and with aging developed autoimmune phenomena. They went onto cross the tgRHOA mice with mice with a TET2 deletion throughout the haematopoietic system and carried out monthly immunisations of these mice with intraperitoneal injections of 100µg NP40-Ovalbumin with 50% Alum in 100 mL total volume, up to a maximum of 7 injections. 40% of the mice went onto develop T cell lymphomas with characteristics of AITL, several others developed myeloid tumours. Transplantation of tumour cells from the mice developing lymphoma to immunosuppressed Nod.SCID.IL2rγ<sup>-/-</sup> (NSG) mice led to rapid lymphoma development and was used to test the activity of everolimus. The mice were treated with 10 mg/kg everolimus or 10% DMSO in PBS by oral gavage and those treated with everolimus showed reductions in spleen size and harvested cells showed reduced phosphorylation of Akt, S6 and 4EBP1 suggesting reduced mTORC1 activity and on-target drug activity.

Zang et al isolated T cells from WT and TET2<sup>-/-</sup> mice and transduced them with retroviruses encoding tagged RHOA<sup>G17V</sup> (186). Downregulation of Fas ligand and reduced apoptosis of CD4<sup>+</sup> T cells in the TET2<sup>-/-</sup> RHOA<sup>G17V</sup> group compared to the other groups (WT; TET2<sup>-/-</sup>; RHOA<sup>G17V</sup>) was shown. They demonstrated a reduction in Th17 and Treg cells in the TET2<sup>-/-</sup> group compared to the WT. The addition of the RHOA<sup>G17V</sup> to TET2<sup>-/-</sup> led to the return of Th17 cells to normal levels but a further decrease in Treg cells. The impact of RHOA<sup>G17V</sup> alone on CD4<sup>+</sup> T cell subtype was minimal suggesting it is the combination of mutations which drives the abnormalities. Transcriptome analysis suggested that FoxO1 was a key target of these mutations with TET2<sup>-/-</sup> leading to reduced expression and RHOA<sup>G17V</sup> producing increased phosphorylation which leads to

transport of FoxO1 to the cytoplasm from the nucleus with subsequent degradation (188). They suggest that the abnormalities seen in CD4<sup>+</sup> T cell proliferation, survival and differentiation are due to the reduction in FoxO1 activity (186).

The transduced cells were then injected into TCR $\alpha$  deficient mice who were studied (186). Those receiving TET2<sup>-/-</sup> cells transduced with RHOA<sup>G17V</sup> showed shorter survival due to the development of weight loss and skin lesions and were found to have B and T cell infiltration of several organs. In this study the combination of TET2 deletion and RHOA<sup>G17V</sup> expression led to increased proliferation of CD4<sup>+</sup> T cells over CD8<sup>+</sup> T cells and increased Tfh numbers with a reduction in Treg numbers. Their comparator mice received untransduced TET2<sup>-/-</sup> cells rather than cells transduced with RHOA<sup>WT</sup>.

#### 1.10.4 Patient derived xenografts

Another method of tumour modelling is patient derived xenografts (PDX). These were initially developed in solid tumours but more recently groups have developed PDX models of lymphoproliferative diseases (189-191). As part of a larger study Ng et al were able to develop four PDX models of AITL along with 13 other PDX models of T cell lymphoma, they also described analysis of various T cell lymphoma cell lines. The AITL PDX models showed some of the mutations expected in the patient population using DNA sequencing with one carrying a RHOA mutation, two carrying multiple TET2 mutations, one with a DNMT3a mutation and three with TCR signalling mutations (1 in CD28 and 2 in PLCG1). RNA sequencing showed a VAV1-SF1 gene fusion in one PDX and a FYN-BACH2 gene fusion in another (192).

Using cell lines of different T cell lymphoma subtypes, they show that E3 ubiquitin-protein ligase, MDM2, and MDMX are targetable in the cell lines with wild type p53 function. They went on to test ALRN-6924 an inhibitor of MDM2 and MDMX in cell lines and PDX models including 2 of the AITL models, comparing the effect of ALRN-6924 to romidepsin over an 8-day treatment period. Both the AITL models showed a reduction in spleen volume compared to vehicle treated mice (192).

PDX models are usually produced in immunosuppressed mice to reduce the risk of graft versus host disease or rejection of the tumour tissue (189).

#### 1.10.5 Summary of mouse models

There is no established model of T cell lymphoma that is widely used. Whilst the recently developed models based on RHOA mutants and other strains bearing TET2 mutation or disruption suggest these alterations are necessary and sufficient for the development of lymphoma they are not representative of the variety of mutation in human disease. The same criticism applies to models based on translocations that are found in only a small fraction of T cell lymphomas. The san roque mouse model is unique in being a source of genetically diverse T cell lymphomas derived from Tfh cells.

The PDX models are a potential method of recapitulating more accurately human disease, however engraftment of AITL is challenging and there are likely to be differences between those tumours which engraft and those which do not.

### 1.11 DEVELOPMENT OF AITL

#### 1.11.1 Speculation about clonal evolution

The prevalence of TET2 and DNMT3A mutations in the haemopoietic cells of elderly individuals with clonal haematopoiesis (193,194) has led to the suggestion that mutations in epigenetic modifiers occur in haemopoietic progenitor cells of AITL patients. This is then followed by RHOA or other mutations in T cells leading to the development of AITL (195). Supporting this are sequencing results demonstrating the same TET2 and/or DNMT3A mutation in AITL tumour and B cells or CD34+ progenitors from the same individual (88,182). The variant allele frequency of RHOA<sup>G17V</sup> mutation was lower than that of TET2 mutation in two cases described by Sakata-Yanagimoto et al, which would also support the presence of TET2 mutation in a higher proportion of cells (196).

More recently two groups have shown the presence of mutations of TET2 and DNMT3A in both PD-1<sup>+</sup> and CD20<sup>+</sup> cells micro-dissected from T cell lymphoma tumour samples (197,198). Nguyen et al (197) also showed that RHOA<sup>G17V</sup> and IDH2 mutations were found in the PD-1<sup>+</sup> cells but not the CD20<sup>+</sup> cells and in most cases the allele frequency was higher in the PD-1<sup>+</sup> population than the matched whole tumour sample. Although the IDH2 mutations co-existed with TET2 mutations in the PD1<sup>+</sup> cells they were not

found in the CD20<sup>+</sup> cells. Interestingly this group also describe the presence of likely activating NOTCH1 mutations in 3 of 87 cases, in each case this mutation was found restricted to the CD20<sup>+</sup> cells and was not present in the PD-1<sup>+</sup> cells. NOTCH1 was among 9 genes found to be hypomethylated and overexpressed in the *Tet2*<sup>-/-</sup> *DNMT3A*<sup>R882H</sup> murine model developed by Scourzic et al (181). These findings suggest that mutations in B cells in the microenvironment of AITL may play a significant role in the pathogenesis.

These findings support the theory that mutations in TET2 and/or DNMT3A occur in progenitor cells potentially making cells more prone to further mutations such as RHOA, TCR-signalling pathway genes or IDH2 which drive lymphomagenesis.

#### 1.11.2 Do mutations in epigenetic modifiers cause T cell lymphoma?

Despite these mutations being well described their functional contribution to the development of Tfh lymphoma remains incompletely understood.

Nishizawa et al (199) has shown methylation levels of BCL6 locus at the CpG islands 27 and 39 using bisulfite sequencing after deep sequencing of AITL and PTCL-NOS samples. They show that cases with TET2 mutation have higher rates of hypermethylation of the BCL6 locus than unmutated cases. In this small series the effect of IDH2 mutation had no additional effect on hypermethylation. They also assessed BCL6 expression by immunohistochemistry in some cases and showed high expression in 5 of 5 cases with hypermethylation samples and 6 of 16 cases without hypermethylation suggesting a correlation between hypermethylation of BCL6 and increased expression. This suggests that epigenetic alterations may cause changes in BCL6 expression, which is known to be vital in Tfh differentiation.

Scourzic et al report a murine bone marrow transplant model in which *Tet2*<sup>-/-</sup> *DNMT3A*<sup>R882H</sup> mice were produced (181). This DNMT3A mutation has dominant negative activity by preventing the active formation of the WT protein (200) and is a frequent site of mutation in AITL (90). Of the 18 primary transplants five developed haematological malignancies – one AITL-like, 2 AML-like and 2 T-ALL-like. Following serial transplantation of the *Tet2*<sup>-/-</sup> *DNMT3A*<sup>R882H</sup> progenitors there was a bias towards

the T cell compartment in peripheral blood and the development of an AITL-like disease in 75% of mice. They conclude that concomitant DNMT3A<sup>R882H</sup> expression and loss of Tet2 in mouse HSPC leads to both myeloid and lymphoid malignancies, suggesting that the low number of transformation in primary recipients is due to TET2 and DNMT3A mutations being insufficient to drive full transformation.

Lemonnier et al (96) developed mouse models to assess the functional impact of three common IDH2<sup>R172</sup> mutations (IDH1<sup>R132H</sup>, IDH2<sup>R140Q</sup>, and IDH2<sup>R172K</sup>) demonstrating a dramatic decrease in 5hmC in DNA of IDH2<sup>R172K</sup> knock in T cells and impaired lymphoid development which was not seen with the other mutations. The IDH2<sup>R172K</sup> mouse also had the highest levels of 2HG in serum, myeloid cells and lymphoid cells.

Wang et al (90) assessed the gene expression profiles of a cohort of AITL cases (n = 37) and found that those with IDH2 mutations formed a single cluster in unsupervised hierarchical clustering analysis suggesting a unique gene expression profile compared to IDH2<sup>WT</sup> cases. Following transduction of Jurkat cells and primary CD4+ cells with an IDH2<sup>R172K</sup> mutant, a global increase in 5-methylcytosine (5mC) and a global decrease in 5-hydroxymethyl cytosine (5hmC) was observed compared with cells expressing wild-type IDH2 or empty vector. However, analysis of AITL cases (n = 18) by reduced representation bisulfite sequencing showed only moderate differences in genome-wide methylation between IDH2/TET2 double-mutants and TET2 single-mutants suggesting that changes in DNA methylation alone cannot explain the differences in gene expression caused by IDH2<sup>R172K</sup> mutation. They went on to show that IDH2<sup>R172K</sup> mutations can dysregulate the post-translational modification of histones in T cells showing in vitro and in vivo increase in H3K27me3, suggesting that 2HG also interferes with the Jumonji family of histone demethylases.

### 1.11.3 What is the role of the RHOA pathway in lymphomagenesis?

The finding that RHOA<sup>G17V</sup> appears to augment VAV1 activation alongside the finding of VAV1 mutations leading to increased downstream signalling in AITL suggest that this pathway may be important in the pathogenesis of AITL (114,145). Secondly, the presence of activating mutations along the TCR pathway (73) suggest that over-activation of this has an important role to play in lymphomagenesis.

The mouse models described in section 1-9 propose different roles for RHOA<sup>G17V</sup> in the development of T cell lymphoma but show that co-operating epigenetic mutations are vital.

Although the initial descriptions of RHOA<sup>G17V</sup> suggested it acted in a dominant negative fashion by sequestration of GEFs more recent work suggests that the mutated RHOA leads to activation of the TCR-signalling pathway via the PI3K-mTOR pathway possibly by inducing ICOS expression (58,201). This may occur through the activation of VAV1. Mouse models suggest that both epigenetic dysregulation and alterations in the TCR signalling pathway are required for lymphomagenesis and that the microenvironment plays a role in stimulation of the T cells.

Gene expression profiling has demonstrated the importance of the microenvironment in AITL (8,85) which suggests that alterations in cell-cell interactions and cell motility due to dysregulation of RHOA may have an important role to play in lymphomagenesis.

## 1.12 AIMS

- 1) To understand the role of mutated RHOA in T cell lymphomagenesis by:
  - a. carrying out an assessment of RHOA stability and expression using bacterial expression of RHOA constructs;
  - b. assessing the expression of RHOA constructs by mammalian cells and investigating the activity of RHOA.
- 2) To further characterise the Roquin<sup>san/+</sup> mouse strain as a model system for investigating T cell lymphoma.
- 3) To develop a method of utilising the T cell lymphoma in the Roquin<sup>san/+</sup> mouse in pre-clinical study of the effect of ITK inhibition by ibrutinib on the T cell lymphomas.

## 2 METHODS

---

### 2.1 BUFFERS

Tissue lysis buffer	100mM Tris HCl (Fisher Scientific, Loughborough, UK) pH 8.5 200mM sodium chloride (NaCl; Fisher Scientific) 5mM Ethylenediaminetetraacetic acid (EDTA; Sigma, Gillingham, UK) 0.2% (w/v) Sodium dodecyl sulphate (SDS; Fisher Scientific)
Agarose gel electrophoresis running buffer (0.5x TBE)	50mM Tris (Fisher Scientific) 50mM Boric acid (Sigma) 1mM EDTA (Sigma)
Bacterial lysis buffer	B-PER Bacterial Protein Extraction Reagent (ThermoFisher, Waltham, Massachusetts, US) DNase (ThermoFisher) Lysozyme (ThermoFisher) cOmplete™, Mini, EDTA-free Protease Inhibitor Cocktail – 1 tablet per 50ml buffer (Roche applied science, Penzburg, Germany)
Protein wash buffer	50mM Tris Hcl pH 7.4 (Fisher Scientific) 150mM NaCl (Fisher Scientific) 5mM Dithiothreitol (DTT; Sigma)
SDS Loading buffer (1X)	50mM Tris-HCl pH 6.8 (Fisher Scientific) 2% SDS (Fisher Scientific) 10% glycerol (Sigma) 1% β-mercaptoethanol (Sigma) 12.5mM EDTA (Sigma) 0.02% bromophenol blue (Sigma)

Protein electrophoresis running buffer (1X)	25mM Tris (Fisher Scientific) 190mM Glycine (Sigma) 0.1% SDS (Fisher Scientific)
Tris-Buffered saline with Tween 20 (TBST)	20mM Tris (Fisher Scientific) 150mM NaCl (Fisher Scientific) 0.1% Tween 20 (Sigma)
Blocking Buffer	5% milk in TBST (New England Biolabs, Ipswich, Massachusetts, US)
Cell separation buffer (Miltenyi)	1 x Phosphate Buffered Saline (PBS; Oxoid, Basingstoke, UK) 0.5% bovine serum albumin (BSA; Sigma) 2mM EDTA (Sigma)
STE Buffer	10mM Tris pH 8.0 (Fisher Scientific) 150mM NaCl (Fisher Scientific) 1mM EDTA (Sigma)
5 X MG Buffer	125mM Hepes pH7.5 (Sigma) 750mM NaCl (Fisher Scientific) 5% NP-40 50mM MgCl <sub>2</sub> (Fisher Scientific) 5mM EDTA (Sigma)
1 X MG Buffer (prepared in this order)	5X MG buffer 25mM sodium fluoride (NaF; Sigma) 1mM Sodium Orthovanate (Na <sub>3</sub> VO <sub>4</sub> ; Santa Cruz Biotechnology, Dallas, Texas, US) 10% glycerol (Sigma) Ultra-pure water cOmplete™, Mini, EDTA-free Protease inhibitor Cocktail (Roche) 100ug Phenylmethylsulfonyl fluoride (PMSF; Sigma)

## 2.2 RHOA EXPRESSION CONSTRUCTS FOR BACTERIAL AND MAMMALIAN CELLS

### 2.2.1 Quantification of nucleic acids

DNA and RNA concentrations were determined spectrophotometrically using a Nanodrop 2000c (ThermoFisher) according to the manufacturer's instructions.

### 2.2.2 DNA sequencing

DNA Sanger sequencing was performed by the Protein and Nucleic Acid Chemistry Laboratory (PNACL) at the University of Leicester. Results were analysed using SequenceAnalyser (Applied Biosystems, Foster City, California, US).

### 2.2.3 Expression plasmids

An expression plasmid containing the open reading frame (ORF) of RHOA cDNA and a 6x histidine tag on a pDEST26 backbone was purchased from SourceBioscience (Nottingham, UK). The cDNA sequence was subsequently cloned into the pLEICS-12 and pLEICS-14 vectors by the PROTEX service at the University of Leicester (Figure 2-1) using the primers shown in Table 2-1 and the above expression plasmid as the template.

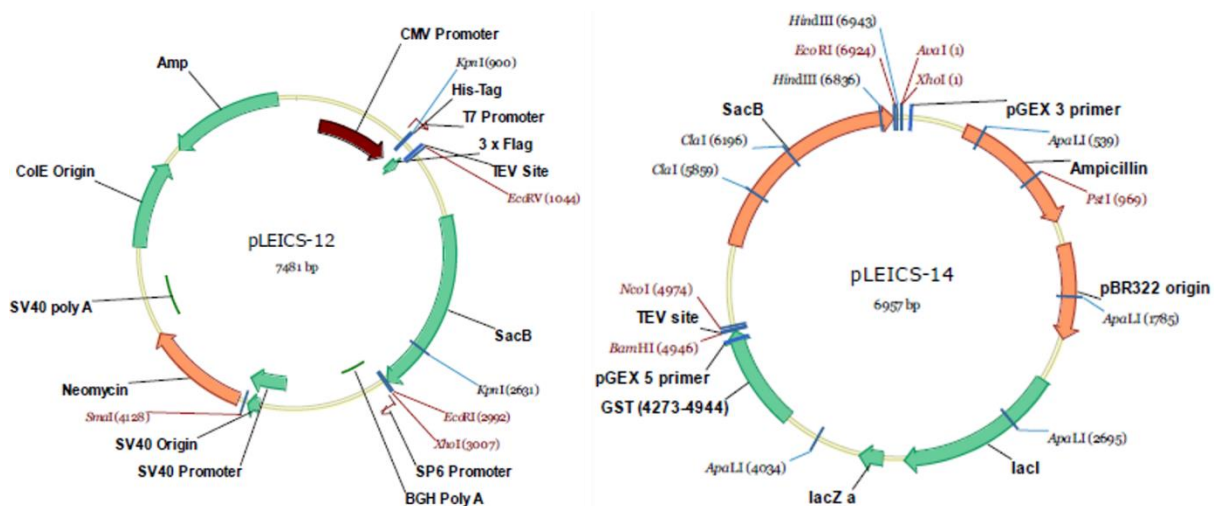


**Figure 2-1: PROTEX expression vectors.**

Diagrammatic representation of the expression vectors used for mammalian and bacterial protein expression. pLEICS-12 produced a His-FLAG tagged protein for mammalian expression. pLEICS-14 produced a GST-tagged protein for bacterial expression

Primer	Sequence
Fwd	GTATTTTCAGGGCGCCGCAGGCTCCATGGCTGCCAT
Rev	GACGGAGCTCGAATTTTCAGGTTCTACAAGACAAGGCA

**Table 2-1: Primers used to insert RHOA cDNA into pLEICS vectors**

#### 2.2.4 Bacterial transformation

Three ultra-competent *Escherichia coli* were used in this project. For plasmid propagation for DNA production DH5 $\alpha$  (Invitrogen, Carlsbad, California, US) or XL10-Gold Ultracompetent Cells (Agilent Technologies, Santa Clara, California, US) were used. For protein expression Rosetta BL21 (DE3) (Novagen<sup>®</sup>, Merck Millipore, Darmstadt, Germany) were used due to their optimisation for mammalian protein production.

Briefly, cells were defrosted on ice and aliquots made. Plasmid was added to the aliquot of cells and incubated on ice for 30 minutes before a 45 second heat shock at 42°C. Super Optimal Catabolite (SOC) media (Invitrogen) was added to the cells and they were incubated shaking at 37°C for 1 hour. Cells were then plated onto Luria broth (LB) agar (Medical Research Council Toxicology Unit, Leicester, UK) with appropriate antibiotics (Table 2-2Table 2-2).

Antibiotic	Concentration used
Chloramphenicol (Sigma)	34 $\mu$ g/ml
Ampicillin (Melford)	50-100 $\mu$ g/ml
Kanamycin (Sigma)	50 $\mu$ g/ml

**Table 2-2: Concentration of antibiotics used for bacterial selection**

#### 2.2.5 Small scale purification of plasmid DNA

5ml LB media (MRC Toxicology Unit) was supplemented with the appropriate antibiotic(s) and inoculated with a single colony from a transformation. Following overnight incubation shaking at 37°C the bacteria were centrifuged at 4440 x g at room temperature for 5 minutes and the supernatant discarded. Plasmid DNA was extracted and purified from the bacterial pellet using a QIAprep spin mini-prep kit (Qiagen, Hilden, Germany) according to the manufacturer's instructions and eluted in ultra-pure water. Following quantification, the purified plasmid was stored at -20°C

### 2.2.6 Large scale purification of plasmid DNA for mammalian cell transfection

5ml LB media was supplemented with the appropriate antibiotic(s) and inoculated with a single colony from a transformation. Following 8 hours of incubation shaking at 37°C 1ml of the culture was added to 200ml of LB media with appropriate antibiotic(s) and cultured overnight shaking at 37°C. The culture was centrifuged at 4440 x g at 4°C for 30 minutes and the supernatant discarded. Plasmid DNA was purified using Maxi Prep kit (Qiagen) according to the manufacturer's instructions. DNA was precipitated in isopropanol (Chemistry Department, University of Leicester) and washed with 70% ethanol (Chemistry Department, University of Leicester). The DNA pellet was dissolved in ultrapure water and quantified prior to storage at -20°C.

### 2.2.7 Site Directed Mutagenesis

Introduction of a point mutation was performed using QuikChange II XL Site-Directed Mutagenesis Kit (Agilent Technologies) which uses a high-fidelity DNA polymerase (*PfuUltra* High Fidelity DNA polymerase). Primers were designed using the web-based QuikChange Primer Design Program found at [www.agilent.com/genomics/qcpd](http://www.agilent.com/genomics/qcpd). The sequences are shown in Table 2-3; primers were used in 50µl reactions at 0.25µM.

Primer	Sequence
<b>Forward G17V</b>	GGTGATGGAGCCTGTGTAAAGACATGCTTGCTC
<b>Reverse G17V</b>	GAGCAAGCATGTCTTTACACAGGCTCCATCACC
<b>Forward G14V</b>	ATGTCTTTCCACAGGCTACATCACCAACAATCACC
<b>Reverse G14V</b>	GGTGATTGTTGGTGATGTAGCCTGTGGAAAGACAT
<b>Forward F25L</b>	GAAGTGGTCCTTGCTGAGGACTATGAGCAAGCATG
<b>Reverse F25L</b>	CATGCTTGCTCATAGTCCTCAGCAAGGACCAGTTC

**Table 2-3: Primers used for site directed mutagenesis**

Reactions were set up according to the manufacturer's instructions including 10-100ng of template DNA in a 50µl reaction. Thermocycling was carried out in a Veriti® Thermal Cycler (Applied Biosystems). Cycling parameters were used as per the manufacturer's protocol with an extension time (at 68°C) of 10 minutes. The parental DNA was digested by addition of *Dpn* and incubation at 37°C for 1 hour. Reactions were then frozen and stored at -20°C prior to bacterial transformation.

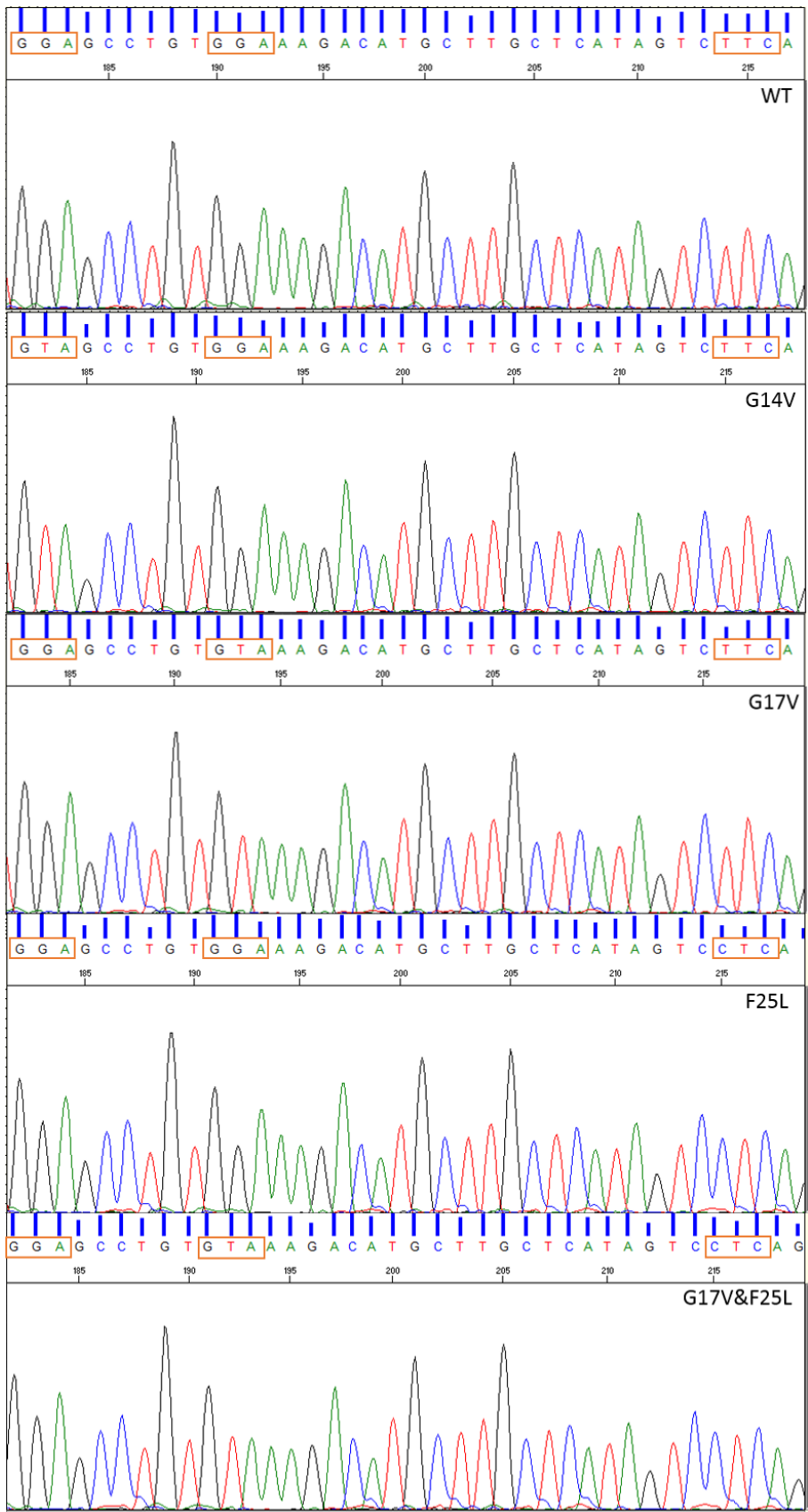


**Figure 2-2: Sanger Sequencing Chromatograms.**  
 These show the sequence from bases 40-76 demonstrating the 3 mutations of interest

## 2.3 PROTEIN EXPRESSION AND PURIFICATION OF BACTERIAL CULTURE

Following transformation of Rosetta BL21 (DE3) (Novagen) cells with pLEICS-14 vector containing the desired RHOA cDNA sequence cells were plated onto LB agar with ampicillin and chloramphenicol (Table 2-2Table 2-2). Subsequently colonies were picked and incubated in LB media with ampicillin and chloramphenicol. Initial incubation was carried out at 37°C in an orbital shaker. Following the initiation of bacterial growth 50µM Isopropylthio-β-galactoside (IPTG; ThermoFisher) was added and incubation was continued at 20°C in an orbital shaker. Following this incubation cells were pelleted at 16000 x g and if lysis was not carried out immediately the pellets were stored at -80°C.

### 2.3.1 Cell Lysis

Cells were resuspended in B-PER Bacterial Protein Extraction Reagent (ThermoFisher) with lysozyme and DNase I on ice and incubated for 15 minutes. Sonication was performed; cells were kept on ice and 5 cycles of sonication with 5 seconds on and 5 seconds off were carried out. Cells were centrifuged at 30000 x g at 4°C for 30 minutes to remove the cell debris.

### 2.3.2 Protein purification

Pierce Glutathione Agarose (ThermoFisher) was washed with protein wash buffer (Section 2.1) and the supernatant from cell lysis was added. This was incubated on a shaker at 4°C for 1-2 hours. Sample centrifuged at 700 x g for 2 minutes at 4°C and supernatant removed. The resin was washed with 1 x PBS & 1% Triton (Sigma) five times then with protein wash buffer three times. Following a final wash, the sample was resuspended in protein wash buffer with Tobacco Etch Virus (TEV) protease (PROTEX, University of Leicester). The sample was incubated overnight under rotation at 4°C then centrifuged at 700 x g for 2 minutes at 4°C and the supernatant containing protein was carefully removed.

### 2.3.3 Protein concentration

The supernatant from the purification steps was added to a washed Amicon® Ultra-Centrifugal Filter with Ultracel-10 membrane (Sigma) of an appropriate volume. The

sample was concentrated following the manufacturer's protocol to the required volume. The sample was then filtered through a Corning® Costar® Spin-X® centrifuge tube filters with cellulose acetate membrane, pore size 0.22 µm (Sigma) to remove any residual agarose.

#### 2.3.4 Protein quantification

To quantify protein 1mL Bicinchoninic acid (BCA; Sigma) was mixed with 20µl copper sulphate solution (Sigma). 5µl of sample was added to this mix and incubated in a heat block at 37°C for 30 minutes. After blanking the spectrophotometer absorbance readings for each sample were recorded. These were read alongside a standard curve prepared with known concentrations of BSA (Sigma) to calculate the protein concentration in mg/ml.

#### 2.3.5 Protein Electrophoresis

Protein electrophoresis was carried out using Mini-Protean® TGX™ Precast Gels or Criterion™ TGX™ Gels (Bio-Rad Laboratories, Hercules, California, US). 12% gels were used. Protein electrophoresis was carried out using reducing and denaturing conditions with protein electrophoresis running buffer (Section 2-1). The sample of protein lysate was diluted to the required concentration and incubated at 95°C with the appropriate volume of SDS loading buffer for 5 minutes. Samples were added to the gel along with an appropriate ladder and SDS loading buffer with water to un-used wells. The gel was run to an appropriate distance at 100 -150 v.

#### 2.3.6 Immuno-blotting

Following protein electrophoresis, the gel was transferred to a Polyvinylidene difluoride (PVDF) membrane using the Trans-Blot Turbo Transfer System (Bio-Rad Laboratories). The membrane was then incubated in blocking buffer for at least 1 hour. The membrane was then incubated with the required primary antibody (Table 2-4Table 2-4) overnight at 4°C with gentle shaking. The membrane was washed with TBST three times for 10 minutes then incubated with the secondary antibody, Anti-rabbit IgG, HRP-linked Antibody (Cell Signalling Technology, #7074) at a concentration of 1:10000 in blocking buffer for 1 hour at room temperature. The membrane was then washed again 3 times

with TBST for 10 minutes. During the final wash Clarity™ Western enhanced chemiluminescence (ECL) substrate was prepared by mixing equal volumes of the luminol and enhancer reagents (BioRad Laboratories). The membrane was incubated in the ECL substrate for 5 minutes. Excess solution was removed, and the membrane placed into a developing cassette. Blots were imaged (SRX-101A X-Ray Film Processor, Konica Minolta, Bloxham Mill, UK) using medical X-ray film (Fujifilm, Tokyo, Japan). Film was exposed for the required time and then developed.

Where further staining was necessary the membrane was then washed with TBST three times for 10 minutes then incubated in Restore Stripping Buffer (ThermoScientific) for 30 minutes at 37°C with gentle agitation. The membrane was washed with TBST three times for 10 minutes and was then incubated in blocking buffer prior to further antibody staining.

<b>Antibody</b>	<b>Concentration</b>
<b>RHOA (67B9) Rabbit mAb (#2117 Cell Signalling Technologies, Danvers, Massachusetts, US)</b>	1:1000
<b>DYKDDDDK (FLAG) Tag (D6W5B) Rabbit mAb (#14793 Cell Signalling Technologies)</b>	1:5000
<b>GAPDH (D16H11) XP® Rabbit mAb (Cell Signalling Technologies)</b>	1:10000
<b>ITK Rabbit mAb (ab137359, Abcam, Cambridge, UK)</b>	1:1000

*Table 2-4: Antibodies used for immunoblotting*

### 2.3.7 Coomassie staining

Following protein electrophoresis, the gel was washed in ultra-pure water 3 times for 10 minutes. PageBlue Protein Staining Solution (ThermoScientific) was added to the gel and incubated for 1 hour with gentle shaking at room temperature. The staining solution was removed, and the gel was washed with ultra-pure water three/four times to destain the gel so that bands could be clearly visualised.

### 2.3.8 Circular Dichroism

Circular dichroism spectroscopy was carried out using Chirascan™ circular dichroism spectrometer (Applied Photophysics, Leatherhead, UK) and Pro-Data Viewer software (Applied Photophysics). Following quantification, the protein samples were diluted to

1mg/ml with protein wash buffer. An initial background spectrum of the buffer was acquired between wavelengths of 210nm and 280nm with a step of 1nm. For each protein construct spectra were acquired in triplicate. A melting curve was then obtained at a wavelength of 220nm from 22°C to 90°C with measurements in triplicate at 1°C intervals.

The circular dichroism spectra for each construct was averaged and the background was subtracted using the Pro-Data Viewer software. Further analysis of the curves was performed with GraphPad Prism7 software (GraphPad Software, La Jolla, California, US).

## 2.4 MAMMALIAN CELL CULTURE

HEK293 cells were maintained in Dulbecco's Modified Eagle Medium (DMEM) with GlutaMAX™ (Gibco™, ThermoFisher) with 10% Fetal Calf Serum (FCS; Gibco™, ThermoFisher). Upon approaching confluence cells were washed with 1 x PBS then 1 x Trypsin EDTA (TE) was added. For regular passage, an appropriate volume was then added to fresh media in a new flask. For transfection PBS was added to the cells and TE and transferred to a 50ml tube. Cells were pelleted then resuspended in media and counted. Cells were then plated at  $3 \times 10^5$  cells/ml, e.g. for a 10cm<sup>2</sup> plate a total of  $3 \times 10^6$  cells were plated in 10ml media.

Jurkat cells were cultured in Roswell Park Memorial Institute (RPMI) 1640 Medium (Gibco™, ThermoFisher) with 10% FCS and 1% GlutaMAX™ supplement (Gibco™, ThermoFisher). Cells were passaged as required by the addition of supplemental media and transfer to a new flask.

### 2.4.1 Cell counting

Cell counting was performed with the TC20™ Automated Cell Counter (BioRad, Laboratories). 10µl Trypan blue (BioRad Laboratories) was added to 10µl sample of cells and then added to a counting slide. The slide was placed in the counter and the total cell number/ml and live cell number/ml was measured.

#### 2.4.2 Mammalian cell transfection

Cells were plated at  $3 \times 10^5$  cells/ml 24 hours prior to transfection. Polyethylenimine (PEI; Sigma) was dissolved in water to a concentration of 100 $\mu$ g/ml and filtered through a 22 $\mu$ m filter and stored at 4°C. For transfection of cells in a 10cm<sup>2</sup> plate 150 $\mu$ l of PEI was added to 2ml sterile PBS and 20 $\mu$ g of plasmid DNA and incubated at room temperature for 30 minutes. Following this incubation 3ml of serum free DMEM + GlutaMAX (Gibco™, ThermoFisher) was added. The cells were washed twice with sterile PBS then the media with transfection reagents was added to the plate. The cells were then incubated at 37°C and 5% CO<sub>2</sub> for 6 hours. 5ml DMEM + GlutaMAX with 10% FCS (Gibco™, ThermoFisher) was then added to the plate and cells returned to the incubator.

#### 2.4.3 Mammalian cell lysis

After the required incubation period cells were used for protein or RNA extraction. Cells were washed with sterile PBS then TE was added. The plate was incubated to allow cells to detach. An equal volume of PBS was added, and the cells were transferred to two microcentrifuge tubes (one for RNA extraction and one for protein extraction). Cells were then pelleted at 300 x g for 5 minutes at 4°C and supernatant discarded.

#### 2.4.4 RNA extraction

Cells for RNA extraction were resuspended in 1ml TRIzol™ reagent (ThermoFisher) and lysed by pipetting up and down. If not proceeding to RNA extraction immediately the sample was then frozen at -80°C. For phase separation 200 $\mu$ l of 1-bromo-3-chloropropane (BCP; Sigma) was added and the sample transferred to a pre-spun 5PRIME Phase Lock Gel tube (Quantabio, Beverly, Massachusetts, US) and shaken vigorously. After a 2-minute incubation at room temperature the sample was spun at 12000 x g for 10 minutes at 4°C. The Phase Lock Gel forms a barrier between the aqueous phase containing RNA and the organic and interface material. The aqueous phase was then transferred to a fresh microcentrifuge tube and an equal volume of 70% ethanol (Chemistry Department, University of Leicester) was added. The sample was vortexed then transferred to a column of the PureLink® RNA Micro Scale Kit (Invitrogen). RNA was bound to the column and then washed with a DNase step as per the

manufacturers protocol. The RNA was eluted with the addition of 15µl of ultra-pure water and quantified. RNA was used in reverse transcription reactions or frozen and stored at -80°C.

#### 2.4.5 Protein extraction

Cells for protein extraction were resuspended in Radioimmunoprecipitation assay (RIPA) buffer (ThermoFisher) with protease and phosphatase inhibitor (New England Biolabs). Sample was vortexed and incubated on ice for 30 minutes. The sample was centrifuged at 10000 x g for 10 minutes at 4°C to remove the cell debris, and the supernatant transferred to a fresh tube. Protein lysate was quantified and used for immunoblotting or stored at -80°C.

#### 2.4.6 Rhotekin pull down

To determine the proportion of RHOA bound to GTP (i.e. the active form) for the different mutant proteins a pulldown assay was performed using a protocol designed by Professor Anne Ridley's group (202). Rhotekin is a Rho family effector protein which binds preferentially to GTP-bound RHOA by the Rho-binding domain (RBD) (203). First GST-Rhotekin protein was produced. A plasmid kindly supplied by Professor Ridley was used to transform Rosetta BL21 (DE3) cells as before and these were plated on LB agar with ampicillin and chloramphenicol. Following overnight incubation, a colony was picked from the plate and added to 5mL LB media with ampicillin and chloramphenicol and incubated overnight at 37°C shaking. This was added to 400ml LB media and incubated at 37°C for a further 3-4 hours. The temperature was then reduced to 20°C and 50µM of IPTG was added to induce protein expression. After overnight incubation, the media was divided into 50ml tubes and centrifuged at 4400 x g for 30 minutes and the supernatant discarded. The cell pellets were stored at -80°C.

To prepare the GST-Rhotekin agarose 50ml STE buffer (Section 2-1) was prepared and 10ml taken to prepare STE-PMSF buffer by the addition of 1mM Phenylmethylsulfonyl fluoride (PMSF; Sigma). One 50ml tube of pelleted cells was taken for each condition and cells lysed by the addition of 5ml STE-PMSF buffer to the first tube and then each

subsequent tube to produce a single tube of lysed cells. These were homogenised by passing through a 19G needle eight-ten times.

Lysozyme was prepared by dissolving 50mg in 500µl of STE buffer and 20µl added to the lysed cells and mixed gently. This was incubated on ice for 20 minutes then 5mM DTT, 1% Tween-20 and 0.03% SDS were added and mixed gently. The sample was centrifuged at 14000 x g for 20 minutes at 4°C and the supernatant added to washed glutathione agarose (using 30µl agarose per condition). The agarose with supernatant was incubated under rotation at 4°C for 1-2 hours. Subsequently the agarose was washed three times with STE buffer and after the final wash left in a small volume of buffer (around 50µl/sample) and a 10µl sample taken for a gel.

The agarose with GST-Rhotekin bound was then used to pulldown the GTP-bound RHOA. 20ml 1 x MG buffer (Section 2-1) was prepared and used to wash the prepared agarose once. The beads were resuspended in around 50µl / sample of 1 x MG buffer and kept on ice. HEK293 cells which had been transfected 48 hours previously in 10cm<sup>2</sup> plates were washed twice with cold PBS then 500µl of 1 X MG buffer was added. Cells were scraped from the plate and transferred to 1.5ml microcentrifuge tubes. The samples were centrifuged at 14000 rpm for 5 minutes at 4°C. From the supernatant 50µl was taken for the total lysate and added to SDS loading buffer boiled and stored at -20°C. The remaining supernatant was added to the 50µl agarose and incubated under rotation at 4°C for 1-2 hours. The agarose was then washed 3 times with 1 X MG buffer then the supernatant removed and SDS loading buffer.

Two 12% Mini-Protean® TGX™ Precast Gels were run – one with the total lysate samples and one with the agarose. Immunoblotting was performed as described previously to detect RHOA, FLAG (total lysate and pull down) and GAPDH (total lysate only).

#### 2.4.7 Gel analysis with Image J

Developed films were scanned to produce image files. These were opened in ImageJ (204,205) for quantification of the density of the bands as described at <https://imagej.nih.gov/ij/docs/menus/analyze.html#gels>.

#### 2.4.8 Ibrutinib treatment of cells

Jurkat cells in culture were treated with ibrutinib (Janssen, Beerse, Belgium) dissolved in Dimethyl sulfoxide (DMSO; Sigma) and 10% 2-Hydroxypropyl- $\beta$ -cyclodextrin (2-HBD) solution (Sigma). Cells were plated at  $1 \times 10^5$  cells/ml into a 96-well white bottomed plate with 150 $\mu$ l added to each well. A range of concentrations of ibrutinib were added to the wells (0.5 $\mu$ M to 20 $\mu$ M) in triplicate. The plate was incubated for 48 hours before a CellTiter-Glo<sup>®</sup> (CTG) Luminescent Cell Viability Assay (Promega, Madison, Wisconsin, US) was carried out as described in section 2.5.12.

## 2.5 A MOUSE MODEL OF T-CELL LYMPHOMA

### 2.5.1 Husbandry and colony management

Mouse work was carried out at the Department of Biomedical Science (DBS) Preclinical Research Facility (PRF) at the University of Leicester in accordance with the home office regulations under the project licences 60/4371 and subsequently P8E5F4055. Animal care and husbandry was carried out by technicians at the PRF.

Roquin<sup>san/+</sup> mice were crossed with C57Bl/6J mice to maintain a population of heterozygote mice and wild type littermates. After weaning ear snips were taken for identification and genotyping, which was carried out by Transnetyx<sup>®</sup> (Cordova, Tennessee, US). Roquin<sup>san/+</sup> mice were set aside for ageing to allow for the development of tumours. Littermate control Roquin<sup>+/+</sup> (WT) mice were also set aside for tissue culture work and to use as a control population.

Once the heterozygous mice reached 6 months of age they were assessed for tumour development by palpation and those with palpable tumours were identified for entry into further study. Those with no tumour development by 12 months of age were culled for tissue culture work.

### 2.5.2 Adoptive transfer

Cell suspensions were produced from the enlarged lymph nodes of aged Roquin<sup>san/+</sup> mice as described in section 1.5.8 using sterile conditions. Cells were delivered to

recipients by intravenous tail vein injection using 25G needles. Mice were placed in an incubator at 37°C for 5 minutes prior to injection.

SCID-Beige mice were used as recipients initially, these were obtained from Dr Ruth Barber who assisted with the design and delivery of these experiments. Six mice received  $3 \times 10^7$  cells in 100µl and six received  $5 \times 10^6$  cells in 100µl. Mice were reviewed daily for signs of ill health and soggy food provided if signs of weight loss.

Further adoptive transfer used WT littermates as recipients, mice selected were approximately 8 weeks old. Prior to tail vein injection half of the recipient mice underwent sub-lethal irradiation to determine if this would produce a better chance of engraftment and subsequent tumour development. Irradiation was carried out in an Xstrahl X-Ray Machine by myself and Dr Ruth Barber. Mice were transported to the machine inside transport boxes after a period of acclimatisation. Mice received a radiation dose of 250cGy approximately one hour prior to the receipt of cells.

Three irradiated and three non-irradiated mice received  $8 \times 10^5$  cells in 100µl and two weeks later a further 3 irradiated and 3 non-irradiated mice received  $5 \times 10^6$  cells in 100µl. Mice were reviewed daily for signs of ill health and soggy food provided if signs of weight loss.

### 2.5.3 Imaging

Magnetic Resonance Imaging (MRI) was carried out at the PRF imaging facility by Dr M Kelly and J Janus. MRI scanning was performed on a 9.4T Agilent scanner (Agilent Technologies, Santa Claire, CA, USA) with a 310mm bore diameter and 6cm inner-diameter gradient (1000mT/m maximum gradient strength). A 4cm millipede RF coil was used for RF transmission and reception. Physiological monitoring was achieved using a custom monitoring and gating system (SA Instruments, Stony Brook, NY, USA). Mouse body temperature was maintained at 37°C using a warm air fan and rectal temperature probe. Respiration was measured using a pneumatic pillow. All scans were performed during the light cycle under anaesthesia with 1-2% isoflurane in oxygen. T2-weighted images were acquired using a respiratory-gated fast spin echo (FSE) sequence with TR/TE=3000/40ms, 40x40mm field of view (256x256 matrix), 32x0.8mm slices and

two signal averages (scan duration = 6min 30secs). This scan was run twice to produce axial slices of both the axillary and inguinal regions. Following completion of imaging the mice were recovered and returned to their cage, they were reviewed the following day by a technician.

#### 2.5.4 Image analysis

ImageJ (204,205) was used to carry out analysis of the images and calculate tumour and lymph node volumes. Scan images were opened as a stack in ImageJ. For each file the lymph nodes were identified and highlighted as a region of interest (ROI) using freehand drawing on each slice when present. The area of the ROI for each slice was recorded. This was performed separately for right and left sided inguinal, axillary and brachial lymph nodes. Lymph node volume was calculated for each slice using the known slice thickness (0.8 mm) and the volumes added to produce a total node volume. For each scan the following lymph node volumes were calculated when they could be identified—right & left axillary, right & left brachial and right & left inguinal.

#### 2.5.5 Drug treatments

During drug treatments mice were weighed 3 times a week, or more frequently if there were concerns about their condition, and soggy diet provided in cases of weight loss. Palpable lymph nodes were measured in 2 dimensions using calipers three times a week.

Cyclophosphamide (Sigma) was made up into solution with sterile PBS at a concentration of 20mg/ml. It was then passed through a 22µm filter. Cyclophosphamide was delivered as an intraperitoneal injection at a dose of 200mg/kg on day 1. An equivalent volume of filtered sterile PBS was delivered as an intraperitoneal injection to the vehicle dosed mice on day 1.

Ibrutinib (Janssen) was made up in a 10% 2-Hydroxypropyl-β-cyclodextrin (2-HBD) solution (Sigma) at a concentration of 25mg/ml and stored at -20°C. This was diluted to 2.5mg/ml in 1% 2-HBD for delivery by oral gavage at a dose of 25mg/kg each day. Vehicle treated mice received an equivalent volume of 1% 2-HBD.

### 2.5.6 Lymph Node Dissection

To ensure that lymph nodes were reliably identified a mouse was injected with 5% Evans Blue dye (Sigma) subcutaneously into the base of the tail under general anaesthetic as described by Harrell et al (206). Anaesthesia was maintained for 20 minutes prior to schedule 1 killing. The mouse was then dissected, lymph node areas observed and photographed. This enabled identification of axillary, brachial and inguinal lymph nodes whilst the peritoneum was intact (Figure 2-3) (207).

In most cases mice were killed for dissection by cervical dislocation and death confirmed by cutting of the femoral artery. Dissection was then performed making a midline incision through the skin and fascia but maintaining the integrity of the peritoneum. Inguinal lymph nodes were dissected and removed. Axillary and brachial lymph nodes were identified and removed. Enlarged lymph nodes were kept separate from non-enlarged nodes and placed into sterile PBS on ice. The peritoneal cavity was then opened and the spleen removed and placed in sterile PBS on ice. The abdomen was inspected for masses and if enlarged mesenteric lymph nodes were found these were removed and placed in sterile PBS on ice. The liver was removed if tissue was required for constitutional DNA extraction.

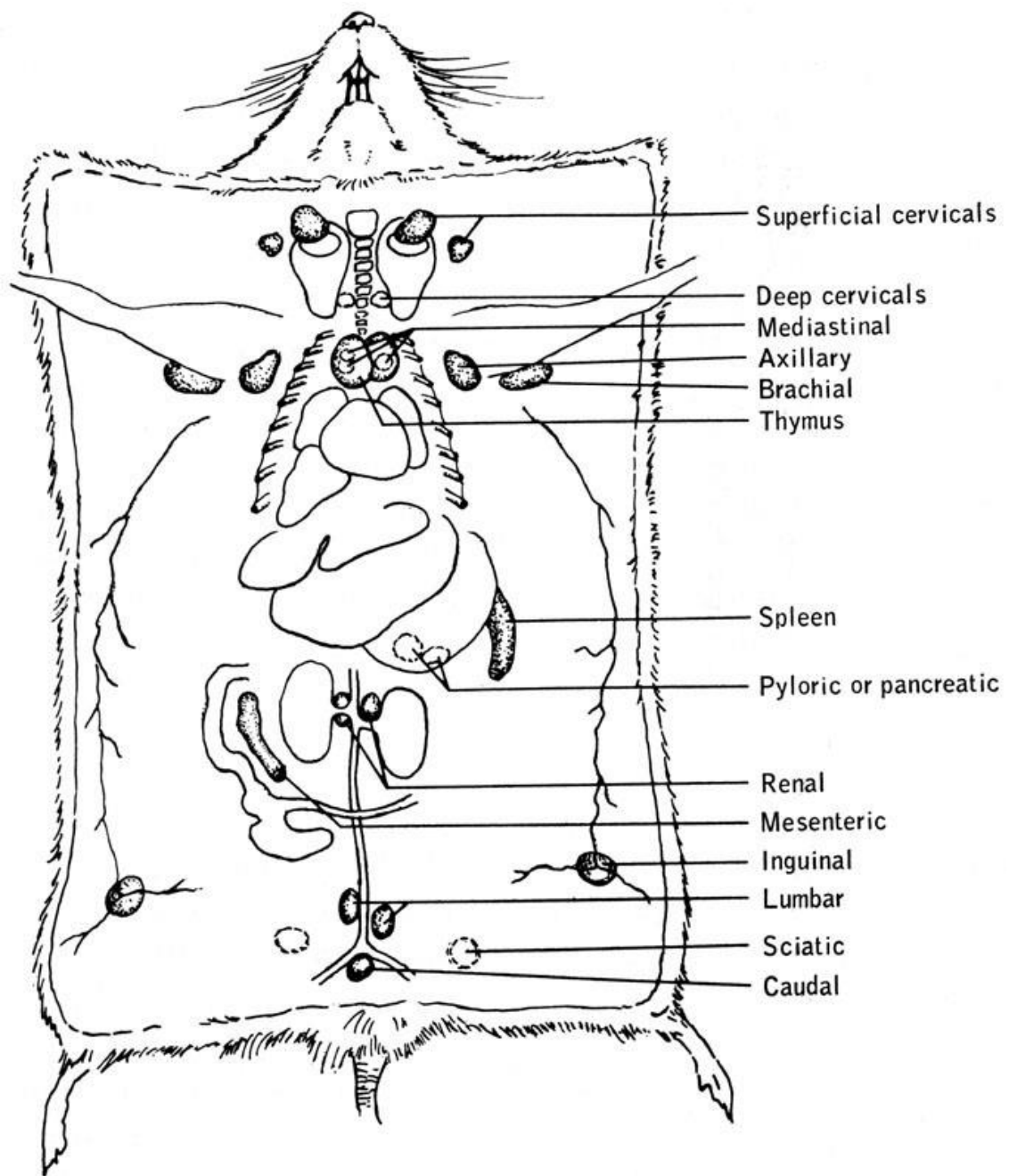


**Figure 2-3: Lymph node anatomy of the mouse from Dunn (207)**

### 2.5.7 Serum IL-21 measurement

At the time of killing the mice were placed under terminal anaesthesia and a blood sample obtained by cardiac puncture carried out by trained PRF staff. The samples were taken into a plain 1.5mL tube and kept at room temperature to allow the preparation of serum. Samples were kept at room temperature undisturbed for at least 30 minutes.

Samples were centrifuged at 4°C at 3000 rpm for 15 minutes with the brake off. The serum was removed and placed in a fresh tube then stored at -20C.

Serum IL-21 was measured using an IL-21 mouse enzyme-linked immunosorbent assay (ELISA) kit (ab100707, Abcam, Cambridge, Massachusetts, US) following the manufacturer's instructions. Briefly a series of IL-21 standard dilutions were prepared and measured in duplicate. Serum samples were defrosted and measured in triplicate where possible or duplicate if insufficient material. After a period of incubation, the plate was washed then biotinylated IL-21 detection antibody added and allowed to bind. After washing, horseradish peroxidase (HRP) -streptavidin solution was added and allowed to bind. After final washing steps the 3,3',5,5'-tetramethylbenzidine (TMB) substrate was added and the plate incubated in darkness. After addition of the stop solution the absorbance at 450nm was read using Infinite® 200 PRO (Tecan, Switzerland) with i-control™ software (Tecan).

Analysis was then carried out using GraphPad Prism v7 (GraphPad) with generation of a standard curve. The concentration of IL-21 in the serum samples was then read from the standard curve (Figure 2-4).

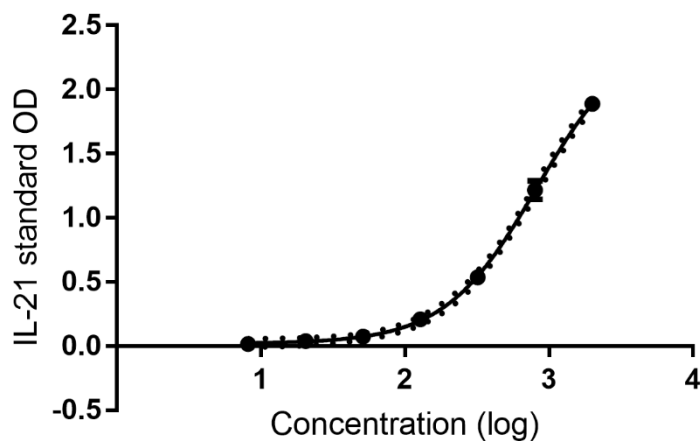


**Figure 2-4: Standard curve generated for the IL-21 ELISA.**

*Log<sup>10</sup> IL-21 concentration is shown on the x-axis and absorbance at 450 nm on the y-axis. Black dots represent the mean of the standard samples (n=3) with error bars showing standard deviation.*

### 2.5.8 Cell suspension preparation

All centrifugation to pellet cells was carried out at 300 x g for 5 minutes at 4°C unless specified. The procedures were carried out in sterile conditions in class 2 biological safety cabinet.

When tissue was to be used for sections and immunohistochemistry it was snap frozen in liquid nitrogen and stored at -80°C. The remaining lymphoid tissues were used to produce cell suspensions. The tissue was placed in a 70µm cell strainer and the plunger of a syringe was used to push the tissue through the strainer with pre-cooled sterile PBS into a 50ml tube. Following centrifugation, the supernatant was removed. Where red cells were present (spleen tissue and enlarged vascular lymph nodes) the cell pellet was resuspended in 3ml 1 x red cell lysis buffer (BioLegend, San Diego, California, US) and incubated at room temperature for 5 minutes. 7ml PBS was then added and the sample centrifuged, the supernatant discarded and the pellet resuspended in 5 – 10 ml PBS. If there were minimal red cells present the pellet was simply resuspended in 5 -10 ml PBS. The suspension was then passed through a 40µm cell strainer into a fresh 50ml tube and a 10µl sample taken for counting. Further processing was then carried out as required.

### 2.5.9 Cell counting

Cell counting was performed with the TC20™ Automated Cell Counter (BioRad). 10µl Trypan blue was added to 10µl sample of cells and then added to a counting slide. The slide was placed in the counter and the total cell number/ml and live cell number/ml was measured.

### 2.5.10 Cell separation

Cell separation was carried out to separate CD4<sup>+</sup> T cells using CD4<sup>+</sup> T cell Isolation Kit, mouse (Miltenyi Biotec, Bergisch Gladbach, Germany). This produces an untouched population of CD4<sup>+</sup> T cells and the remaining labelled cells can also be collected if required. A 1 x 10<sup>5</sup> cell sample was taken following preparation of the cell suspension prior to cell separation to carry out flow cytometry (FACS) analysis. The remaining cells were then pelleted and resuspended in 40µl cell separation buffer per 1 x 10<sup>7</sup> cells and

10µl of Biotin-Antibody Cocktail was added per  $1 \times 10^7$  cells. After mixing the samples were incubated in the fridge for 5 minutes. 30µl cell separation buffer and 20µl Anti-Biotin MicroBeads per  $1 \times 10^7$  cells were added and after mixing the samples were incubated for 10 minutes in the fridge.

During the second incubation the LS Columns were placed into a MACS Separator on a cool tray and washed with 3ml cell separation buffer. The sample was then made up to 500µl with cell separation buffer, if required, and added to the column and the flow through collected into a 15ml tube. The column was washed with 3ml cell separation buffer and the flow through collected into the same tube. If the non-CD4<sup>+</sup> cells were required, the column was removed from the separator and placed over a new 15ml tube. 5ml cell separation buffer was added and the magnetically labelled cells were flushed out using the plunger.

A 10µl sample of the unlabelled CD4<sup>+</sup> cells was taken and cells were counted.  $1 \times 10^5$  cells were taken to carry out flow cytometry to assess the purity of the selected cells.

#### 2.5.11 FACS staining

FACS antibodies were obtained from Becton Dickinson Biosciences, Franklin Lakes, New Jersey, US unless otherwise specified. For cell separation analysis FACS was carried out on  $1 \times 10^5$  cells. Cells were centrifuged and the supernatant removed. Cells were resuspended in 50µl 1 x PBS with 1:100 anti-CD4-FITC, 1:50 anti-B220-PE and 1:50 anti-CD8-APC and incubated in the dark at room temperature for 30 minutes. 400µl PBS was added and cells were centrifuged and supernatant removed. Cells were resuspended in 500µl PBS and transferred to FACS tube. Flow cytometry was carried out using a FACS Canto to assess proportions of CD4 cells, CD8 cells and B cells before separation and purity of CD4 cells after separation. In some cases, the CD4 cell sample post separation was stained with 1:1000 anti-CD4-FITC, 1:10 anti-CXCR5-APC and 1:20 PD1-PE to determine the proportion of Tfh cells in the CD4 cell population.

For tumour / tissue characterisation analysis FACS was carried out on  $1 \times 10^6$  cells. Cells were centrifuged and the supernatant removed. Cells were resuspended in 100µl PBS & 1% BSA with antibodies as shown in Table 2-5 and incubated in the dark at

room temperature for 30 minutes. 400µl PBS was added and cells were centrifuged and supernatant removed. Cells were resuspended in 500µl PBS and transferred to FACS tubes. Flow cytometry was carried out using a FACS Canto (BD Bioscience) with BD FACSDIVA™ software to assess lymphocyte subsets and Tfh cells. Further analysis was performed using FlowJo® v10 (Ashland, Oregon, USA).

Antibody Specificity	Fluorophore	Clone	Panel
CD4	FITC	GK1.5	Lymphocyte subsets, Tfh
B220	PE	RA3-6B2	Lymphocyte subsets
CD8	APC	53-6.7	Lymphocyte subsets
PD1 (CD279)	PE	J43	Tfh
CXCR5	APC	2G8	Tfh

**Table 2-5: Antibodies used in FACS panels**

#### 2.5.12 CD4<sup>+</sup> cell culture

CD4<sup>+</sup> cells were cultured in RPMI medium with 10% FCS, penicillin (50 U/ml) and streptomycin (50µg/ml) (Gibco™, ThermoFisher). 1 x 10<sup>5</sup> cells were added to each well of a round-bottomed 96 well plate in 100µl of medium.

To stimulate cells, the plate was pre-coated with purified NA/LE hamster anti-mouse CD3e (aCD3, clone 145-2C11, BD Bioscience). At least 12 hours prior to cell culture aCD3 was diluted to 10µg/ml with sterile PBS and 50µl (0.5µg) added to required wells, the plate was sealed and kept at 4°C until required. Prior to plating the wells were washed with sterile PBS.

Further stimulation was provided by purified NA/LE hamster anti-mouse CD28 (aCD28, clone 37.51, BD Bioscience). This was added to culture medium at a concentration of 2µg/ml.

Treatment of cells was undertaken with ibrutinib (Janssen). For cell culture ibrutinib was dissolved in DMSO at 50mg/ml and stored at -20°C. Prior to use in culture a 100µM stock in medium was prepared. An equivalent volume of DMSO was added to medium for control samples. Ibrutinib / DMSO was added to wells at the required concentration for treatment.

### 2.5.13 CellTiter-Glo® Luminescent Cell Viability Assay

The CellTiter-Glo® (CTG) Luminescent Cell Viability Assay (Promega) assesses the number of viable cells based upon quantitation of ATP. Cells were cultured in 100µl of media with required additional conditions in an opaque 96-well plate (Corning Inc, Corning, New York, US). Following an appropriate incubation period, the plate was removed from the incubator and the CTG reagent removed from the fridge. Reagent and cells were allowed to equilibrate to room temperature for 15 minutes. 50µL of CTG reagent was added to each experimental well and the plate was shaken at 200rpm for 2 minutes. Following a further 10-minute incubation the luminescence was read using the Infinite® 200 PRO (Tecan) with i-control™ software (Tecan).

### 2.5.14 Cell proliferation & differentiation

Following separation CD4<sup>+</sup> cells were stained with Cell Trace Violet (CTV; Thermo Fisher). 5µM CTV was added to cells at a concentration of  $1 \times 10^6$ /ml in pre-warmed PBS and cells were incubated for 20 minutes at 37°C protected from light.

Cells were centrifuged then resuspended at  $1 \times 10^6$ /ml in culture medium. For each condition 100µl of cells was plated into 10 wells of a round-bottomed 96 well plate (total of 1ml for each condition) with recombinant mouse IL-12 (R&D Systems, Minneapolis, Minnesota, US) at a final concentration of 10ng/ml and /or recombinant mouse IL-21 (R&D Systems) at a final concentration of 50ng/ml. Stimulation and drug or vehicle treatment was added as required.

Plates were incubated at 37°C and 5% CO<sub>2</sub> for 6 days before the cells were harvested. On the day of analysis frozen CD4 cells were defrosted and  $1 \times 10^6$  cells were stained with CTV as above.

Cells were washed with PBS then resuspended in 50µl PBS with 1:1000 anti-CD4-FITC, 1:20 anti-PD1-PE and 1:10 anti-CXCR5-APC and incubated at room temperature in darkness for 20 minutes. 400µl PBS was added and cells were centrifuged and supernatant removed. Cells were resuspended in 500µl PBS and transferred to a FACS tube. Flow cytometry was carried out using FACS Aria (BD Bioscience) with BD

FACSDIVA™ software with assistance from Dr Lucia Pinon, CTV was detected in the Pacific Blue channel. Further analysis was performed using FlowJo® v10.

#### 2.5.15 RNA extraction

Frozen cell suspensions from mice which had undergone ibrutinib / placebo therapy were defrosted and counted.  $1 \times 10^6$  cells were taken for RNA extraction and the remaining cells were separated. The CD4<sup>+</sup> cells and non-CD4<sup>+</sup> cells were then collected for RNA extraction. Cells were centrifuged and the supernatant removed. The cells were resuspended in 800µl TRIzol™ reagent (ThermoFisher) and transferred to a prepared 5Prime Phase Lock Gel tube (QuantaBio). 160µl of BCP (Sigma) was added to each sample and tubes shaken vigorously. Phase separation was carried out by centrifugation at 12000 x g for 10 minutes at 4°C. The aqueous phase was transferred to a fresh 1.5ml tube and an equal volume of 70% ethanol was added. This mixture was vortexed then added to a PureLink™ RNA Micro column (Invitrogen) and the protocol followed to bind RNA, wash RNA with a DNase step and elute RNA with 15µl of ultrapure water.

RNA to be used for microarray was passed to the Nucleus Genomics service and quantity and quality assessed using a 2100 Bioanalyzer (Agilent Genomics). Samples with sufficient good quality RNA were chosen for a microarray (RNA Integrity Number (RIN) greater than 7, or satisfactory trace).

Further RNA extractions carried out from CD4<sup>+</sup> spleen cells were carried out by the Nucleus Genomic service using the Maxwell® 16 LEV simplyRNA Purification Kit (Promega) for cells in the Maxwell® 16 Instrument (Promega). Following separation of CD4<sup>+</sup> cells from mouse spleen the cells were centrifuged and supernatant removed. The cell pellet was then snap frozen in liquid nitrogen and stored at -80°C until RNA extraction. Quality and quantity of the extracted RNA was assessed as before.

#### 2.5.16 Gene Expression Profiling by Microarray

A total of 100ng of total RNA was reverse transcribed, converted into complementary RNA (cRNA) and labelled with Cy3 using the LowInput QuickAmp Labeling Kit One-Color according to manufacturer's protocol (Agilent Genomics). Labelled cRNA was then hybridized over night at 65°C onto the SurePrint G3 Mouse Gene Exp v2 Array, which

permits the quantification of about 60,000 transcripts. Each microarray was scanned on an Agilent DNA microarray C-scanner. Extraction and quality check of the raw data was performed using the Agilent Feature extraction software 10.5.1.1. The microarray hybridisation and scanning were performed by Nucleus Genomics at the University of Leicester (Dr Nicolas Sylvius & Dr Spencer Gibson).

Data was normalised using Partek software (Partek Inc., St. Louis, MO, USA) and further analysis was carried out using MeV v4.8.1 from the TM4 suite of software developed by The Institute for Genomic Research (208). The two-class unpaired Significance Analysis of Microarrays (SAM) was used to produce a list of differentially expressed genes.

Further analysis of the differentially expressed genes was carried out using The Database for Annotation, Visualization and Integrated Discovery (DAVID) v6.8 (209,210). The gene list was submitted to the website and a number of databases are searched to explore functional relationship or over-represented pathways. The functional annotation clustering tool was used to search the databases shown in Table 2-6.

Category	Terms
<b>Functional Categories</b>	COG_ontology Up_Keywords Up_Seq_Feature
<b>Gene Ontology</b>	GOTERM_BP_Direct GOTERM_CC_Direct GOTERM_MF_Direct
<b>Pathways</b>	BIOCARTA KEGG_Pathway REACTOME_Pathway
<b>Protein Domains</b>	INTERPRO PIR_Superfamily SMART

**Table 2-6: Databases used in Functional Annotation Clustering analysis**

#### 2.5.17 DNA extraction

DNA was extracted from enlarged lymph nodes and livers of mice – DNA from the liver was considered constitutional DNA. 200 µl of tissue lysis buffer (Section 2-1) was added

to the tissue with 1µl Proteinase K (Qiagen) and the sample was vortexed. Samples were incubated at 55°C at 800rpm in a ThermoMixer C (Eppendorf, Hamburg, Germany) for 2 hours then centrifuged at 14000 x g for 2 minutes at room temperature. The supernatant was transferred to a fresh tube containing 200µl isopropanol (Department of Chemistry, University of Leicester) and the tubes shaken. The samples were centrifuged at 14000 x g for 2 minutes at room temperature and the supernatant removed. The DNA pellet was air dried for 5 minutes then resuspended in ultra-pure water.

#### 2.5.18 Whole exome sequencing

Whole exome sequencing (WES) was carried out in collaboration with the Mouse Genome Project led by Thomas Keane at the Sanger Institute (Cambridge). DNA from a tumour and liver of 2 heterozygous mice, the liver from a heterozygous mouse with no tumour development at 8 months and the liver of a WT mouse was sent to Sanger. They performed WES using SureSelectXT Mouse All Exon Kit (Agilent Genomics) to develop the library which was sequenced on an Illumina HiSeq producing 75bp paired-end reads.

##### *2.5.18.1 Mapping reads to the reference genome*

Bioinformatic analysis was carried out with support from Anthony Doran at the Sanger Institute using the analysis pipeline they have previously described (211). After removal of Illumina tag sequences and poor-quality bases the sequencing reads from each sample were aligned to the C57BL/6J GRCm38 (mm10) mouse reference genome using BWA-MEM (v0.7.5) with default parameters. Each BAM file (one per sample) was then sorted and filtered for possible PCR and optical duplicates using Picard Tools (v1.64). To improve SNP and indel calling, the GATK v3.0 'IndelRealigner' tool, was used to realign reads around indels using default options.

##### *2.5.18.2 Variant Calling & Effect Prediction*

After mapping the WES libraries to the reference genome bioinformatic tools were used to generate files containing lists of variations from the reference genome. There are a number of tools available to analyse variation from WES and using more than one piece of software is useful to detect variants which may be of interest. Those that are found

by more than one method may be of particular interest. The variation arises from the use of different quality filters.

Filter	Description	Value
<b>MinMQ</b>	Minimum mapping quality supporting variant	20
<b>QUAL</b>	Minimum value of the sample specific QUAL score	20
<b>MinGQ</b>	Minimum genotype quality	20
<b>MinDP</b>	Minimum good quality read depth	20
<b>MinHetDP</b>	Minimum quality relating to depth and genotype (Hetrozygotes)	10
<b>MinAltDP</b>	Minimum likelihood of alternative genotype	4 / 10
<b>StrandBias</b>		0.0001
<b>MaxDP</b>	Maximum read depth	5000

*Table 2-7: Filters used for determining variant quality.*

Dr Anthony Doran used SAMtools (v 1.3.1) mpileup to generate VCF files and BCFtools (v 1.3.1) to filter the variants. The filters used to determine variant quality are shown in Table 2-7.

Further analyses were carried out using the high-performance computing system at the University of Leicester (SPECTRE). Varscan2 is a software programme from Washington University (212,213) which takes paired tumour & constitutional BAM files and analyses them to produce lists of somatic, germline and loss of heterozygosity (LOH) variants.

Further analysis of files was carried out with Varscan2 to compare the constitutional and tumour samples. To generate a list of variants the somatic programme is used. This was run with the following modifications to the default settings:

- Min-coverage-tumour 30
- Min-coverage-normal 10
- Tumour-purity 0.1

Next the variants were classified as high or low confidence using the processSomatic command with default settings.

The Ensembl Variant Effect Prediction (VEP) tool version 88 or version 91 was used to predict the effect of the filtered SNVs and Indels on gene transcripts (214). Further analysis of the gene lists produced was carried out by submitting the gene lists to InnateDB (215). InnateDB is a publicly available database, which allows online submission of a gene list to assess if there are over-represented pathways.

#### 2.5.19 Clonality

To assess for the presence of T cell clonality genomic DNA was extracted from mouse lymph node tissue using PureLink Genomic DNA kit (Invitrogen). Four polymerase chain reactions (PCR) were carried out using pooled primers, sequences are shown in Table 2-8 (176,216). Pool 1 (V-J1) included the 20 primers located within the V $\beta$  segments and the downstream primer from the 3' region of J $\beta$ 1.6. Pool 2 (V-J2) included the 20 primers located within the V $\beta$  segments and the downstream primer from the 3' region of J $\beta$ 2.7. Pool 3 (D-J1) included the 2 primers located immediately 5' of D $\beta$ 1 and D $\beta$ 2 with the downstream J $\beta$ 1.6 primer. Pool 4 (D-J2) included the two D $\beta$  primers and J $\beta$ 2.7. The J $\beta$ -3'-Primers were labelled at the 5' end with 6-FAM to enable GeneScanning.

PCR reactions were 25 $\mu$ l containing 50ng of genomic DNA with 3pmol of forward primers and 3pmol of the 6-FAM labelled reverse primer and MyFi (Bioline, London, UK) buffer and DNA Polymerase. Thermocycling was carried out in a Veriti<sup>®</sup> Thermal Cycler (Applied Biosystems) with three minutes at 95°C followed by 35 cycles of 30 seconds at 94°C, 30 seconds at 60°C and 1 minute at 72°C then a final extension for 10 minutes at 72°C.

The PCR products were analysed by capillary electrophoresis using GeneScan-ABI 3100 using the 500LIZ standard ladder. Plates were set up with each well containing 0.5 $\mu$ l of a single PCR reaction with 0.5 $\mu$ l of ladder and 9 $\mu$ l of formamide. The GeneScanning was performed by PNAFL at the University of Leicester. Peak Scanner Software v1.0 (Applied Biosystems) was used to analyse the results.

Designation	Sequence (5'→3')
<b>Vβ-5'-Primer</b>	
<b>TCRB-V1</b>	AAATGAGACGGTGCCAGTCGTT
<b>TCRB-V2</b>	TCCTGGGGACAAAGAGGTCAAATC
<b>TCRB-V3</b>	GAAAAACGATTCTCTGCTGAGTGTCC
<b>TCRB-V4</b>	AGCTATCAAAAATTATGGACAATCAG
<b>TCRB-V5</b>	CAGCAGATTCTCAGTCCAACAGTTT
<b>TCRB-V6</b>	AAGGCGATCTATCTGAAGGCTATGA
<b>TCRB-V7</b>	AGCTGATTTATATCTCATACGATGTTG
<b>TCRB-V8</b>	TATATGTACTGGTATCGGCAGGACA
<b>TCRB-V9</b>	TTCCAATCCAGTCGGCCTAACAAT
<b>TCRB-V10</b>	GCGCTTCTCACCTCAGTCTTCAG
<b>TCRB-V11</b>	TTCTCAGCTCAGATGCCCAATCAG
<b>TCRB-V12</b>	AGCTGAGATGCTAAATTCATCCTTC
<b>TCRB-V13</b>	CTGCTGTGAGGCCTAAAGGAACTAA
<b>TCRB-V14</b>	AGAGTCGGTGGTGCAACTGAACCT
<b>TCRB-V15</b>	CCCATCAGTCATCCCACTTATCC
<b>TCRB-V16</b>	GATTTTAGGACAGCAGATGGAGTTTC
<b>TCRB-V17</b>	TCGAAATGAAGAAATTATGGAACAAAC
<b>TCRB-V18</b>	CCGGCCAAACCTAACATTCTCAAC
<b>TCRB-V19</b>	CTACAAGAAACCGGGAGAAGAACTC
<b>TCRB-V20</b>	CTGGTATCAACAAAAGCAGAGCAAA
<b>Dβ-5'-Primer</b>	
<b>TCRB-D1</b>	GAGGAGCAGCTTATCTGGTGGTTT
<b>TCRB-D2</b>	GTAGGCACCTGTGGGGAAGAACT
<b>Jβ-3'-Primer</b>	
<b>TCRB-J1</b>	CACAACCCCTCCAGTCAGAAATG
<b>TCRB-J2</b>	TGAGAGCTGTCTCCTACTATCGATT

**Table 2-8: Primers used for the assessment of T cell clonality**

## 3 CHARACTERISATION OF RHOA MUTATIONS

---

### 3.1 INTRODUCTION

As described in section 1.8.3 it is not fully understood how the mutations described in RHOA effect its function. Although the groups describing the presence of the RHOA<sup>G17V</sup> mutation in AITL investigated its functional impact their descriptions of a “dominant negative” mutation depends on assumptions about the genetics i.e. that the mutation is heterozygous, which have not been clearly established. When considered alongside the work of Cleverley et al (37,127), who demonstrate thymic lymphomas in mice bearing homozygous deficiency of RHOA, it seems plausible that this mutation may cause a loss of function and this contributes to lymphoma development.

Our laboratory has carried out targeted deep sequencing of cfDNA from plasma obtained at diagnosis from a cohort of 16 patients with AITL or PTCL-NOS. The panel included RHOA and 11 other genes. A novel mutation of RHOA, c.73A>G (p.Phe25Leu-F25L) was detected (217). The mutation leading to F25L has not previously been reported but p.Phe25Val has recently been described in lung cancer (218).

To clarify the functional impact of the G17V mutation described in the literature and F25L as found in our laboratory bacterial and mammalian expression systems were used. We have also compared the effects to those seen following a G14V mutation which has been shown to be a gain of function mutation. Finally, a pulldown assay was carried out to assess the GTP-binding activity of the mutant RHOA proteins compared to the WT protein.

### 3.2 BACTERIAL EXPRESSION & PURIFICATION OF RHOA MUTANT PROTEINS

Following transformation of Rosetta DE3 cells with the required plasmids the cells were incubated and allowed to grow prior to induction of protein expression with IPTG and further growth as described in section 2.3.

Protein was extracted from the cells as described in section 2.3.2 and a sample of supernatant was taken for assessment prior to addition of the remaining supernatant to the glutathione agarose. Figure 3-1 shows the GST-RHOA protein in column A for

each construct. This shows that higher amounts of the GST-RHOA<sup>WT</sup>, GST-RHOA<sup>G14V</sup> and GST-RHOA<sup>F25L</sup> were produced than GST-RHOA<sup>G17V</sup> with GST-RHOA<sup>G17V&F25L</sup> barely detectable.

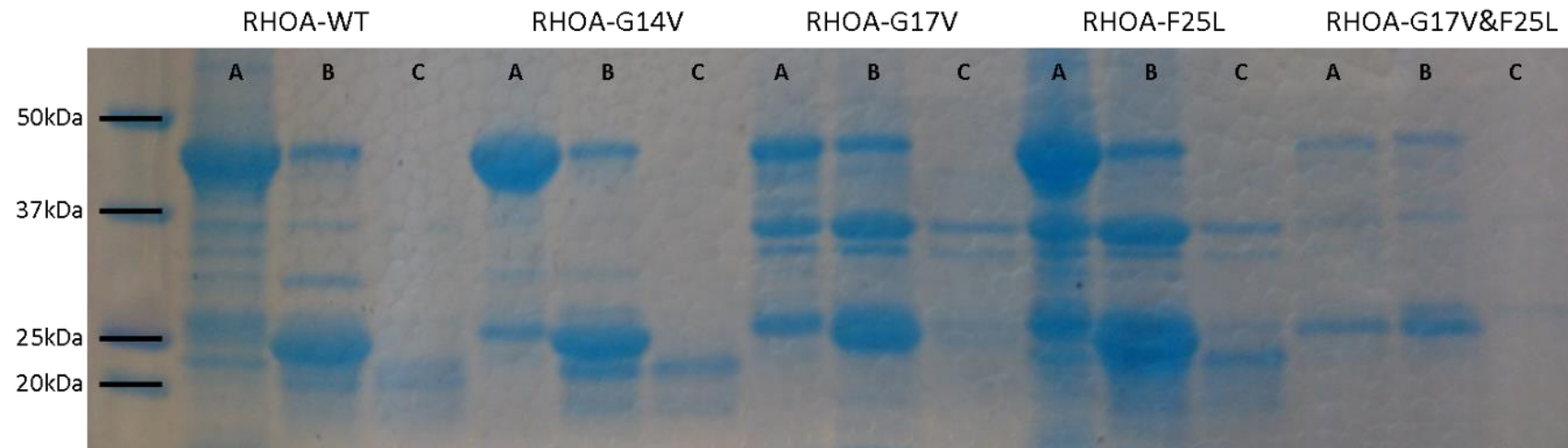


**Figure 3-1: Coomassie stained gel showing proteins produced following bacterial expression.**

The 5 constructs are displayed above the relevant lanes. For each construct lane A shows the protein supernatant following protein extraction with the band at ~45kDa representing the GST-RHOA protein. Lane B shows the beads following TEV cleavage with the band at ~45kDa representing uncleaved GST-RHOA and the band at ~25kDa representing GST. Lane C shows the supernatant following TEV cleavage prior to filtration and concentration with the band at 21kDa representing RHOA.

### 3.2.1 Circular dichroism of RHOA proteins

The proteins were filtered and concentrated then their concentrations were quantified using the BCA assay. There was insufficient RHOA<sup>G17V&F25L</sup> protein produced to carry out any further analysis. The other proteins were diluted to 1mg/ml and 200µl added to the CD cuvette to perform CD spectroscopy and melting curve analysis. The curves of each construct follow a similar pattern consistent with the presence of an α-helix (Figure 3-2). This is in keeping with the known structure of RHOA<sup>WT</sup>.

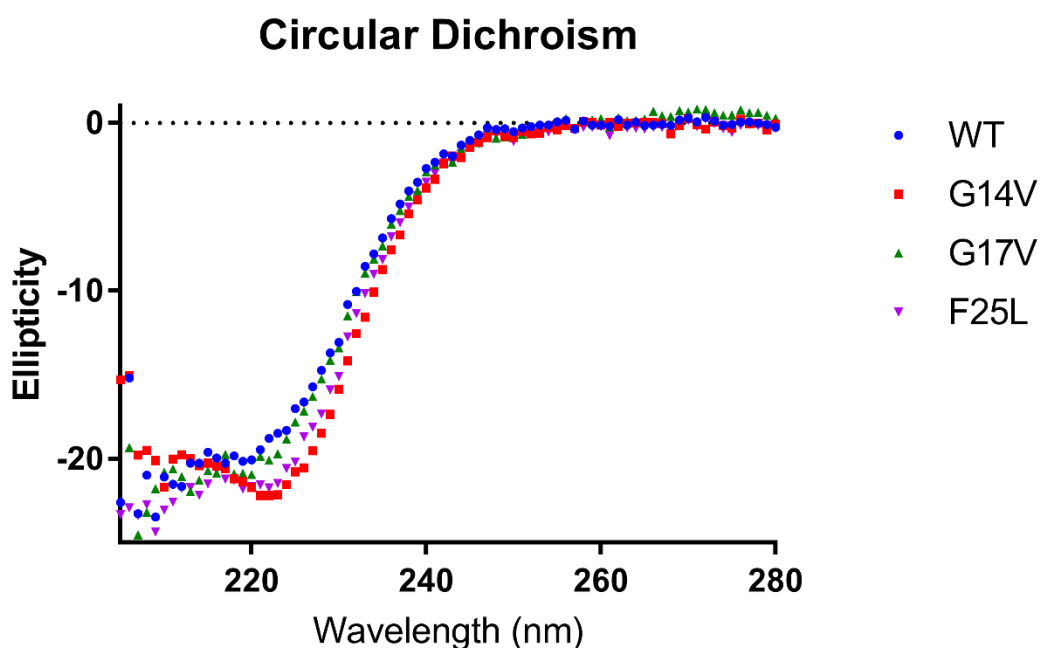


**Figure 3-2: Circular dichroism curves for RHOA constructs.**

The ellipticity is shown against the light wavelength from 210nm – 280nm for the four RHOA constructs as shown in the legend to the right of the graph. RHOA<sup>WT</sup> is shown by blue circles, RHOA<sup>G14V</sup> by red squares, RHOA<sup>G17V</sup> by green triangles and RHOA<sup>F25L</sup> by purple triangles. The curves shown are the mean of 3 spectra with the baseline buffer spectrum subtracted.

After obtaining the CD spectrum the protein was denatured by melting and a melting curve produced taking three measurements at a wavelength of 220nm at each degree change between 22°C and 90°C. The constructs all denature with rising temperatures (Figure 3-3). The melting temperature of each protein is the temperature at which 50% of the protein is unfolded. RHOA<sup>WT</sup> remains folded at higher temperatures than the

RHOA-mutant constructs suggesting increased stability of the WT *in vitro* proteins (Table 3-1).

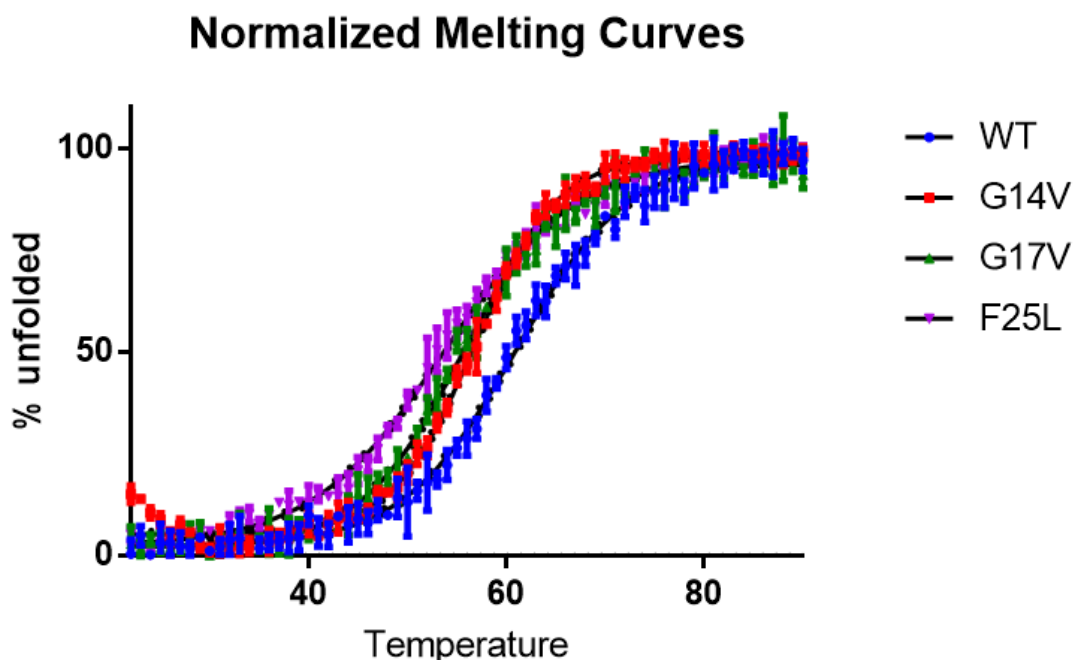


**Figure 3-3: Normalised melting curves of RHOA constructs.**

Melting curves showing the proportion of unfolded protein at each degree of temperature between 22°C and 90°C for the RHOA constructs as shown in the legend to the right of the graph. Each point represents the mean of 3 readings with the error bars showing the standard deviation. RHOA<sup>WT</sup> is shown by blue circles, RHOA<sup>G14V</sup> by red squares, RHOA<sup>G17V</sup> by green triangles and RHOA<sup>F25L</sup> by purple triangles.

Protein	Melting temperature (°C)	95% confidence (°C)
RHOA <sup>WT</sup>	60.9	60.6-61.3
RHOA <sup>G14V</sup>	56.8	56.6-57.0
RHOA <sup>G17V</sup>	55.4	55.1-55.8
RHOA <sup>F25L</sup>	53.7	53.3-54.0

**Table 3-1: Melting temperatures of RHOA constructs.**

Calculated from triplicate readings from one protein construct.

Taken together, these results show reduced expression of RHOA<sup>G17V</sup> and RHOA<sup>G17V&F25L</sup> by a bacterial system when compared to RHOA<sup>WT</sup>, RHOA<sup>G14V</sup> and RHOA<sup>F25L</sup>. The four constructs analysed all showed similar structure with the presence of an  $\alpha$ -helix. There is a suggestion that the mutant proteins may be less stable than the RHOA<sup>WT</sup> proteins.

### 3.3 MAMMALIAN EXPRESSION OF RHOA PROTEINS

Next, to assess the protein expression in mammalian cells, HEK293T cells were transfected with plasmids encoding FLAG-RHOA proteins using PEI as described in section 2.4.2. A total of 5 plasmids were used for transfection and one flask was treated with transfection agent but no plasmid to act as an untransfected control. Following a period of incubation, the cells were lysed and protein extracted. An equal amount of total protein from each cell population was loaded into a PAGE-gel for protein electrophoresis and immunoblotting, GAPDH was used as an additional loading control.

Immunoblotting was performed for RHOA, FLAG and GAPDH as described in section 2.3.6. Due to the similarity in size of the proteins the membrane was stained with each antibody before being stripped and restained with the next antibody.

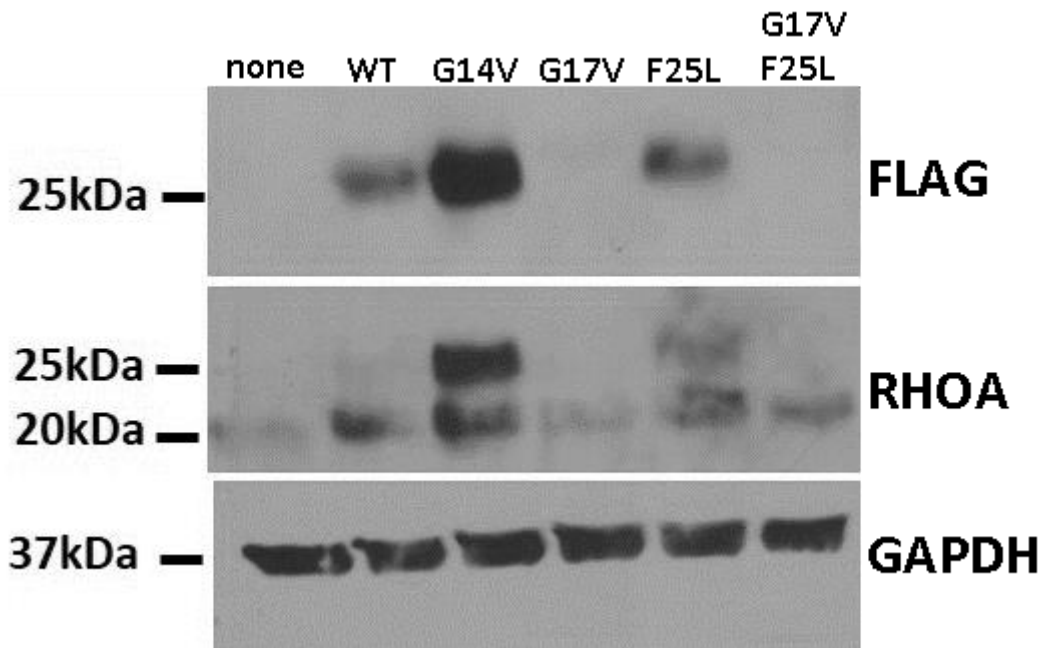


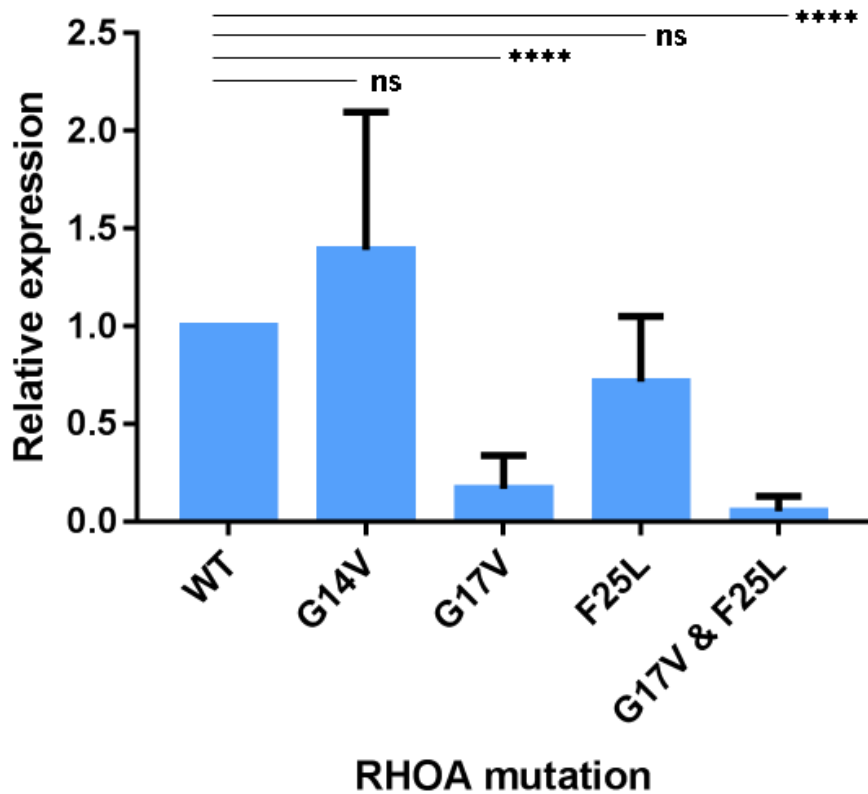
**Figure 3-4: Representative Western blots showing FLAG, RHOA and GAPDH.**

The upper panel shows the detection of the FLAG-RHOA protein. The middle panel shows the detection of the endogenous RHOA protein at 21kDa and the FLAG-RHOA protein at ~25kDa. The lower panel shows the detection of the GAPDH loading control. Lane 1 contains protein from untransfected cells, lane 2 from FLAG-RHOA<sup>WT</sup> transfected cells, lane 3 from FLAG-RHOA<sup>G14V</sup> transfected cells, lane 4 from FLAG-RHOA<sup>G17V</sup> transfected cells, lane 5 from FLAG-RHOA<sup>F25L</sup> transfected cells and lane 6 from FLAG-RHOA<sup>G17V&F25L</sup> transfected cells.

ImageJ was used to analyse the images and assess the relative amount of FLAG-RHOA produced compared to the FLAG-RHOA<sup>WT</sup> transfected cells after controlling for the total protein using the GAPDH loading control. There were higher amounts of RHOA<sup>G14V</sup> expressed compared to RHOA<sup>WT</sup> with lower amounts of RHOA<sup>F25L</sup> and RHOA<sup>G17V</sup>. There were very small amounts of RHOA<sup>G17V&F25L</sup> expressed (Figure 3-4 & Figure 3-5A).

These differences in expression were consistent across several experiments (n=8) and several of the comparisons reached statistical significance (Figure 3-5). As seen in the bacterial system there is a lower expression of RHOA<sup>G17V</sup> (as a single mutation or in combination with a second mutation) when compared to RHOA<sup>WT</sup>, RHOA<sup>G14V</sup> and RHOA<sup>F25L</sup>. The expression of RHOA<sup>G14V</sup> appears to be higher than the expression of RHOA<sup>WT</sup> but this does not reach statistical significance.

## A Protein expression relative to RHOA-WT



## B

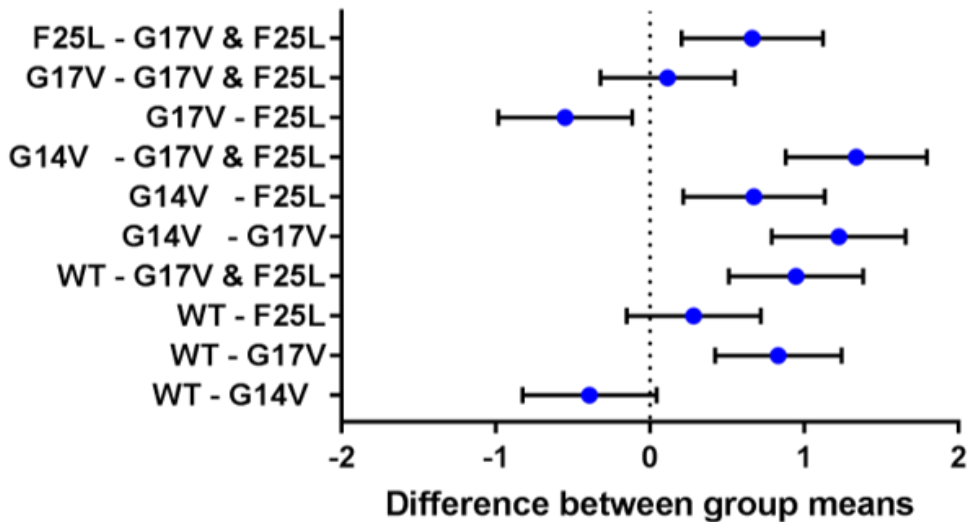


**Figure 3-5: Graph showing the relative expression of FLAG-RHOA protein by HEK293 cells.**

A- Bars represent the relative expression of FLAG-RHOA protein compared to the FLAG-RHOA-WT transfected cells after controlling for amount of protein loaded. The error bars represent the standard deviation (for WT and G17V  $n=10$ , for G14V, F25L and G17V&F25L  $n=8$ ). B- results of one-way ANOVA analysis with Tukey correction for multiple analyses showing the difference in the means of the expression of the two constructs (blue dot) and the 95% confidence intervals (error bars)

### 3.4 ASSESSMENT OF RHOA ACTIVITY

The proportion of RHOA-GTP was used as a marker of RHOA activity as this represents the active form of RHOA. HEK293 cells were transfected with the FLAG-RHOA plasmids as before. To perform the pulldown assay GST-Rhotekin was prepared and bound to glutathione agarose beads as described in section 2.4.6 (Figure 3-6). 48 hours after transfection the HEK293 cells were lysed using a magnesium containing lysis buffer on ice to prevent hydrolysis of the GTP bound to RHOA by Rho-GAPs during the cell lysis and subsequent processing. A small volume of whole cell lysate was taken to assess for total FLAG-RHOA and the remaining was incubated with the agarose carrying GST-Rhotekin.

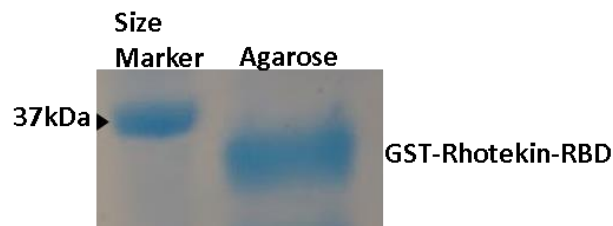


**Figure 3-6: Coomassie stained gel showing the GST-Rhotekin-RBD.**

*The Coomassie stained gel shows the GST-Rhotekin-RBD from a sample of the agarose with the expected size of ~35kDa.*

The whole cell lysates and the agarose were then loaded onto a gel for protein electrophoresis. GAPDH was used as a loading control for the whole cell lysate. The same volume of agarose was loaded for each sample. Figure 3-7 shows a Western blot which again demonstrates differences in expression of FLAG-RHOA depending upon the presence of mutations. This makes assessment of the proportion of activated RHOA difficult – particularly for the proteins expressed at the lowest level.

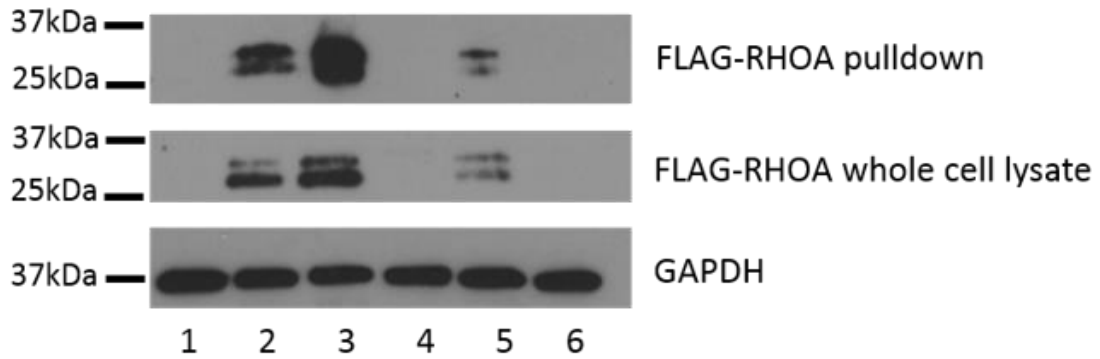


**Figure 3-7: Representative Western blot showing the results of the active RHOA pulldown.** The upper panel shows the detection of FLAG-RHOA bound to GST-Rhotekin agarose and representing the active GTP-bound RHOA. The central panel shows the total FLAG-RHOA in the cell lysate. The lower panel shows the detection of the GAPDH loading control from the whole cell lysate. Lane 1 contains protein from untransfected cells, lane 2 from FLAG-RHOA<sup>WT</sup> transfected cells, lane 3 from FLAG-RHOA<sup>G14V</sup> transfected cells, lane 4 from FLAG-RHOA<sup>G17V</sup> transfected cells, lane 5 from FLAG-RHOA<sup>F25L</sup> transfected cells and lane 6 from FLAG-RHOA<sup>G17V&F25L</sup> transfected cells.

Figure 3-8 shows the combined results of 2 experiments and shows that a higher proportion of the FLAG-RHOA<sup>G14V</sup> is active and GTP bound when compared to FLAG-RHOA<sup>WT</sup> which is consistent with previous work suggesting that it is an activating mutation. The presence of an F25L or G17V mutation leads to a lower proportion of active RHOA and the combined mutation leads to such low levels of protein expression that it was not possible to assess the proportion of active RHOA.

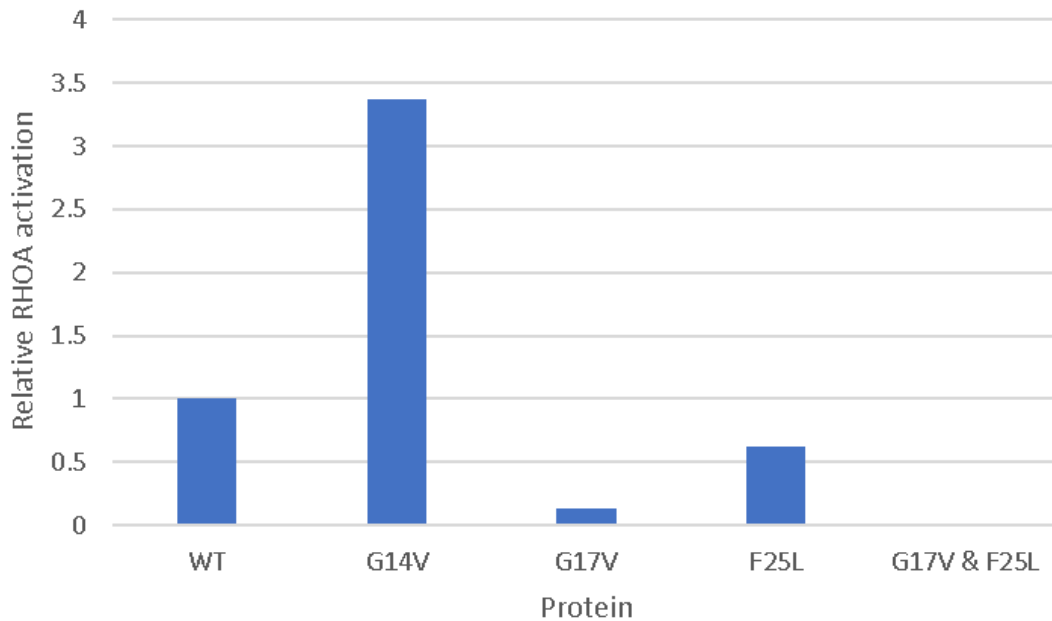


**Figure 3-8: Relative activation of RHOA compared to RHOA<sup>WT</sup>.**  
 Graph showing the relative level of RHOA activation compared to RHOA<sup>WT</sup>. (n=2)

### 3.5 DISCUSSION

The presence of point mutations in RHOA which have been discovered in cases of AITL and PTCL-NOS which lead to the substitution of a single amino acid. The mutations appear to influence the protein structure and in the cases of mutations found in AITL and PTCL-NOS (RHOA<sup>G17V</sup> and RHOA<sup>F25L</sup>) they lead to reduced expression and activation. Other groups have also found that the exogenous expression of RHOA<sup>G17V</sup> was lower than of RHOA<sup>WT</sup> in various cell lines (99,143). Although we have not excluded the possibility that RHOA<sup>G17V</sup> may be found in inclusion bodies in bacteria and not be found in the lysate this seems less likely as the result mirrors that seen in the mammalian system.

Both G17V and F25L mutations lead to reduced exogenous expression of RHOA and reduced GTP binding. It remains unclear how this leads to the development of AITL.

The substitution of valine for glycine at amino acid 17 occurs within the GTP-binding site and is likely to alter the interaction between RHOA, GDP and GTP as demonstrated by

this work and others (97-99). The bulkier amino acid may also alter the stability of RHOA folding leading to the apparent reduced expression seen in this work (Figure 3-9).

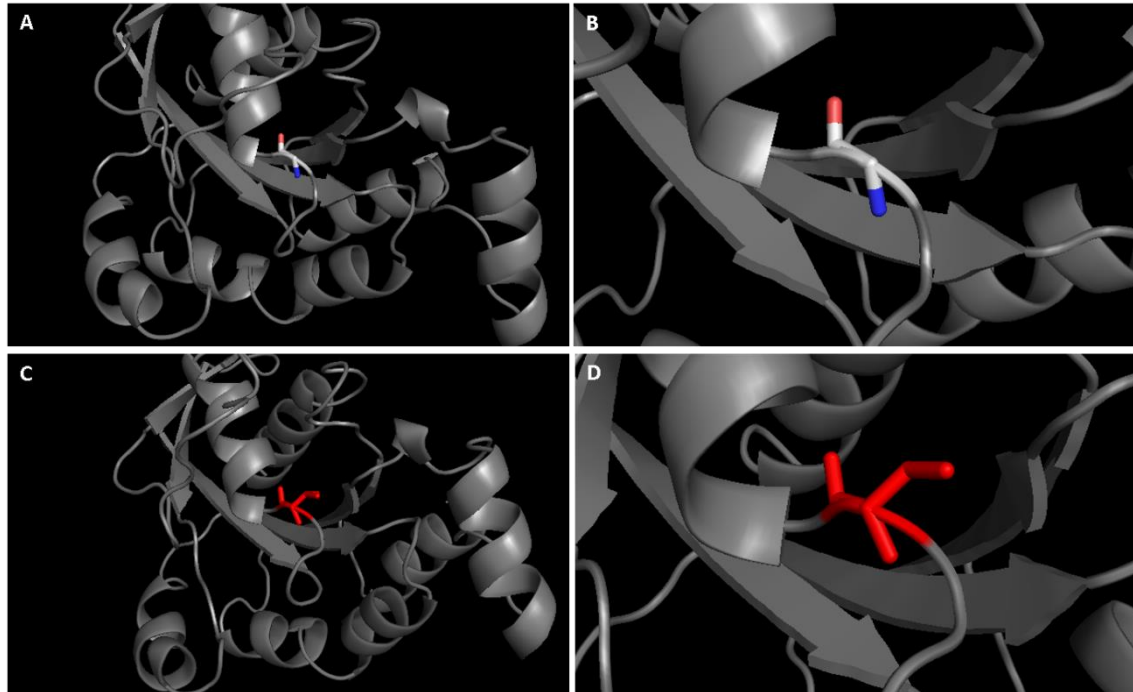


**Figure 3-9: Representation of RHOA generated in PYMOL.**

(A & B) show the WT protein with Gly highlighted at amino acid position 17. (C & D) show the G17V mutated protein with Val highlighted at amino acid position 17.

The substitution of leucine for phenylalanine at amino acid 25 is not with the GTP binding site but in the WT protein there is an interaction between this amino acid and the phenylalanine residue at position 171 (Figure 3-10). The alteration in the side chain may alter the interaction between these amino acids leading to disruption of the  $\alpha$ -helix and reduced protein stability.

Further assessment of the cause for reduced expression could be carried out using proteasome inhibitors to reduce protein breakdown in the cell to assess if this led to higher expression of the mutated protein.

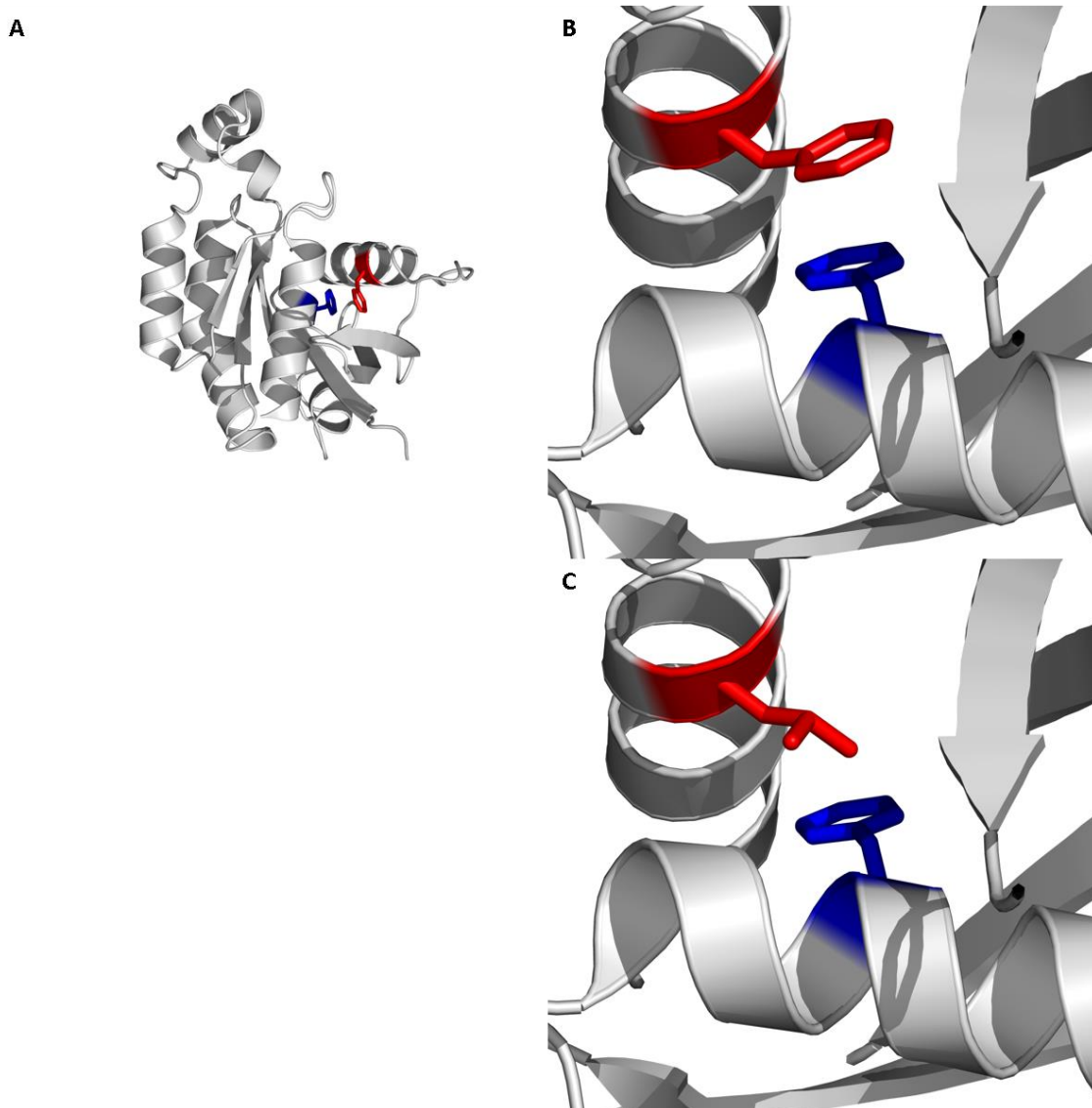


**Figure 3-10: Representation of RHOA generated by Louise Fairall in PYMOL.**

(A) WT RHOA with amino acids 25 (Phe) and 171 (Phe) highlighted in red and blue respectively. (B & C) show the interaction between amino acid 25 in the WT (B) and F25L-mutated (C) forms of RHOA demonstrating the change in side chain between Phe and Leu at amino acid position 25.

Further assessment of the effect of the mutations on cell phenotype could be achieved using CRISPR/Cas9 techniques to introduce the point mutations and assess the effect of heterozygous and homozygous mutations on the cell behaviour at endogenous expression levels.

## 4 CHARACTERISATION OF THE SAN ROQUE MOUSE MODEL

---

### 4.1 INTRODUCTION TO THE MODEL

As described in section 1.10 a proportion of mice with a heterozygous point mutation in the Roquin gene develop lymphadenopathy between 6 and 12 months of age. Work published by Ellyard et al (176) has described some of the features of this model. We have carried out work to confirm their findings in our colony and gain a better understanding of the model. Throughout the chapter Roquin<sup>san/+</sup> mice are referred to as SRQ mice and littermate control Roquin<sup>+/+</sup> mice as WT mice, at no point did our work involve Roquin<sup>san/san</sup> mice.

### 4.2 THE SAN ROQUE COLONY

Over the course of the work we assessed the proportion of mice developing enlarged lymph nodes. In our colony 74 of 240 mice over 100 days old (31%) developed lymphadenopathy. Of those developing lymphadenopathy 65% were female and 35% were male, as was seen in the original description of these mice (176). There were a few cases in which mice were found to have enlarged lymph nodes by palpation which subsequently reduced in size spontaneously. Figure 4-1 shows an example of enlarged lymph nodes and normal lymph nodes dissected from a mouse found to have bilateral axillary lymph node enlargement.

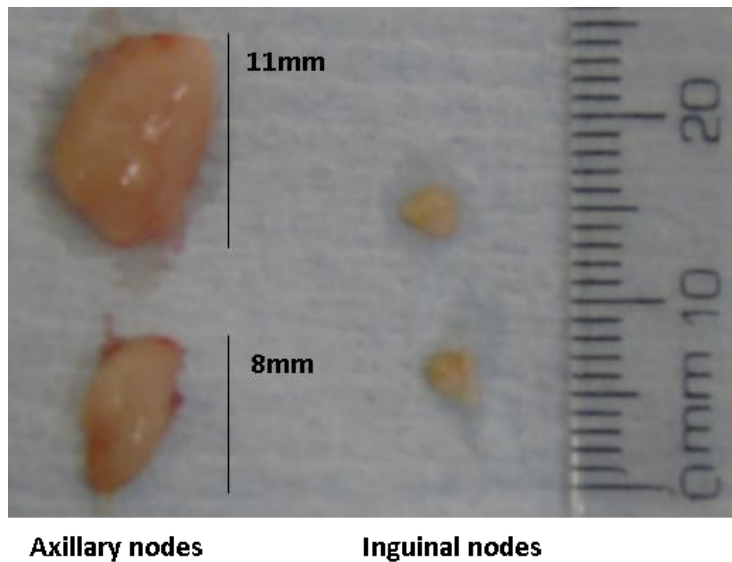


**Figure 4-1: Lymph nodes extracted from SRQ5211.**

The enlarged axillary lymph nodes are shown on the left and the normal inguinal lymph nodes on the right.

Sections from an enlarged lymph node showed an absence of normal germinal centres and infiltration with larger cells (Figure 4-2).

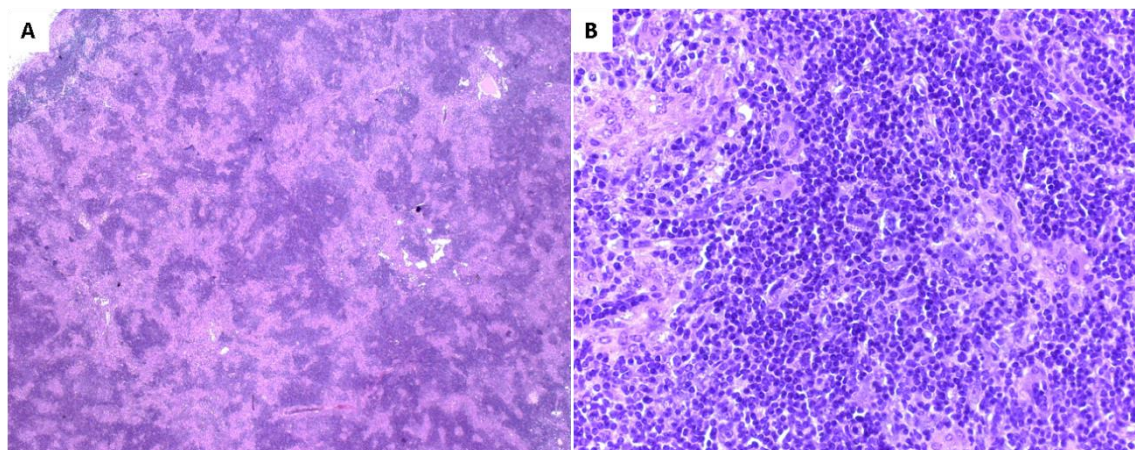


**Figure 4-2: Haematoxylin and eosin stained sections of an enlarged axillary lymph node**

(staining performed by S Mamand). (A) shows a section at x2.5 magnification and (B) a section at x40 magnification.

### 4.3 FLOW CYTOMETRY ASSESSMENT

Ellyard et al showed flow cytometric analysis of normal lymph nodes from SRQ and WT mice and tumour lymph nodes from SRQ mice. In this section analysis of cell content will be carried out to compare 1) spleens from wild-type and SRQ mice without tumours 2) normal lymph nodes from SRQ mice without tumour development and enlarged lymph nodes and 3) paired comparisons of enlarged lymph nodes and spleen.

#### 4.3.1 Comparison of SRQ and WT spleens

To assess differences in cell composition between the SRQ and WT spleens we carried out flow cytometry of cell suspensions produced from the spleens (Figure 4-3). T-tests with correction for multiple analyses show that the lymphocyte composition of the spleens was the same in WT and SRQ mice with similar proportions of B cells ( $p=0.3$ ),  $CD4^+$  T cell ( $p=0.7$ ) and  $CD8^+$  T cells ( $p=0.1$ ) ( $n=21$ ). However, there was a difference in the  $CD4^+$  subsets with an increased proportion of Tfh cells seen in the SRQ spleen compared to the WT spleen ( $p<0.0001$ ;  $n=21$ ).

These findings show that the differences in the WT and SRQ spleens are found in the  $CD4^+$  T cell subsets. The Tfh cells make up only a small proportion of the total  $CD4^+$  T cells in both populations. The proportion of B cells seen in the WT mouse population is higher than typically reported for mouse spleens at 60% compared to 45-50%.

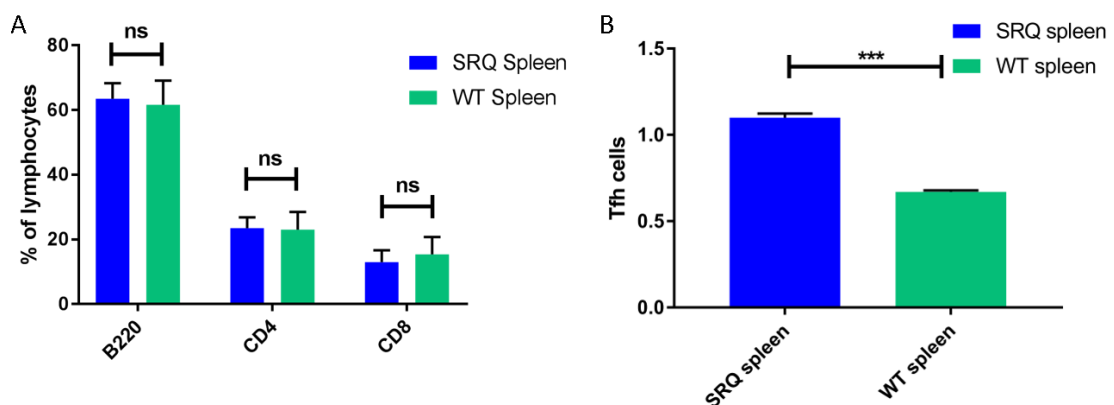


**Figure 4-3: FACS assessment for lymphocyte subsets in WT and SRQ spleens.**

Bars represent the mean subset percentage of the total lymphocyte population ( $n=21$ ) and the error bars standard deviation. A- shows the percentage of each lymphocyte subset of the total lymphocyte population. B- shows the percentage of Tfh cells from the  $CD4$  cell population.

#### 4.3.2 Assessment of lymph nodes

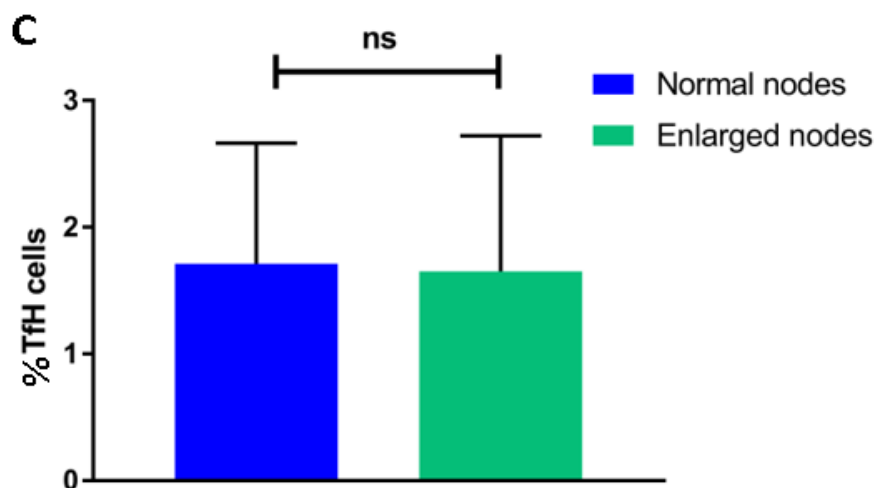
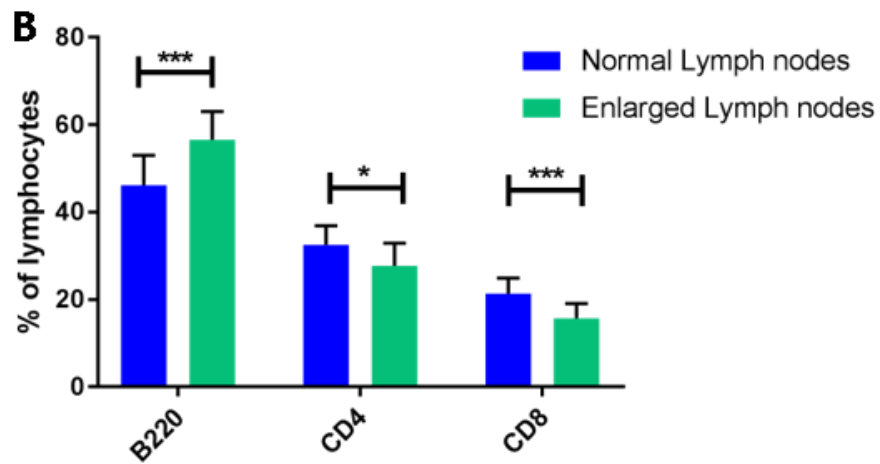
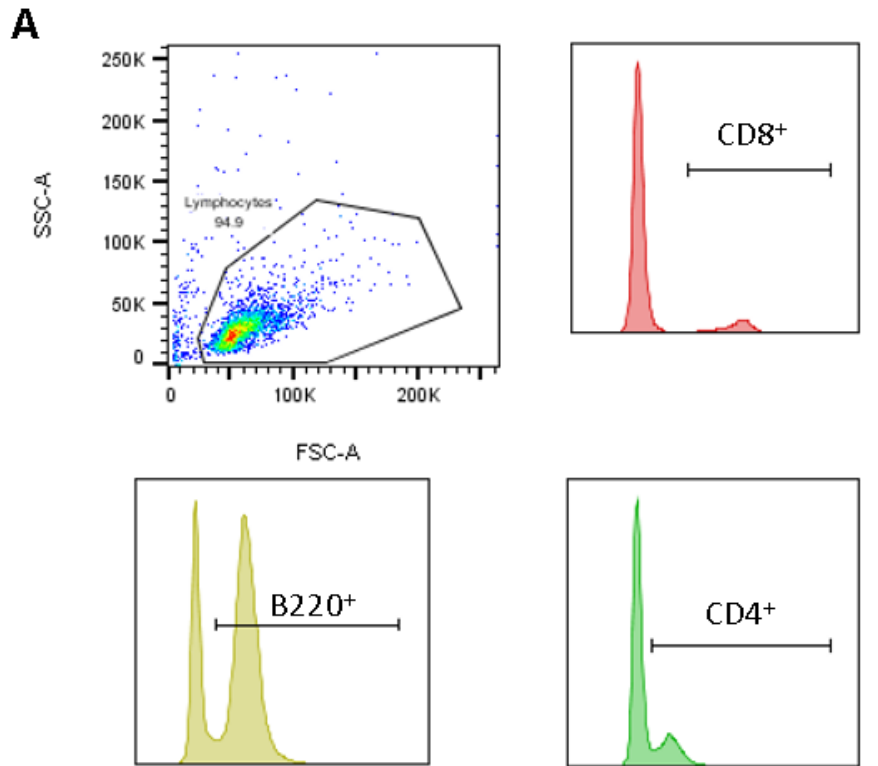
To confirm the findings of Ellyard et al (176) we carried out flow cytometry of tumour and normal lymph nodes from a number of SRQ mice. The proportion of B220 positive cells, CD4 positive cells and CD8 positive cells was measured from the lymphocyte population (Figure 4-4 A). In keeping with Ellyard et al (176), we found that the tumour lymph nodes had an increased proportion of B cells ( $p=0.0003$ ) with a reduction in both CD4<sup>+</sup> ( $p=0.014$ ) and CD8<sup>+</sup> ( $p=0.0002$ ) proportions (Figure 4-4B) when analysed by t-tests with correction for multiple analyses. Similar proportions of B cells (40-50%) and T cells (CD4<sup>+</sup> 30-40% & CD8<sup>+</sup> 20-25%) were found in the lymph nodes from the WT mice which is consistent with the values seen in the paper from Ellyard et al (176) but demonstrates a higher proportion of B cells than typically reported in murine lymph nodes.

We assessed the Tfh proportion of cells using high PD1 and CXCR5 expression on CD4<sup>+</sup> lymphocytes (Figure 4-6 A shows an example of the gating strategy). We found that the proportion of CD4<sup>+</sup> T cells which we defined as Tfh cells was not significantly different between the normal and enlarged lymph nodes (Figure 4-4 C) when analysed by t-test with correction for multiple analyses. However, as the enlarged lymph nodes had an increased number of cells the total number of Tfh cells was higher in the enlarged nodes.

These findings are consistent with those shown by Ellyard et al (176) and the suggestion that these tumours have features similar to AITL. The presence of a malignant Tfh population is thought to lead to an excess of B cells through increased germinal centre activity and abnormal B cell help.

**Figure 4-4: FACS to determine lymphocyte subset proportions in normal and tumour lymph nodes in SRQ mice (page 84)**

*A- gating strategy to select lymphocytes and then histograms showing separation of positive and negative cells from a representative sample. B- chart showing the mean percentage of each cell type from the total lymphocyte population with the error bars showing the standard deviation (normal nodes  $n=12$ ; tumour nodes  $n=17$ ). C- chart showing the mean % of Tfh cells from the CD4 cell population with the error bars representing standard deviation ( $n = 5$ ).*



### 4.3.3 Paired comparison of tumour lymph nodes and spleen

To further characterise the lymphoid populations in the mice we assessed the cellular composition of spleens in the SRQ mice and compared this to the composition of the tumours. Four mice with tumours were selected and cell suspensions produced from the spleen and tumours.

#### 4.3.3.1 Lymphocyte subsets

A sample of the cell suspension was used for flow cytometry to assess the B cell, CD4<sup>+</sup> T cell and CD8<sup>+</sup> T cell proportions. This showed that the B cell proportion was similar between the spleen and enlarged lymph node but with a slightly higher CD4<sup>+</sup> cell proportion in the spleen ( $p = 0.02$ ) and consequent lower CD8<sup>+</sup> cell proportion ( $p = 0.003$ ) when analysed by t-tests with correction for multiple comparisons (Figure 4-5).

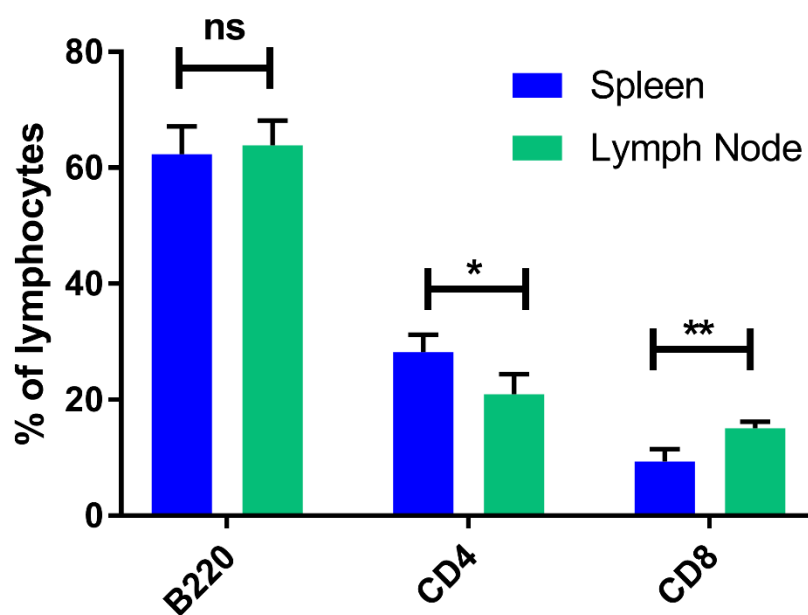


**Figure 4-5: Lymphocyte subsets in paired spleen and enlarged lymph node samples.**

Chart showing the mean percentage of each lymphocyte subset from the total lymphocyte population with the error bars representing standard deviation ( $n=4$ )

#### 4.3.3.2 *Tfh population*

After separation from total splenocytes or total lymph nodes, CD4<sup>+</sup> T cells were analysed by FACS to 1) determine the purity of the separation and 2) the Tfh proportion as assessed by measuring the PD1<sup>hi</sup>CXCR5<sup>hi</sup> population (Figure 4-6 A). There was a higher proportion of Tfh cells found in the spleens than the lymph nodes of these mice ( $p=0.007$ ) which is reflected in the higher expression of PD1 ( $p=0.03$ ) although there was no significant difference in the CXCR5 expression ( $p=0.100$ ) (Figure 4-6 B & Figure 4-6 C). Significance was calculated by t-tests with a correction for multiple comparisons.

This demonstrates that there are differences in composition between the enlarged lymph nodes and spleens. The majority of the lymphocytes in both tissues are B cells but there are slight differences in the proportion of CD4<sup>+</sup> and CD8<sup>+</sup> T cells. Within the CD4<sup>+</sup> T cell population there was higher expression of PD1 in the cells from the spleen and a consequent increase in the Tfh population defined as PD1<sup>hi</sup>CXCR5<sup>hi</sup>. However, these enlarged nodes showed a lower proportion of Tfh cells than those used in the comparison with normal lymph nodes which is difficult to explain.

Tfh cells generally make up less than 0.5% of CD4<sup>+</sup> T cells in normal mouse spleens and lymph nodes (219) so these results do show an increase in Tfh proportions in the SRQ mice compared to normal mice.

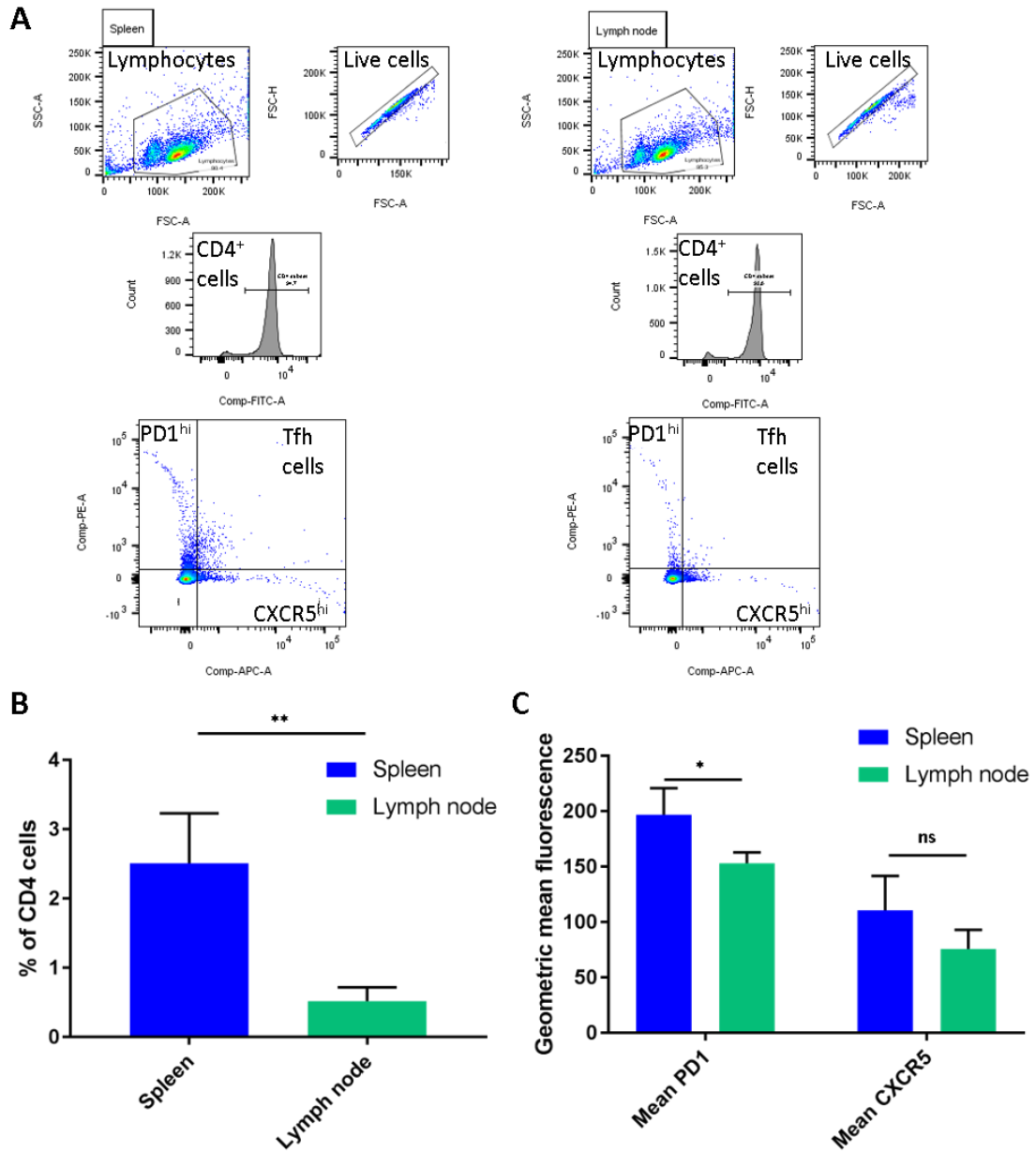


**Figure 4-6: FACS assessment for Tfh populations in spleen and tumour pairs.**

A- shows representative FACS plots and gating strategies for the spleens (left) and lymph nodes (right) from the SRQ mice analysed. Following the lymphocyte gate doublets were excluded and the CD4 population gated. The CD4 population was plotted with CXCR5-APC expression on the x-axis and PD1-PE expression on the y-axis. A quadrant gate was used to select the PD1<sup>hi</sup>CXCR5<sup>hi</sup> population representing Tfh cells. B- shows the mean proportion of Tfh cells as a percentage of CD4 cells (n=4) with error bars representing standard deviation. C- shows the geometric mean fluorescence of PD1-PE and CXCR5-APC from the CD4 cell population (n=4) with error bars representing standard deviation.

#### 4.4 T CELL CLONALITY

Overall while there are differences in cell composition between normal and enlarged lymph nodes these are subtle and in particular there is no major increase in T<sub>H</sub> cell fraction in enlarged lymph nodes. It was, therefore, necessary to assess for the presence of T cell clones in lymph nodes using spectratyping as described in section 2.5.19 in a selection of SRQ mice. We detected three cases in which there was a consistent clonal peak found across different enlarged lymph nodes and in two cases the same peak was seen in non-enlarged lymph nodes. The presence of T cell clones was detected by spectratyping in 7 of 12 mice.

Figure 4-7 shows representative examples of results from 2 mice. SRQ 5283 had enlarged right axillary and bilateral inguinal lymph nodes. A peak was seen at 180bp in all three lymph nodes, this was particularly marked in the left inguinal node but was present in the others with an increase in polyclonal background.

This is consistent with Ellyard et al (176) who showed the presence of a T cell clone in a high proportion of mice carrying enlarged lymph nodes. We have also demonstrated the presence of a consistent clone within different enlarged nodes of the same mouse suggesting that the malignant clone only arises once.

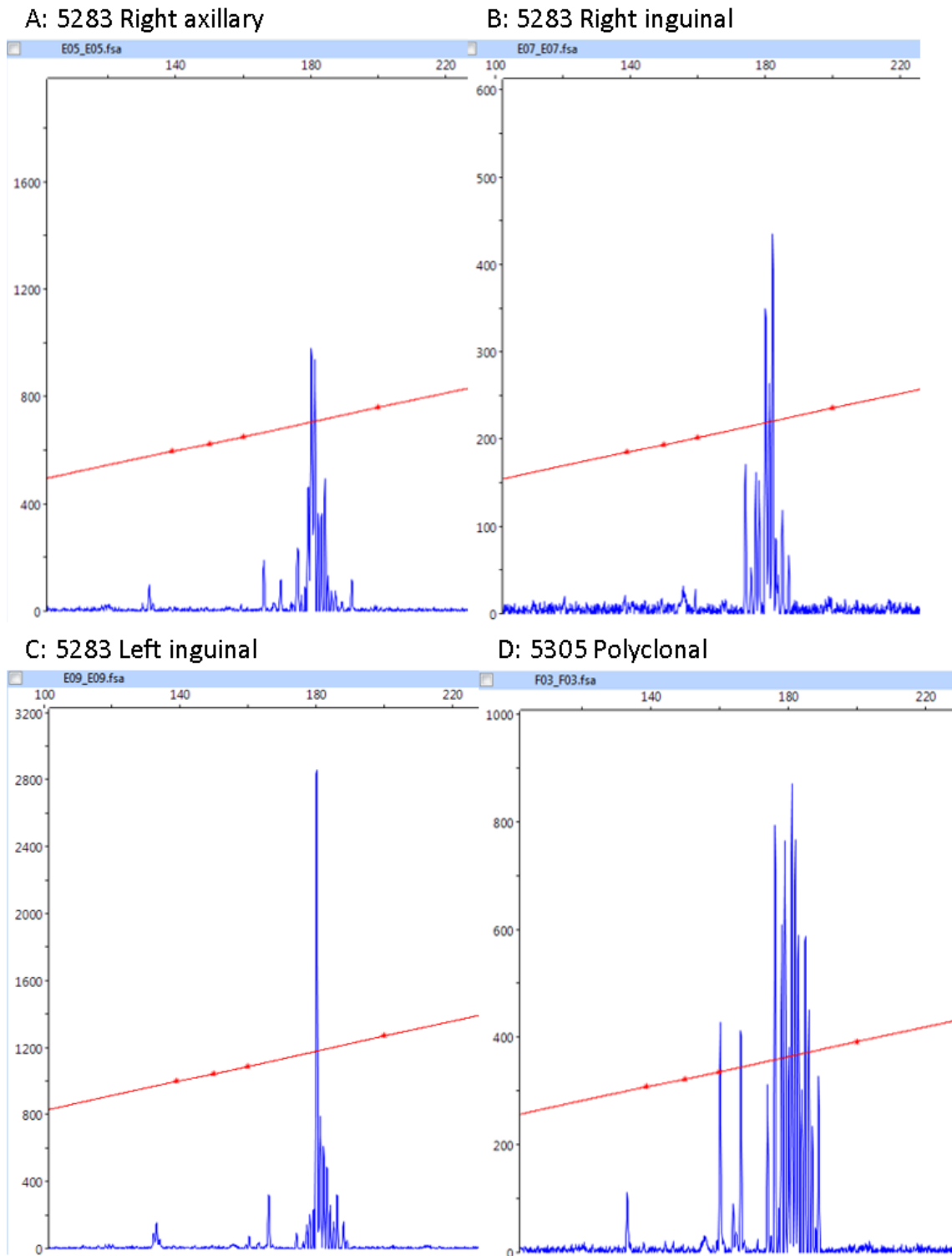


**Figure 4-7: TCR spectratyping results of V2-J PCR products.**

Panels A-C show the results from three enlarged lymph nodes from SRQ5283 with a consistent peak at approximately 180bp, this is on a polyclonal background in the right axillary and inguinal lymph nodes. Panel D shows the results from the enlarged right inguinal lymph node with polyclonal T cells demonstrated. The red line represents the size standards.

## 4.5 IN VITRO CHARACTERISATION

Experiments were performed to characterise the response of CD4<sup>+</sup> T cells from both WT and SRQ mice to stimulation and treatment in culture. For all culture experiments the CD4<sup>+</sup> T cells were isolated from spleens or tumour lymph nodes of the SRQ mice and from spleens of the WT mice as described in section 2.5.8.

As discussed in section 1.9 ITK is an important molecule in T cell activation and signalling. We used ibrutinib as an ITK inhibitor in the CD4<sup>+</sup> T cell population in culture to demonstrate its effect upon cell survival and differentiation after stimulation.

### 4.5.1 CD4<sup>+</sup> T cell ITK expression

Firstly, we assessed the expression of ITK in CD4<sup>+</sup> T cells isolated from SRQ and WT mouse spleens using Western blots for ITK and GAPDH. This demonstrated that ITK was expressed by CD4<sup>+</sup> T cells in SRQ and WT mice, in this single experiment the expression of ITK was slightly lower in the SRQ cells when adjusted for GAPDH expression (Figure 4-8).

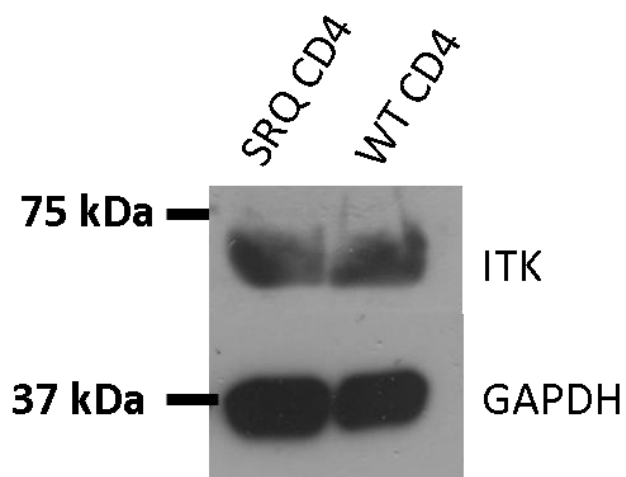


**Figure 4-8: Western blot showing expression of ITK in SRQ and WT mice**

*ITK is shown at approximately 72kDa and GAPDH at approximately 36kDa. Protein from SRQ CD4 cells is on the left and WT CD4 cells on the right as labelled.*

#### 4.5.2 T cell stimulation and ITK inhibition

Subsequently, to assess the effect of ITK inhibition, using ibrutinib, upon stimulation of CD4<sup>+</sup> T cells in culture with anti-CD3 and anti-CD28 viability and proliferation were measured using an ATP luminescence method as described in section 2.5.13.

##### 4.5.2.1 Ibrutinib treatment of CD4<sup>+</sup> T cells

First, we determined an appropriate concentration of ibrutinib to use for further experiments. CD4<sup>+</sup> T cells from SRQ spleens were cultured with anti-CD3 and anti-CD28 stimulation in a range of ibrutinib concentrations (0 – 50µM). A concentration of 2.5µM ibrutinib was selected for further experiments as this concentration led to reduced cell viability but did not kill all the cells (Figure 4-9), the mean relative luminescence at 2.5µM was 81%.

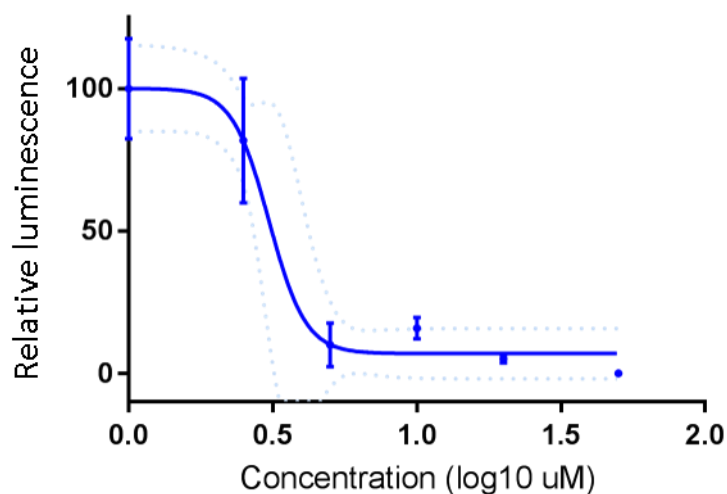


**Figure 4-9: Response curve showing effect of ibrutinib treatment on stimulated CD4<sup>+</sup> T cells.**

The x-axis shows the concentration (log<sub>10</sub> µM) and the y-axis the luminescence relative to cells treated with vehicle alone. The points represent the mean (n=3) and error bars the standard deviation with the lines representing the standard curve with the 95% confidence intervals shown by the dotted lines.

#### 4.5.2.2 WT vs SRQ CD4<sup>+</sup> T cells from spleen

Experiments to compare the difference between CD4<sup>+</sup> T cells extracted from the spleens of WT and SRQ mice were performed. This enabled assessment of the response to stimulation and any difference in the effect of ITK inhibition.

After extraction and purification from the spleens of WT and SRQ mice CD4<sup>+</sup> T cells were cultured as described in section 2.5.12. Stimulated CD4<sup>+</sup> T cells from both WT and SRQ mice showed increased viability represented by increased luminescence compared to unstimulated cells (SRQ p=0.0015, WT p < 0.0001) using a two-way ANOVA with Tukey's multiple comparison test. In both cases the addition of ibrutinib reduced the effect of stimulation (SRQ p=0.0308, WT p < 0.0001) (Figure 4-10).

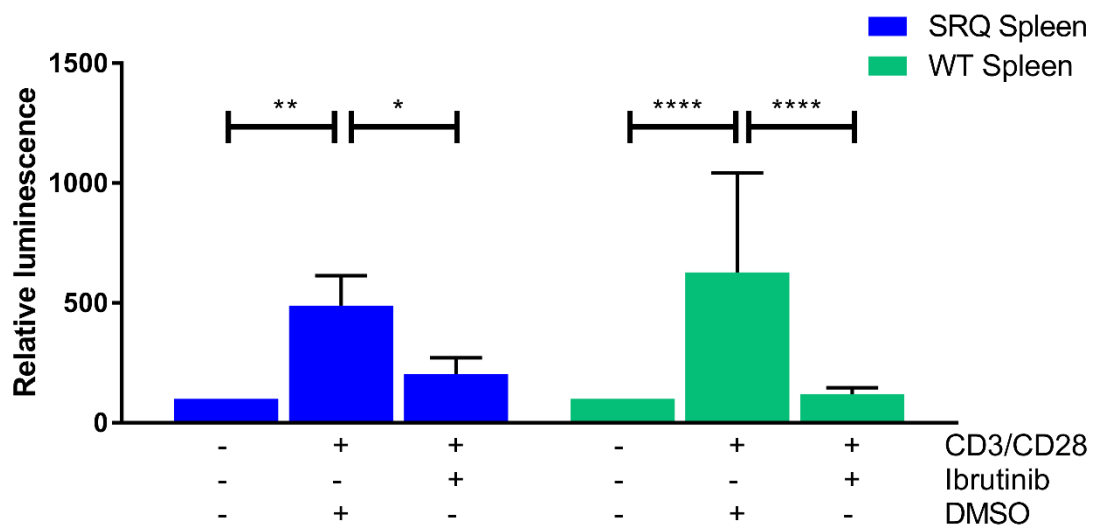


**Figure 4-10: Effect of stimulation and treatment on splenic CD4<sup>+</sup>T cells.**

Graph showing the relative luminescence of unstimulated cells (100) and cells which have been stimulated with or without ibrutinib treatment. Bars represent the mean and error bars the standard deviation (WT n= 10, SRQ n= 7)

#### 4.5.2.3 Paired spleen and tumour samples

Next experiments to determine the effect of ITK inhibition on CD4<sup>+</sup> T cells from enlarged lymph nodes were performed. The effect of stimulation with anti-CD3 +/- anti-CD28

was assessed and compared to the effect in the spleen from the same mouse. The effect of ITK inhibition on cells stimulated with anti-CD3 and anti-CD28 was measured.

CD4<sup>+</sup> T cells were purified from the enlarged lymph nodes and spleens of four SRQ mice with tumours. The cells were then cultured with stimulation in the presence or absence of ibrutinib treatment (2.5µM) for 48 hours.

When compared to unstimulated cells the cells stimulated with anti-CD3 +/- anti-CD28 showed an increase in luminescence suggesting increased cell viability. This increase was less in the presence of ibrutinib. Paired t-tests with correction for multiple comparisons showed no significant differences between the responses of CD4<sup>+</sup> T cells from spleens or tumours (Figure 4-11).

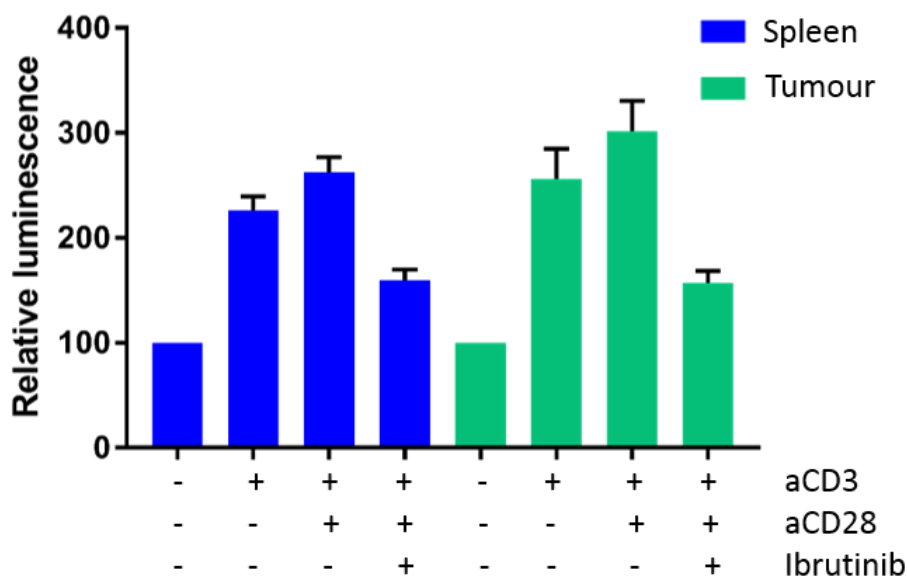


**Figure 4-11: Graph showing effect of stimulation and ibrutinib treatment on CD4<sup>+</sup> T cells from SRQ spleens and tumours.**

Bars represent the mean relative luminescence compared to unstimulated cells (n=4; blue-spleen; green-tumour) and the error bars the standard deviation. The culture conditions are described on the x-axis.

These experiments show that in the presence of an ITK inhibitor (ibrutinib) the effect of CD4<sup>+</sup> T cell stimulation with anti-CD3 and anti-CD28 is reduced. This is consistent across WT CD4<sup>+</sup> T cells and SRQ CD4<sup>+</sup> T cells isolated from spleens and enlarged lymph nodes.

### 4.5.3 Interleukin stimulation and proliferation

Work on human T cell lines and primary patient T cells in our laboratory (220) showed that ITK inhibition affected the differentiation of CD4<sup>+</sup> T cells in response to cytokine stimulation. The addition of cytokines to T cell culture altered the proportion of CD4<sup>+</sup> T cell subsets and showed CD4<sup>+</sup> T cell plasticity as discussed in section 1.3.2. IL-21 is established as an important cytokine in Tfh differentiation, it is also secreted by Tfh cells (221,222). IL-12 has been shown to induce IL-21 expression in CD4<sup>+</sup> T cells and play a role in Tfh differentiation (223,224).

Firstly, we assessed the effect of ibrutinib on Tfh differentiation of CD4<sup>+</sup> T cells in the presence of IL-12 and/or IL-21 in culture. Then, we assessed the effect of IL-12 and IL-21 on the differentiation and proliferation of CD4<sup>+</sup> Tfh cells from WT and SRQ mice in culture. The experiment is described in section 2.5.14.

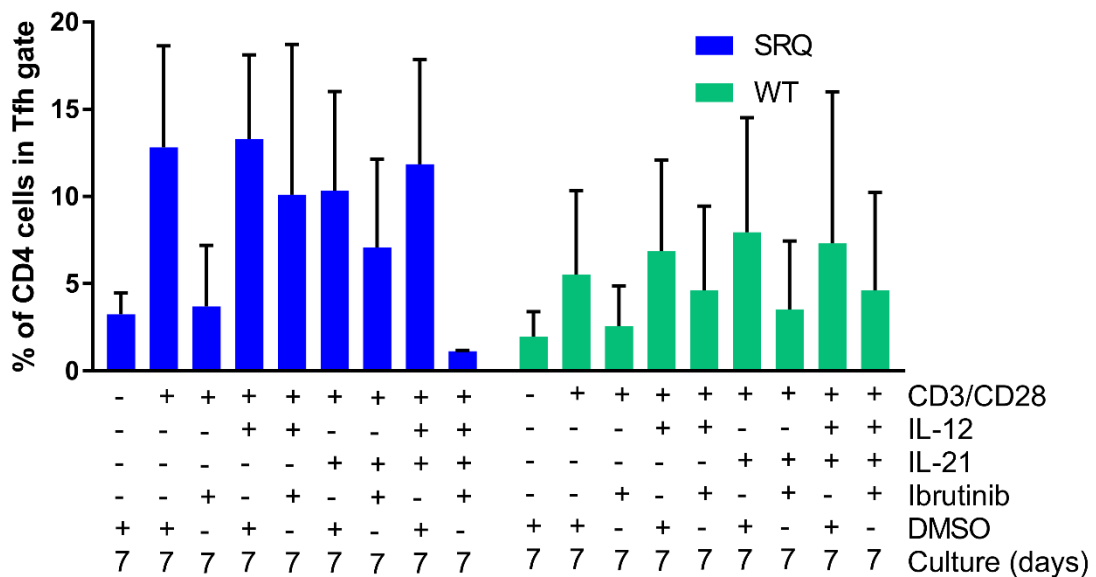


**Figure 4-12: Tfh proportions following culture with interleukins +/- ibrutinib.** The bars show the mean Tfh population as a proportion of CD4 cells (n=3) with blue representing SRQ and green WT. The error bars represent the standard deviation. The culture conditions are shown beneath the x-axis.

These experiments showed a low proportion of Tfh cells in unstimulated culture and an increase in Tfh differentiation following stimulation with anti-CD3 and anti-CD28. In these experiments the addition of IL-12, IL-21 or both interleukins appeared to have no effect on the Tfh proportion. Treatment with ibrutinib appeared to reduce the differentiation to Tfh cells in all conditions although the differences are not statistically significant (Figure 4-12).

To assess changes in proliferation the cells were labelled with Cell trace violet (CTV) prior to culture. Higher amounts of proliferation lead to reduced fluorescence as the marker is divided between the daughter cells. A lower average fluorescence represents increased proliferation. CTV is detected by the Aria (BD Biosciences) in the Pacific Blue position. Lymphocytes were subsequently gated by CD4 positivity and divided into Tfh ( $PD1^{hi}CXCR5^{hi}$ ) and non-Tfh ( $PD1^{lo}CXCR5^{lo}$ ) cells (Figure 4-13 A). Examination of the Pacific Blue fluorescence for the Tfh population showed that cells treated with ibrutinib appeared to show less proliferation compared to cells in the same culture conditions without ibrutinib (Figure 4-13 B & C). These variations did not meet statistical significance but appeared similar in both WT and SRQ Tfh cells.

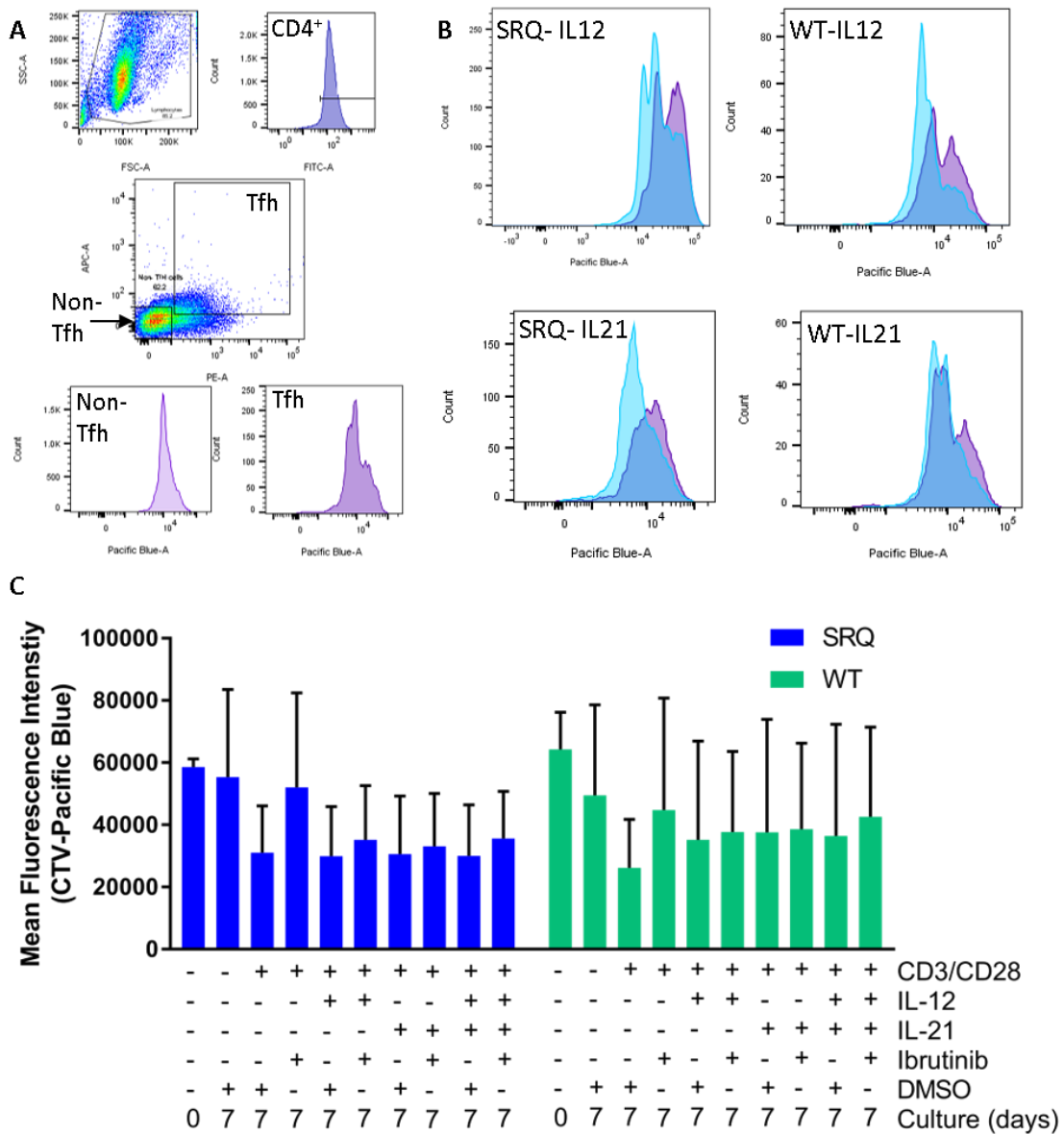


**Figure 4-13: Summary of CTV and proliferation of Tfh cells.**

A- representative FACS plot showing the gating strategy used to gate lymphocytes then CD4<sup>+</sup> positive cells in the upper panels followed by the gates for Tfh and non-Tfh cells in the middle panel based upon PD1 and CXCR5 expression. The lower panels show the Pacific-Blue fluorescence representing the CTV in the Non-Tfh and Tfh populations. B- overlying Pacific-Blue fluorescence for cells cultured with the labelled interleukin and anti-CD3/anti-CD28 with the blue peak showing DMSO treated and the purple peak ibrutinib treated cells (representative panels shown). C- the average arithmetic mean fluorescence intensity is shown by the bars with standard deviation shown by error bars. The culture conditions are shown below the x-axis.

#### 4.5.4 Conclusions from *in vitro* experiments

In vitro experiments confirm that ITK is present in the CD4<sup>+</sup> T cells and it has a role to play in T cell signalling as demonstrated by the reduced cell viability and reduced differentiation to Tfh cells seen in stimulated cells treated with ibrutinib. This effect is seen in CD4<sup>+</sup> T cells from both WT mice and SRQ mice.

#### 4.6 ASSESSMENT OF GENE EXPRESSION BY MICROARRAY

As described in section 1.10 the ROQUIN protein binds to *Icos* mRNA and regulates its stability. The mutated ROQUIN protein encoded by *Roquin<sup>san</sup>* binds with greater affinity so the *Icos* mRNA decays more slowly leading to increased ICOS protein expression. To assess the effect of this on gene expression we carried out a microarray experiment using CD4<sup>+</sup> T cells extracted from the spleens of SRQ and WT mice as described in section 2.5.16. A total of 14 samples (7 SRQ and 7 WT) were analysed.

Using the two-class unpaired Significance Analysis of Microarrays (SAM) a list of differentially expressed genes was generated using a random selection of 100 permutations (Figure 4-14). Using a delta-value of 0.304 a total of 15 genes were differentially expressed, with a false discovery rate of 22.5%.

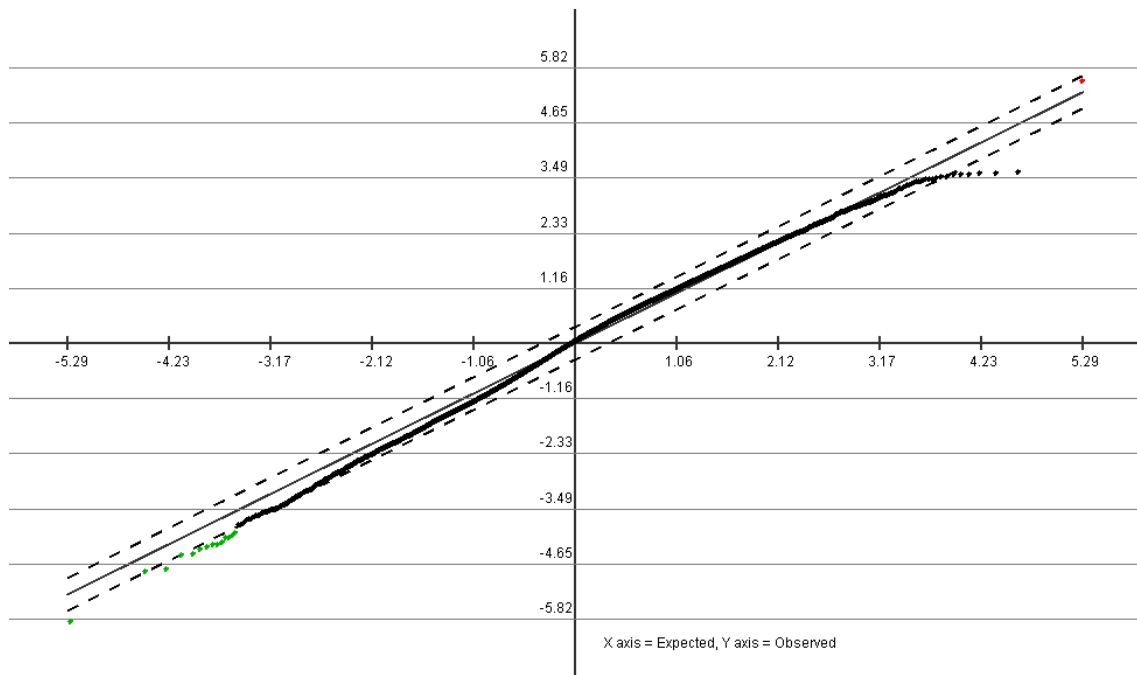


**Figure 4-14: SAM graph from MeV**

*This graph from MeV shows the initial output of SAM with genes which are significantly more highly expressed in the SRQ mice shown in red and those which are significantly less expressed in green.*

One gene was found to be positively significant in SRQ CD4<sup>+</sup> T cells – ENSMUST00000130888 a transcript of RCC1 domain-containing protein 1 (RCCD1). This protein has been described as a co-regulator of KMD8 in human studies with a role in chromatin regulation (225) and possibly cytoskeletal microtubule stability (226). The genes which are differentially expressed in the SRQ CD4<sup>+</sup> T cells are shown in Figure 4-15.

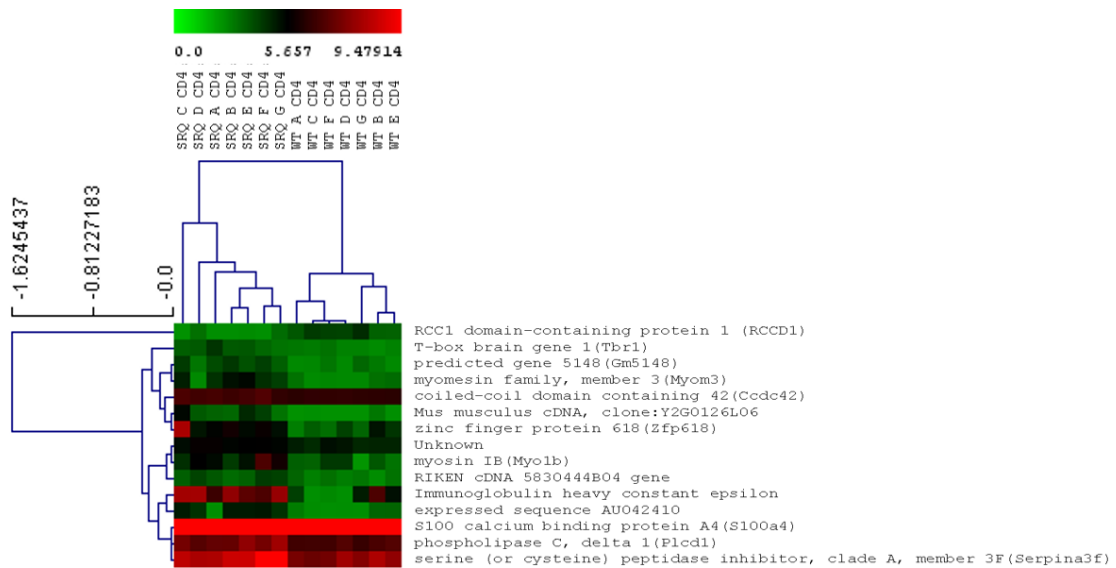


**Figure 4-15: Hierarchical clustering generated from differentially expressed genes.**  
 Samples are listed above the heat map and the gene names on the right.

Further analysis of the significant negative genes was carried out using DAVID v6.8 (209,210) as described in section 2.5.16.

There were several pairs of genes which are found in categories or pathways determined by DAVID and a single cluster produced in the functional analysis clustering. This is a cluster based on location in the cell and the function of metal ion binding. No clusters were found which appeared to have functional implications related to tumorigenesis by this analysis.

Further analysis using the genes identified by Iqbal et al (8,85) and used in the AITL gene classifiers did not show sample clustering along genotype (**Figure 4-16**). However, the published analyses assessed whole tumour samples whereas this analysis was of selected CD4 cells. The expression of ICOS was high in both the SRQ mice and the WT littermate control samples.

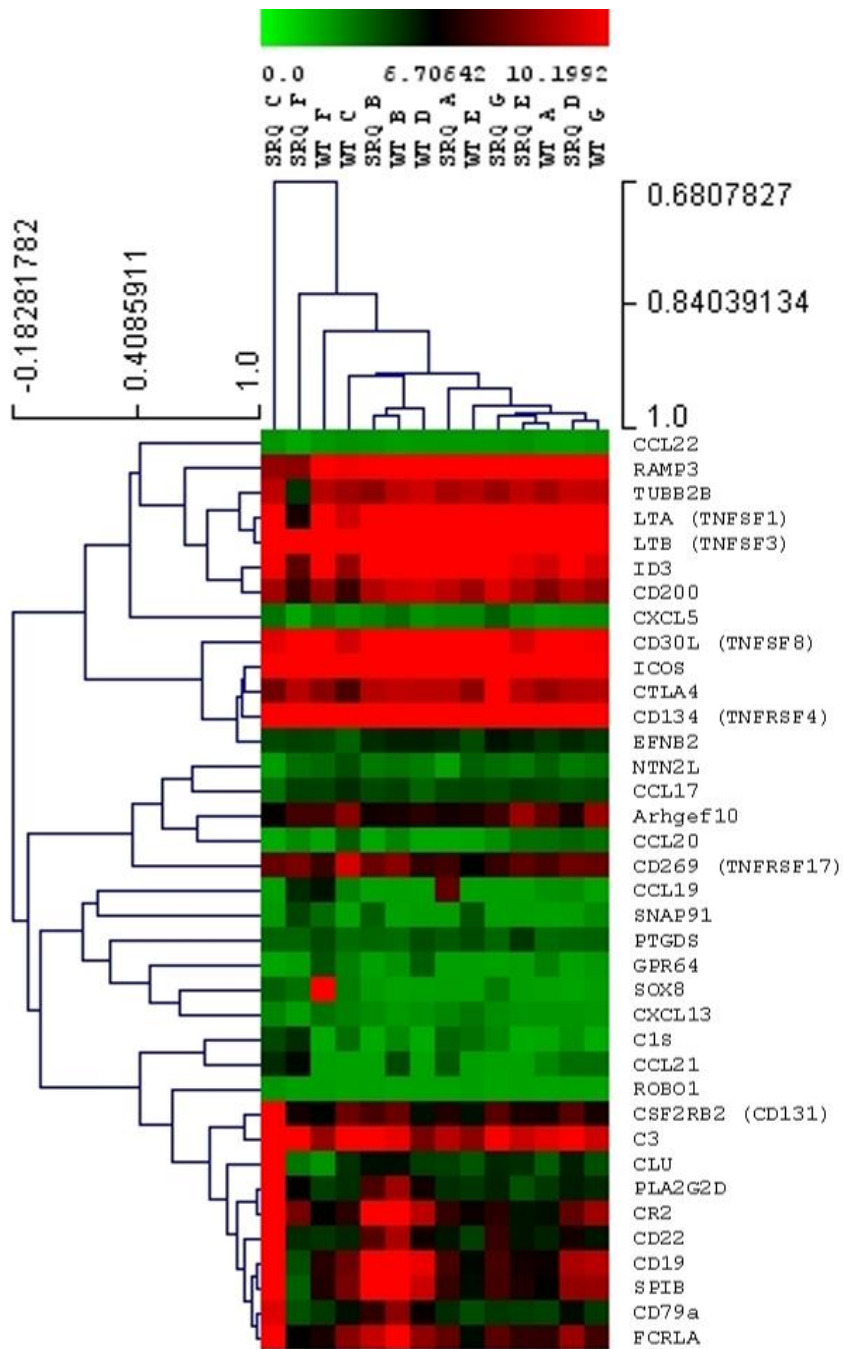


**Figure 4-16: Heat map of hierarchical clustering of genes from AITL gene classifiers.**  
 Genes are listed to the right of the heat map and samples above.

Although the flow cytometry analysis has shown an alteration in the Tfh proportion in the spleens of SRQ mice the Tfh cells remain a small proportion of the CD4 cells. This may explain why we did not detect the over-expression of other genes associated with

Tfh cell differentiation. These results also suggest that there are minimal transcriptional differences between the SRQ and WT mice.

## 4.7 WHOLE EXOME SEQUENCING

Although all SRQ mice carry a point mutation in Roquin, only a proportion develop lymphoma during their lifetime. The cause of this incomplete penetrance is not understood. WES was carried out to look for genetic variation that might play a role in lymphoma development. Six DNA samples were sequenced by the Sanger Institute in collaboration with Dr Thomas Keane's laboratory as described in section 2.5.18.

The samples consisted of constitutional DNA from the livers of a WT mouse, an SRQ mouse (SRQ control) with no tumour development and two SRQ mice (SRQ5293 and SRQ5301) with tumours. Matched tumour DNA from the enlarged lymph nodes of these mice was also sequenced.

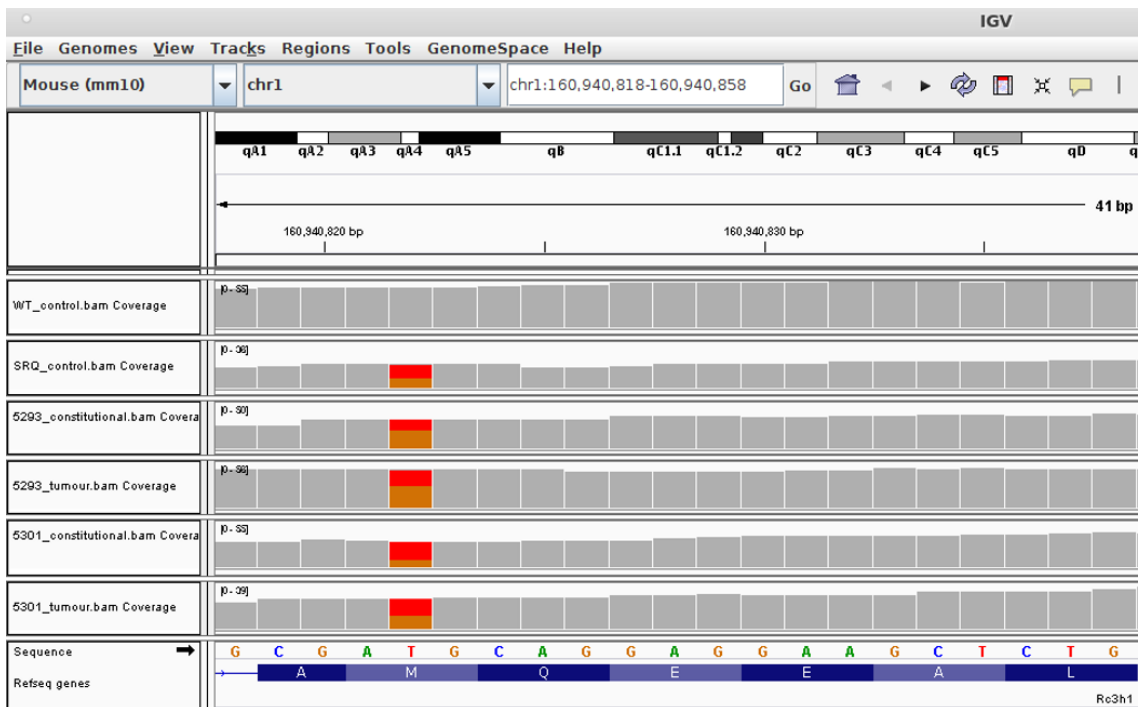
### 4.7.1 Analysis of reads and Mapping to the reference genome

To carry out further analysis of the WES libraries various bioinformatic steps must be undertaken. BAM files were generated, sorted and filtered by Dr Anthony Doran of the Sanger Institute as described in section 2.5.18.1, aligning each sample to the C57BL/6J GRCm38 (mm10) mouse reference genome. Details of the reads generated, and the quality of the mapping are shown in Table 4-1. This shows that over 99% of reads in each sample were mapped to the reference genome and over 98% of paired reads were properly paired.

In order to demonstrate the presence of the expected heterozygous mutation in Rc3h1 at Chr1: 160,940,825 in the five SRQ samples Integrated Genomic Viewer was used (Figure 4-17). This provides an indication that the WES is of reasonable quality as the expected mutation is found in the SRQ samples and not the WT sample. In each SRQ sample both the normal base and the mutant base are found in the proportions which would be expected in a heterozygous mouse.

Sample	5301 tumour	5301 constitutional	5293 tumour	5293 constitutional	SRQ control	WT control
QC passed reads total (n)	86962026	98439457	110294088	117582295	97539351	106171148
Mapped reads (n)	86822933	98290519	110089219	117413405	97393433	106003901
Mapped reads (%)	99.84	99.85	99.81	99.86	99.85	99.84
Properly paired (n)	85573964	97732356	109264538	116666754	96798758	105421112
Properly paired (%)	98.52	99.31	99.12	99.26	99.28	99.32

**Table 4-1: BAM file statistics showing the numbers and proportions of properly mapped reads and properly paired reads for each sample.**



Sample	Coverage	T (WT)	G (MUT)
WT control	46	46	0
SRQ control	18	10	8
5293 constitutional	31	12	19
5293 tumour	45	19	26
5301 constitutional	30	21	9
5301 tumour	25	14	11

**Figure 4-17: Integrated Genomics Viewer confirming the genotype of each sample in the Roquin gene. Variation at Chr1: 160,940,825 (exon 5 of Rc3h1) is shown in the five SRQ samples with the red block representing the WT allele (T) and the gold block representing the variant allele (G) and the total block height representing the coverage (range 18-46) at this site. The total number of reads at this nucleotide and the number of each allele is shown in the table.**

#### 4.7.2 Generating variants of interest

After determining that the WES data was of good quality and each sample had been mapped to the reference genome we went on to look for variation from the reference genome which could have a potential impact upon on the development of lymphoma in these mice.

Numerous bioinformatic tools exist to call single nucleotide variants (SNVs) which have primarily been developed for variant calling in human samples. Groups have shown that there is not always consensus between the tools when calling SNVs which means that use of more than one method should be considered (227,228).

To analyse the WES data two methods of analysis were used to produce lists of SNVs of interest. The process is summarised in Figure 4-18 and described in the text below.

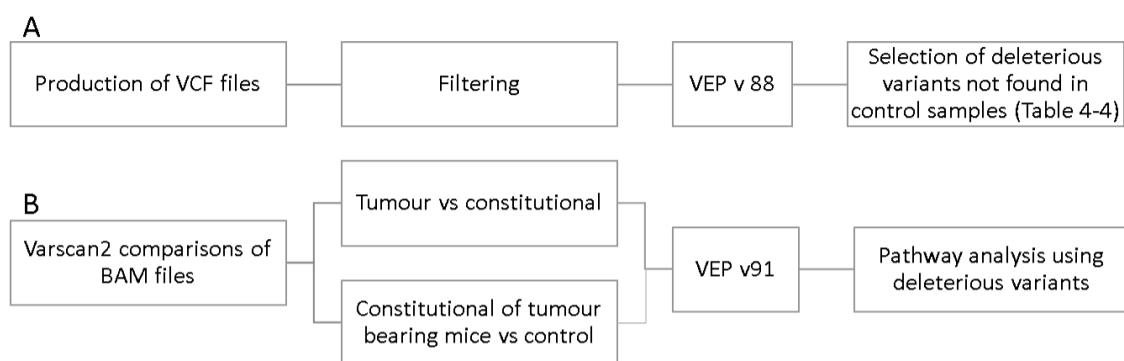


**Figure 4-18: Summary of WES analysis to produce SNVs of interest.**

As described in section 2.5.18.2 Dr Doran produced a list of high quality variants from each sample and used VEP version 88 to predict the effect of each SNV (211,214). He then compared the lists to produce SNVs, which were found in the tumour samples and the constitutional samples from the tumour bearing mice, which were not found in the control samples.

	Total variants	Passed filters	Intronic SNVs	Deleterious
<b>WT control</b>	201728	1760	868	187
<b>SRQ control</b>	195088	1758	901	211
<b>5293 constitutional</b>	217651	1890	875	209
<b>5293 tumour</b>	212005	1900	878	191
<b>5301 constitutional</b>	190177	1796	935	203
<b>5301 tumour</b>	186028	1680	897	208

**Table 4-2: VCF file statistics.**

*The total numbers of variants in each sample, the number passing the quality filters, the number of high quality SNVs predicted to occur in intronic regions with coding consequences and the number of high quality SNVs predicted to have deleterious effects on protein production.*

Analysis of the VCF files showed similar amounts of variation from the reference genome in each of the six samples (Table 4-2). VEP analysis predicted that around half the SNVs found in each sample occurred in intronic DNA with coding consequences and a proportion of these were likely to have deleterious effects on protein production.

As described in section 2.5.18.2 analysis was also carried out using Varscan2 to produce lists of SNVs which are somatic, germline or loss of heterozygosity (LOH) and subsequently a list of high confidence SNVs in each category (212,213). The high confidence somatic SNVs were then further analysed using VEP version 91 to predict the effect of each SNV (214). This was used to compare the tumour and constitutional DNA from the two tumour bearing mice (Figure 4-19Figure 4-19). It was also used to compare the constitutional DNA from the tumour bearing mice with the control mouse to look for variation which may predispose to tumour development (Figure 4-20Figure 4-20).

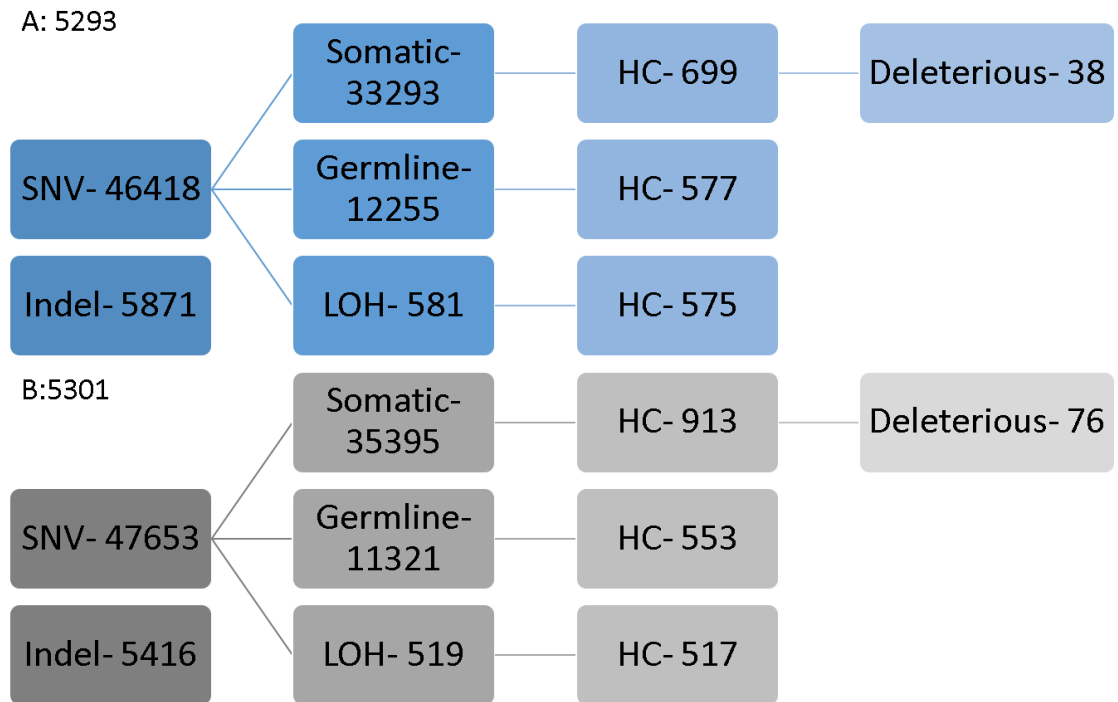


**Figure 4-19: Variants analysed by Varscan showing the number of variants found at each stage of the analysis for 5293 (A) and 5301 (B).**

The initial analysis produces the number of SNV and indels which vary between the germline and tumour DNA. The SNVs are then divided into those found in the tumour sample (Somatic), those showing LOH and those in the Germline sample. Each of these is then divided into high confidence (HC) and low confidence variants. Following VEP analysis of the Somatic high confidence variants those producing deleterious amino acid changes were counted.

As part of the VEP analysis the SNVs were assigned a SIFT score which predicts the effect of the SNV on protein production (229). The SNVs assigned a deleterious label by the SIFT score were then reviewed.

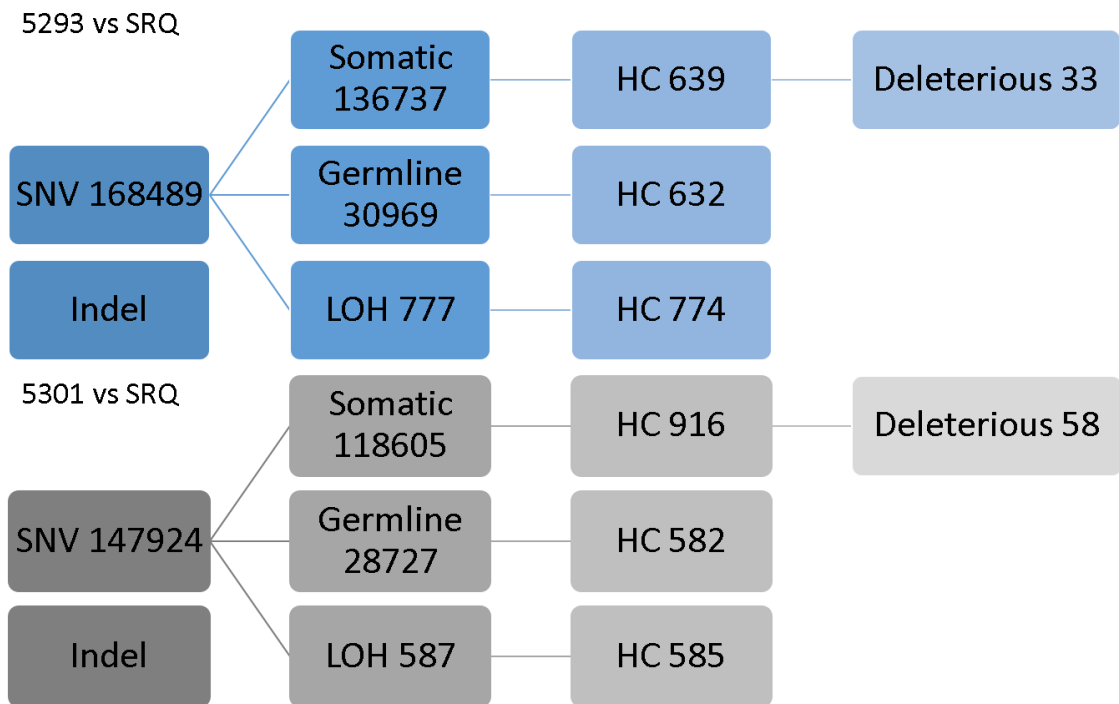


**Figure 4-20: Variants analysed by Varscan showing the number of variants found at each stage of the analysis for 5293 and 5301 constitutional samples compared to SRQ control sample.**

The initial analysis produces the number of SNV and indels which vary between the germline and tumour DNA. The SNVs are then divided into those found in the tumour sample (Somatic), those showing LOH and those in the Germline sample (SRQ control). Each of these is then divided into high confidence (HC) and low confidence variants. Following VEP analysis of the Somatic high confidence variants those producing deleterious amino acid changes were counted.

#### 4.7.3 Description of Variants

The above bioinformatic analysis produced several lists of SNVs in genes which may be of interest. From the comparison of filtered VCF files four lists of genes were produced:

- 1) SNVs in 5293 tumour not found in the SRQ or WT control samples
- 2) SNVs in 5301 tumour not found in the SRQ or WT control samples
- 3) SNVs in 5293 constitutional not found in the SRQ or WT control samples
- 4) SNVs in 5301 constitutional not found in the SRQ or WT control samples

Following comparison of the VCF files the genes containing SNVs in one or both tumour samples but not found in the control samples are shown in Table 4-3 which also indicates whether the gene was shown to contain SNVs in the matched constitutional sample. Some genes contained more than one SNV.

Gene Name (MGI)	5293 Tumour	5301 Tumour	5293 Constitutional	5301 Constitutional
Mroh2a	X	X	X	X
Hjurp	X	X	X	X
Vmn2r116	X	X	X	
Ccnb3	X	X		
Rrs1	X		X	
Ugt1a9	X	X	X	X
Pfdn2	X		X	X
Pdzrn4	X			
Vmn2r114	X	X	X	X
Vmn2r115	X	X		
Hsp90ab1	X			
Rhoa	X			

**Table 4-3: List of genes generated by comparison of filtered VCF files.**

Genes shown were found to have mutations predicted to have a deleterious effect in the samples shown by an X and not in the SRQ or WT control samples.

Genes which contained an SNV in one or both tumour samples but not the matched constitutional samples were cyclin B3 (Ccnb3), PDZ domain containing RING finger 4 (Pdzrn4), heat shock protein 90 alpha (cytosolic), class B member 1 (Hsp90ab1), ras homolog family member A (Rhoa) and vomeronasal 2, receptor 115 (Vnm2r115).

From the VarScan2 analysis four lists of genes were produced:

- 1) SNVs in 5293 tumour not found in 5293 constitutional sample
- 2) SNVs in 5301 tumour not found in 5301 constitutional sample
- 3) SNVs in 5293 constitutional not found in SRQ control sample
- 4) SNVs in 5301 constitutional not found in SRQ control sample

These lists were reviewed and compared to the lists produced from the filtered VCF files. VarScan analysis also confirmed the presence of an SNV in Rhoa in the 5293 tumour sample, it also showed SNVs in Hsp90ab1 in both tumour samples.

Further review of the SNVs using IGV viewer showed several SNVs in Hsp90ab1 in both tumour samples, and these varied between the tumours (Table 4-4 & Figure 4-21A). The deleterious variants were all predicted in the transcript ENSMUST00000024739.13.

Tumour	cDNA change	Amino acid substitution	VAF
5293	c.1810C>T	Arg604Trp	0.11
5293	c.1820A>C	Lys607Thr	0.16
5301	c.1885A>T	Asn629Tyr	0.14
5301	c.1889C>T	Pro630Leu	0.15
5301	c.2015A>T	Asp672Val	0.21
5301	c.2035C>A	Arg679Ser	0.23
5301	c.2044C>T	Arg682Cys	0.29

**Table 4-4: Details of predicted effects of SNVs on Hsp90ab1-201.**

The SNV found in Ccnb3 was the same in both tumours and was predicted to produce a c.354A>C mutation in transcript ENSMUST00000115752 which leads to an asparagine to glutamic acid substitution (p.Asn75Glu) (Figure 4-21B). This variant had a variant allele frequency (VAF) of 0.46 in the 5293 tumour sample and 0.43 in the 5301 tumour sample.

Rhoa was predicted to have a single SNV with a deleterious effect in the 5293 tumour sample (Figure 4-21C). This was predicted to produce a c.575T>C mutation in transcript ENSMUST00000007959 leading to a phenylalanine to leucine substitution (p.Phe25Leu) which we have also examined following the detection of this mutation in patient samples as described in section 3.1 (217). There was a difference in coverage between the samples for the Rhoa exons with higher coverage in the 5293 tumour sample (253 x compared to 83 x in the 5301 tumour sample) which may suggest copy number variation. The VAF was 0.41. On review of IGV viewer other heterozygous variants in exons 3 and 6 of the 5293 tumour sample could also be seen which on further review showed no change in amino acid.

Pdzrn4 had an SNV in the 5293 tumour sample predicted to cause a c.2376G>A mutation in transcript ENSMUST000000035399 leading to an arginine to glutamine substitution (p.Arg705Gln) (Figure 4-21D). This SNV had a VAF of 0.54.

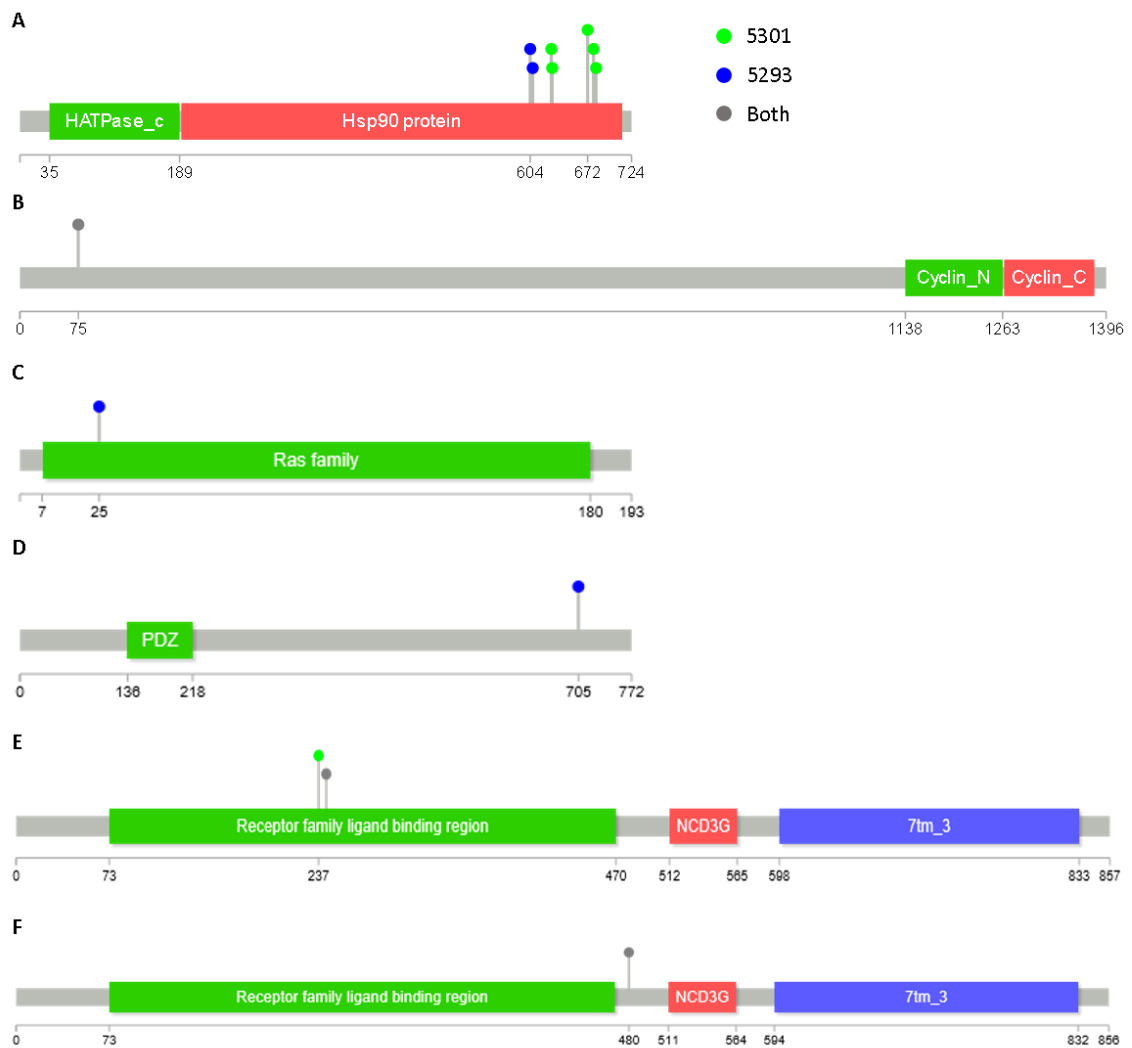


**Figure 4-21: Gene lollipop diagrams representing the six genes found to have SNVs predicted to impact protein production in tumour samples only.**  
 (A) *Hsp90* (B) *Ccnb3* (C) *Rhoa* (D) *Pdzrn4* (E) *Vmn2r115* & (F) *Vmn2r116*. The grey bar represents the base sequence and repeats and motifs are highlighted and coloured according to the Pfam database (230,231)

*Vmn2r115* had an SNV in both tumour samples predicted to cause a c.727A>G mutation in transcript ENSMUST00000168175 leading to an asparagine to aspartic acid substitution (p.Asn243Asp) with a VAF of 0.24 in the 5293 tumour sample and 0.25 in the 5301 tumour sample. There was also a SNV found in the 5301 tumour sample predicted to cause a c.709A>C mutation in the same transcript leading to an isoleucine to leucine substitution (p.Ile273Leu) with a VAF of 0.24 (Figure 4-21Figure 4-21E).

Vmn2r116 had an SNV in both tumour samples and the constitutional samples from 5293. The SNV was predicted to cause a c1440A>C mutation in transcript ENSMUST00000164856 leading to a lysine to asparagine substitution (p.Lys480Asn) and had a VAF of 0.22 in the 5293 tumour sample, 0.28 in the 5301 tumour sample and 0.33 in the 5293 constitutional sample (Figure 4-21F).

Hsp90ab1 is a member of the heat shock protein (HSP) family which support the folding of other proteins and maintain protein stability (232). HSPs have been found to be up-regulated in several cancer types although only a small proportion of haematological malignancy cases have been found to have a mutation in HSP90AB1 (109).

Ccnb3 has been associated with a subtype of bone sarcoma where tumours containing a fusion between the BCL6 co-repressor gene and Ccnb3 gene have been shown to be distinct from Ewing sarcoma (233).

Pdzrn4 has limited association with cancer although according to the COSMIC database mutations have been found in 0.4% of haematological malignancy (109).

Vmn2r115 and Vmn2r116 are G-protein coupled receptors which is part of the mouse olfactory system, along with Vmn2r114. SNVs were also found in Vmn2r114 in tumour and constitutional samples. These genes have been shown to alter behaviour in response to specific stimuli.

cDNA change	Amino acid substitution	5293T VAF	5293C VAF	5301T VAF	5301C VAF
c.648G>A	V146M		0.17	0.21	
c.817C>T	T202M	0.23	0.18	0.16	0.13
c.1321G>A	C370Y	0.31	0.31	0.36	0.35
c.1405G>A	R398H	0.77	0.84	0.82	0.83
c.1936C>T	A575V	0.83	0.85	0.86	0.87
c.3157G>A	C982Y			0.17	0.19
c.3522C>T	L1104F			0.2	0.16
c.4570T>C	V1453A			0.17	
c.5100C>T	R1630C			0.16	

**Table 4-5: SNVs found in Mroh2a.**

The Variant Allele Fractions (VAFs) are listed for SNVs which passed the quality filters. 5293T and 5301T indicate the VAF within tumour and 5293C and 5301C are VAF within non-tumour tissue.

Other genes which were found to have SNVs in the tumour-bearing mice but not the SRQ control or WT control samples are also shown in Table 4-3. These included Maestro heat like repeat family member 2A (Mroh2a; Table 4-5) and Holliday junction recognition protein (Hjurp; Table 4-6) in which a number of SNVs were found, Ribosome Biogenesis Regulator Homolog (Rrs1) and UDP Glucuronosyltransferase Family 1 Member A9 (Ugt1a9) in which 2 SNVs were found and Prefoldin Subunit 2 (Pfdn2) in which 1 SNV was found (Figure 4-22). These genes have not been associated with lymphoma in previous studies (109).

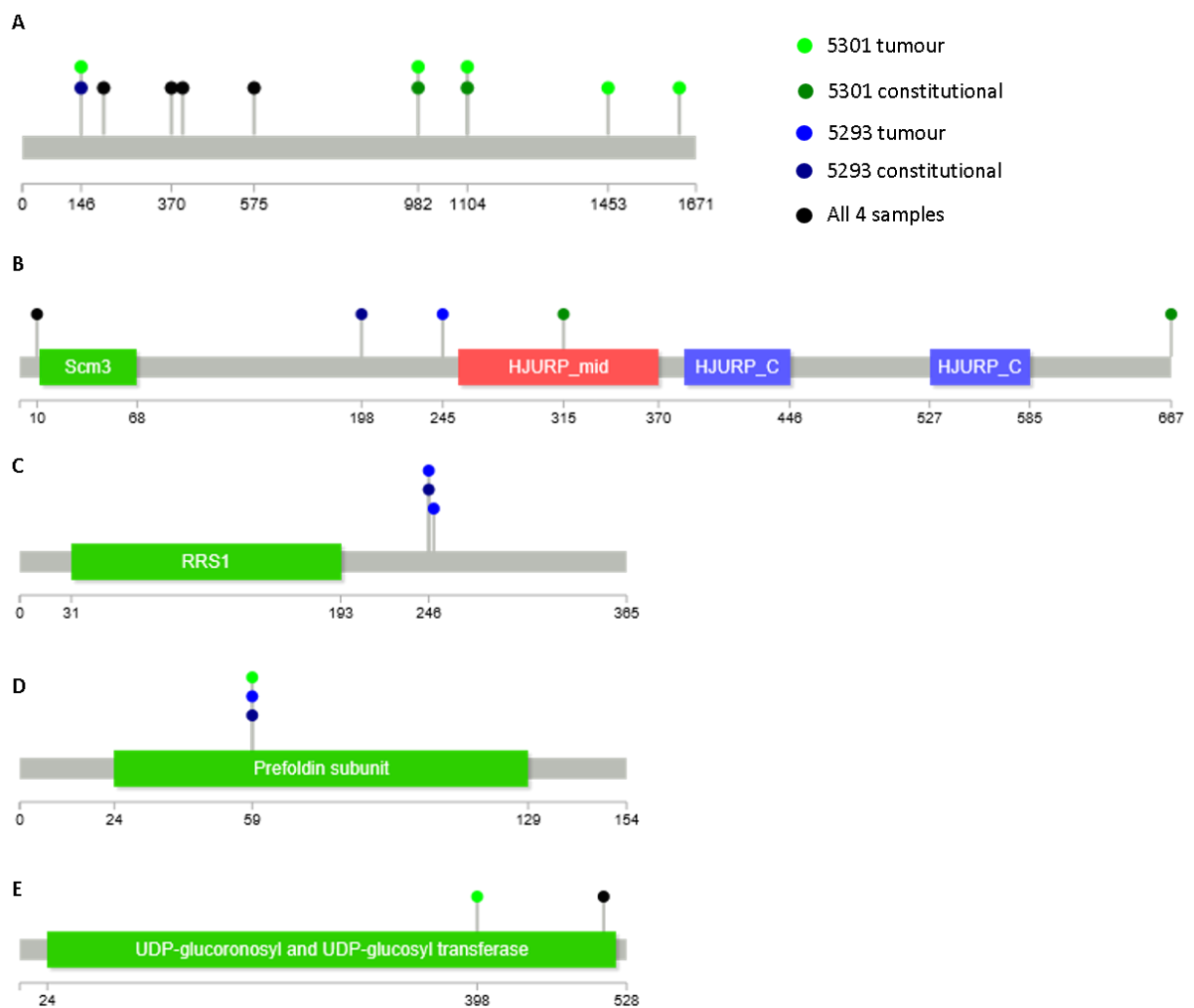


**Figure 4-22: Gene lollipop diagrams showing the genes mutated in the tumour and constitutional samples of the tumour-bearing mice.**

Genes shown are *Mroh2a* (A), *Hjurp* (B), *Rrs1* (C), *Pfdn2* (D) and *Ugt1a9* (E). The grey bar represents the base sequence and repeats and motifs are highlighted and coloured according to the Pfam database (230,231)

cDNA change	Amino acid substitution	5293T VAF	5293C VAF	5301T VAF	5301C VAF
c.192A>T	R10W	0.42	0.4	0.43	0.41
c.757G>T	G198V		0.2		
c.897G>A	D245N	0.17			
c.1108C>A	P315H				0.17
c.2164C>T	P667L				0.23

**Table 4-6: SNVs found in Hjurp.**

The Variant Allele Fractions (VAFs) are listed for SNVs which passed the quality filters. 5293T and 5301T indicate the VAF within tumour and 5293C and 5301C are VAF within non-tumour tissue.

#### 4.7.4 Pathway analysis

The gene lists from the Varscan analysis were also submitted to InnateDB to determine if there were over-represented pathways (215). Analysis of the lists of gene found in the tumours but not the constitutional DNA showed over-represented pathways including molecules associated with elastic fibres, regulation of the actin cytoskeleton and focal adhesion. This is of interest as RHOA is known to be of importance in the regulation of the actin cytoskeleton and cell-cell interactions suggesting that these variations may be contributing to lymphomagenesis in this mouse model.

Analysis of the genes found in the constitutional DNA of the tumour bearing mice but not in the control sample showed over-represented pathways including CD28 dependent PI3K/AKT signalling, PI3K/AKT activation and CD28 co-stimulation. These are pathways, which have been associated with the development of T cell lymphoma as part of the TCR signalling pathway (73).

Speculatively, this suggests that over-activity in T cell signalling may produce a tendency towards the development of lymphoma and a second hit in genes regulating cell motility and cell to cell interaction lead to lymphomagenesis.

#### 4.7.5 Discussion of WES results

Other genes which have been found to be mutated in AITL (PLCG1, CD28 and JAK2) were reviewed in IGV and showed no evidence of variation. TP53 was also examined and showed no variation from the reference genome in these samples.

Due to the low tumour burden thought to be present in the sample the results may underestimate the genetic variation in the malignant cells themselves. The variant allele frequencies which have been discussed may be found in non-tumour cells due to their frequency.

#### 4.8 CHARACTERISATION OF THE SRQ MOUSE MODEL SUMMARY

In this chapter it is shown that a proportion of the SRQ colony go onto develop AITL like tumours with evidence of T cell clonality. Tumour composition showed a high proportion of B220<sup>+</sup> cells in keeping with previous work by Ellyard et al (176). *In vitro* work showed that ITK inhibition affects the differentiation and proliferation of CD4<sup>+</sup> T cells from both WT and SRQ mice.

Gene expression analysis was carried out on CD4<sup>+</sup> T cells from the spleens of WT and SRQ mice and few differences were detected. Although increased expression of Tfh markers was observed, Tfh cells make up only a small proportion of the CD4<sup>+</sup> T cells which may explain the limited differences seen.

WES analysis revealed the presence of SNVs which may be contributing to tumour development in the colony and confirmed that lymphomas produced are genetically diverse. Further assessment of the genetic drivers of tumour development would require sequencing of larger numbers. Detailed analysis of the VAFs demonstrated allele frequencies varied within tumours suggesting sub-clonal variation. By flow cytometry for Tfh cells the tumour burden was estimated at <5%. However, allele frequencies of SNVs in tumour tissue are significantly higher than this. The same problem exists in studies of human T-cell lymphoma (see Supp Table 7 from Sakata-Yanagimoto et al (99) and Supp Table 6 from Palomero et al (97)) and this is likely to be due to 1) complex genetics within the T-cell population with copy number variation and possibly mixtures of heterozygous and homozygous changes and, 2) some mutations might be present in the non-tumour populations of B-cells as has been reported for TET2 (197).

## 5 RESULTS OF PRECLINICAL EXPERIMENTS

---

### 5.1 INTRODUCTION

The published mouse models of T-cell lymphoma are difficult to employ for pre-clinical testing either due to long latency of tumour development or because the genetic driver is not representative e.g. the ITK:SYK transgenic mouse produces T-cell lymphomas but the t(ITK;SYK) is found in 20% of follicular T-cell lymphoma.

The san roque strain of mouse also develops tumours with a long latency. However, the tumours are genetically diverse (as described in Chapter 1). As less than half of the heterozygous san roque mice developed easily detectable lymphadenopathy we considered various methods to utilise the model in the most effective way.

In this chapter a failed adoptive transfer approach to produce large numbers of mice with genetically identical tumours is first described. Subsequent experiments describe studies on san roque mice with lymphomas including a pilot study demonstrating firstly, the usefulness of MRI and secondly, the effects of cyclophosphamide treatment. Finally, a pre-clinical study to investigate the ITK/BTK inhibitor, ibrutinib, in san roque mice is described.

### 5.2 ADOPTIVE TRANSFER TO PRODUCE COHORTS OF MICE WITH GENETICALLY IDENTICAL LYMPHOMAS?

We hoped that by transferring cell suspensions produced from tumours extracted from the aged heterozygous mice we would generate consistent tumour development. Groups have had success in developing myeloma models with this method (234). Cell suspensions were produced in a sterile environment then delivered via intravenous injection (tail vein) to recipient mice as described in Section 2.x.x.

Our efforts were unsuccessful with significant toxicity seen following transfer of cells to SCID/Beige mice thought to be secondary to graft versus host disease. The mice receiving cells became unwell with weight loss, diarrhoea and behaviour suggestive of illness after four to five days. Haematoxylin and eosin (H & E) staining of bowel fixed in

formalin at the time of post mortem suggested an increase in inflammatory infiltrate (Figure 5-1).

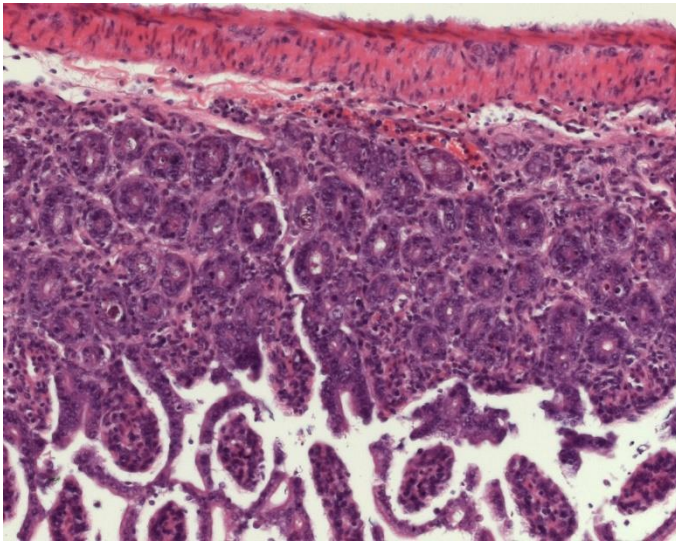


**Figure 5-1: H & E stained section of bowel taken from a mouse at post mortem 5 days after receipt of adoptive transfer of tumour cells.**

We went on to perform adoptive transfer of tumour cell suspensions to wild type littermates, half of whom received prior irradiation as described in section 2.x.x. No tumour development occurred in the recipients after an observation period of 6 months.

### 5.3 VISUALISING MOUSE LYMPHOMA BY MAGNETIC RESONANCE IMAGING (MRI)

Following the failure to develop a cohort of mice with identical lymphomas by adoptive transfer we considered ways in which the mice with spontaneous tumour development could be used as a model for preclinical studies.

The ability to visualise and accurately measure the volumes of enlarged lymph nodes using MRI scans enabled us to perform pre- and post- treatment images. Initially we carried out post mortem scans to determine the feasibility of this approach to demonstrate that we could detect abnormalities. We went on to perform a series of scans of mice at 3 age points – 6 months, 8 months and 12 months. These scans demonstrated that lymph nodes could be identified in the inguinal and brachial region

whether enlarged or not and in the axillary region when enlarged and sometimes when not.

From this series of scans (Figure 5-2 & Figure 5-3) we were able to determine that enlarged inguinal lymph nodes could be palpated enabling mice to be identified for further studies.

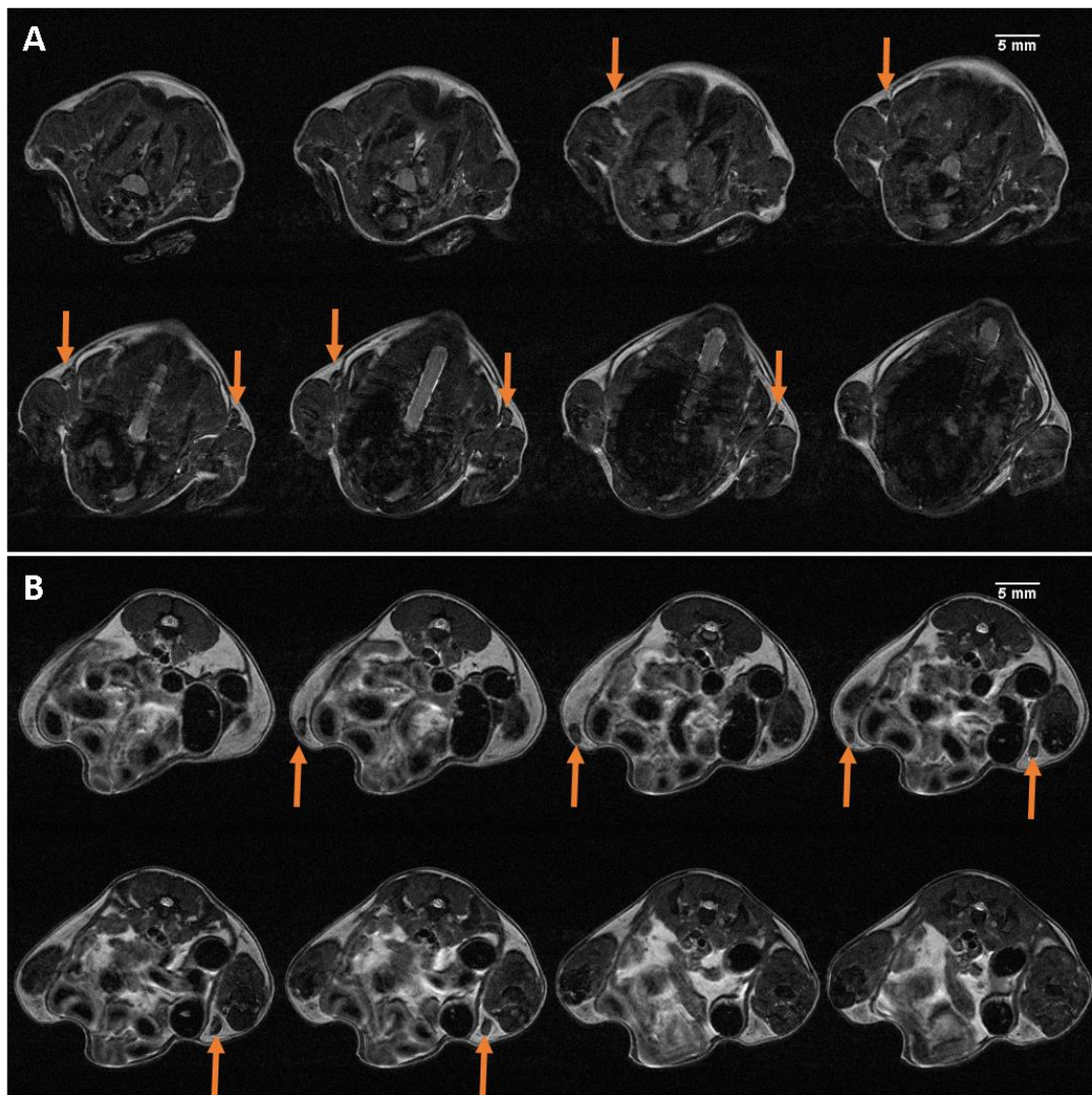


**Figure 5-2: Montage of T2 weighted MRI scan images of axial slices (0.8mm) from a 12-month-old mouse with no enlarged lymph nodes.**

The image in the upper left of each series is the most cranial. A: images from the axillary region with orange arrows highlighting the normal sized brachial lymph nodes. The axillary lymph nodes cannot be seen clearly. B: images from the inguinal region with orange arrows highlighting normal sized inguinal lymph nodes.

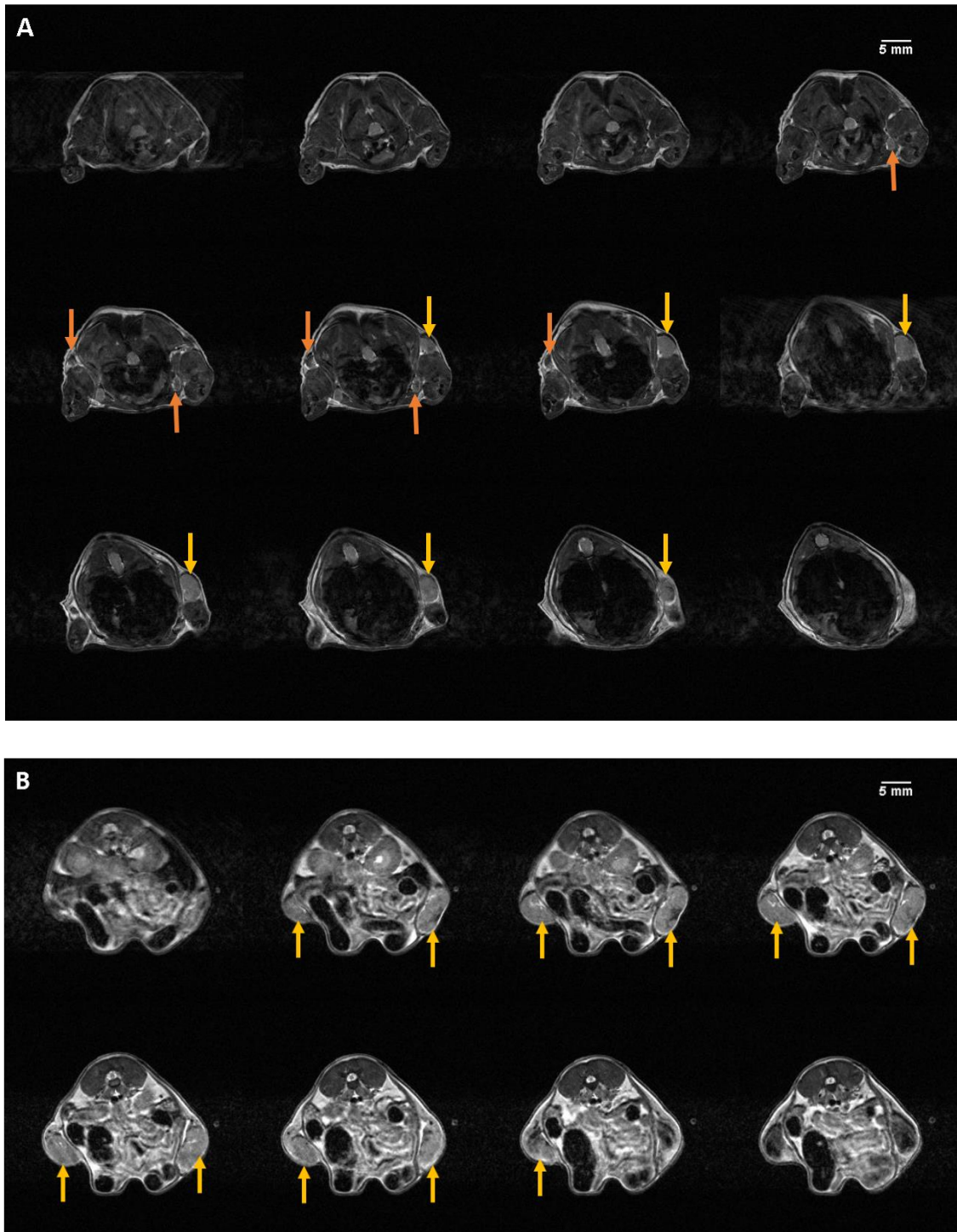


**Figure 5-3: Montage of T2 weighted MRI scan images of axial slices (0.8mm) from an 8-month-old mouse.**

The image in the upper left of each series is the most cranial. A: images from the axillary region where the orange arrows highlight a normal axillary lymph node and a normal brachial lymph node. The yellow arrow highlights an enlarged brachial lymph node. B: images from the inguinal region with yellow arrows highlighting the bilateral enlargement of inguinal lymph nodes.

The scans from a mouse with palpable lymph nodes (Figure 5-3) show that enlarged lymph nodes have a higher signal intensity when compared to the normal lymph nodes in T2 weighted scans.

#### 5.4 PILOT STUDY TO DEMONSTRATE SENSITIVITY TO CYCLOPHOSPHAMIDE TREATMENT

To assess the response of the enlarged lymph nodes to treatment with chemotherapy we designed an experiment to assess the response to cyclophosphamide therapy. Cyclophosphamide is a widely used chemotherapy drug, which is a key component of treatment regimens for lymphoid malignancies. It has been used in treatment of mouse models of lymphoid malignancies at a range of doses (235-237) and we selected 200mg/kg as likely to be therapeutic without excessive toxicity. After the identification of 3 mice with enlarged inguinal lymph nodes they underwent MRI scans and 2 were subsequently treated with a single intra-peritoneal (IP) injection of cyclophosphamide (200mg/kg) in sterile PBS and the other with a single IP injection of the equivalent volume of sterile PBS. The age, sex and location of enlarged lymph nodes in the mice are shown in Table 5-1.

Mouse	Sex	Age (days)	Enlarged node location	Treatment
5336	M	315	Left inguinal	Placebo
5395	F	246	Left inguinal & left brachial	Cyclophosphamide
5396	F	246	Right inguinal & left axillary	Cyclophosphamide

**Table 5-1: Details of mice treated with cyclophosphamide/placebo with the age measured on the day of treatment**

The mice were observed as described in section 2.5.5 with regular health checks including weight and tumour measurements. There was a clear reduction in the palpable lymph node caliper measurements in the two cyclophosphamide-treated mice within 3 days of treatment and no evidence of recurrence in the period (Figure 5-4). These mice also showed a weight reduction approximately 7 days after treatment, which was likely to be due to cyclophosphamide toxicity, both mice recovered with additional dietary support.

The placebo-treated mouse underwent a repeat MRI scan on day 24 and the cyclophosphamide-treated mice underwent the repeat scan on day 22. All mice were culled on day 28 and tissues harvested for post-mortem analysis.

Scans show the reduction in size of the enlarged lymph nodes following treatment with cyclophosphamide (Figure 5-5) with no reduction in lymph node size in the placebo treated mouse (Figure 5-6). The lymph node volumes were calculated using ImageJ and the changes in size between the scans is represented in a waterfall plot (Figure 5-7).

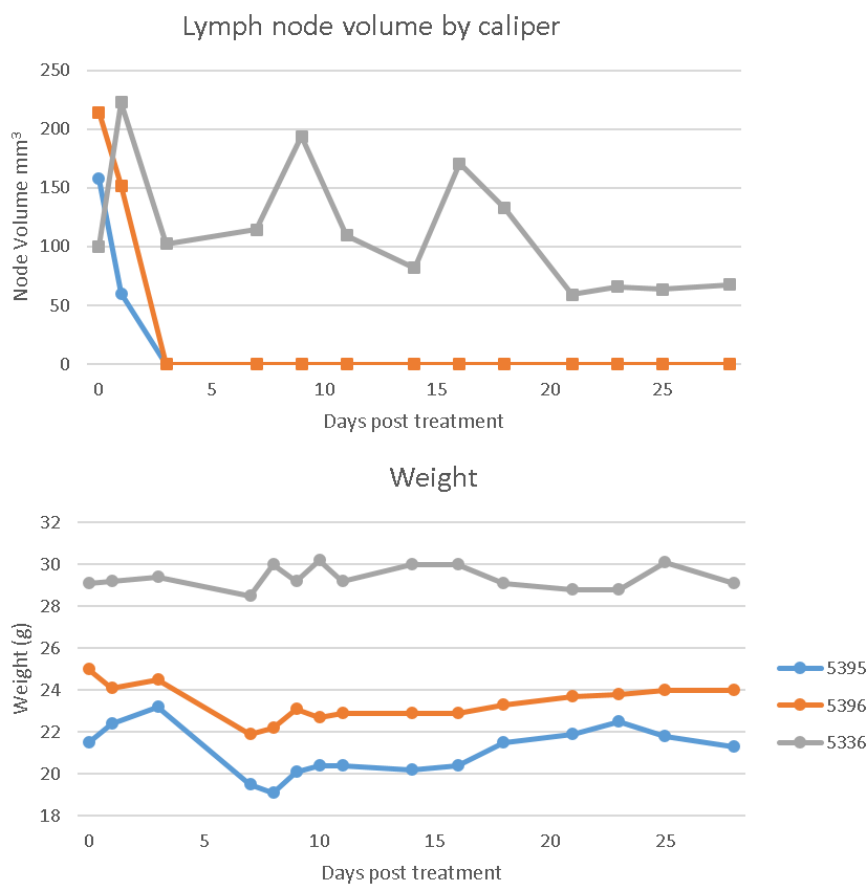


**Figure 5-4: Graphs showing the lymph node volume by caliper measurement and the weight of mice in the cyclophosphamide study**

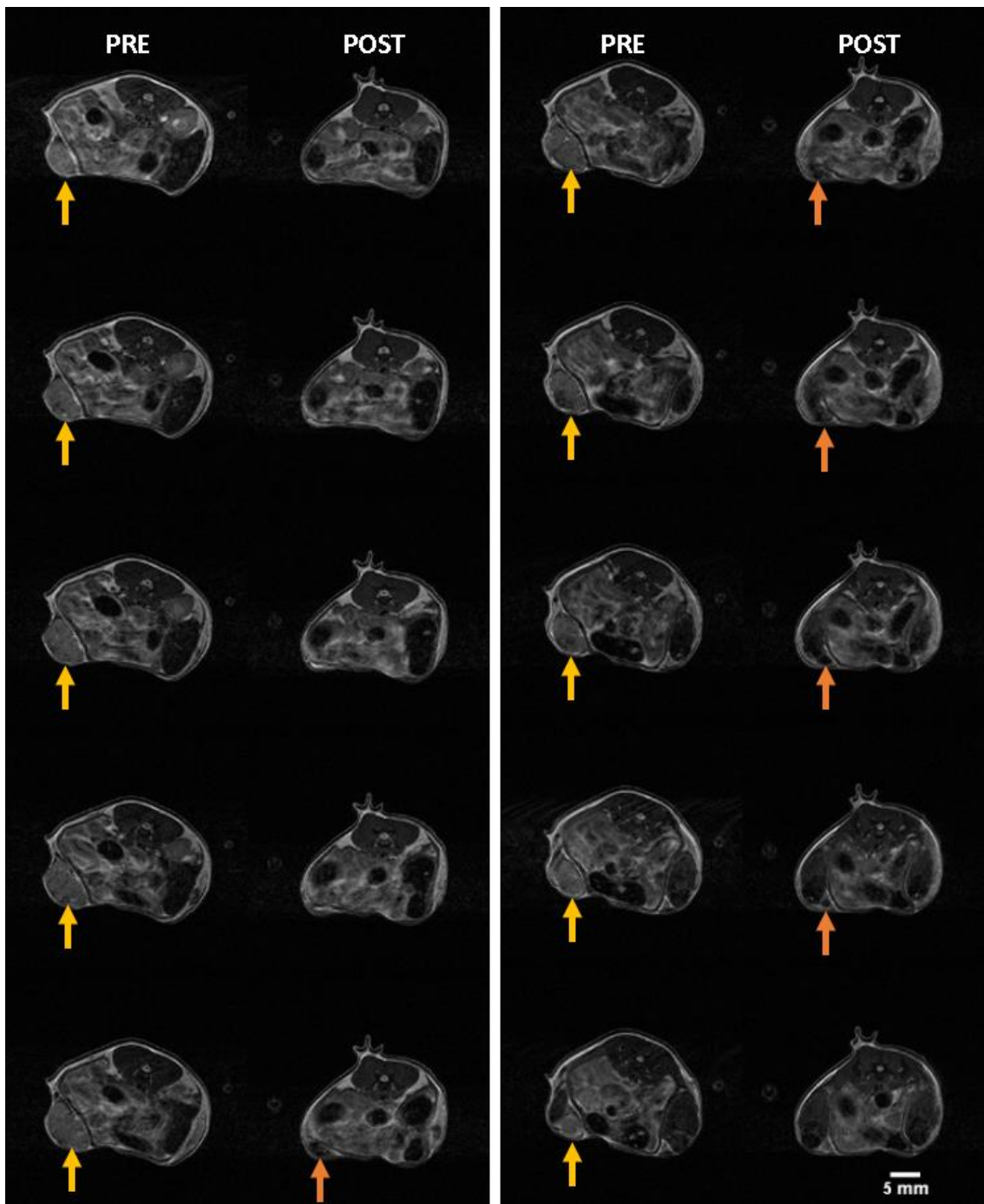


**Figure 5-5: Series of MRI scan images from SRQ5396**

Images from prior to treatment are in the left-hand column of each panel and a follow up scan after 4 weeks in the right-hand column of each panel. Sequential axial images (0.8mm slices) are shown from the most cranial slices at the top of the columns in the left panel. The yellow arrow highlights the enlarged lymph node prior to treatment and the orange arrow highlights the same lymph node following treatment.

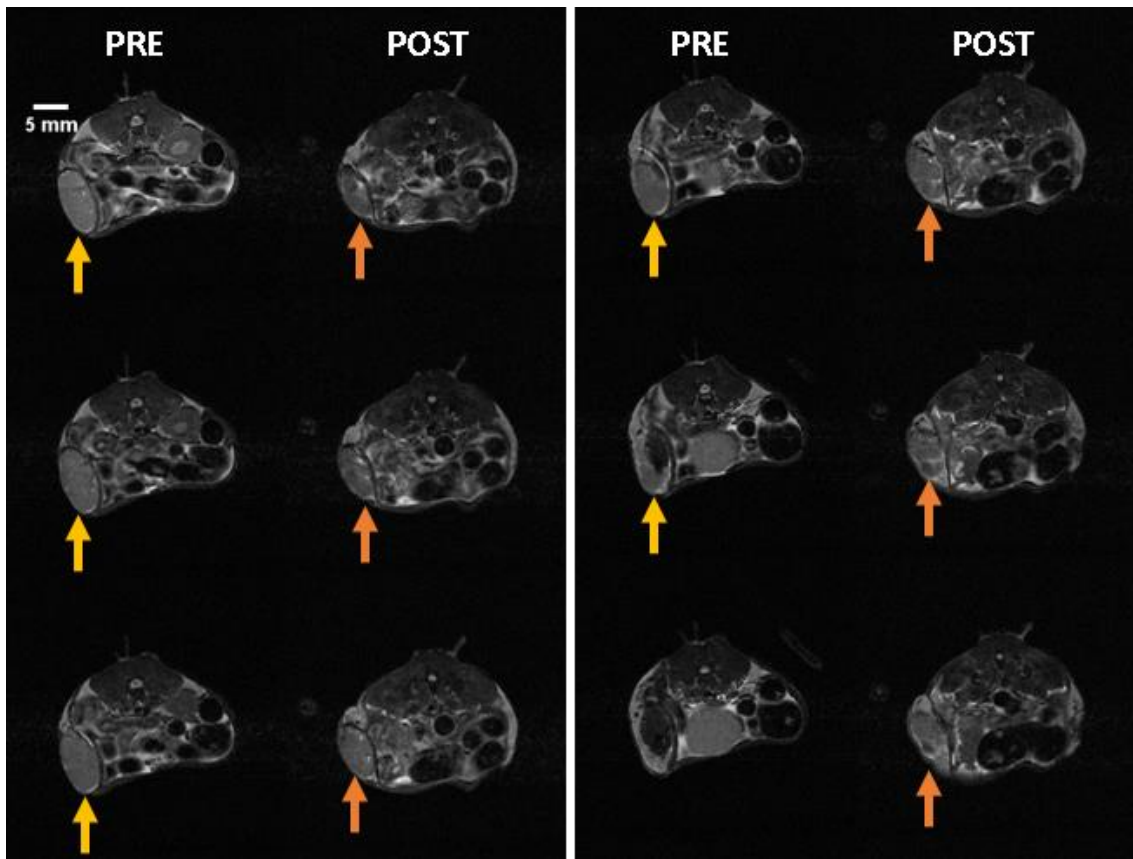


**Figure 5-6: Series of MRI scan images from SRQ5336**

Images from prior to treatment are in the left-hand column of each panel and a follow up scan after 4 weeks in the right-hand column of each panel. Sequential axial images (0.8mm slices) are shown from the most cranial slice at the top. The yellow arrow highlights the enlarged lymph node prior to treatment and the orange arrow highlights the same lymph node following treatment.

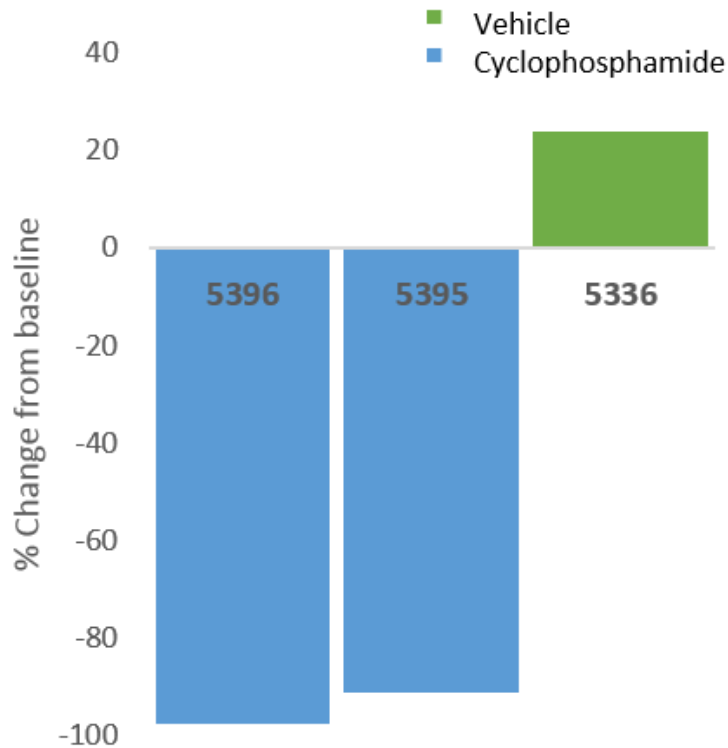


**Figure 5-7: Water fall plot demonstrating the response to cyclophosphamide**

*This waterfall plot shows the percentage change in lymph node volume of the lymph nodes which were enlarged at baseline after treatment with cyclophosphamide or placebo. The blue bars represent the mice treated with cyclophosphamide and the green bar the mouse treated with vehicle only. The x-axis label shows the number assigned to the mouse as an identifier at birth.*

Cell suspensions were produced from the harvested lymph nodes and flow cytometry performed to assess the proportions of B cells, CD4<sup>+</sup> T cells and CD8<sup>+</sup> T cells (Figure 5-8). There was a reduction in the proportion of B cells in the enlarged lymph nodes of the treated mice, producing a profile in keeping with that of non-enlarged lymph nodes. Due to the small numbers involved no statistical tests were performed.

This pilot study showed that the enlarged lymph nodes reduced in response to treatment with a chemotherapy agent suggesting that the model was useful for the preclinical assessment of novel agents.

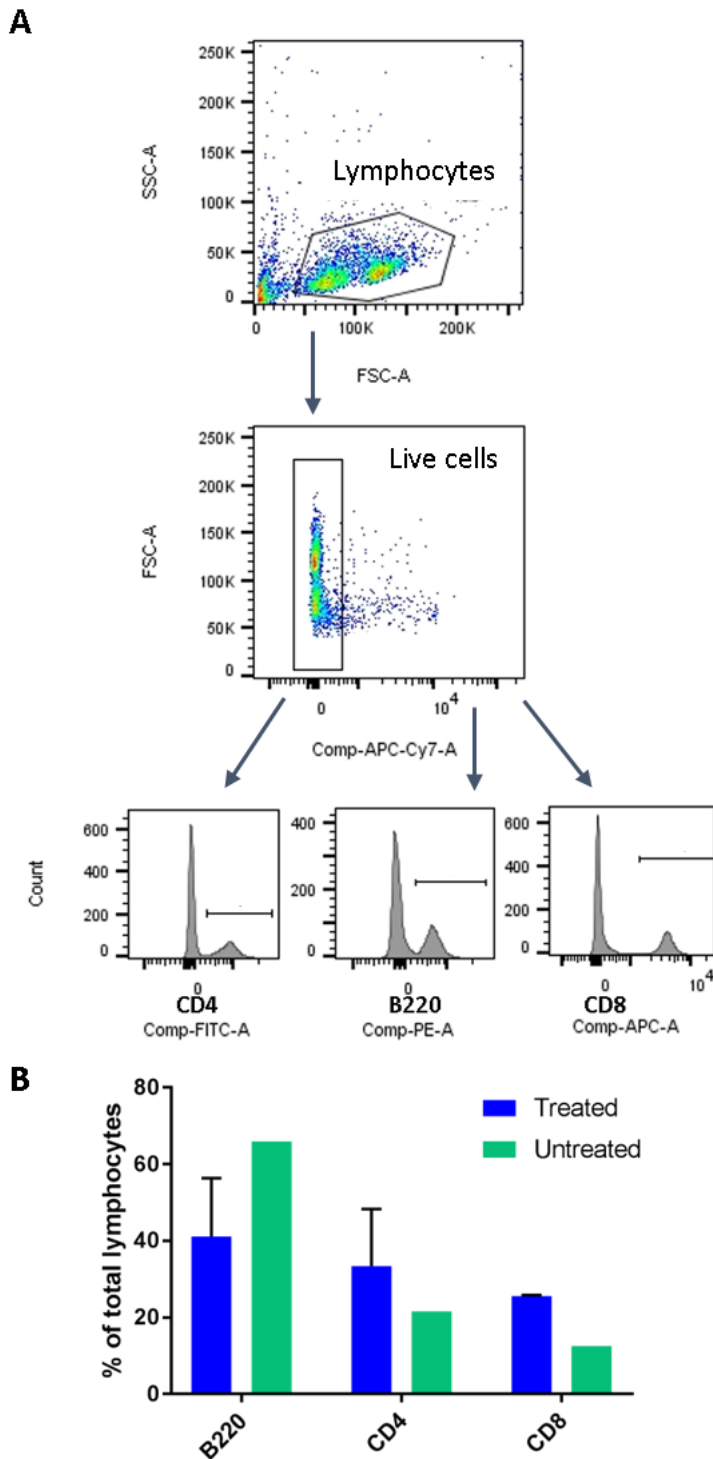


**Figure 5-8: Results of FACS analysis of lymph nodes following treatment of mice with cyclophosphamide/placebo.**

*A: representative FACS plots showing the lymphocyte gate and selection of live cells using Draq7 staining followed by determination of cells stained with appropriate surface markers in the three histograms. B: graph showing the proportions of B cells, CD4<sup>+</sup> cells and CD8<sup>+</sup> cells from enlarged lymph nodes in the untreated mouse (green bars) and two treated mice (blue bars) with the bars representing the mean percentage and error bars the standard deviation.*

## 5.5 A PRECLINICAL STUDY WITH THE ITK/BTK INHIBITOR, IBRUTINIB

Our next aim was to determine the effect of ITK inhibition on the san roque tumours using ibrutinib and assess its potential as a therapy for AITL. Ibrutinib has previously been used in preclinical studies of CLL treatment at a dose of 25mg/kg daily. Ibrutinib was dissolved in 1% 2-HBC and delivered by oral gavage each day.

To show that the vehicle did not alter the effect of ibrutinib on T cell survival we compared the effect of ibrutinib dissolved in DMSO and 2-HBC on Jurkat cells. Ibrutinib was dissolved in DMSO or 10% 2-HBC and added to Jurkat cells cultured in RPMI with 10% FCS and 1% Glutamax at a range of concentrations. This showed similar IC50 concentrations of 6.79 $\mu$ M (5.73-8.05) for DMSO and 6.10 $\mu$ M (5.01-7.32) for 2-HBC (Figure 5-9).

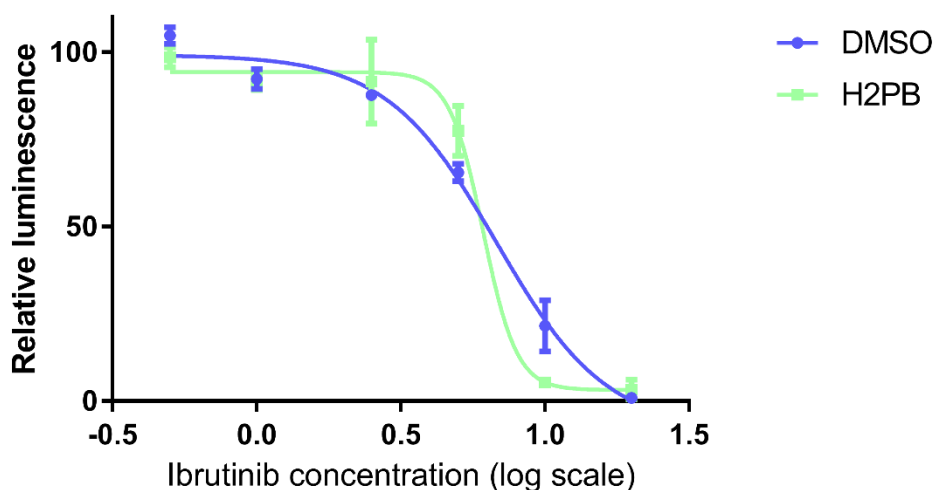


**Figure 5-9: Graph showing the effect of ibrutinib vehicle on Jurkat cells assessed by CTG assay.**

The relative luminescence of Jurkat cells treated with ibrutinib at a range of concentrations as shown in the x-axis (log<sub>10</sub> scale of  $\mu$ M concentrations). The mean of 3 readings is shown with the standard deviation represented by the error bars and luminescence calculated relative to cells cultured with vehicle alone. The green line shows the results when ibrutinib was dissolved in H2PB and the blue line in DMSO.

### 5.5.1 Cohort 1

In the first cohort we identified 12 mice with palpable tumours and 4 were treated with vehicle alone and 8 with ibrutinib. To determine if there was a progressive treatment effect over time one mouse received 7 days ibrutinib, one received 14 days, one received 21 days and the remaining received 28 days. All vehicle treated mice received

28 days of treatment. Prior to the initiation of treatment mice underwent an MRI scan under general anaesthetic. During treatment mice were weighed 3 times a week and tumour measurements were carried out with calipers. Treatment was well tolerated with no significant changes in weight or health concerns during the course. Details of the mice in this cohort are shown in Table 5-2.

Following completion of treatment, the mice underwent a second MRI scan under general anaesthetic. The following week the mice were anaesthetised, blood collected via cardiac puncture and death confirmed by cervical dislocation. Lymph nodes, spleen and liver were harvested for further analysis.

Mouse	Sex	Age (days)	Treatment group	Enlarged lymph nodes
5349	M	377	Ibrutinib 28 days	Left inguinal & right axillary
5350	F	377	Ibrutinib 28 days	Right inguinal
5412	F	332	Ibrutinib 28 days	Left inguinal & left axillary
5468	F	267	Ibrutinib 28 days	Left inguinal
5488	F	270	Ibrutinib 28 days	Right inguinal & left axillary
5547	F	209	Ibrutinib 21 days	Right inguinal & right axillary
5469	F	281	Ibrutinib 14 days	Right inguinal
5535	F	231	Ibrutinib 7 days	Right inguinal
5403	F	327	Vehicle	Left inguinal & bilateral axillary
5427	F	318	Vehicle	Left inguinal
5498	F	256	Vehicle	Right inguinal & right axillary
5524	F	227	Vehicle	Right inguinal & left axillary

**Table 5-2: Details of mice in cohort 1 with the age measured on the first day of treatment**

### 5.5.2 Cohort 2

To assess the effect of a longer treatment period a further 8 mice with palpable tumours were identified 4 of whom were treated with ibrutinib and 4 with vehicle for a total of 7 weeks. As previously mice underwent an MRI scan under general anaesthetic prior to the start of treatment and regular health monitoring during treatment. Additional diffusion weighted images were captured for this cohort where possible. The details of the mice in this cohort are shown in Table 5-3.

Following completion of treatment, the mice underwent a second MRI scan under general anaesthetic. The following week the mice were anaesthetised, blood collected via cardiac puncture and death confirmed by cervical dislocation. Lymph nodes and spleen were harvested for further analysis. On this occasion the cardiac puncture yielded insufficient blood for further analysis in 5 of the 8 subjects so no further analysis was undertaken.

Mouse	Sex	Age (days)	Treatment group	Enlarged node location
5617	F	335	Ibrutinib 56 days	Left inguinal
5700	F	241	Ibrutinib 56 days	Bilateral inguinal
5528	F	475	Ibrutinib 56 days	Bilateral inguinal & left brachial
5690	F	248	Ibrutinib 56 days	Left inguinal & right axillary
5580	F	410	Vehicle	Right inguinal
5680	F	260	Vehicle	Left inguinal
5560	F	439	Vehicle	Left inguinal
5684	F	255	Vehicle	Left inguinal, left brachial & left axillary

**Table 5-3: Details of mice in cohort 2 with the age measured on the first day of treatment**

### 5.5.3 Response assessment by MRI

Lymph node volumes before and after treatment were calculated using ImageJ and change in enlarged lymph nodes used to assess response to treatment.

A range of treatment responses were seen (Figure 5-11) and one of the vehicle-treated mice in cohort 1 showed a spontaneous tumour regression with a reduction in tumour size of 50%. In the second cohort with longer treatment duration a response was seen in 3 of the 4 treated mice and progressive or stable disease seen in 3 of the 4 vehicle treated mice. One of the vehicle treated mice showed a small reduction in lymph node volume between the two scans. Overall the mice treated with ibrutinib showed a higher rate of lymph node size reduction and this was more apparent with longer treatment durations as can be seen in a waterfall plot (Figure 5-10).

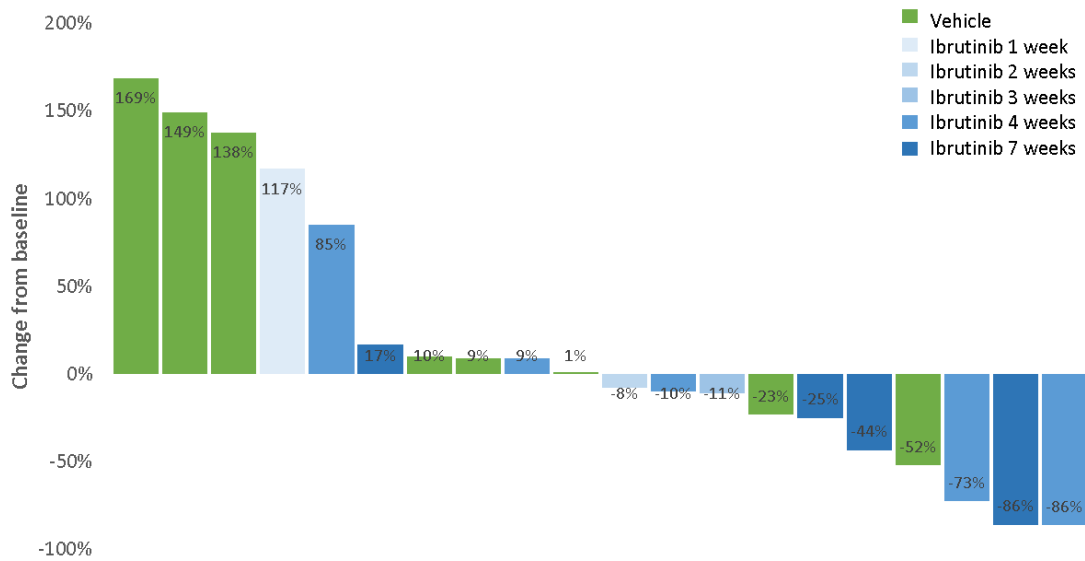


**Figure 5-10: Water fall plot showing the change in volume of enlarged pre-treatment lymph nodes following therapy.**

Each bar represents the change in volume of all enlarged lymph nodes in an individual mouse measured from the end of treatment scan when compared to the pre-treatment scan, with the % change shown alongside each bar. Green bars represent mice treated with placebo and blue bars mice treated with ibrutinib, with increasing length of treatment represented by darker shades.

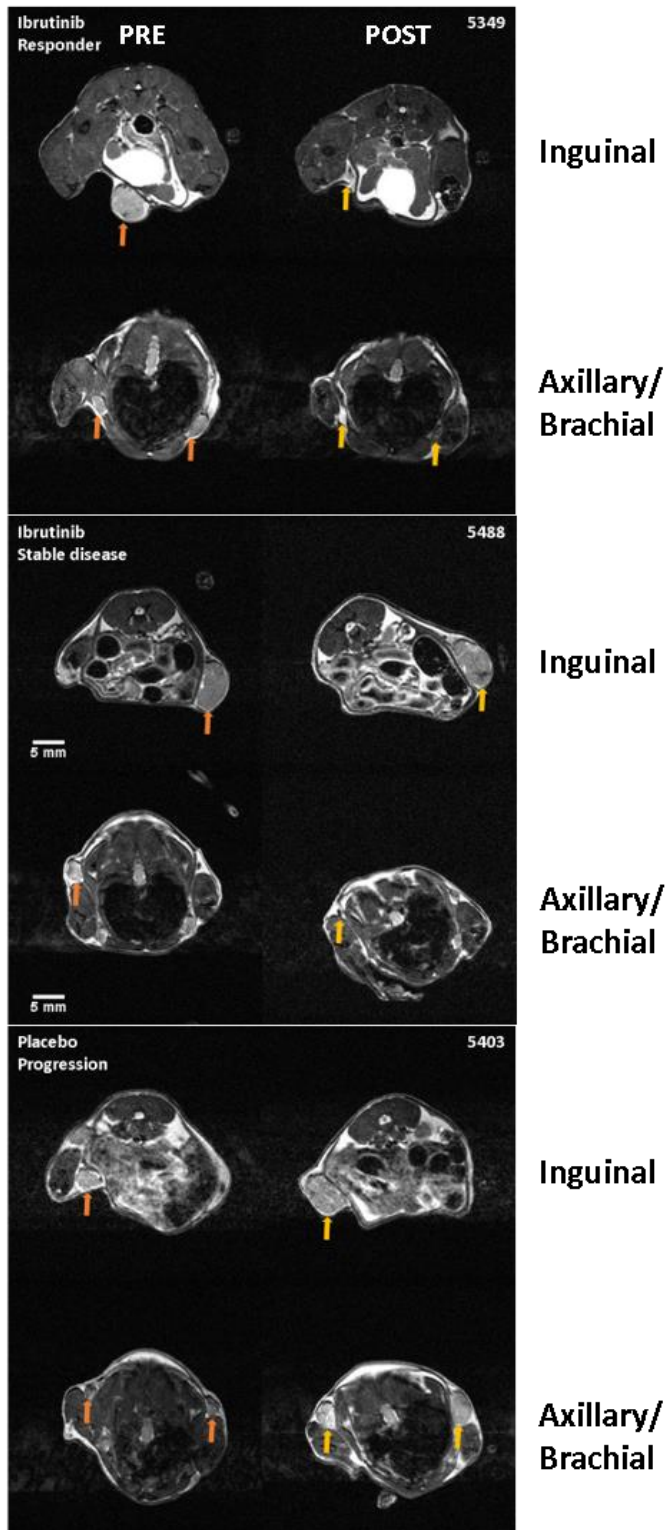


**Figure 5-11: Representative MRI scan images from the first cohort of mice treated with ibrutinib or vehicle.**

MRI scan images from the inguinal and axillary/brachial regions before and after treatment showing examples of response, stable disease and progression from the first cohort of mice in the ibrutinib study with the orange arrows highlighting lymph nodes prior to treatment and the yellow arrows showing the same lymph nodes following treatment.

#### 5.5.4 Post mortem analysis

To better understand the effect of ibrutinib on the lymph node composition several experiments were carried out on cell suspensions produced from the enlarged lymph nodes and serum collected at the time of post mortem.

##### *5.5.4.1 Assessment of lymph node composition after ibrutinib therapy with FACS*

Flow cytometry was used to analyse the proportion of B cells, CD4<sup>+</sup> and CD8<sup>+</sup> T cells in enlarged lymph nodes following treatment. This showed that the proportions of these lymphocyte subsets were no different following treatment with ibrutinib in the post-mortem samples (Figure 5-12 A). There was also no difference when the treated mice were analysed by response (Figure 5-12 B) with progressive disease (PD; n=2) defined as an increase of greater than 50% in lymph node volume, partial response (PR; n=4) defined as a reduction of greater than 50% in lymph node volume and stable disease (SD; n=6) as all others. Differences between treated and untreated mice were assessed using t-tests with a correction for multiple comparisons.

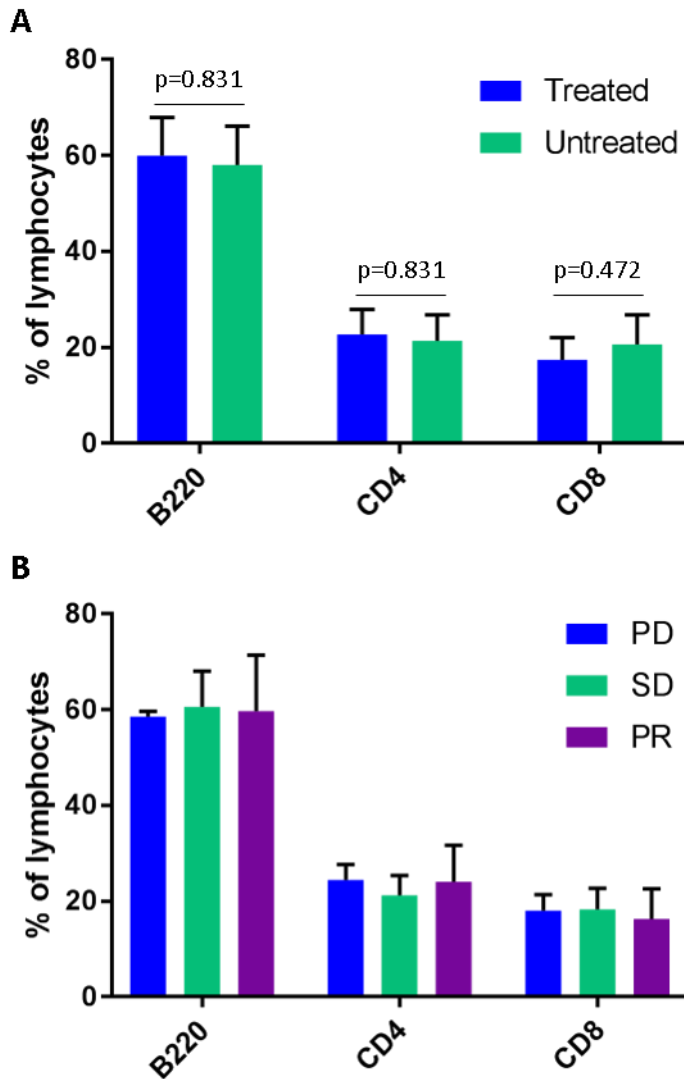


**Figure 5-12: FACS to assess lymphocyte subsets following ibrutinib treatment.**

Both charts show the mean percentage of all lymphocytes with standard deviation shown by the error bars. The p-values were calculated by t-tests with a correction for multiple comparisons. A- shows the results for treated (blue; n=12) and untreated (green; n=8) mice. B- shows the results for treated mice when categorised by response (see text).

Flow cytometry was also used to assess the proportion of Tfh cells within the CD4<sup>+</sup> T cell population. As with the lymphocyte subset analysis there were no differences in the proportion of Tfh cells based upon treatment (Figure 5-13 A) using t-tests with correction for multiple comparisons. The numbers of mice when categorised by response are small but the proportion of Tfh cells is shown in Figure 5-13 B.

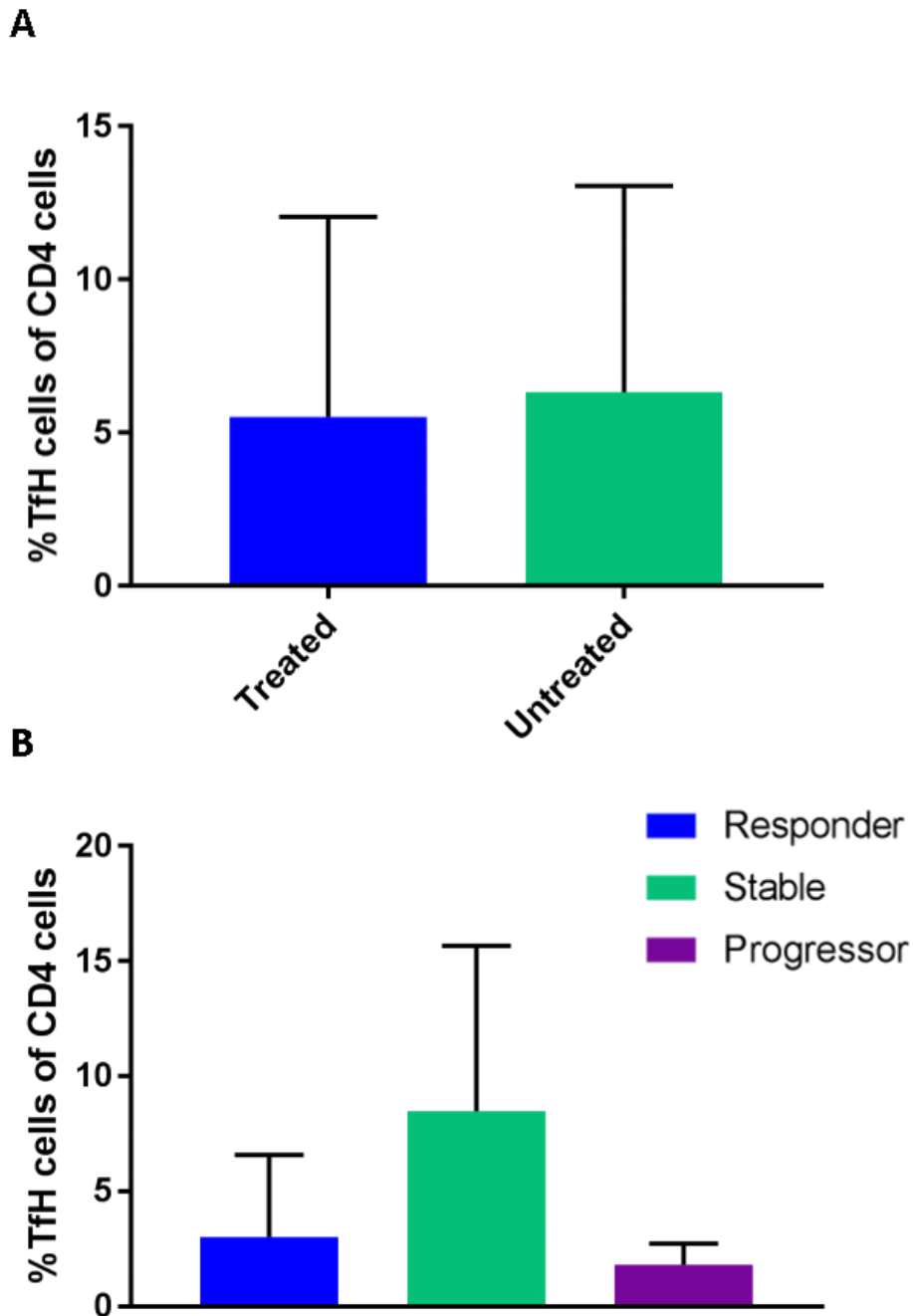


**Figure 5-13: FACS to assess Tfh populations following ibrutinib treatment.**

Both charts show the mean Tfh percentage of CD4<sup>+</sup> lymphocytes with the standard deviation shown by error bars. A- shows the results for treated (blue n=12) and untreated (green n=8) mice. B- shows the results for treated mice when categorised by response.

#### 5.5.4.2 Assessment of ibrutinib effect on serum IL-21

IL-21 is an important cytokine in Tfh differentiation and is secreted by Tfh cells. In order to assess if it could be used as a biomarker to show response to therapy we collected

serum from the mice in cohort 1 and an IL-21 ELISA was performed as described in section 2.5.7.

A standard curve was generated with a line of best fit plotted. Results from the mouse samples showed an undetectable level of IL-21 in 7 mice (<8 pg/ml). The results from the other 5 mice enabled the IL-21 level to be determined from the standard curve, 2 of these mice were untreated and 3 were treated and showed SD. There was no association between treatment (Figure 5-14) or response and the IL-21 level.

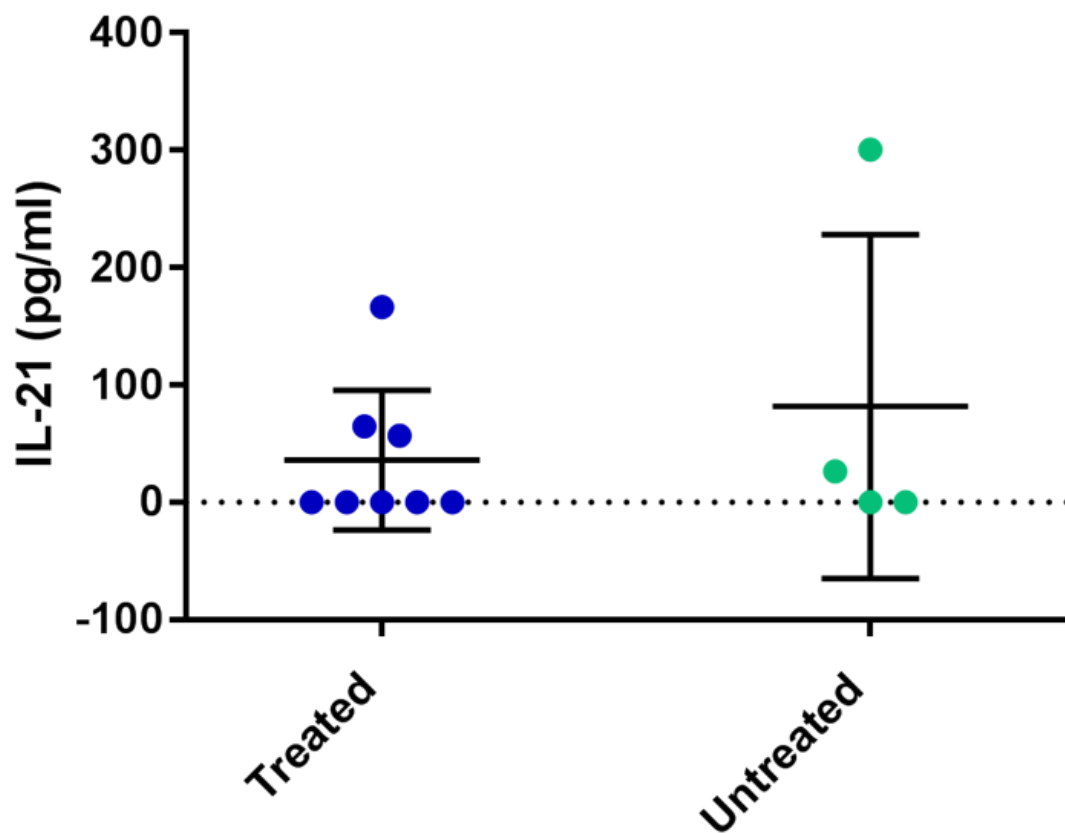


**Figure 5-14: Assessment of serum IL-21.**

Individual IL-21 serum levels are shown by dots with undetectable samples plotted at 0. Blue dots represent treated mice (n=8) and green dots represent untreated mice (n=4). Error bars show the standard deviation.

#### 5.5.4.3 Microarray to assess effect of ibrutinib treatment on gene expression

To assess the difference in gene expression between lymph nodes in mice treated with ibrutinib compared to those treated with placebo a microarray was carried out. RNA was extracted from cell suspensions produced from the enlarged lymph nodes of

treated and untreated mice. A total of 6 samples (4 treated and 2 untreated) were analysed using SurePrint G3 Mouse GeneExpression v2 Microarray Kit from Agilent as described in section 2.5.16. Samples selected were those with sufficient good quality RNA. Three of the treated mice showed stable disease and the other progressed on treatment. One of the untreated mice showed progressive disease over the course of the treatment period (4 weeks) and the other showed stable disease.

Results were normalised using Partek® Genomics Suite® software, version 7.0 Copyright ©; 2018 Partek Inc., St. Louis, MO, USA. Further analysis was performed using MultiExperiment Viewer (MeV) from the TM4 suite of software developed by The Institute for Genomic Research (208).

Using the two-class unpaired Significance Analysis of Microarrays (SAM) a list of differentially expressed genes was generated using a random selection of 100 permutations. Using a delta-value of 1.76 a total of 54 genes were differentially expressed (Figure 5-15) with a median false discovery rate of 10%. All genes were more highly expressed in the untreated mice (Figure 5-16).

The list of differentially expressed genes was analysed using The Database for Annotation, Visualization and Integrated Discovery (DAVID ) v6.8 (209,210).

Using the Functional Annotation Clustering tool with the selected databases shown in Table 2-6 Table 2-6 there were 4 annotation clusters produced based upon Up\_Keywords in the functional categories. These categories may also be based upon cellular location and although the genes are thought to have similar functions there were no over-represented pathways found.

Cluster one includes genes associated with cell membranes, particularly G-protein coupled receptors. Cluster two includes genes which produce secreted proteins. Cluster three includes genes which produce cytoplasmic proteins with a role in the cytoplasmic skeleton. Cluster four includes genes encoding phosphoproteins.

These categories are primarily location based and do not represent any over-represented pathways or indicate any clear effect of ibrutinib on gene expression related to cell survival pathways.

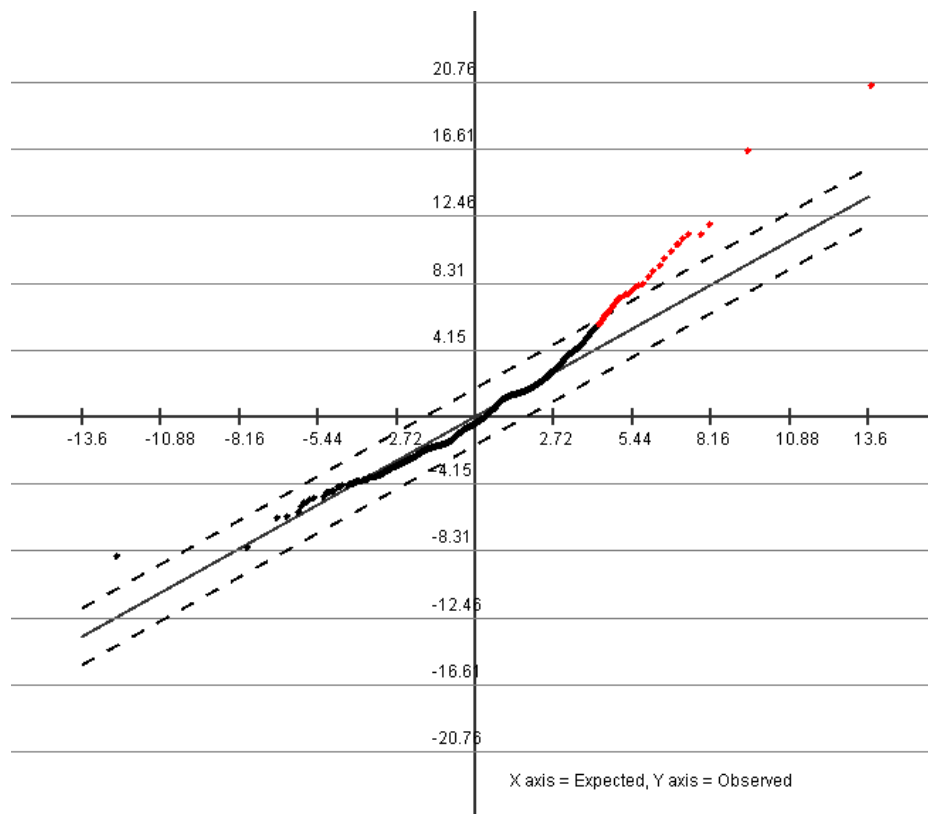


**Figure 5-15: SAM graph from MeV**

*This graph from MeV shows the initial output of SAM with genes which are significantly more highly expressed in the untreated mice shown in red.*

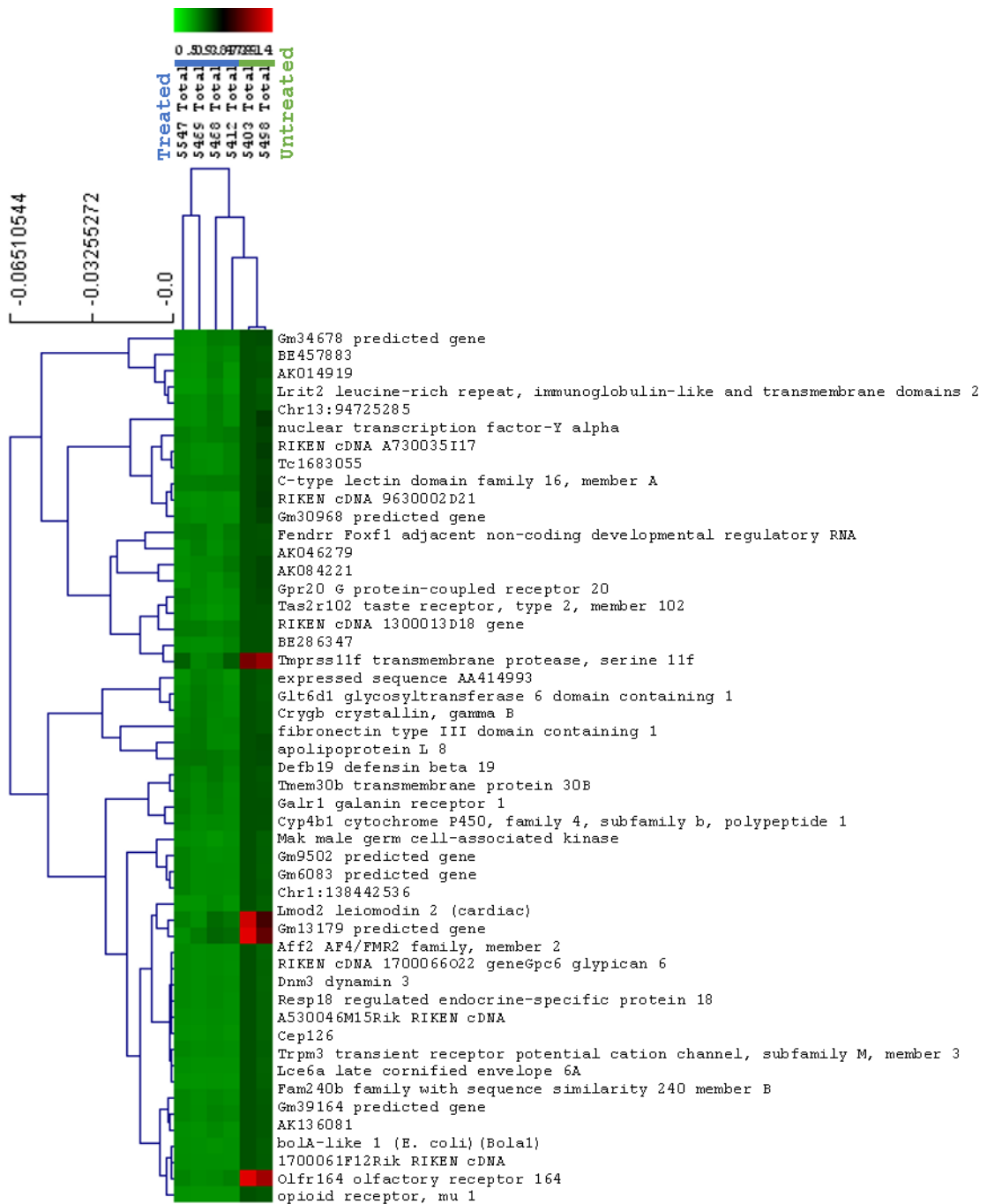


**Figure 5-16: Hierarchical clustering generated from genes with significantly different upregulation by SAM analysis**

The mice analysed are listed across the top and the 4 treated mice are the left-hand columns and the 2 untreated are the right-hand columns. Genes which are significantly different in the level of upregulation in untreated mice by SAM analysis are listed to the right of the heat map.

#### 5.5.4.4 Assessment of CD4<sup>+</sup> T cell response to stimulation using *in Vitro* cell culture

To assess changes in CD4<sup>+</sup> T cell response to stimulation after *in vivo* ibrutinib treatment culture of cells was carried out. Following tissue harvest from mice in cohort 2, CD4<sup>+</sup> T cells were selected from a portion of the lymph node cell as described in section 2.5.8. These cells were then added to culture medium and cultured with or without stimulation in a 96 well plate. Stimulation was performed using anti-CD3 +/- anti-CD28. After 48 hours the cells were analysed for viability using an ATP luminescence assay as described in section 2.5.13. Each condition was performed in triplicate.

There was no difference in the effect of stimulation with anti-CD3 between the cells from lymph nodes in untreated mice compared to the treated mice ( $p=0.531$ ) or in the effect of stimulation with anti-CD3 and anti-CD28 ( $p=0.602$ ) using t-test with correction for multiple analyses. The addition of anti-CD28 to anti-CD3 had no effect upon the level of viability seen using the CTG assay in CD4<sup>+</sup> T cells from the lymph nodes of treated or untreated mice (Figure 5-17). There was no difference in the raw luminescence values for the unstimulated cells when comparing treated and untreated mice ( $p=0.856$ ).

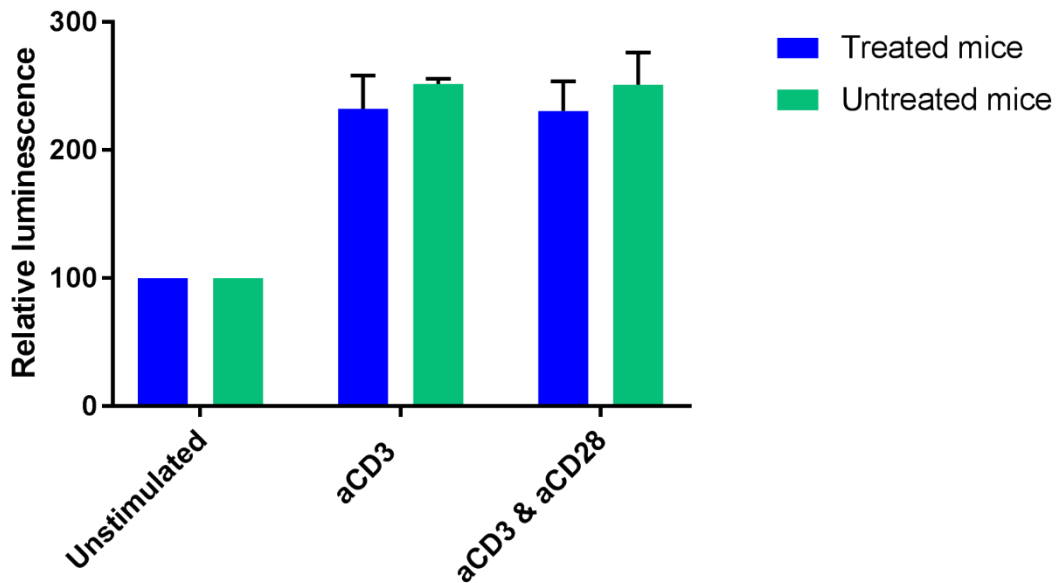


**Figure 5-17: Bar graph showing the effects of stimulation of CD4<sup>+</sup> T cells in cell culture.**

The bars represent the relative luminescence from an ATP luminescence assay comparing cells in experimental conditions to unstimulated cells. The CD4<sup>+</sup> T cells were extracted from the enlarged lymph nodes of ibrutinib-treated (blue n=4) or untreated (green n=4) mice.

## 5.6 DISCUSSION

As described in section 1.10 there is a lack of mouse models that are faithful representations of human T cell lymphoma. Here the san roque mouse strain has been explored as a model for pre-clinical testing. The novel aspects of this strain are that it is immunocompetent and produces genetically diverse lymphomas. The implications of the model are that, as with genetically heterogeneous human disease, only a proportion would be expected to respond to any particular treatment.

Our attempts to generate an adoptive transfer model were unsuccessful with transfer of lymph node cell suspensions into SCID-Beige mice causing rapid and severe illness. The SCID-Beige mice are deficient in T cells, B cells and NK cells. Although these mice have been used for xenograft models (238) we found that all recipient mice were euthanized or died within 10 days of intravenous cell injection. It may be possible to carry out subcutaneous injection or intraperitoneal injection (239) of cells to produce mice with identical tumours.

Transfer of cells to the immunocompetent WT littermates did not produce any tumour development despite the use of sublethal irradiation. We may have had greater success if we had selected cells for transfer rather than using the entire lymph node population given that any tumour cells are only a small proportion and these recipients would have provided a microenvironment for tumour development. Other methods of xenografting such as subcutaneous injection could also have been considered.

Our imaging and drug treatment work included a high proportion of female mice as the majority of tumour bearing mice were female (65%) and this also enabled mice receiving the same treatment to be housed together and limited the need for single housing.

The concept of "mouse hospital" has been developed to support the idea that animal models faithful to human disease can be used to inform clinical trial design by providing pharmacokinetic and pharmacodynamic data as well as data on responses in different contexts (240). The work here sits within this framework and suggests that some patients with ITK expressing T-cell lymphoma will respond to ibrutinib. The genetic basis for these responses will need further work to elucidate.

MRI scans enabled assessment of tumour volume and were used to monitor response to treatment in this mouse model of lymphoma. The mice tolerated the scans suggesting that scans could be carried out multiple times over the course of a longer treatment period.

The san roque model shows similarities to AITL as shown by the increase in B cells present in tumour lymph nodes described in section 4.3.2 and occasional cases of spontaneous regression (241-243). The benefit of a genetically diverse model is that it offers a more accurate representation of human disease and the genetic diversity seen amongst patients.

Ibrutinib treatment in our cohort produced a mixed response but there is a suggestion that longer treatment times produced more responses. Treatment was well tolerated, and further assessment of longer treatment durations could be considered.

The results of the post mortem analysis did not show many significant changes between treated mice and untreated mice. This may be explained by the period of up to 10 days between the last dose of ibrutinib and the post mortem due to the design of the experiment and timing of the MRI scans.

In an assessment of the effect of ibrutinib on the transcriptome in CLL the authors describe the results of both WES and RNA-sequencing (244). They profiled the CLL transcriptome in 14 patients at baseline and after 1 month and 6 months of ibrutinib therapy. They showed that of genes with differential expression at baseline and after treatment the majority (498 of 653 genes) were down-regulated. They found that changes became more pronounced with longer treatment duration. Consistent with this finding, in our study the differentially expressed genes were all down-regulated in the treated cohort. Although we have not demonstrated pathways regulated by ibrutinib it is possible that some of the genes whose expression is altered might be biomarkers of response.

## 6 CONCLUSIONS

---

### 6.1 RHOA MUTATION: COULD LOSS OF PROTEIN EXPRESSION CONTRIBUTE TO LYMPHOMAGENESIS?

Recent advances in T cell lymphoma include the discovery of recurrent mutations in Tfh lymphoma which suggest that the combination of epigenetic dysregulation and RHOA<sup>G17V</sup> mutation along with activation of the TCR-signalling pathway are important contributors to the development of T cell lymphoma (73,245,246). The co-operation between TET2 and RHOA mutations has been confirmed in mouse models which have suggested that RHOA<sup>G17V</sup> leads to activation of signalling pathways (184-186) despite the fact the G17V mutation leads to reduced activation.

To better understand the role of mutated RHOA in T cell lymphomagenesis the expression of RHOA constructs in bacterial and mammalian cells was determined and demonstrated that the induced expression of RHOA<sup>G17V</sup> is lower than that of RHOA<sup>WT</sup>. This may be due to reduced protein stability as suggested by the lower melting point of the RHOA<sup>G17V</sup> protein. This reduced expression is mentioned in a review paper from one group (143) but is not commented upon by the papers which originally described the RHOA mutation in T cell lymphoma.

The mutations found in RHOA in AITL appear to alter both the amount of protein and its function. The G17V mutation occurs within the GTP-binding domain with the larger valine subunit likely to lead to altered GTP binding and potentially protein stability. The mutation at F25L shown by our laboratory (217) does not occur within the GTP-binding site but alters the interaction with amino acid 171 which may alter the GTP binding site conformation along with changes in the protein stability.

Assessment of the role of protein degradation in reduced expression could be determined by using proteasome inhibitors and assessing their effect upon the expression of RHOA in WT and mutant forms.

A mouse strain with RHOA deficient T cell precursors has been shown to develop T cell lymphoma (127). This is potentially interesting and might suggest that PTCL could have a very early origin in the thymus as has been suggested for ALCL (247). However, it seems that RHOA<sup>G17V</sup> is an acquired mutation and sequencing studies have suggested that RHOA mutations occur subsequent to TET2 mutations (196,197).

A more recently described mouse model (185) in which RHOA<sup>G17V</sup> was expressed under the control of the CD4 regulatory elements demonstrated mRNA expression of RHOA<sup>G17V</sup> but protein immunoblotting cannot differentiate between endogenous RHOA<sup>WT</sup> expression and RHOA<sup>G17V</sup>.

It remains an open question as to whether the effect of the RHOA<sup>G17V</sup> mutation is due primarily to a RHOA deficiency or, as has been suggested by one group, dysregulation of signalling downstream of RHOA (145). These authors showed that RHOA<sup>G17V</sup> binds to VAV1 leading to its activation (145). They also found markedly lower levels of RHOA<sup>G17V</sup> expression compared to RHOA<sup>WT</sup>, although this is not commented upon.

Several models have now shown alterations in downstream signalling pathways in the presence of the RHOA<sup>G17V</sup> mutation suggesting that the mutated RHOA protein interacts either directly or indirectly with components of the TCR signalling pathway (145,184-186). The prevalence of mutations in the TCR signalling pathway in cases of AITL suggests that activation of the TCR pathway plays an important role in the development of AITL.

A better understanding of the effect of the RHOA<sup>G17V</sup> and RHOA<sup>F25L</sup> mutations could be developed with the use of CRISPR/Cas9 techniques to introduce the mutation and assess the subsequent RHOA expression and effect upon cell behaviour. Although the lack of model Tfh cell lines might be problematic this technique could elucidate the molecular mechanism of action of RHOA and potentially guide whether targeting of the TCR or other signalling pathway would be a useful therapeutic target.

## 6.2 THE SAN ROQUE MOUSE STRAIN IS A USEFUL PRE-CLINICAL MODEL FOR TESTING NOVEL AGENTS THAT MIGHT BE BENEFICIAL IN T-CELL LYMPHOMA

Clinical trials are currently the only means of bringing new drugs into clinical practice, but they are expensive to carry out and carry a high risk of failure. It is recognised that cancers are genetically heterogeneous and that even within the same histological group there are different molecular drivers of disease. There is, therefore, interest in "de-risking" trials by targeting agents to specific groups of patients for whom pre-clinical testing has suggested a benefit. Using animal models that are faithful to the human disease has an important role in this process.

The SRQ mouse model was developed a few years ago (Ellyard et al (176)) and preliminary work suggested that animals heterozygous for an activating mutation leading to increased numbers of Tfh cells, develop Tfh lymphomas with fairly long latency and in about 50%. There are no standard pre-clinical models of Tfh lymphoma and, therefore, the SRQ mouse strain could form a useful part of pre-clinical testing. There appear to be few, if any, cell lines representative of Tfh cells and, therefore, cell line testing will always be limited. Pre-clinical testing in animal models is a routine part of drug development as molecules developed and tested in vitro in cell lines require pharmacodynamic and pharmacokinetic assessment in preclinical models prior to first in man trials.

The SRQ mouse model produces genetically diverse Tfh lymphoma on an immunocompetent background, which, in keeping with human Tfh lymphoma, shows a proliferation of reactive B cells in the microenvironment. I undertook a limited sequencing study of two tumours to try to assess genetic drivers of disease. This produced complex results. While certain genes were mutated in lymphomas and not in other tissues from the diseased mouse or littermate controls the study did not reveal mutations in the group of genes involved human lymphoma with the exception that RhoA was altered at a residue close to the GTP binding site in one case. Further work will be necessary to understand if genes found in this study (Hsp90ab1, Ccnb3 and Pdzn4) are drivers of the mouse disease.

In order to carry out a study as close as possible to a clinical trial, tumour volumes were assessed by MRI scanning before and after treatment. This method of imaging was used partly because of local expertise but it also represents a feasible means to obtain *in vivo* tumour measurements and enabled the assessment of response to treatment. Potentially diffusion weighted MRI imaging is a technique that can be used for functional imaging while the T2 weighted imaging (reported in this thesis) was used to obtain structural information.

ITK is a target for therapy in Tfh lymphoma because it is highly expressed in Tfh lymphoma and the ITK:SYK translocation, which is present in a minority of follicular Tfh provides a genetic link to the disease. In addition mutations leading to increased TCR signalling are recognised in PTCL (73) and ITK is a constituent of the proximal TCR signalling pathway. VAV1 is also a target for mutation in PTCL and a potential target for treatment (114,145). ITK is upstream of VAV1 and inhibition of ITK might be a route to abolish VAV1 effects. There is now extensive experience with the BTK inhibitor, ibrutinib, in B-cell lymphomas (248-250) and this drug also inhibits ITK (161). An action of ibrutinib in Tfh lymphoma may be due to the combined effect upon inhibition of ITK in T cells and BTK in B cells with subsequent effects upon the microenvironment.

ITK inhibition with ibrutinib led to reduced proliferation and differentiation of CD4<sup>+</sup> T cells from WT and SRQ mice in response to stimulation *in vitro* without any prominent differences in gene expression. This could have been because of the experimental conditions used or reflect the fact that most of the important changes are post-transcriptional.

Mice were treated with ibrutinib for varying lengths of time. Although treated mice showed definite evidence of response that was not observed in the control group there were confounding factors such as spontaneous regression of tumours. Spontaneous regression has been reported in human AITL (242) and this does not, therefore, diminish the usefulness of this animal model. In addition, the modifying effects of mutations could play a role in generating variation in response with some lymphomas being truly resistant to ITK inhibitors due to indirect genetic mechanisms, while others might need longer periods of treatment before an effect is observed.

A recently published pilot trial of ibrutinib in T cell lymphoma (both PTCL and cutaneous T cell lymphoma) included 13 patients of whom only one responded to therapy (251). In this study, most patients had Sézary Syndrome (a cutaneous and peripheral blood type of T cell lymphoma) and none of the patients had AITL/Tfh lymphoma. The results obtained in this thesis with the san roque preclinical model suggest that ibrutinib may be effective in a proportion of cases of Tfh lymphoma suggesting that further study of ibrutinib in patients with Tfh lymphoma, and particularly those expressing ITK, is warranted.

Collectively the san roque mouse is a promising model system for pre-clinical studies in Tfh lymphoma. Further characterisation of the molecular drivers of the lymphomas produced by these animals might help to define markers associated with response or resistance to treatment and inform the design of future clinical trials.

### 6.3 FUTURE DIRECTIONS

Further assessment of the genetic drivers of the Tfh lymphoma occurring in the san roque mice could be established with further WES and subsequent targeted sequencing. Given the importance of mutations in genes involved in epigenetic changes an assessment of the methylation patterns in the san roque mice may add to the validity of the model.

Those mice which were unresponsive to ITK inhibition also offer a useful source of information and assessment of genetic changes in these mice could offer an insight into mechanisms of resistance.

The addition the RHOA<sup>G17V</sup> mutation to T cells of the san roque mouse would potentially be interesting, offering an opportunity to assess the effect upon tumour prevalence and behaviour.

## 7 REFERENCES

---

- (1) Smith A, Crouch S, Lax S, Li J, Painter D, Howell D, et al. Lymphoma incidence, survival and prevalence 2004-2014: sub-type analyses from the UK's Haematological Malignancy Research Network. *Br J Cancer* 2015;112(9):1575-1584.
- (2) Swerdlow SC, Campo E, Harris NL, Jaffe ES, Pileri SA, Stein H, et al. WHO Classification of Tumours of Haematopoietic and Lymphoid Tissues. revised 4th ed. Lyon, France: International Agency for Research on Cancer; 2017.
- (3) Federico M, Rudiger T, Bellei M, Nathwani BN, Luminari S, Coiffier B, et al. Clinicopathologic characteristics of angioimmunoblastic T-cell lymphoma: analysis of the international peripheral T-cell lymphoma project. *J Clin Oncol* 2013;31(2):240-246.
- (4) Vose J, Armitage J, Weisenburger D, International T-Cell LP. International peripheral T-cell and natural killer/T-cell lymphoma study: pathology findings and clinical outcomes. *J Clin Oncol* 2008;26(25):4124-4130.
- (5) Xu B, Liu P. No survival improvement for patients with angioimmunoblastic T-cell lymphoma over the past two decades: a population-based study of 1207 cases. *PLoS One* 2014;9(3):e92585.
- (6) de Leval L, Rickman DS, Thielen C, Reynies A, Huang YL, Delsol G, et al. The gene expression profile of nodal peripheral T-cell lymphoma demonstrates a molecular link between angioimmunoblastic T-cell lymphoma (AITL) and follicular helper T (TFH) cells. *Blood* 2007;109(11):4952-4963.
- (7) Piccaluga PP, Agostinelli C, Califano A, Carbone A, Fantoni L, Ferrari S, et al. Gene expression analysis of angioimmunoblastic lymphoma indicates derivation from T follicular helper cells and vascular endothelial growth factor deregulation. *Cancer Res* 2007;67(22):10703-10710.
- (8) Iqbal J, Wright G, Wang C, Rosenwald A, Gascoyne RD, Weisenburger DD, et al. Gene expression signatures delineate biological and prognostic subgroups in peripheral T-cell lymphoma. *Blood* 2014;123(19):2915-2923.
- (9) Bellei M, Foss FM, Shustov AR, Horwitz SM, Marcheselli L, Kim WS, et al. The outcome of peripheral T-cell lymphoma patients failing first-line therapy: a report from the prospective, International T-Cell Project. *Haematologica* 2018;103(7):1191-1197.
- (10) Moskowitz AJ, Lunning MA, Horwitz SM. How I treat the peripheral T-cell lymphomas. *Blood* 2014;123(17):2636-2644.

- (11) Binder C, Ziepert M, Pfreundschuh M, Dührsen U, Eimermacher H, Aldaoud A, et al. CHO(E)P-14 followed by alemtuzumab consolidation in untreated peripheral T cell lymphomas: final analysis of a prospective phase II trial. *Ann Hematol* 2013;92(11):1521-1528.
- (12) Kim JG, Sohn SK, Chae YS, Cho YY, Yang DH, Lee J, et al. Alemtuzumab plus CHOP as front-line chemotherapy for patients with peripheral T-cell lymphomas: a phase II study. *Cancer Chemother Pharmacol* 2007;60(1):129-134.
- (13) Lee J, Suh C, Kang HJ, Ryoo B-, Huh J, Ko YH, et al. Phase I study of proteasome inhibitor bortezomib plus CHOP in patients with advanced, aggressive T-cell or NK/T-cell lymphoma. *Ann Oncol* 2008;19(12):2079-2083.
- (14) Gleeson M, Peckitt C, To YM, Edwards L, Chau I, Johnson P, et al. CHOP VERSUS GEM-P IN THE FIRST-LINE TREATMENT OF T-CELL LYMPHOMA (PTCL): INITIAL RESULTS OF THE UK NRCI PHASE II RANDOMISED CHEMO-T TRIAL. *Hematol Oncol* 2017;35:75-76.
- (15) Dupuis J, Morschhauser F, Ghesquières H, Tilly H, Casasnovas O, Thieblemont C, et al. Combination of romidepsin with cyclophosphamide, doxorubicin, vincristine, and prednisone in previously untreated patients with peripheral T-cell lymphoma: a non-randomised, phase 1b/2 study. *The Lancet Haematology* 2015;2(4):e165.
- (16) Johnston PB, Cashen AF, Nikolinakos PG, Beaven AW, Barta SK, Bhat G, et al. Safe and Effective Treatment of Patients with Peripheral T-Cell Lymphoma (PTCL) with the Novel HDAC Inhibitor, Belinostat, in Combination with CHOP: Results of the Bel-CHOP Phase 1 Trial. *Blood* 2015;126(23):253.
- (17) Shustov A, Johnston PB, Barta SK, Bhat G, Reddy G, Oki Y. Pralatrexate in Combination with Cyclophosphamide, Doxorubicin, Vincristine, and Prednisone (CHOP) in Previously Untreated Patients with Peripheral T-Cell Lymphoma (PTCL): A Phase 1 Dose-Escalation Study. *Blood* 2017;130(Suppl 1):818.
- (18) Kharfan-Dabaja M, Kumar A, Ayala E, Hamadani M, Reimer P, Gisselbrecht C, et al. Clinical Practice Recommendations on Indication and Timing of Hematopoietic Cell Transplantation in Mature T Cell and NK/T Cell Lymphomas: An International Collaborative Effort on Behalf of the Guidelines Committee of the American Society for Blood and Marrow Transplantation. *Biol Blood Marrow Transplant* 2017.
- (19) d'Amore F, Relander T, Lauritzsen GF, Jantunen E, Hagberg H, Anderson H, et al. Up-front autologous stem-cell transplantation in peripheral T-cell lymphoma: NLG-T-01. *J Clin Oncol* 2012;30(25):3093-3099.
- (20) Chihara D, Fanale MA, Miranda RN, Noorani M, Westin JR, Nastoupil LJ, et al. The survival outcome of patients with relapsed/refractory peripheral T-cell lymphoma-not

otherwise specified and angioimmunoblastic T-cell lymphoma. *Br J Haematol* 2017;176(5):750-758.

(21) Falchi L, Lue JK, Amengual JE, Sawas A, Deng C, Marchi E, et al. A Phase 1/2 Study of Oral 5-Azacytidine and Romidepsin in Patients with Lymphoid Malignancies Reveals Promising Activity in Heavily Pretreated Peripheral T-Cell Lymphoma (PTCL). *Blood* 2017;130(Suppl 1):1515.

(22) Cheminant M, Bruneau J, Kosmider O, Lefrere F, Delarue R, Gaulard P, et al. Efficacy of 5-azacytidine in a TET2 mutated angioimmunoblastic T cell lymphoma. *Br J Haematol* 2015;168(6):913-916.

(23) Lemonnier F, Dupuis J, Sujobert P, Tournillhac O, Cheminant M, Sarkozy C, et al. Treatment with 5-azacytidine induces a sustained response in patients with angioimmunoblastic T-cell lymphoma. *Blood* 2018;132(21):2305-2309.

(24) Hopfinger G, Nosslinger T, Lang A, Linkesch W, Melchardt T, Weiss L, et al. Lenalidomide in combination with vorinostat and dexamethasone for the treatment of relapsed/refractory peripheral T cell lymphoma (PTCL): report of a phase I/II trial. *Ann Hematol* 2014;93(3):459-462.

(25) Morschhauser F, Fitoussi O, Haioun C, Thieblemont C, Quach H, Delarue R, et al. A phase 2, multicentre, single-arm, open-label study to evaluate the safety and efficacy of single-agent lenalidomide (Revlimid) in subjects with relapsed or refractory peripheral T-cell non-Hodgkin lymphoma: the EXPECT trial. *Eur J Cancer* 2013;49(13):2869-2876.

(26) Toumishey E, Prasad A, Dueck G, Chua N, Finch D, Johnston J, et al. Final report of a phase 2 clinical trial of lenalidomide monotherapy for patients with T-cell lymphoma. *Cancer* 2015;121(5):716-723.

(27) Coiffier B, Pro B, Prince HM, Foss F, Sokol L, Greenwood M, et al. Results from a pivotal, open-label, phase II study of romidepsin in relapsed or refractory peripheral T-cell lymphoma after prior systemic therapy. *J Clin Oncol* 2012;30(6):631-636.

(28) Horwitz SM, Advani RH, Bartlett NL, Jacobsen ED, Sharman JP, O'Connor OA, et al. Objective responses in relapsed T-cell lymphomas with single-agent brentuximab vedotin. *Blood* 2014;123(20):3095-3100.

(29) Damaj G, Gressin R, Bouabdallah K, Cartron G, Choufi B, Gyan E, et al. Results From a Prospective, Open-Label, Phase II Trial of Bendamustine in Refractory or Relapsed T-Cell Lymphomas: The BENTLY Trial. *Journal of Clinical Oncology* 2013;31(1):104-110.

- (30) O'Connor OA, Pro B, Pinter-Brown L, Bartlett N, Popplewell L, Coiffier B, et al. Pralatrexate in patients with relapsed or refractory peripheral T-cell lymphoma: results from the pivotal PROPEL study. *J Clin Oncol* 2011;29(9):1182-1189.
- (31) O'Connor OA, Horwitz S, Masszi T, Van Hoof A, Brown P, Doorduijn J, et al. Belinostat in Patients With Relapsed or Refractory Peripheral T-Cell Lymphoma: Results of the Pivotal Phase II BELIEF (CLN-19) Study. *J Clin Oncol* 2015;33(23):2492-2499.
- (32) Foss F, Advani R, Duvic M, Hymes KB, Intragumtornchai T, Lekhakula A, et al. A Phase II trial of Belinostat (PXD101) in patients with relapsed or refractory peripheral or cutaneous T-cell lymphoma. *Br J Haematol* 2015;168(6):811-819.
- (33) Ogura M, Ishida T, Hatake K, Taniwaki M, Ando K, Tobinai K, et al. Multicenter phase II study of mogamulizumab (KW-0761), a defucosylated anti-CC chemokine receptor 4 antibody, in patients with relapsed peripheral T-cell lymphoma and cutaneous T-cell lymphoma. *J Clin Oncol* 2014;32(11):1157-1163.
- (34) Barr PM, Li H, Spier C, Mahadevan D, LeBlanc M, Ul-Haq M, et al. Phase II Intergroup Trial of Alisertib in Relapsed and Refractory Peripheral T-Cell Lymphoma and Transformed Mycosis Fungoides: SWOG 1108. *J Clin Oncol* 2015;33(21):2399-2404.
- (35) Witzig TE, Reeder C, Han JJ, LaPlant B, Stenson M, Tun HW, et al. The mTORC1 inhibitor everolimus has antitumor activity in vitro and produces tumor responses in patients with relapsed T-cell lymphoma. *Blood* 2015;126(3):328-335.
- (36) Horwitz S, O'Connor OA, Pro B, Illidge T, Fanale M, Advani R, et al. Brentuximab vedotin with chemotherapy for CD30-positive peripheral T-cell lymphoma (ECHELON-2): a global, double-blind, randomised, phase 3 trial. *Lancet* 3 Dec 2018. doi: 10.1016/S0140-6736(18)32984-2. [Epub ahead of print]
- (37) Cleverley S, Henning S, Cantrell D. Inhibition of Rho at different stages of thymocyte development gives different perspectives on Rho function. *Current Biology* 1999;9(12):S1.
- (38) Rothenberg EV. Transcriptional drivers of the T-cell lineage program. *Curr Opin Immunol* 2012;24(2):132-138.
- (39) Cher DJ, Mosmann TR. Two types of murine helper T cell clone. II. Delayed-type hypersensitivity is mediated by TH1 clones. *J Immunol* 1987;138(11):3688-3694.
- (40) Mosmann TR, Cherwinski H, Bond MW, Giedlin MA, Coffman RL. Two types of murine helper T cell clone. I. Definition according to profiles of lymphokine activities and secreted proteins. *J Immunol* 1986;136(7):2348-2357.

- (41) Zhu J, Yamane H, Paul WE. Differentiation of Effector CD4 T Cell Populations. *Annual Review of Immunology* 2009;28(1):445-489.
- (42) Zhou L, Chong MMW, Littman DR. Plasticity of CD4 + T Cell Lineage Differentiation. *Immunity* 2009;30(5):646-655.
- (43) Hirahara K, Poholek A, Vahedi G, Laurence A, Kanno Y, Milner JD, et al. Mechanisms underlying helper T-cell plasticity: implications for immune-mediated disease. *J Allergy Clin Immunol* 2013;131(5):1276-1287.
- (44) Laslo P, Spooner CJ, Warmflash A, Lancki DW, Lee H, Sciammas R, et al. Multilineage transcriptional priming and determination of alternate hematopoietic cell fates. *Cell* 2006;126(4):755-766.
- (45) Wilson CB, Rowell E, Sekimata M. Epigenetic control of T-helper-cell differentiation. *Nat Rev Immunol* 2009;9(2):91-105.
- (46) Martin-Orozco N, Chung Y, Chang SH, Wang Y, Dong C. Th17 cells promote pancreatic inflammation but only induce diabetes efficiently in lymphopenic hosts after conversion into Th1 cells. *Eur J Immunol* 2009;39(1):216-224.
- (47) Hegazy AN, Peine M, Helmstetter C, Panse I, Fröhlich A, Bergthaler A, et al. Interferons direct Th2 cell reprogramming to generate a stable GATA-3(+)T-bet(+) cell subset with combined Th2 and Th1 cell functions. *Immunity* 2010;32(1):116-128.
- (48) Baumjohann D, Ansel KM. MicroRNA-mediated regulation of T helper cell differentiation and plasticity. *Nat Rev Immunol* 2013;13(9):666-678.
- (49) Maul J, Baumjohann D. Emerging Roles for MicroRNAs in T Follicular Helper Cell Differentiation. *Trends Immunol* 2016;37(5):297-309.
- (50) Baumjohann D, Kageyama R, Clingan JM, Morar MM, Patel S, de Kouchkovsky D, et al. The microRNA cluster miR-17~92 promotes TFH cell differentiation and represses subset-inappropriate gene expression. *Nat Immunol* 2013;14(8):840-848.
- (51) Crotty S. A brief history of T cell help to B cells. *Nat Rev Immunol* 2015;15(3):185-189.
- (52) Johnston RJ, Poholek AC, DiToro D, Yusuf I, Eto D, Barnett B, et al. Bcl6 and Blimp-1 are reciprocal and antagonistic regulators of T follicular helper cell differentiation. *Science* 2009;325(5943):1006-1010.
- (53) Nurieva RI, Chung Y, Martinez GJ, Yang XO, Tanaka S, Matskevitch TD, et al. Bcl6 mediates the development of T follicular helper cells. *Science* 2009;325(5943):1001-1005.

- (54) Chtanova T, Tangye SG, Newton R, Frank N, Hodge MR, Rolph MS, et al. T follicular helper cells express a distinctive transcriptional profile, reflecting their role as non-Th1/Th2 effector cells that provide help for B cells. *J Immunol* 2004;173(1):68-78.
- (55) Kim CH, Lim HW, Kim JR, Rott L, Hillsamer P, Butcher EC. Unique gene expression program of human germinal center T helper cells. *Blood* 2004;104(7):1952-1960.
- (56) Yu D, Rao S, Tsai LM, Lee SK, He Y, Sutcliffe EL, et al. The Transcriptional Repressor Bcl-6 Directs T Follicular Helper Cell Lineage Commitment. *Immunity* 2009;31(3):457-468.
- (57) Choi YS, Kageyama R, Eto D, Escobar TC, Johnston RJ, Monticelli L, et al. ICOS receptor instructs T follicular helper cell versus effector cell differentiation via induction of the transcriptional repressor Bcl6. *Immunity* 2011;34(6):932-946.
- (58) Gigoux M, Shang J, Pak Y, Xu M, Choe J, Mak TW, et al. Inducible costimulator promotes helper T-cell differentiation through phosphoinositide 3-kinase. *Proc Natl Acad Sci U S A* 2009;106(48):20371-20376.
- (59) Rolf J, Fairfax K, Turner M. Signaling pathways in T follicular helper cells. *J Immunol* 2010;184(12):6563-6568.
- (60) Hatzi K, Nance JP, Kroenke MA, Bothwell M, Haddad EK, Melnick A, et al. BCL6 orchestrates Tfh cell differentiation via multiple distinct mechanisms. *J Exp Med* 2015;212(4):539-553.
- (61) Crotty S. Follicular helper CD4 T cells (TFH). *Annu Rev Immunol* 2011;29:621-663.
- (62) Baumjohann D, Preite S, Reboldi A, Ronchi F, Ansel KM, Lanzavecchia A, et al. Persistent antigen and germinal center B cells sustain T follicular helper cell responses and phenotype. *Immunity* 2013;38(3):596-605.
- (63) Yusuf I, Kageyama R, Monticelli L, Johnston RJ, Ditoro D, Hansen K, et al. Germinal center T follicular helper cell IL-4 production is dependent on signaling lymphocytic activation molecule receptor (CD150). *J Immunol* 2010;185(1):190-202.
- (64) McCausland MM, Yusuf I, Tran H, Ono N, Yanagi Y, Crotty S. SAP regulation of follicular helper CD4 T cell development and humoral immunity is independent of SLAM and Fyn kinase. *J Immunol* 2007;178(2):817-828.
- (65) Hu JK, Crompton JC, Locci M, Crotty S. CRISPR-Mediated Slamf1 $\Delta/\Delta$  Slamf5 $\Delta/\Delta$  Slamf6 $\Delta/\Delta$  Triple Gene Disruption Reveals NKT Cell Defects but Not T Follicular Helper Cell Defects. *PLOS ONE* 2016;11(5):e0156074.

- (66) Good-Jacobson KL, Szumilas CG, Chen L, Sharpe AH, Tomayko MM, Shlomchik MJ. PD-1 regulates germinal center B cell survival and the formation and affinity of long-lived plasma cells. *Nat Immunol* 2010;11(6):535-542.
- (67) Haynes NM, Allen CDC, Lesley R, Ansel KM, Killeen N, Cyster JG. Role of CXCR5 and CCR7 in follicular Th cell positioning and appearance of a programmed cell death gene-1high germinal center-associated subpopulation. *J Immunol* 2007;179(8):5099-5108.
- (68) Attridge K, Wang CJ, Wardzinski L, Kenefeck R, Chamberlain JL, Manzotti C, et al. IL-21 inhibits T cell IL-2 production and impairs Treg homeostasis. *Blood* 2012;119(20):4656-4664.
- (69) Sage PT, Francisco LM, Carman CV, Sharpe AH. The receptor PD-1 controls follicular regulatory T cells in the lymph nodes and blood. *Nat Immunol* 2013;14(2):152-161.
- (70) Berg LJ, Finkelstein LD, Lucas JA, Schwartzberg PL. Tec family kinases in T lymphocyte development and function. *Annu Rev Immunol* 2005;23:549-600.
- (71) Schaeffer EM, Debnath J, Yap G, McVicar D, Liao XC, Littman DR, et al. Requirement for Tec kinases Rlk and Itk in T cell receptor signaling and immunity. *Science* 1999;284(5414):638-641.
- (72) Schwartzberg PL, Finkelstein LD, Readinger JA. TEC-family kinases: regulators of T-helper-cell differentiation. *Nat Rev Immunol* 2005;5(4):284-295.
- (73) Vallois D, Dobay MPD, Morin RD, Lemonnier F, Missiaglia E, Juilland M, et al. Activating mutations in genes related to TCR signaling in angioimmunoblastic and other follicular helper T-cell-derived lymphomas. *Blood* 2016;128(11):1490-1502.
- (74) Swerdlow SH, Campo E, Pileri SA, Harris NL, Stein H, Siebert R, et al. The 2016 revision of the World Health Organization classification of lymphoid neoplasms. *Blood* 2016;127(20):2375-2390.
- (75) Dorfman DM, Brown JA, Shahsafaei A, Freeman GJ. Programmed death-1 (PD-1) is a marker of germinal center-associated T cells and angioimmunoblastic T-cell lymphoma. *Am J Surg Pathol* 2006;30(7):802-810.
- (76) Xerri L, Chetaille B, Serriari N, Attias C, Guillaume Y, Arnoulet C, et al. Programmed death 1 is a marker of angioimmunoblastic T-cell lymphoma and B-cell small lymphocytic lymphoma/chronic lymphocytic leukemia. *Hum Pathol* 2008;39(7):1050-1058.
- (77) Dupuis J, Boye K, Martin N, Copie-Bergman C, Plonquet A, Fabiani B, et al. Expression of CXCL13 by neoplastic cells in angioimmunoblastic T-cell lymphoma

(AITL): a new diagnostic marker providing evidence that AITL derives from follicular helper T cells. *Am J Surg Pathol* 2006;30(4):490-494.

(78) Marafioti T, Paterson JC, Ballabio E, Chott A, Natkunam Y, Rodriguez-Justo M, et al. The inducible T-cell co-stimulator molecule is expressed on subsets of T cells and is a new marker of lymphomas of T follicular helper cell-derivation. *Haematologica* 2010;95(3):432-439.

(79) Roncador G, García Verdes-Montenegro J, Tedoldi S, Paterson JC, Klapper W, Ballabio E, et al. Expression of two markers of germinal center T cells (SAP and PD-1) in angioimmunoblastic T-cell lymphoma. *Haematologica* 2007;92(8):1059-1066.

(80) Piccaluga PP, Fuligni F, De Leo A, Bertuzzi C, Rossi M, Bacci F, et al. Molecular Profiling Improves Classification and Prognostication of Nodal Peripheral T-Cell Lymphomas: Results of a Phase III Diagnostic Accuracy Study. *JCO* 2013;31(24):3019-3025.

(81) Attygalle A, Al-Jehani R, Diss TC, Munson P, Liu H, Du MQ, et al. Neoplastic T cells in angioimmunoblastic T-cell lymphoma express CD10. *Blood* 2002;99(2):627-633.

(82) Zhou Y, Attygalle AD, Chuang S, Diss T, Ye H, Liu H, et al. Angioimmunoblastic T-cell lymphoma: histological progression associates with EBV and HHV6B viral load. *Br J Haematol* 2007;138(1):44-53.

(83) Zettl A, Lee S, Rüdiger T, Starostik P, Marino M, Kirchner T, et al. Epstein-Barr virus-associated B-cell lymphoproliferative disorders in angioimmunoblastic T-cell lymphoma and peripheral T-cell lymphoma, unspecified. *Am J Clin Pathol* 2002;117(3):368-379.

(84) Willenbrock K, Bräuninger A, Hansmann M. Frequent occurrence of B-cell lymphomas in angioimmunoblastic T-cell lymphoma and proliferation of Epstein-Barr virus-infected cells in early cases. *Br J Haematol* 2007;138(6):733-739.

(85) Iqbal J, Weisenburger DD, Greiner TC, Vose JM, McKeithan T, Kucuk C, et al. Molecular signatures to improve diagnosis in peripheral T-cell lymphoma and prognostication in angioimmunoblastic T-cell lymphoma. *Blood* 2010;115(5):1026-1036.

(86) Shaffer AL, Wright G, Yang L, Powell J, Ngo V, Lamy L, et al. A library of gene expression signatures to illuminate normal and pathological lymphoid biology. *Immunol Rev* 2006;210:67-85.

(87) Lemonnier F, Couronne L, Parrens M, Jais JP, Travert M, Lamant L, et al. Recurrent TET2 mutations in peripheral T-cell lymphomas correlate with TFH-like features and adverse clinical parameters. *Blood* 2012;120(7):1466-1469.

- (88) Couronne L, Bastard C, Bernard OA. TET2 and DNMT3A mutations in human T-cell lymphoma. *N Engl J Med* 2012;366(1):95-96.
- (89) Odejide O, Weigert O, Lane AA, Toscano D, Lunning MA, Kopp N, et al. A targeted mutational landscape of angioimmunoblastic T-cell lymphoma. *Blood* 2014;123(9):1293-1296.
- (90) Wang C, McKeithan TW, Gong Q, Zhang W, Bouska A, Rosenwald A, et al. IDH2R172 mutations define a unique subgroup of patients with angioimmunoblastic T-cell lymphoma. *Blood* 2015;126(15):1741-1752.
- (91) Cairns RA, Iqbal J, Lemonnier F, Kucuk C, de Leval L, Jais JP, et al. IDH2 mutations are frequent in angioimmunoblastic T-cell lymphoma. *Blood* 2012;119(8):1901-1903.
- (92) Mason EF, Kuo FC, Hasserjian RP, Seegmiller AC, Pozdnyakova O. A distinct immunophenotype identifies a subset of NPM1-mutated AML with TET2 or IDH1/2 mutations and improved outcome. *Am J Hematol* 2018;93(4):504-510.
- (93) Figueroa ME, Abdel-Wahab O, Lu C, Ward PS, Patel J, Shih A, et al. Leukemic IDH1 and IDH2 mutations result in a hypermethylation phenotype, disrupt TET2 function, and impair hematopoietic differentiation. *Cancer Cell* 2010;18(6):553-567.
- (94) Ward PS, Patel J, Wise DR, Abdel-Wahab O, Bennett BD, Collier HA, et al. The Common Feature of Leukemia-Associated IDH1 and IDH2 Mutations Is a Neomorphic Enzyme Activity Converting  $\alpha$ -Ketoglutarate to 2-Hydroxyglutarate. *Cancer Cell* 2010;17(3):225-234.
- (95) Sasaki M, Knobbe CB, Itsumi M, Elia AJ, Harris IS, Chio IIC, et al. D-2-hydroxyglutarate produced by mutant IDH1 perturbs collagen maturation and basement membrane function. *Genes Dev* 2012;26(18):2038-2049.
- (96) Lemonnier F, Cairns RA, Inoue S, Li WY, Dupuy A, Broutin S, et al. The IDH2 R172K mutation associated with angioimmunoblastic T-cell lymphoma produces 2HG in T cells and impacts lymphoid development. *Proc Natl Acad Sci U S A* 2016;113(52):15084-15089.
- (97) Palomero T, Couronne L, Khiabani H, Kim MY, Ambesi-Impiombato A, Perez-Garcia A, et al. Recurrent mutations in epigenetic regulators, RHOA and FYN kinase in peripheral T cell lymphomas. *Nat Genet* 2014;46(2):166-170.
- (98) Yoo HY, Sung MK, Lee SH, Kim S, Lee H, Park S, et al. A recurrent inactivating mutation in RHOA GTPase in angioimmunoblastic T cell lymphoma. *Nat Genet* 2014;46(4):371-375.

- (99) Sakata-Yanagimoto M, Enami T, Yoshida K, Shiraishi Y, Ishii R, Miyake Y, et al. Somatic RHOA mutation in angioimmunoblastic T cell lymphoma. *Nat Genet* 2014;46(2):171-175.
- (100) Nagata Y, Kontani K, Enami T, Kataoka K, Ishii R, Totoki Y, et al. Variegated RHOA mutations in adult T-cell leukemia/lymphoma. *Blood* 2016;127(5):596-604.
- (101) O'Hayre M, Inoue A, Kufareva I, Wang Z, Mikelis CM, Drummond RA, et al. Inactivating mutations in GNA13 and RHOA in Burkitt's lymphoma and diffuse large B-cell lymphoma: A tumor suppressor function for the Gα13/RhoA axis in B cells. *Oncogene* 2016;35(29):3771-3780.
- (102) Rohde M, Richter J, Schlesner M, Betts MJ, Claviez A, Bonn BR, et al. Recurrent RHOA mutations in pediatric Burkitt lymphoma treated according to the NHL-BFM protocols. *Genes Chromosomes Cancer* 2014;53(11):911-916.
- (103) Reddy A, Zhang J, Davis NS, Moffitt AB, Love CL, Waldrop A, et al. Genetic and Functional Drivers of Diffuse Large B Cell Lymphoma. *Cell* 2017;171(2):494.e15.
- (104) Kakiuchi M, Nishizawa T, Ueda H, Gotoh K, Tanaka A, Hayashi A, et al. Recurrent gain-of-function mutations of RHOA in diffuse-type gastric carcinoma. *Nat Genet* 2014;46(6):583-587.
- (105) Zhou J, Hayakawa Y, Wang TC, Bass AJ. RhoA mutations identified in diffuse gastric cancer. *Cancer Cell* 2014;26(1):9-11.
- (106) Lawrence MS, Stojanov P, Mermel CH, Robinson JT, Garraway LA, Golub TR, et al. Discovery and saturation analysis of cancer genes across 21 tumour types. *Nature* 2014;505(7484):495-501.
- (107) Nagao R, Kikuti YY, Carreras J, Kikuchi T, Miyaoka M, Matsushita H, et al. Clinicopathologic Analysis of Angioimmunoblastic T-cell Lymphoma with or Without RHOA G17V Mutation Using Formalin-fixed Paraffin-embedded Sections. *Am J Surg Pathol* 2016;40(8):1041-1050.
- (108) Ondrejka SL, Grzywacz B, Bodo J, Makishima H, Polprasert C, Said JW, et al. Angioimmunoblastic T-cell lymphomas with the RHOA p.Gly17Val mutation have classic clinical and pathologic features. *Am J Surg Pathol* 2016;40(3):335-341.
- (109) Forbes SA, Beare D, Boutselakis H, Bamford S, Bindal N, Tate J, et al. COSMIC: somatic cancer genetics at high-resolution. *Nucleic Acids Res* 2017;45(D1):D783.
- (110) Rohr J, Guo S, Huo J, Bouska A, Lachel C, Li Y, et al. Recurrent activating mutations of CD28 in peripheral T-cell lymphomas. *Leukemia* 2016;30(5):1062-1070.

- (111) Lee SH, Kim JS, Kim J, Kim SJ, Kim WS, Lee S, et al. A highly recurrent novel missense mutation in CD28 among angioimmunoblastic T-cell lymphoma patients. *Haematologica* 2015;100(12):505.
- (112) Rohr J, Guo S, Huo J, Bouska A, Lachel C, Li Y, et al. Recurrent activating mutations of CD28 in peripheral T-cell lymphomas. *Leukemia* 2015.
- (113) Yoo HY, Kim P, Kim WS, Lee SH, Kim S, Kang SY, et al. Frequent CTLA4-CD28 gene fusion in diverse types of T-cell lymphoma. *Haematologica* 2016;101(6):757-763.
- (114) Abate F, da Silva-Almeida AC, Zairis S, Robles-Valero J, Couronne L, Khiabani H, et al. Activating mutations and translocations in the guanine exchange factor VAV1 in peripheral T-cell lymphomas. *Proceedings of the National Academy of Sciences* 2017;114(4):764-769.
- (115) Streubel B, Vinatzer U, Willheim M, Raderer M, Chott A. Novel t(5;9)(q33;q22) fuses ITK to SYK in unspecified peripheral T-cell lymphoma. *Leukemia* 2006;20(2):313-318.
- (116) Attygalle AD, Feldman AL, Dogan A. ITK/SYK translocation in angioimmunoblastic T-cell lymphoma. *Am J Surg Pathol* 2013;37(9):1456-1457.
- (117) Liang P, Chang S, Lin M, Hsieh Y, Chu P, Chen C, et al. Angioimmunoblastic T-cell lymphoma in Taiwan shows a frequent gain of ITK gene. *Int J Clin Exp Pathol* 2014;7(9):6097-6107.
- (118) Etienne-Manneville S, Hall A. Rho GTPases in cell biology. *Nature* 2002;420(6916):629-635.
- (119) Dransart E, Olofsson B, Cherfils J. RhoGDI revisited: novel roles in Rho regulation. *Traffic* 2005;6(11):957-966.
- (120) Ridley AJ, Hall A. The small GTP-binding protein rho regulates the assembly of focal adhesions and actin stress fibers in response to growth factors. *Cell* 1992;70(3):389-399.
- (121) Cantrell D. Lymphocyte signalling: a coordinating role for Vav? *Curr Biol* 1998;8(15):535.
- (122) Glotzer M. Animal cell cytokinesis. *Annu Rev Cell Dev Biol* 2001;17:351-386.
- (123) Chircop M. Rho GTPases as regulators of mitosis and cytokinesis in mammalian cells. *Small GTPases* 2014;5:10.4161/sgtp.29770. Epub 2014 Jul 2.
- (124) Tybulewicz VL, Henderson RB. Rho family GTPases and their regulators in lymphocytes. *Nat Rev Immunol* 2009;9(9):630-644.

- (125) Henning SW, Galandrini R, Hall A, Cantrell DA. The GTPase Rho has a critical regulatory role in thymus development. *EMBO J* 1997;16(9):2397-2407.
- (126) Galandrini R, Henning SW, Cantrell DA. Different functions of the GTPase Rho in prothymocytes and late pre-T cells. *Immunity* 1997;7(1):163-174.
- (127) Cleverley SC, Costello PS, Henning SW, Cantrell DA. Loss of Rho function in the thymus is accompanied by the development of thymic lymphoma. *Oncogene* 2000;19(1):13-20.
- (128) Rubin EJ, Gill DM, Boquet P, Popoff MR. Functional modification of a 21-kilodalton G protein when ADP-ribosylated by exoenzyme C3 of *Clostridium botulinum*. *Mol Cell Biol* 1988;8(1):418-426.
- (129) Mullin M, Lightfoot K, Clarke R, Miller M, Lahesmaa R, Cantrell D. The RhoA transcriptional program in pre-T cells. *FEBS Lett* 2007;581(22):4309-4317.
- (130) Yang J-, Kalim KW, Li Y, Zhang S, Hinge A, Filippi M-, et al. RhoA orchestrates glycolysis for TH2 cell differentiation and allergic airway inflammation. *J Allergy Clin Immunol* 2016;137(1):245.e4.
- (131) Zhang S, Konstantinidis DG, Yang J, Mizukawa B, Kalim K, Lang RA, et al. Gene targeting RhoA reveals its essential role in coordinating mitochondrial function and thymocyte development. *J Immunol* 2014;193(12):5973-5982.
- (132) Julian L, Olson MF. Rho-associated coiled-coil containing kinases (ROCK): structure, regulation, and functions. *Small GTPases* 2014;5:e29846.
- (133) Rozo C, Chinenov Y, Maharaj RK, Gupta S, Leuenberger L, Kirou KA, et al. Targeting the RhoA-ROCK pathway to reverse T-cell dysfunction in SLE. *Ann Rheum Dis* 2017;76(4):740-747.
- (134) Pernis AB, Ricker E, Weng C, Rozo C, Yi W. Rho Kinases in Autoimmune Diseases. *Annu Rev Med* 2016;67:355-374.
- (135) Isgro J, Gupta S, Jacek E, Pavri T, Duculan R, Kim M, et al. Enhanced rho-associated protein kinase activation in patients with systemic lupus erythematosus. *Arthritis Rheum* 2013;65(6):1592-1602.
- (136) Weiss JM, Chen W, Nyuydzefe MS, Trzeciak A, Flynn R, Tonra JR, et al. ROCK2 signaling is required to induce a subset of T follicular helper cells through opposing effects on STATs in autoimmune settings. *Sci Signal* 2016;9(437):ra73.
- (137) Vielkind S, Gallagher-Gambarelli M, Gomez M, Hinton HJ, Cantrell DA. Integrin regulation by RhoA in thymocytes. *J Immunol* 2005;175(1):350-357.

- (138) Pasvolsky R, Grabovsky V, Giagulli C, Shulman Z, Shamri R, Feigelson SW, et al. RhoA is involved in LFA-1 extension triggered by CXCL12 but not in a novel outside-in LFA-1 activation facilitated by CXCL9. *J Immunol* 2008;180(5):2815-2823.
- (139) Giagulli C, Scarpini E, Ottoboni L, Narumiya S, Butcher EC, Constantin G, et al. RhoA and zeta PKC control distinct modalities of LFA-1 activation by chemokines: critical role of LFA-1 affinity triggering in lymphocyte in vivo homing. *Immunity* 2004;20(1):25-35.
- (140) Ihara K, Muraguchi S, Kato M, Shimizu T, Shirakawa M, Kuroda S, et al. Crystal structure of human RhoA in a dominantly active form complexed with a GTP analogue. *J Biol Chem* 1998;273(16):9656-9666.
- (141) Longenecker K, Read P, Lin SK, Somlyo AP, Nakamoto RK, Derewenda ZS. Structure of a constitutively activated RhoA mutant (Q63L) at 1.55 Å resolution. *Acta Crystallogr D Biol Crystallogr* 2003;59:876-880.
- (142) Ghosh PM, Ghosh-Choudhury N, Moyer ML, Mott GE, Thomas CA, Foster BA, et al. Role of RhoA activation in the growth and morphology of a murine prostate tumor cell line. *Oncogene* 1999;18(28):4120-4130.
- (143) Chiba S, Enami T, Ogawa S, Sakata-Yanagimoto M. G17V RHOA: Genetic evidence of GTP-unbound RHOA playing a role in tumorigenesis in T cells. *Small GTPases* 2015;6(2):100-103.
- (144) Warner K, Crispatzu G, Al-Ghaili N, Weit N, Florou V, You MJ, et al. Models for mature T-cell lymphomas—A critical appraisal of experimental systems and their contribution to current T-cell tumorigenic concepts. *Crit Rev Oncol* 2013;88(3):680-695.
- (145) Fujisawa M, Sakata-Yanagimoto M, Nishizawa S, Komori D, Gershon P, Kiryu M, et al. Activation of RHOA-VAV1 signaling in angioimmunoblastic T-cell lymphoma. *Leukemia* 2018;32(3):694-702.
- (146) Corre I, Gomez M, Vielkind S, Cantrell DA. Analysis of Thymocyte Development Reveals that the GTPase RhoA Is a Positive Regulator of T Cell Receptor Responses In Vivo. *J Exp Med* 2001;194(7):903-914.
- (147) Gomez-Rodriguez J, Kraus ZJ, Schwartzberg PL. Tec family kinases Itk and Rlk/Txk in T lymphocytes: cross-regulation of cytokine production and T-cell fates. *FEBS J* 2011;278(12):1980-1989.
- (148) Liu KQ, Bunnell SC, Gurniak CB, Berg LJ. T cell receptor-initiated calcium release is uncoupled from capacitative calcium entry in Itk-deficient T cells. *J Exp Med* 1998;187(10):1721-1727.

- (149) Dombroski D, Houghtling RA, Labno CM, Precht P, Takesono A, Caplen NJ, et al. Kinase-independent functions for Itk in TCR-induced regulation of Vav and the actin cytoskeleton. *J Immunol* 2005;174(3):1385-1392.
- (150) Woods ML, Kivens WJ, Adelman MA, Qiu Y, August A, Shimizu Y. A novel function for the Tec family tyrosine kinase Itk in activation of beta 1 integrins by the T-cell receptor. *EMBO J* 2001;20(6):1232-1244.
- (151) Takesono A, Horai R, Mandai M, Dombroski D, Schwartzberg PL. Requirement for Tec kinases in chemokine-induced migration and activation of Cdc42 and Rac. *Curr Biol* 2004;14(10):917-922.
- (152) Fischer AM, Mercer JC, Iyer A, Ragin MJ, August A. Regulation of CXC chemokine receptor 4-mediated migration by the Tec family tyrosine kinase ITK. *J Biol Chem* 2004;279(28):29816-29820.
- (153) Fowell DJ, Shinkai K, Liao XC, Beebe AM, Coffman RL, Littman DR, et al. Impaired NFATc translocation and failure of Th2 development in Itk-deficient CD4+ T cells. *Immunity* 1999;11(4):399-409.
- (154) Gomez-Rodriguez J, Sahu N, Handon R, Davidson TS, Anderson SM, Kirby MR, et al. Differential expression of interleukin-17A and -17F is coupled to T cell receptor signaling via inducible T cell kinase. *Immunity* 2009;31(4):587-597.
- (155) Gomez-Rodriguez J, Meylan F, Handon R, Hayes ET, Anderson SM, Kirby MR, et al. Itk is required for Th9 differentiation via TCR-mediated induction of IL-2 and IRF4. *Nat Commun* 2016;7:10857.
- (156) Forssell J, Sideras P, Eriksson C, Malm-Erfjält M, Rydell-Törmänen K, Ericsson P, et al. Interleukin-2-inducible T cell kinase regulates mast cell degranulation and acute allergic responses. *Am J Respir Cell Mol Biol* 2005;32(6):511-520.
- (157) Ferrara TJ, Mueller C, Sahu N, Ben-Jebria A, August A. Reduced airway hyperresponsiveness and tracheal responses during allergic asthma in mice lacking tyrosine kinase inducible T-cell kinase. *J Allergy Clin Immunol* 2006;117(4):780-786.
- (158) Sun Y, Peng I, Webster JD, Suto E, Lesch J, Wu X, et al. Inhibition of the kinase ITK in a mouse model of asthma reduces cell death and fails to inhibit the inflammatory response. *Sci Signal* 2015;8(405):ra122.
- (159) von Bonin A, Rausch A, Mengel A, Hitchcock M, Krüger M, von Ahsen O, et al. Inhibition of the IL-2-inducible tyrosine kinase (Itk) activity: a new concept for the therapy of inflammatory skin diseases. *Exp Dermatol* 2011;20(1):41-47.

- (160) Cho H, Shin HM, Haberstock-Debic H, Xing Y, Owens TD, Funk JO, et al. A Small Molecule Inhibitor of ITK and RLK Impairs Th1 Differentiation and Prevents Colitis Disease Progression. *J Immunol* 2015;195(10):4822-4831.
- (161) Dubovsky JA, Beckwith KA, Natarajan G, Woyach JA, Jaglowski S, Zhong Y, et al. Ibrutinib is an irreversible molecular inhibitor of ITK driving a Th1-selective pressure in T lymphocytes. *Blood* 2013;122(15):2539-2549.
- (162) Schutt SD, Fu J, Nguyen H, Bastian D, Heinrichs J, Wu Y, et al. Inhibition of BTK and ITK with Ibrutinib Is Effective in the Prevention of Chronic Graft-versus-Host Disease in Mice: e0137641. *PLoS ONE* 2015;10(9):e0137641.
- (163) Miklos D, Cutler CS, Arora M, Waller EK, Jagasia M, Pusic I, et al. Ibrutinib for chronic graft-versus-host disease after failure of prior therapy. *Blood* 2017;130(21):2243-2250.
- (164) Honigberg LA, Smith AM, Sirisawad M, Verner E, Loury D, Chang B, et al. The Bruton tyrosine kinase inhibitor PCI-32765 blocks B-cell activation and is efficacious in models of autoimmune disease and B-cell malignancy. *Proc Natl Acad Sci U S A* 2010;107(29):13075-13080.
- (165) Chang BY, Huang MM, Francesco M, Chen J, Sokolove J, Magadala P, et al. The Bruton tyrosine kinase inhibitor PCI-32765 ameliorates autoimmune arthritis by inhibition of multiple effector cells. *Arthritis Res Ther* 2011;13(4):R115.
- (166) de Gorter, David J. J., Beuling EA, Kerseboom R, Middendorp S, van Gils JM, Hendriks RW, et al. Bruton's tyrosine kinase and phospholipase Cgamma2 mediate chemokine-controlled B cell migration and homing. *Immunity* 2007;26(1):93-104.
- (167) de Rooij, Martin F. M., Kuil A, Geest CR, Eldering E, Chang BY, Buggy JJ, et al. The clinically active BTK inhibitor PCI-32765 targets B-cell receptor- and chemokine-controlled adhesion and migration in chronic lymphocytic leukemia. *Blood* 2012;119(11):2590-2594.
- (168) Sagiv-Barfi I, Kohrt HEK, Czerwinski DK, Ng PP, Chang BY, Levy R. Therapeutic antitumor immunity by checkpoint blockade is enhanced by ibrutinib, an inhibitor of both BTK and ITK. *Proc Natl Acad Sci U S A* 2015;112(9):966.
- (169) Campbell R, Chong G, Hawkes EA. Novel Indications for Bruton's Tyrosine Kinase Inhibitors, beyond Hematological Malignancies. *J Clin Med* 2018;7(4):62.
- (170) Berglöf A, Hamasy A, Meinke S, Palma M, Krstic A, Månsson R, et al. Targets for Ibrutinib Beyond B Cell Malignancies. *Scand J Immunol* 2015;82(3):208-217.
- (171) Huang Y, Moreau A, Dupuis J, Streubel B, Petit B, Le Gouill S, et al. Peripheral T-cell lymphomas with a follicular growth pattern are derived from follicular helper T

cells (TFH) and may show overlapping features with angioimmunoblastic T-cell lymphomas. *Am J Surg Pathol* 2009;33(5):682-690.

(172) Agostinelli C, Rizvi H, Paterson J, Shende V, Akarca AU, Agostini E, et al. Intracellular TCR-signaling pathway: novel markers for lymphoma diagnosis and potential therapeutic targets. *Am J Surg Pathol* 2014;38(10):1349-1359.

(173) Frith CH, Ward JM, Chandra M. The morphology, immunohistochemistry, and incidence of hematopoietic neoplasms in mice and rats. *Toxicol Pathol* 1993;21(2):206-218.

(174) Pechloff K, Holch J, Ferch U, Schweneker M, Brunner K, Kremer M, et al. The fusion kinase ITK-SYK mimics a T cell receptor signal and drives oncogenesis in conditional mouse models of peripheral T cell lymphoma. *J Exp Med* 2010;207(5):1031-1044.

(175) Wartewig T, Kurguis Z, Keppler S, Pechloff K, Hameister E, Öllinger R, et al. PD-1 is a haploinsufficient suppressor of T cell lymphomagenesis. *Nature* 2017;552(7683):121-125.

(176) Ellyard JI, Chia T, Rodriguez-Pinilla S, Martin JL, Hu X, Navarro-Gonzalez M, et al. Heterozygosity for Roquinsan leads to angioimmunoblastic T-cell lymphoma-like tumors in mice. *Blood* 2012;120(4):812-821.

(177) Yu D, Tan AH, Hu X, Athanasopoulos V, Simpson N, Silva DG, et al. Roquin represses autoimmunity by limiting inducible T-cell co-stimulator messenger RNA. *Nature* 2007;450(7167):299-303.

(178) Linterman MA, Rigby RJ, Wong R, Silva D, Withers D, Anderson G, et al. Roquin differentiates the specialized functions of duplicated T cell costimulatory receptor genes CD28 and ICOS. *Immunity* 2009;30(2):228-241.

(179) Vinuesa CG, Cook MC, Angelucci C, Athanasopoulos V, Rui L, Hill KM, et al. A RING-type ubiquitin ligase family member required to repress follicular helper T cells and autoimmunity. *Nature* 2005;435(7041):452-458.

(180) Muto H, Sakata-Yanagimoto M, Nagae G, Shiozawa Y, Miyake Y, Yoshida K, et al. Reduced TET2 function leads to T-cell lymphoma with follicular helper T-cell-like features in mice. *Blood Cancer J* 2014;4:e264.

(181) Scourzic L, Couronné L, Pedersen MT, Della Valle V, Diop M, Mylonas E, et al. DNMT3A(R882H) mutant and Tet2 inactivation cooperate in the deregulation of DNA methylation control to induce lymphoid malignancies in mice. *Leukemia* 2016;30(6):1388-1398.

- (182) Quivoron C, Couronné L, Della Valle V, Lopez CK, Plo I, Wagner-Ballon O, et al. TET2 Inactivation Results in Pleiotropic Hematopoietic Abnormalities in Mouse and Is a Recurrent Event during Human Lymphomagenesis. *Cancer Cell* 2011;20(1):25-38.
- (183) Beachy SH, Onozawa M, Chung YJ, Slape C, Bilke S, Francis P, et al. Enforced expression of Lin28b leads to impaired T-cell development, release of inflammatory cytokines, and peripheral T-cell lymphoma. *Blood* 2012;120(5):1048-1059.
- (184) Cortes JR, Ambesi-Impiombato A, Couronné L, Quinn SA, Kim CS, da Silva Almeida, Ana C., et al. RHOA G17V Induces T Follicular Helper Cell Specification and Promotes Lymphomagenesis. *Cancer Cell* 2018;33(2):273.e7.
- (185) Ng SY, Brown L, Stevenson K, deSouza T, Aster JC, Louissaint A, et al. RhoA G17V is sufficient to induce autoimmunity and promotes T-cell lymphomagenesis in mice. *Blood* 2018;132(9):935-947.
- (186) Zang S, Li J, Yang H, Zeng H, Han W, Zhang J, et al. Mutations in 5-methylcytosine oxidase TET2 and RhoA cooperatively disrupt T cell homeostasis. *J Clin Invest* 2017;127(8):2998-3012.
- (187) Chang T, Zeitels LR, Hwang H, Chivukula RR, Wentzel EA, Dews M, et al. Lin-28B transactivation is necessary for Myc-mediated let-7 repression and proliferation. *PNAS* 2009;106(9):3384-3389.
- (188) Ouyang W, Li MO. Foxo: in command of T lymphocyte homeostasis and tolerance. *Trends Immunol* 2011;32(1):26-33.
- (189) Pizzi M, Inghirami G. Patient-derived tumor xenografts of lymphoproliferative disorders: are they surrogates for the human disease? *Curr Opin Hematol* 2017;24(4):384-392.
- (190) Tentler JJ, Tan AC, Weekes CD, Jimeno A, Leong S, Pitts TM, et al. Patient-derived tumour xenografts as models for oncology drug development. *Nat Rev Clin Oncol* 2012;9(6):338-350.
- (191) Townsend EC, Murakami MA, Christodoulou A, Christie AL, Köster J, DeSouza TA, et al. The Public Repository of Xenografts Enables Discovery and Randomized Phase II-like Trials in Mice. *Cancer Cell* 2016;29(4):574-586.
- (192) Ng SY, Yoshida N, Christie AL, Ghandi M, Dharia NV, Dempster J, et al. Targetable vulnerabilities in T- and NK-cell lymphomas identified through preclinical models. *Nat Commun* 2018;9(1):2024.
- (193) Buscarlet M, Provost S, Zada YF, Barhdadi A, Bourgoïn V, Lépine G, et al. DNMT3A and TET2 dominate clonal hematopoiesis and demonstrate benign phenotypes and different genetic predispositions. *Blood* 2017;130(6):753-762.

- (194) Busque L, Patel JP, Figueroa M, Vasanthakumar A, Provost S, Hamilou Z, et al. Recurrent Somatic TET2 Mutations in Normal Elderly Individuals With Clonal Hematopoiesis. *Nat Genet* 2012;44(11):1179-1181.
- (195) Lemonnier F, Mak TW. Angioimmunoblastic T-cell lymphoma: more than a disease of T follicular helper cells. *J Pathol* 2017;242(4):387-390.
- (196) Sakata-Yanagimoto M. Multistep tumorigenesis in peripheral T cell lymphoma. *Int J Hematol* 2015;102(5):523-527.
- (197) Nguyen TB, Sakata-Yanagimoto M, Asabe Y, Matsubara D, Kano J, Yoshida K, et al. Identification of cell-type-specific mutations in nodal T-cell lymphomas. *Blood Cancer J* 2017;7(1):e516.
- (198) Schwartz FH, Cai Q, Fellmann E, Hartmann S, Mäyränpää MI, Karjalainen-Lindsberg M, et al. TET2 mutations in B cells of patients affected by angioimmunoblastic T-cell lymphoma. *J Pathol* 2017;242(2):129-133.
- (199) Nishizawa S, Sakata-Yanagimoto M, Hattori K, Muto H, Nguyen T, Izutsu K, et al. BCL6 locus is hypermethylated in angioimmunoblastic T-cell lymphoma. *Int J Hematol* 2017;105(4):465-469.
- (200) Russler-Germain DA, Spencer DH, Young MA, Lamprecht TL, Miller CA, Fulton R, et al. The R882H DNMT3A mutation associated with AML dominantly inhibits wild-type DNMT3A by blocking its ability to form active tetramers. *Cancer Cell* 2014;25(4):442-454.
- (201) Rolf J, Bell SE, Kovesdi D, Janas ML, Soond DR, Webb LM, et al. Phosphoinositide 3-kinase activity in T cells regulates the magnitude of the germinal center reaction. *J Immunol* 2010;185(7):4042-4052.
- (202) Cernuda-Morollón E, Millán J, Shipman M, Marelli-Berg FM, Ridley AJ. Rac activation by the T-cell receptor inhibits T cell migration. *PLoS ONE* 2010;5(8):e12393.
- (203) Ren X, Kiosses WB, Schwartz MA. Regulation of the small GTP-binding protein Rho by cell adhesion and the cytoskeleton. *The EMBO Journal* 1999;18(3):578-585.
- (204) Rueden CT, Schindelin J, Hiner MC, DeZonia BE, Walter AE, Arena ET, et al. ImageJ2: ImageJ for the next generation of scientific image data. *BMC Bioinformatics* 2017;18(1):529.
- (205) Schindelin J, Arganda-Carreras I, Frise E, Kaynig V, Longair M, Pietzsch T, et al. Fiji: an open-source platform for biological-image analysis. *Nat Methods* 2012;9(7):676-682.

- (206) Harrell MI, Iritani BM, Ruddell A. Lymph node mapping in the mouse. *J Immunol Methods* 2008;332(1-2):170-174.
- (207) Dunn TB. Normal and pathologic anatomy of the reticular tissue in laboratory mice, with a classification and discussion of neoplasms. *J Natl Cancer Inst* 1954;14(6):1281-1433.
- (208) Saeed AI, Sharov V, White J, Li J, Liang W, Bhagabati N, et al. TM4: a free, open-source system for microarray data management and analysis. *BioTechniques* 2003;34(2):374-378.
- (209) Dennis G, Sherman BT, Hosack DA, Yang J, Gao W, Lane HC, et al. DAVID: Database for Annotation, Visualization, and Integrated Discovery. *Genome Biol* 2003;4(5):P3.
- (210) Huang DW, Sherman BT, Lempicki RA. Systematic and integrative analysis of large gene lists using DAVID bioinformatics resources. *Nat Protoc* 2009;4(1):44-57.
- (211) Doran AG, Wong K, Flint J, Adams DJ, Hunter KW, Keane TM. Deep genome sequencing and variation analysis of 13 inbred mouse strains defines candidate phenotypic alleles, private variation and homozygous truncating mutations. *Genome Biol* 2016;17(1):167.
- (212) Koboldt DC, Larson DE, Wilson RK. Using VarScan 2 for Germline Variant Calling and Somatic Mutation Detection. *Curr Protoc Bioinformatics* 2013;44:17.
- (213) Koboldt DC, Zhang Q, Larson DE, Shen D, McLellan MD, Lin L, et al. VarScan 2: somatic mutation and copy number alteration discovery in cancer by exome sequencing. *Genome Res* 2012;22(3):568-576.
- (214) McLaren W, Gil L, Hunt SE, Riat HS, Ritchie GRS, Thormann A, et al. The Ensembl Variant Effect Predictor. *Genome Biol* 2016;17(1):122.
- (215) Breuer K, Foroushani AK, Laird MR, Chen C, Sribnaia A, Lo R, et al. InnateDB: systems biology of innate immunity and beyond--recent updates and continuing curation. *Nucleic Acids Res* 2013;41(Database issue):1228.
- (216) Gärtner F, Alt FW, Monroe R, Chu M, Sleckman BP, Davidson L, et al. Immature thymocytes employ distinct signaling pathways for allelic exclusion versus differentiation and expansion. *Immunity* 1999;10(5):537-546.
- (217) Ottolini B, Nawaz N, Mamand S, Allchin RL, Fields P, Dillon R, et al. Heterogenous Mutations at RHOA exon 2 revealed by targeted sequencing of cell free DNA and peripheral blood mononuclear cell DNA in Peripheral T Cell Lymphoma. *HemaSphere* 2018;2(S1):273.

- (218) Zehir A, Benayed R, Shah RH, Syed A, Middha S, Kim HR, et al. Mutational landscape of metastatic cancer revealed from prospective clinical sequencing of 10,000 patients. *Nat Med* 2017;23(6):703-713.
- (219) Baumjohann D, Ansel KM. Identification of T follicular helper (Tfh) cells by flow cytometry. *Protocol Exchange* 2013.
- (220) Mamand S, Allchin RL, Ahearne MJ, Wagner SD. Comparison of interleukin-2-inducible kinase (ITK) inhibitors and potential for combination therapies for T-cell lymphoma. *Sci Rep* 2018;8(1):14216.
- (221) Spolski R, Leonard WJ. IL-21 and T follicular helper cells. *Int Immunol* 2010;22(1):7-12.
- (222) Ding Y, Li J, Yang P, Luo B, Wu Q, Zajac AJ, et al. Interleukin-21 promotes germinal center reaction by skewing the follicular regulatory T cell to follicular helper T cell balance in autoimmune BXD2 mice. *Arthritis & Rheumatology (Hoboken, N.J.)* 2014;66(9):2601-2612.
- (223) Ma CS, Deenick EK, Batten M, Tangye SG. The origins, function, and regulation of T follicular helper cells. *J Exp Med* 2012;209(7):1241-1253.
- (224) Jogdand GM, Mohanty S, Devadas S. Regulators of Tfh Cell Differentiation. *Front Immunol* 2016;7.
- (225) Marcon E, Ni Z, Pu S, Turinsky AL, Trimble SS, Olsen JB, et al. Human-chromatin-related protein interactions identify a demethylase complex required for chromosome segregation. *Cell Rep* 2014;8(1):297-310.
- (226) Wu J, He Z, Yang X, Li K, Wang D, Sun F. RCCD1 depletion attenuates TGF- $\beta$ -induced EMT and cell migration by stabilizing cytoskeletal microtubules in NSCLC cells. *Cancer Lett* 2017;400:18-29.
- (227) Cai L, Yuan W, Zhang Z, He L, Chou K. In-depth comparison of somatic point mutation callers based on different tumor next-generation sequencing depth data. *Sci Rep* 2016;6:36540.
- (228) Bohnert R, Vivas S, Jansen G. Comprehensive benchmarking of SNV callers for highly admixed tumor data. *PLoS ONE* 2017;12(10):e0186175.
- (229) Sim N, Kumar P, Hu J, Henikoff S, Schneider G, Ng PC. SIFT web server: predicting effects of amino acid substitutions on proteins. *Nucleic Acids Res* 2012;40(Web Server issue):452.
- (230) Jeremy J Jay, Cory Brouwer. Lollipops in the Clinic: Information Dense Mutation Plots for Precision Medicine. *PLoS One* 2016;11(8):e0160519.

- (231) Finn RD, Coghill P, Eberhardt RY, Eddy SR, Mistry J, Mitchell AL, et al. The Pfam protein families database: towards a more sustainable future. *Nucleic Acids Res* 2016;44(D1):279.
- (232) Haase M, Fitze G. HSP90AB1: helping the good and the bad. *Gene* 2016;575(2 Pt 1):171-186.
- (233) Pierron G, Tirode F, Lucchesi C, Reynaud S, Ballet S, Cohen-Gogo S, et al. A new subtype of bone sarcoma defined by BCOR-CCNB3 gene fusion. *Nat Genet* 2012;44(4):461-466.
- (234) Tompkins VS, Rosean TR, Holman CJ, DeHoedt C, Olivier AK, Duncan KM, et al. Adoptive B-cell transfer mouse model of human myeloma. *Leukemia* 2016;30(4):962-966.
- (235) Zhang Y, Hua C, Cheng H, Wang W, Hao S, Xu J, et al. Distinct sensitivity of CD8+ CD4- and CD8+ CD4+ leukemic cell subpopulations to cyclophosphamide and rapamycin in Notch1-induced T-ALL mouse model. *Leuk Res* 2013;37(11):1592-1601.
- (236) Zacarias Fluck MF, Hess L, Salatino M, Croci DO, Stupirski JC, Di Masso RJ, et al. The aggressiveness of murine lymphomas selected in vivo by growth rate correlates with galectin-1 expression and response to cyclophosphamide. *Cancer Immunol Immunother* 2012;61(4):469-480.
- (237) Motoyoshi Y, Kaminoda K, Saitoh O, Hamasaki K, Nakao K, Ishii N, et al. Different mechanisms for anti-tumor effects of low- and high-dose cyclophosphamide. *Oncol Rep* 2006;16(1):141-146.
- (238) Shibata S, Asano T, Ogura A, Hashimoto N, Hayakawa J, Uetsuka K, et al. SCID-bg mice as xenograft recipients. *Lab Anim* 1997;31(2):163-168.
- (239) Mosier DE, Gulizia RJ, Baird SM, Wilson DB. Transfer of a functional human immune system to mice with severe combined immunodeficiency. *Nature* 1988;335(6187):256-259.
- (240) Clohessy JG, Pandolfi PP. Mouse hospital and co-clinical trial project--from bench to bedside. *Nat Rev Clin Oncol* 2015;12(8):491-498.
- (241) Humeniuk MS, Liang JJ, Howard M, Inwards DJ. Spontaneous complete remission of angioimmunoblastic T-cell lymphoma. *Proc (Bayl Univ Med Cent)* 2014;27(3):242-245.
- (242) Cornish N, Maybury B, Otton S. A four-year spontaneous remission of angioimmunoblastic T-cell lymphoma. *Br J Haematol* 2018;180(2):176.

- (243) Pangalis GA, Moran EM, Nathwani BN, Zelman RJ, Kim H, Rappaport H. Angioimmunoblastic lymphadenopathy. Long-term follow-up study. *Cancer* 1983;52(2):318-321.
- (244) Landau DA, Sun C, Rosebrock D, Herman SEM, Fein J, Sivina M, et al. The evolutionary landscape of chronic lymphocytic leukemia treated with ibrutinib targeted therapy. *Nature communications* 2017;8(1):2185.
- (245) Fukumoto K, Nguyen TB, Chiba S, Sakata-Yanagimoto M. A review of the biologic and clinical significance of genetic mutations in angioimmunoblastic T-cell lymphoma. *Cancer Sci* 2017.
- (246) Lemonnier F, Gaulard P, de Leval L. New insights in the pathogenesis of T-cell lymphomas. *Curr Opin Oncol* 2018;30(5):277-284.
- (247) Malcolm TIM, Villarese P, Fairbairn CJ, Lamant L, Trinquand A, Hook CE, et al. Anaplastic large cell lymphoma arises in thymocytes and requires transient TCR expression for thymic egress. *Nat Commun* 2016;7:10087.
- (248) Herman SEM, Gordon AL, Hertlein E, Ramanunni A, Zhang X, Jaglowski S, et al. Bruton tyrosine kinase represents a promising therapeutic target for treatment of chronic lymphocytic leukemia and is effectively targeted by PCI-32765. *Blood* 2011;117(23):6287-6296.
- (249) Byrd JC, Furman RR, Coutre SE, Flinn IW, Burger JA, Blum KA, et al. Targeting BTK with ibrutinib in relapsed chronic lymphocytic leukemia. *N Engl J Med* 2013;369(1):32-42.
- (250) Byrd JC, Brown JR, O'Brien S, Barrientos JC, Kay NE, Reddy NM, et al. Ibrutinib versus ofatumumab in previously treated chronic lymphoid leukemia. *N Engl J Med* 2014;371(3):213-223.
- (251) Kumar A, Vardhana S, Moskowitz AJ, Porcu P, Dogan A, Dubovsky JA, et al. Pilot trial of ibrutinib in patients with relapsed or refractory T-cell lymphoma. *Blood Adv* 2018;2(8):871-876.